The described method was applied to the 24 prismatic specimens extracted from the panels. In Figure 5.13 (b), the density of fibres, which is defined as the number of fibres digitally counted divided by the sectional area under investigation, is plotted against the orientation number. Values related to 2D and 3D conditions by Schönlin are marked. Additionally, values obtained with Equation 5.3 have been marked with a discontinuous line. To understand the concept behind the theoretical curve, it should be considered that if all fibres are parallel to the surface, then η_φ=0. Conversely, if every fibre is perpendicular to the surface, the orientation number is η_φ=1. When fibres are nearly perpendicular to the surface, their projection onto a line that is perpendicular to the surface will be greater, and the likelihood of being cut by the studied plane increase. The majority of the sections have an η_φ value between 2D and 3D. However, there is a significant scatter of the density of fibres, far from the theoretical curve. According to the authors, this experimental observation may suggest the existence of an anisotropic distribution of fibres. As further findings, it can be concluded that the density of fibres within a section and their orientation are not necessarily related. In the present study, the poker vibrator was introduced to break the discontinuity of fibres across the planes caused by the waiting time between pourings. This internal compaction is expected to have introduced a degree of heterogeneity in the distribution of fibres.

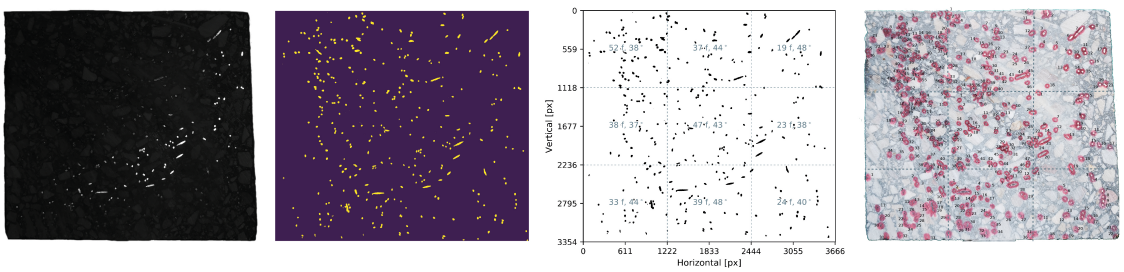

(a) (b) (c) (d)

Figure 5.12: Results of the digital image analysis: (a) single photo of specimen P2D1, (b) collection of photo joined together as a unique matrix of specimen P2D1, (c) number and average angle of the fibres separated by nine equal quadrant of specimen P2D1, and (d) manual counting of sample P2D1.

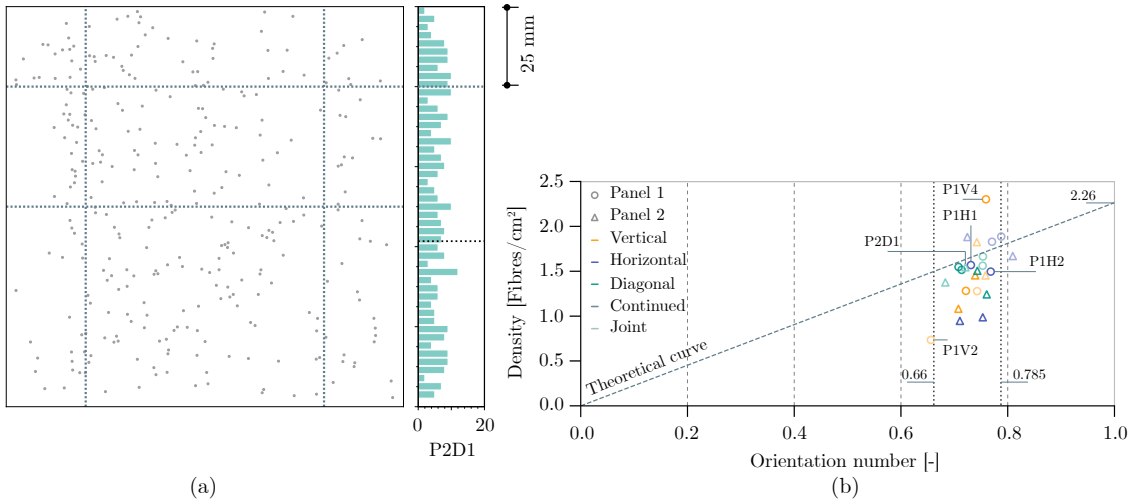

Figure 5.13: Results of the digital image analysis: (a) location of each fibre of the specimen P2D1 and histogram of the distribution of the fibres vertically, and (b) orientation number versus fibre density of the 24 prismatic specimens extracted from the panels.

At this point, the number of fibres, their orientation and distribution within each section can be observed in Figure 5.14 from all the specimens extracted from the panels. Here, the histograms of the vertical distribution of the fibres within each section are presented. Furthermore, each fibre is weighted to account for its individual orientation. The non-weighted bars can be seen in each histogram with a lighter colour. Lastly, the centroids of the weighted fibres within the tensile zone (fibres below the upper 25 mm) are marked with a discontinuous line.

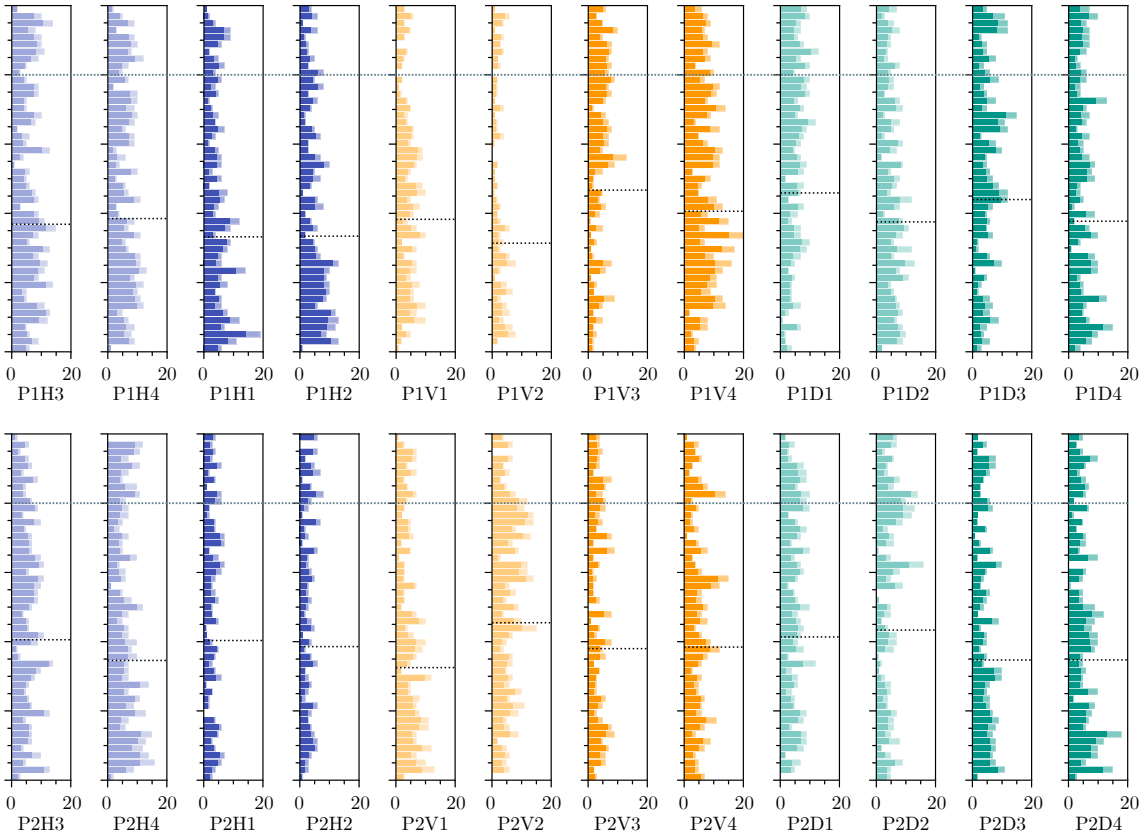

Figure 5.14: Histograms of the fibres vertical distribution of the 24 specimens weighted by the orientation of the fibres.

From the theoretical point of view, there is a relation between the described parameters and the bending nominal strength. In order to validate it experimentally, after testing different regression curves, the best-fitted are presented in Figure 5.15 (a-c), for f_L, f_{R1}, and f_{R3}, respectively. The fibres accounted for are those below the 25 mm considered. The R^2 when all fibres (no weighted) are considered is 0.44 and 0.22 for f_{R1} and f_{R3}, respectively. When only fibres below the hypothetical neutral axis are considered, R^2 increases to 0.52 and 0.26. Lastly, when these fibres are weighted by their orientation, there is a further lighter improvement in R^2, which is the one shown in Figure 5.15 (a-c). Another attempt was also performed to account for the distribution of the fibres below the neutral axis, but the correlation was lower.

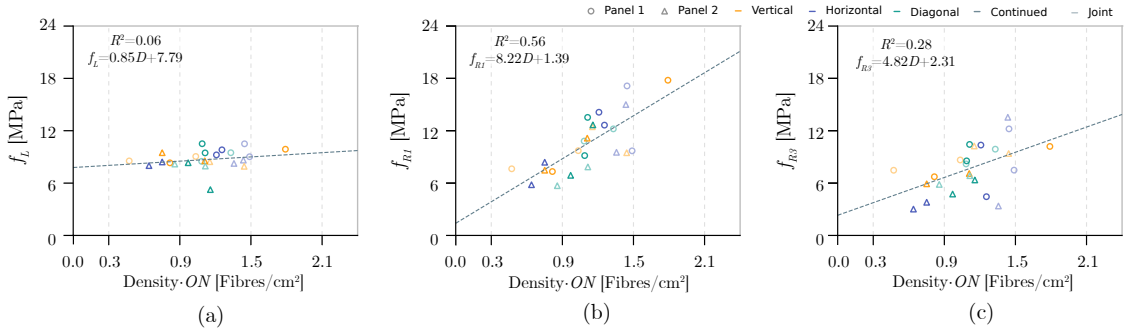

Figure 5.15: Third part of the experimental campaign based on rectangular-shaped panels: (a-c) fibre density weighted by the orientation of each fibre versus the f_L, f_{R1}, and f_{R3}, respectively.

Another technique applied to evaluate the fibre distribution and orientation was the measurement of the inductance of the concrete cylindrical cores extracted from the panels. The employed device, developed by Calavaro et al. [105] and [106], is designed to estimate the fibre content of concrete cores using the inductance measurement variations. Furthermore, the distribution of fibres within a given plane and in a perpendicular direction can be obtained. This work focused on the fibre content. Two cores were extracted from each prismatic specimen tested as illustrated in Figure 5.10 (a), and four additional cores were extracted directly from the panel. Each core was analysed with the inductance apparatus, which was previously calibrated for this specific mix. Subsequently, the cores were broken, and their fibre content was weighted to obtain the precision of this method for this HPFRC. Figure 5.16 shows on a bar graph the V_f (kg/m^3) of each specimen: with a lighter grey being the one obtained through the weighted of the fibres, and with a darker grey the one obtained with the inductance measurements. The average of each of them is shown by the horizontally discontinuous line, and an average difference of 16% is found. All inductance measurements estimate fewer fibre contents than the weighted ones. The inductance method was designed considering that the magnetic fields created by individual fibres do not interact with each other ($V_{f,max}$=60 kg/m^3). According to these results, the application of this technique to a concrete with a fibre content of 80 kg/m^3 increases the inaccuracy obtained.

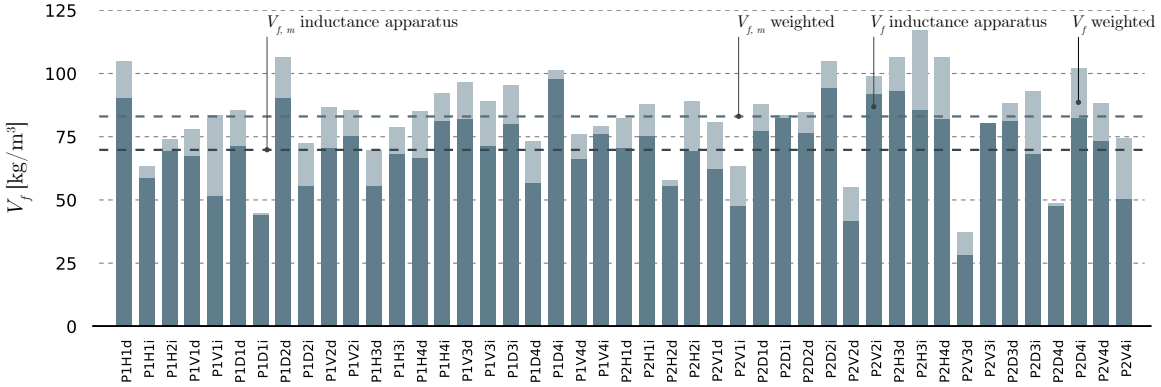

Figure 5.16: Fibre content of the cylindric cores extracted from the panel.

The results of the image analysis of the prismatic specimens, and of the inductance of the cylindrical cores are plotted together in Figure 5.17. A grey colour map with its average value equal to V_f=1% (80 kg/m^3) has been applied to illustrate the distribution of the fibres. To express the fibre density (kg/cm^2) obtained from counting the fibres in the prismatic specimens as kg/m^3, a proportionality is applied. It is considered that a V_f=80 kg/m^3 corresponds to the theoretical number of 1.67 fibres/cm^2 (2.26 fibres/cm^2 multiplied by η_φ=0.738, which is the average orientation number of the 24 specimens).

As main finding, the study of Figure 5.17 endorses that there is no reduction in the number of fibres crossing the notched sections affected by the discontinuity between pours. The average fibre content from all the studied elements is 70 kg/m^3 (-12% with respect to 80 kg/m^3). This difference can be attributed to the previously described inaccuracies of the used inductance technique. The CV of all the elements is 23%, which is similar to the dispersion observed in the 3 point-bending tests. Nonetheless, a significant difference was found between the minimum and maximum fibre content for the panels, ranging in 35-110 kg/m^3 and 28-93 kg/m^3 for, respectively, the panel 1 and 2. However, it should be studied if this dispersion is local (affecting separated elements), or if it reflects some predominantly distribution of fibres which could create a brittle failure plane. Elements from each panel were grouped in 8 horizontal planes. The only clear pattern is observed in the horizontal specimens, which presents in average a V_f=81 kg/m^3 if they are crossed by the discontinuity plane, and V_f=64 kg/m^3 if not. Between the eight horizontal planes of each panel, the dispersion is reduced to a CV=14%, and no further clear patterns are observed. It can be stated that the pouring method followed prevents the creation of cold joints between surfaces.

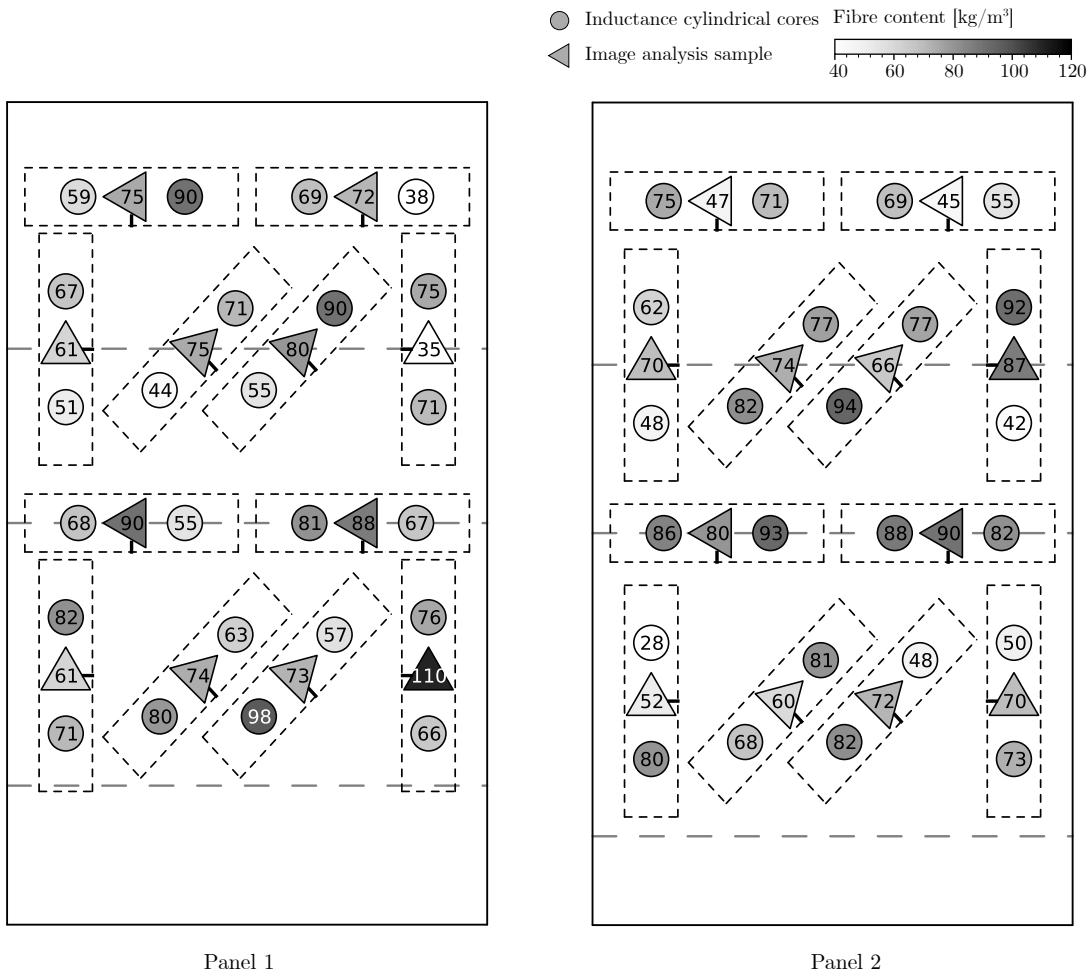

Figure 5.17: Distribution of fibre measured by the digital image analysis and the inductance measurements.

5.5 Conclusions

5.5.1 Conclusions

This Chapter presented the development of a tailor-made HPFRC mix to be used for the construction of segmental 60 m-span U-girder road bridges. The mix, in addition to satisfy specific design requirements, should have a cost not exceeding 2.5-3.0 times the cost of a C70/85 to be competitive from an economic point of view. The bridge design takes advantage of the shear strength contribution of the fibres to eliminate any stirrups in the girder web. Therefore, being so important the role of these fibres, a design-by-testing methodology has

been followed to exactly analyse the casting process of the U-girders.

The following main conclusions are drawn:

- It is possible to develop a cost competitive HPFRC (with a cost only 2.5-3.0 times higher than a C70/85) that reaches strength class C100/115 (f_{ck}=100 MPa) using a cement content of 500 kg/m^3 and 50 kg/m^3 silica fume with a maximum aggregate size of 12 mm. Furthermore, the selected fibre content was 80 kg/m^3 of 4D+60 leading to a 13a class post-cracking strength and a workability class F5 without any sign of segregation or fibre balls.

- Minimum variations from conventional casting techniques will ease the adoption of novel HPFRC by precasters. Therefore, an experimental campaign was designed to allow the use of conventional U-girder formworks for the proposed HPFRC-based solution. Specifically, the formwork remains opened at top face of the bottom slab.

- As expected, the casting of prismatic specimens showed a strong dependency between their casting procedure and their bending post-cracking strength: f_{R1m} and f_{R3m} are reduced by 68% and 76%, respectively, when the specimens were vertically cast.

- The effect of a waiting time between successive pourings without internal compaction with poker vibration has been studied with prismatic specimens. The vertically cast specimens completely lost the post-cracking strength when a waiting time of 3 hours is applied. In contrast, 45 minutes was found to be an acceptable waiting time, as the reduction was not critical (42.6% and 10.6% for f_{R1m} and f_{R3m}, respectively).

- A vibrating table was used for the compaction of the previous specimens. In order to avoid the bending post-cracking strength reduction mentioned above, it was decided to use a poker vibrator to distribute the fibres across the planes between the layers.

- Two real-scale L-shaped panels were cast according to the conventional casting procedure for U-girders. During the internal vibration of the web, a liquefaction of the concrete at the bottom slab occurred with a waiting time of 45 minutes. Hence, the second L-shaped specimen was characterized by a waiting time of 90 minutes between successive layers, and no liquefaction occurred; this waiting time can be considered an adequate value for real-scale production.

- Two rectangular-shaped panels were cast as real-scale mock-ups of the webs of the U-girders. From the test of the extracted prismatic specimens it was concluded: (i) the panel 2 presented lower bending post-cracking strength (-20%), which could be

attributed to the higher free pouring height of the concrete from the container to the formwork, (ii) no difference was detected between the specimens located horizontally or vertically in the panel, (iii) the potential cold joints characterised by a waiting time of 90 minutes do not cause a strength reduction of the prismatic specimens, attributed to the layers stitching of by means of poker vibration.

- The digital image analysis of the fibre counting identified a moderate linear correlation (R^2=0.56) between the density of fibres under the neutral axis, weighted by their orientation, with respect to f_{R1k}.
- Digital image analysis and inductance measurements were used on the elements extracted from the panels to assess the distribution of fibres. These endorsed that there is no reduction in the number of fibres crossing the notched sections affected by the discontinuity between pours. This proved that the methods of pouring and vibration avoided any cold joint.

6

Database of shear tests for prestressed FRC beams without vertical stirrups

6.1 Introduction

Walraven et al. [57] demonstrated that a high-performance fibre reinforced concrete (HPFRC) can achieve a post-cracking hardening behaviour under bending tests showing smeared cracking. In addition, considering the shear contribution of the fibres, it is possible to avoid any transverse reinforcement. The question arises of whether the application of an HPFRC in the design of prestressed precast concrete girders for road girder bridges could be economically attractive compared to conventional concrete bridges. Previous Chapters 2.3 and 4.4 concluded that, for example, a bridge based on precast HPFRC U-girders externally prestressed, spanning 60 m with three segments, can be considered a promising option. Specifically, the solution could be economically competitive due to the removal of conventional stirrups and the savings in concrete consumption (both in the girders and the substructure) if a tailored HPFRC mix, with a f_{ck}=100 MPa and f_{R3k}=12 MPa, is used. Therefore, prestressed HPFRC has the potential for a wide application in the bridge construction sector, and its potential has not been fully exploited. A key point to promote this wide popularization is represented by an accurate evaluation of shear strength, especially for prestressed elements without stirrups.

In an effort to provide a tool that can be used to evaluate design expressions, this work presents a database that collects experimental shear tests on beams made of prestressed steel fibre reinforced concrete without transversal reinforcement. Different existing databases and research papers [89, 94, 121, 122] have been used as a starting point to build this database. The approach described in this Chapter aims to check the conservativeness and accuracy of the relevant design expressions and has been previously adopted by Reineck and Todisco [123] for non-slender beams without stirrups, by Todisco et al. [124, 125] for non-slender beams with vertical stirrups, and by Todisco et al. [126] for non-slender beams with vertical stirrups and horizontal web reinforcement. As additional data, for the convenience of the reader, information about concrete mixes is also provided due to the importance of the fibre type and volume in the shear strength.

The collection database contains 80 tests from 13 different references [13, 60, 65, 88, 89, 94, 122, 127–132]. The evaluation database is then obtained after the application of filters based on the availability of essential data and the ranges of applicability of the formulations. Specifically, four different codes have been considered in this work: the FprEN 1992-1-1:2022 (Issue date: 2022-09) [48], the Model Code 2010 [49], the draft version of Model Code 2020 [50] and the Spanish National Code [70]. All the shear formulations included in these codes are suitable for application to FRC prestressed concrete members without stirrups. The formulations are applied to the evaluation file and the results are critically analysed. Lastly, two additional databases found in the scientific literature of non-prestressed fibre reinforced concrete specimens without stirrups are also analysed. In summary, this work, in an effort to calibrate shear design code expressions for prestressed fibre reinforced concrete members without shear reinforcement, presents the most comprehensive database on the behaviour of these elements. In light of this database, the performances of shear strength expressions of several codes and recommendations are evaluated and discussed.

6.2 Analysis of the collected database

6.2.1 Presentation of the database

The collection database gathers 80 shear tests for prestressed FRC beams without vertical stirrups subjected to point loads. In this study only tests with steel fibres were considered because there is more experience in their use for structural applications. For the convenience of the readers, the collected data are included in the Appendix A of this document, as two separate spreadsheets. Specifically, the first spreadsheet follows the same nomenclature

and structure as the database of Reineck et al. [133], with some specific additional data for FRC (e.g. the quantity of fibres, aggregate size, and nominal flexural strength). The second spreadsheet collects information about concrete mixes, which is important for a correct interpretation of the results.

Research interest in the shear performance of prestressed FRC beams without vertical stirrups is recent. This is shown in Figure 6.1 that illustrates the distribution over time of the tests collected in the database.

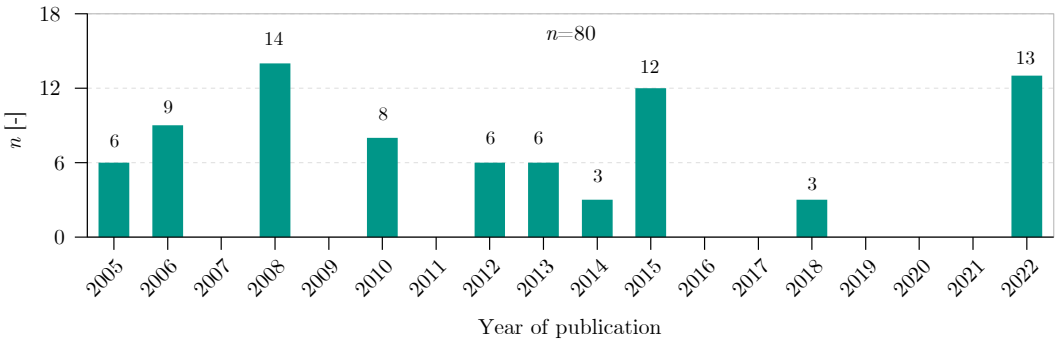

Figure 6.1: Year of publication of the tests collected.

To have a complete overview of the beams collected in the database, Figure 6.2 illustrates their cross-sections. The number located in the bottom right corner of each section indicates the number of tests performed with that section. Furthermore, different colours are used to indicate different concrete compressive strength (mean value of the uniaxial compression strength of concrete (f_{1cm})); specifically, light grey if f_{1cm} is lower than 90 MPa, and dark grey if f_{1cm} is higher than this value. Regarding the beam height, two different groups can be identified. The first includes specimens with a height smaller than 400 mm (Jin et al. [122], Baby et al. [60], Metje and Leutbecher [130], and Hegger and Bertram [127], representing around 30% of the specimens included in the database. The second group comprises beams with larger dimensions up to 1000 mm. The web thicknesses also show a large variability, from 50 to 148 mm. Finally, with the exception of Metje and Leutbecher [130], who employed beams with a rectangular cross-section, all tested specimens (90%) are characterized by an I cross-section.

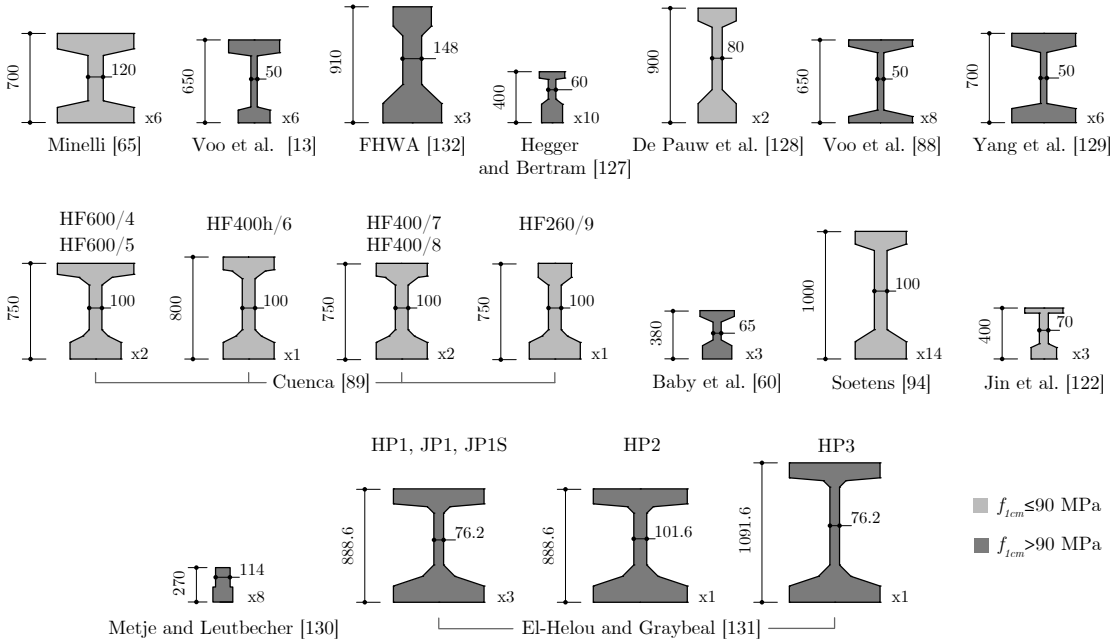

Figure 6.2: Cross-sections of the beams tested.

Regarding the layout of the test, 93% of the tests were performed at 3 points, while the remaining 7% (that is, El-Helou and Graybeal [131]) were performed at 4 points. The main variables studied in all these experimental campaigns were volume content of the fibre (V_f) and the average compressive level (σ_{cp}). Secondary parameters were shear slenderness (a/d) and top flange width (b).

To obtain a wide perspective on the characteristics of all the tests collected in the database, Table 1 presents the maximum and minimum values of the most significant parameters. Furthermore, in an effort to highlight the characteristics of the database, a series of histograms are illustrated in Figure 6.3, where the number of tests is plotted versus the main test parameters. Within these figures, the vertical axes denote the number of tests, while the horizontal axes cover different variables.

Table 6.1: Ranges of parameters in the database.

Parameter	Min value	Max value
f_{1c} [MPa]	42	175
h [mm]	270	1092
d [mm]	209	990
b_w [mm]	50	148
a/d [-]	1.75	4.5
σ_{cp} [MPa]	6.54	35.8
V_f [%]	0.3	2.5
ρ_{pw} [%]	1	7.59
D_{Max} [mm]	0.4	32
λ_f [-]	48	157
σ_{fu} [MPa]	1225	3000

In Figure 6.3 (a), the number n of tests is plotted versus the uniaxial concrete compressive strength f_{1c}(=0.95$f_{c,cyl}$) subdivided into class intervals of Δf_{1c}=10 MPa. Two separate groups can be identified: the first gathers 32 tests (40%) with f_{1c}<90 MPa, while the second group includes 48 tests (60%) with an f_{1c} greater than this limit, and up to 180 MPa. In Figure 6.3 (b), the number of tests is plotted versus the shear span to effective depth ratio (κ=a/d) subdivided into intervals of $\Delta\kappa$=0.5. The minimum and maximum shear slendernesses are, respectively, 1.75 and 4.50. The average value is around 3, while 6.3% of the tests show a κ<2.4 and can be classified as nonslender beams. All other tests (93.7%) can be considered as slender beams. As briefly discussed before, steel fibres can replace conventional transverse reinforcement; therefore, the amount of fibre (V_f) is a representative parameter in the shear strength of the tested beams. Figure 6.3 (c) shows the distribution of V_f subdivided into intervals of ΔV_f=0.20%. The most significant peak is around V_f=1% with 21 tests (26.3%), representing a fibre quantity of approximately 80 kg/m^3. The average compressive stress level (σ_{cp}) indicates the amount of prestressing in the tested beams and also plays a key role in shear strength. In Figure 6.3 (d) the number of tests is plotted versus σ_{cp} subdivided into intervals of $\Delta\sigma_{cp}$=5 MPa. Two separated groups can be identified, the first characterized by a σ_{cp}<20 MPa (with 46 tests, 57.5%) and a second with σ_{cp}>20 MPa (with 34 tests, 42.5%). In the design of the girders, conventionally, an effective compressive level (σ_{cp}/f_{1c}) of 0.20 is used. Consequently, Figure 6.3 (e) illustrates the number of tests versus σ_{cp}/f_{1c}, subdivided into class intervals of $\Delta\sigma_{cp}/f_{1c}$=0.05. This parameter is representative for evaluating the consistency of tests from a designer's perspective. The results show that 51 tests (64%) are within the range 0.20±0.05, but many others (approximately one third) are far from this value. This could be explained by the fact that different levels of prestress

are used to investigate its effect on the shear strength, or that laboratory restrictions make it difficult to achieve higher levels of prestress. The geometric percentage of longitudinal reinforcement (ρ_{pw}) also plays a role in the shear resistance mechanism, precisely, in the concrete contribution to the shear strength of beams without stirrups [62]. Therefore, Figure 6.3 (f) shows the distribution of the number of the beams versus ρ_{pw}, subdivided into class intervals of $\Delta\rho_{pw}$=1. Two separated groups are clearly observed, the first with ρ_{pw}<3.5% with 50 tests (62.5%), and the second one (ρ_{pw}>3.5%) with 30 tests (37.5%).

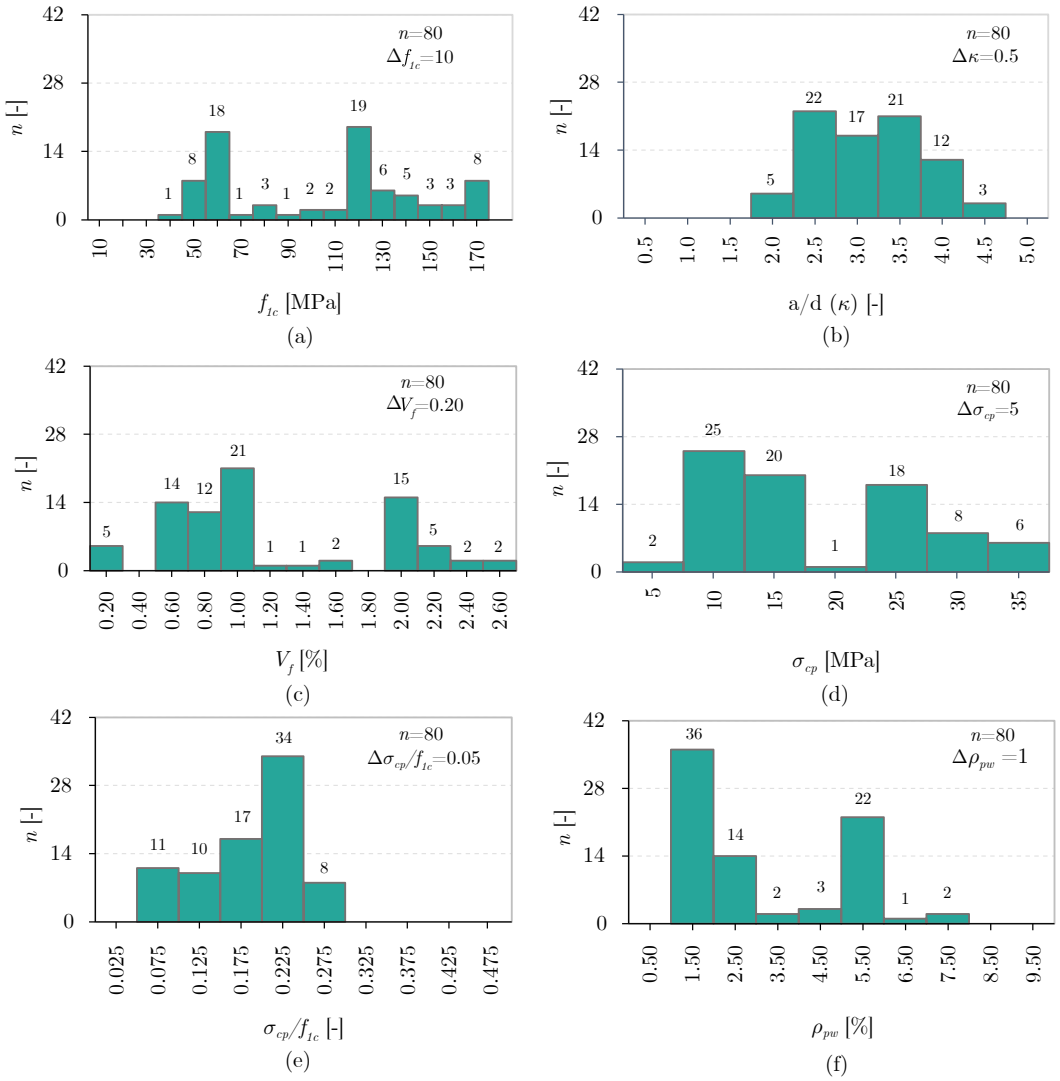

Figure 6.3: Distribution of parameters in database: (a) uniaxial compression strength of concrete f_{1c}, (b) moment-shear-force ratio (κ), (c) fibre content (V_f), (d) axial concrete stress at CGS (σ_{cp}), (e) effective compressive level (σ_{cp}/f_{1c}), and (f) geometrical reinforcement ratio of prestressing steel related to b_w (ρ_{pw}).

6.2.2 Correlation among parameters

This section briefly investigates possible correlations among different parameters of the specimens collected in the database. Figure 6.5 shows f_{1c} (on the vertical axis) versus σ_{cp} (on the horizontal axis). Furthermore, as additional information, the circle size represents the maximum aggregate size (D_{Max}). Finally, the grey colour is used when ρ_{pw}<3.5, and orange otherwise. The limit mentioned above of σ_{cp} /f_{1c}=0.20 is marked by a diagonal black line, while two additional lines indicate the area between σ_{cp} /f_{1c}=0.20±0.05. First, it should be noted that 64% of the tests are within this region. Secondly, as expected, a higher compressive strength generally corresponds to a higher value of the prestress force. Furthermore, the D_{Max} decreases as the f_{1c} increases, indicating that more high-performance concretes are based on aggregates with lower size.

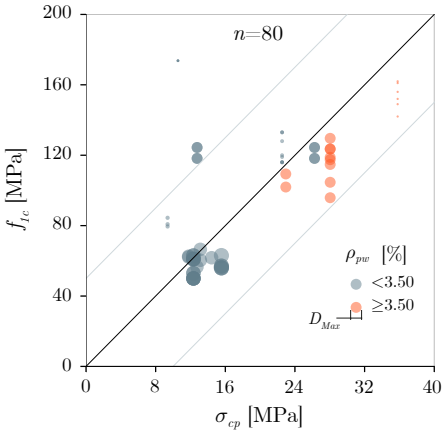

Figure 6.4: Relation between the axial concrete stress at CGS (σ_{cp}) and the uniaxial compression strength of concrete (f_{1c}).

Regarding the aspects related to steel fibres, Figure 6.5 shows in the horizontal axis the fibre volume (V_f) and in the vertical axis the residual strength at a CMOD=2.5 mm (f_{R3m}). The procedure to obtain this value is described in EN-14651 [4], and it is used in several shear formulations (e.g., MC-2010 [49], the draft versions of EC2-2020 [48] and MC-2020 [50], and the Spanish National Code [70]). Fifty-nine percentage of the tests collected in the database reported this value. For further information, the markers have different shapes to indicate the type of fibre (i.e., a circle when it is hooked and a triangle when it is straight). Furthermore, the colour code indicates the direct tensile strength of the steel fibres (σ_{fu}). The mixes developed by Soetens [94] are located in the upper left part of the figure and are represented by six dark red circles. These tests are characterized by the same fibre type with different V_f; therefore, they are used to illustrate a good fit with a linear trend (R^2=0.83) between the

two parameters studied (V_f and f_{R3}). It is interesting to observe that all mixes with hooked fibres have a V_f<0.76%, while those with straight fibres always include a volume fibre greater than 1%. The latter value represents a limit for hooked fibres due to workability issues. The reason is the high geometrical dimensions of the hooked fibres, whose lengths (l_f) range from 30 to 40 mm and whose diameters (d_f) range from 0.38 to 0.62 mm for the mixes under analysis. In contrast, straight fibres have l_f from 12.7 to 20 mm and d_f from 0.15 to 0.40 mm. These lower geometric dimensions of straight fibres explain the possibility of exceeding V_f=1%, but also their lower f_{R3} compared to hooked fibres.

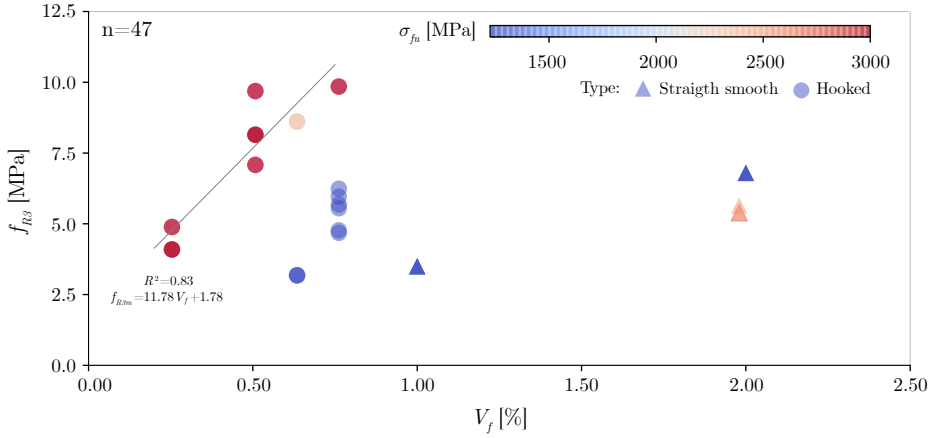

Figure 6.5: Relation between the fibre volume (V_f) and the residual strength at a CMOD=2.5 mm for fibre-reinforced concrete (f_{R3}).

6.3 Comparison with shear strength predictions of fib Model Code, Eurocode and Spanish Code

6.3.1 Brief overview of the shear strength expressions

In light of the presented database, the performance of several shear strength expressions for prestressed FRC beams without vertical stirrups can be evaluated. Specifically, the formulations included in the following documents have been studied: the last draft (issue date: 2022-09) of FprEN 1992-1-1:2022 (EC2-2020) [48], the Model Code 2010 (MC-2010) [49], the last draft of Model Code 2020 (MC-2020) [50] and the Spanish National Code (SNC) [70]. These formulations are collected in Equations 6.1 to 6.8.

FprEN 1992-1-1:2022 (Issue date: 2022-09) [48]

$$V_{Rd,cf} = \left(\eta_{cF} \frac{0.66}{\gamma_V} \left(100 \rho_l f_{ck} \frac{d_{dg}}{d} \right)^{1/3} - k_1 \sigma_{cp} + \ \eta_F f_{Ftud} \ \right) b_w z \tag{6.1}$$

$$V_{Rd,cf} \geq \ V_{Rd,min} = \left(\eta_{cF} \tau_{Rdc,min} \ + \ \eta_F f_{Ftud} \right) b_w z \tag{6.2}$$

$$\tau_{Rd,min} = \frac{11}{\gamma_V} \sqrt{\frac{f_{ck}}{f_{yd}} \frac{d_{dg}}{d}} \tag{6.3}$$

$$k_1 = \frac{0.5}{a_{cs,0}} \left(e_p + \frac{d}{3} \right) \frac{A_c}{b_w z} \leq 0.18 \frac{A_c}{b_w z} \tag{6.4}$$

$$a_{cs,0} = \left| \frac{M_{Ed}}{V_{Ed}} \right| \geq \ d \tag{6.5}$$

$$\eta_{cF} = max \left\{ 1.2 - 0.5 f_{Ftuk}; 0.4 \right\} \leq 1.0; \eta_F = 1.0 \tag{6.6}$$

$$d_{dg} = \begin{cases} 16 + D_{lower} \leq 40 \text{[mm] for concrete with } f_{ck} \leq 60 \text{[MPa]} \\ 16 + D_{lower} \left(60 / f_{ck} \right)^2 \leq 40 \text{[mm] for concrete with } f_{ck} > 60 \text{[MPa]} \end{cases} \tag{6.7}$$

Spanish National Code [70]

$$V_{cF} = 0.7 k \tau_{fd} b_w d + \left(\frac{0.18}{\gamma_c} k \left[100 \rho_l f_{ck} \right]^{\frac{1}{3}} + 0.15 \sigma_{cp} \right) b_w d \tag{6.8}$$

MC-2010 [65]

$$V_{Rd,cf} = \ \left(\frac{0.18}{\gamma_c} k \left[100 \rho_l \left(1 + 7.5 \frac{f_{Ftuk}}{f_{ctk}} \right) f_{ck} \right]^{\frac{1}{3}} + 0.15 \sigma_{cp} \ \right) b_w d \tag{6.9}$$

MC-2010 based on SMCFT [49]

$$V_{Rd,cf} = \frac{1}{\gamma_F} \left(k_v \sqrt{f_{ck}} + k_f f_{Ftuk} cot\theta \right) b_w z \tag{6.10}$$

$$k_v = \frac{0.4}{1 + 1500 \varepsilon_x} \frac{1300}{1000 + k_{dg} z} \tag{6.11}$$

$$\theta = 29 + 7000 \varepsilon_x \tag{6.12}$$

MC-2020 [50]

$$V_{Rd,cf} = \frac{1}{\gamma_F} \left(k_v \sqrt{f_{ck}} + k_f f_{Ftuk} cot\theta \right) b_w z \tag{6.13}$$

$$k_v = \frac{0.4}{1 + 1500 \varepsilon_x + \xi} \frac{1300}{1000 + k_{dg} z} \tag{6.14}$$

$$\theta = 29 + 7000\varepsilon_x \tag{6.15}$$

$$\xi = (20 - 14000\varepsilon_x)\,\frac{K_s f_{Ftuk}}{f_{ck}} \tag{6.16}$$

All these shear strength expressions present a certain degree of empiricism. The formulation of the last draft of EC2-2020 [48] (Annex L, Equations 6.1 to 6.7) is an adaptation of the current EC2 [45] (Eq. 6.2.a) for conventional beams without stirrups. This expression is based on the König and Fisher expression [62], which is an empirical adjustment obtained from a database of conventional concrete beams without stirrups. The formulation of the Spanish National Code (SNC) [70] (Equation 6.8) is based on the referenced formulation, but also considers the final recommendations of RILEM TC 162-TDF [134]. Finally, the formulation of MC-2010, based on the work of Minelli [65] (Equation 6.9), also shares the same origin.

In contrast, the formulation of the MC-2010 (Equations 6.10 to 6.12) located in the comments section is based on the Simplified Modified Compression Field Theory (SMCFT) [64], which is a simplified version of the Vecchio and Collins Modified Compression Field Theory (MCFT) [63]. MCFT describes the behaviour of conventional concrete members reinforced with stirrups, and it is based on the equilibrium, compatibility, and constitutive laws related to a cracked concrete element. The simplification that turns MCFT into the SMCFT is based on a solution to the equation system that the MCFT raises, allowing the SMCFT formulation to be calculated preliminary on the 'back of an envelope'. This solution was reached by performing a parametric analysis of the MCFT with conventional cases for both with and without stirrups members, reaching separated formulations for each case. The draft version of the incoming Model Code, MC-2020 [50] (Equations 6.13 to 6.16) is similar to the comments version of MC-2010, but it considers a new coefficient of the strain factor (Equation 6.16). All these shear formulations consider different parameters, such as the longitudinal bonded reinforcement ratio, the compressive and nominal flexural strengths, the effect of the element size and the size of the aggregates, among others.

6.3.2 Selection of the evaluation database

In order to correctly apply the above-mentioned code shear expressions, the tests have to be sorted according to the applicability ranges of the different codes. Furthermore, the nominal

Table 6.2: Results of the evaluation of the tests in respect of the individual criteria *kon*i.

Individual criteria	Condition for criterion	Test satisfying criterion		Violating criterion
		No.	Percent of 80	No.
*kon*1	f_{R1} and f_{R3} >0	47	59	33
*kon*2	$f_{ck} \leq 100$	32	40	48
*kon*3	$f_{ck} \leq 90$	31	39	49
*kon*4	$f_{ck} \leq 120$	40	50	40
*kon*5	κ>2.4	75	94	5

Table 6.3: Results for the application of criteria for evaluation database.

Individual criteria	Combination of individual criteria	Test satisfying criterion		Violating criterion
		No.	Percent of 80	No.
*kon*125	*kon*1 x *kon*2 x *kon*5	27	34	53
*kon*135	*kon*1 x *kon*3 x *kon*5	26	33	54
*kon*145	*kon*1 x *kon*4 x *kon*5	32[1]	40	48

flexural strength, characterized by EN-14651 [4], must be reported in the tests. These control criteria are defined and checked for:

- *kon*i = 0 not fulfilled; not transferred to the evaluation file.
- *kon*i = 1 fulfilled; transferred to the evaluation file.

The abbreviation '*kon*' is a German acronym for control criterion and 'i' is a running number. The first criterion, *kon*1, is 1 if f_{R1} and f_{R3} are available data; otherwise, it is 0. Next, *kon*2, *kon*3, *kon*4 criteria are applied to check the applicability range of f_{1c}: specifically, $f_{ck} \leq 100$ MPa for the draft version of EC2020, $f_{ck} \leq 90$ MPa for the SNC, and $f_{ck} \leq 120$ MPa for the MC-2010 and the draft of MC-2020. Finally, *kon*5 is also applied to consider only non-slender beams with κ>2.4. Table 6.2 shows the results of the application of the individual selection criteria, while Table 6.3 collects the subsequent application of the specified combinations. The detailed description of all procedures applied in this work to establish evaluation databases can be found in Reineck and Dunkelberg [135], and Reineck and Fitik [136].

6.3.3 Statistical analysis for the model safety factor

All shear strength expressions have been implemented in the evaluation database, and a specific shear strength $V_{u,cal}$ has been calculated for each test. Comparison of this value with

Table 6.4: Comparison of statistical values for γ_{mod}.

Statistical values for γ_{mod}	EC2	SNC	MC10	MC10 SMCFT	MC20 SMCFT
n	27	26	31	31	31
m	1.54	1.59	1.70	1.78	2.07
s	0.36	0.35	0.32	0.62	0.69
$v = s/m$	0.23	0.22	0.19	0.35	0.33
γ_{mod}<1 [%]	0	0	0	0	0

the shear force at failure $V_{u,test}$ allows the definition of a model safety factor as expressed by Equation 6.17.

$$\gamma_{mod} = \frac{V_{u,test}}{V_{u,cal}} \tag{6.17}$$

For the calculation of $V_{u,cal}$, the material safety factors γ_c and γ_F are taken as 1, and the mean values of the material strength are considered. Hence, the γ_{mod} is a model safety factor that characterizes the quality and the accuracy of the model. It does not contain load factors and it is not a global safety factor. These results are gathered in Appendix D. Table 6.4 collects the statistical results of γ_{mod} to facilitate a comparison between the shear formulations. Specifically, the number of tests (n), the mean (m), the standard deviation (s), and the coefficient of variation $v = s/m$ are listed. Finally, the number of tests with γ_{mod}<1 is indicated, expressed as a percentage of the number of tests analysed.

The results show that the design expressions of all documents are conservative. To graphically show all the results, the γ_{mod} is illustrated in Figure 6.6 for design expressions using the box-and-whiskers plot. The SMCFT-based approach of MC-2010 shows a better accuracy of the model, as well as a lower scatter. However, the best statistical indicators are obtained for the EC2-2020 formulation with m=1.54 and v=0.23.

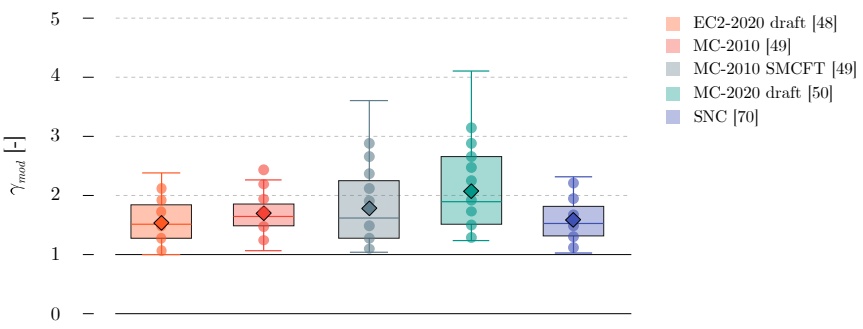

Figure 6.6: Box-and-whiskers plot for the model safety factors (γ_{mod}) values of the presented database.

Next, Figure 6.7 investigates the influence of different variables on the γ_{mod}. The criterion to select this correlation was to identify a linear trend with $R^2 \geq 0.45$. Several parameters were investigated (κ, f_{R3m}, f_{1cm}, ρ_{pw}, d, and σ_{cp}), but Figure 6.7 only shows the parameters that meet that criterion. Specifically, Figures 6.7 (a) and (b) refer to the γ_{mod} obtained for the expression of the last draft of MC-2020. The first two graphs indicate a linear relation (i.e., γ_{mod} increases with increasing ρ_{pw} and σ_{cp}). Therefore, as the main finding, it can be concluded that although the compression level is already considered in the MC-2020 formulations (based on SMCFT), an adjustment with respect to this variable could improve the accuracy of these models. For the SMCFT-based expression of MC-2010, the distributions are very similar and slight changes in R^2 are observed.

A similar finding is obtained by analysing the results of the MC-2010 SMCFT and MC-2020 draft, but with lower values of R^2, respectively 0.40 and 0.39.

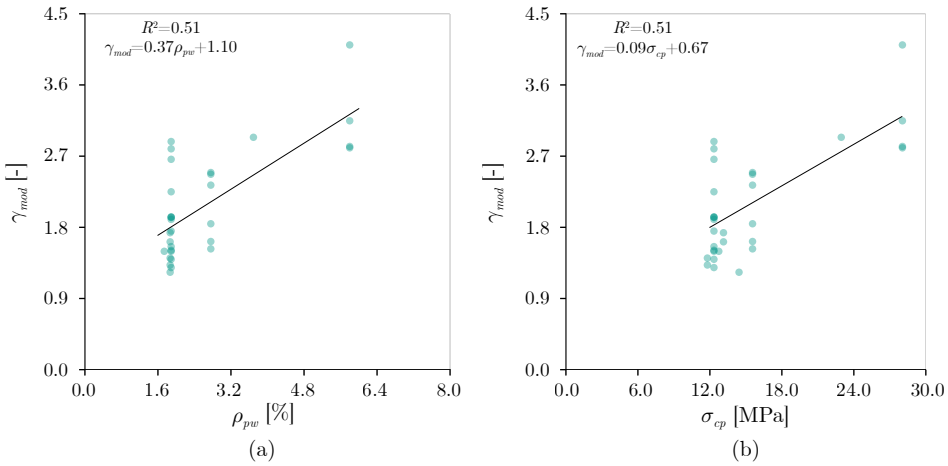

Figure 6.7: Distribution of model safety factors (γ_{mod}) of: (a) MC-2020 draft versus the geometrical reinforcement ratio of prestressing steel related to b_w (ρ_{pw}), and (b) MC-2020 draft versus the axial concrete stress at CGS (σ_{cp}).

6.3.4 Comparison with databases of fibre reinforced concrete beams without stirrups

The database presented in this study collects only prestressed beams. Therefore, to identify the effect of prestress on the model safety factor, two different databases of FRC beams without stirrups have been studied. The first database was assembled by Lantsoght [137] and includes 488 beams. The second database was published by Cuenca et al. [121], and contains 34 beams. The Lantsoght's database does not contain the f_{R3} values required for the application of the shear formulations, while the second does. However, detailed information about the fibres used was provided in the Lantsoght's database. Therefore, two different regressions were applied to obtain f_{R3} from the characteristics of the fibres. The first procedure was based on the work of Faccin [138], while the second one was based on the research of Bairán et al. [139]. Therefore, the Lantsoght's database was first filtered, considering only the FRC hooked fibres to be consistent with the FRC material database from which these regressions were derived. After filtering, 262 tests remained in the database, and the filters already described in Table 6.3 were applied.

The comparisons of the statistical values for γ_{mod} are detailed in Tables 6.5 to 6.7. Specifically, Tables 6.5 and 6.6 refer to the Lantsoght's database, respectively, with Faccin and Bairán et al. regression laws. Table 6.7 is based on Cuenca's database that already included experimental values of f_{R3}.

Table 6.5: Comparison of statistical values for γ_{mod} of Langtsoght database and regression by Faccin [137, 138].

Statistical values for γ_{mod}	EC2	SNC	MC10	MC10 SMCFT	MC20 SMCFT
n	255	239	261	261	261
m	1.30	1.15	1.26	1.02	1.05
s	0.58	0.44	0.50	0.39	0.41
$v = s/m$	0.45	0.38	0.40	0.38	0.39
γ_{mod}<1 [%]	32	44	33	59	56

Table 6.6: Comparison of statistical values for γ_{mod} of Langtsoght database and regression by Bairán et al. [137, 139].

Statistical values for γ_{mod}	EC2	SNC	MC10	MC10 SMCFT	MC20 SMCFT
n	255	239	261	261	261
m	1.50	1.26	1.35	1.15	1.19
s	0.73	0.49	0.56	0.48	0.50
$v = s/m$	0.48	0.39	0.42	0.42	0.42
γ_{mod}<1 [%]	20	31	24	44	40

Table 6.7: Comparison of statistical values for γ_{mod} of Cuenca et al. database [121].

Statistical values for γ_{mod}	EC2	SNC	MC10	MC10 SMCFT	MC20 SMCFT
n	34	34	34	25	25
m	1.21	1.11	1.06	0.87	0.90
s	0.27	0.23	0.20	0.16	0.16
$v = s/m$	0.22	0.20	0.19	0.18	0.18
γ_{mod}<1 [%]	16	26	44	76	76

The graphical comparison in terms of γ_{mod} is presented in Figure 6.8 for all the design expressions and the four databases. Specifically, the results are grouped by shear formulations to compare the results among databases. The average value (m) is graphically indicated with a cross, while the coefficient of variation (v) is indicated with whiskers. Furthermore, the percentages (%) of tests with a γ_{mod}<1 are given for each case at the top of each bar.

The results clearly prove the pronounced conservativeness of the shear models when dealing with prestress beams made of FRC without stirrups. This result is common to all design expressions, although more noticeable in the shear formulation of MC-2010 and MC-2020. The most accurate shear strength predictions are obtained for the SNC.

Furthermore, results obtained with Faccin and Bairán et al. regression laws are similar, although small differences can be observed (e.g., Bairán results present a m value 12% lower on average compared to that of Lantsoght-Faccin). However, when dealing with the experimental values of f_{R1} and f_{R3}, the γ_{mod} is generally lower, with a high percentage of tests below the safe limit of γ_{mod}=1. As final observation, the Cuenca et al. database presents the lowest scatter, and this result is independent of the used shear expression.

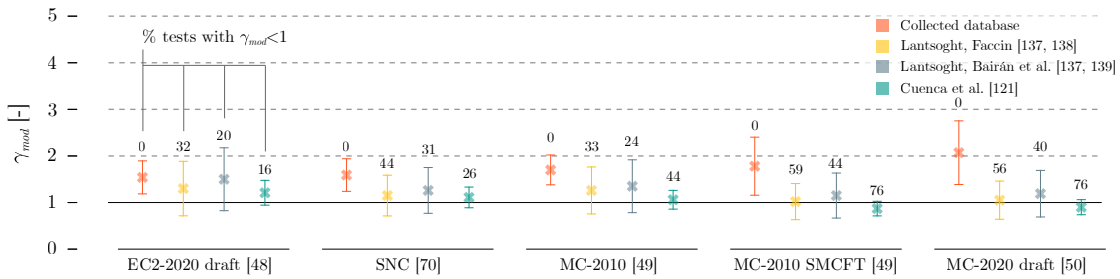

Figure 6.8: Model safety factors (γ_{mod}) for the 4 different databases calculations and the five shear formulations under study.

6.4 Conclusions

6.4.1 Conclusions

This Chapter introduced a large database for shear tests on prestressed FRC beams without stirrups subjected to point loads. The database contained 80 beams obtained from 13 different references. As far as the authors know, this is the largest database on these structural elements. These tests have been filtered to meet the applicability ranges of the different codes. In light of this database, the accuracy of different shear strength formulations is evaluated

with the use of a model safety factor. Additionally, two more databases of non-prestressed FRC beams without stirrups were considered. The main findings of this study are as follows:

- All shear strength predictions yielded clear conservative results (they yielded results that were above the desired 5% fractile). Specifically, MC20 SMCFT present higher conservative values of γ_{mod} with an average value of 2.07. Eurocode 2 presents the best precision with an average value of γ_{mod} of 1.54.
- In the design expression of the MC-2010 SMCFT and MC-2020 draft, there are pronounced trends for the model safety factor with respect to ρ_{pw}, and σ_{cp}. Therefore, the conservatism of these shear models can be improved by increasing the effect of these two factors.
- The comparison of the results with other databases with similar beams but without prestress proves a pronounced conservativeness of the shear models when dealing with prestress beams. The most accurate shear strength predictions are obtained for the SNC. The average value of γ_{mod} for prestressed beams is 25% higher for the design expression of the SNC, but it increases extraordinarily up to 1.98 times when shear model Model Code 2020 is considered.
- Further studies are needed to solve the conservativeness problem observed in this Chapter. Specifically, the relevant contribution of the prestress on the shear strength should be enhanced by the analytical models included in the codes.

Finally, for the convenience of the readers, all the data collected and described in this document are shared with the scientific community. Specifically, Appendix C includes the collection database, while Appendix D comprises all the results consequent to the application of the shear strength predictions.

7

Mechanical analysis of shear-transfer actions based on detailed experimental measurements

7.1 Introduction

In Chapter 4, it was studied the potential of using precast HPFRC U-girders with external unbonded prestressing to span medium-to-large distances (close to 60 m, see Figure 1 (a)). Such structural solution allows avoiding the need for stirrups in the webs while achieving reductions in concrete consumption both in the girders and substructure (as foundations and piles). The most promising solutions were identified for HPFRC mixes with compressive strength (f_{ck}) in the order of 100 MPa and heavily prestressed, with a characteristic residual strength at a CMOD of 2.5 mm (f_{R3k}) ranging from 8 to 10 MPa. In the previous Chapter 4 it was shown the cost-saving of this solution is around 12.5% compared to alternatives based on the use of conventional reinforced concrete.

The design of such members is governed by the shear resistance of the slender webs. For members with shear reinforcement and smeared cracking pattern, conventional design approaches consider strut-and-tie models [140, 141], derived from the truss analogy [142–144], and stress fields [145]. These models allow for consistent design of beam regions (where plane sections remain plane) as well as discontinuity regions (where such condition does not hold true). For elements without shear reinforcement, crack localization may occur

and the previous approaches are not suitable for design. In this case, several models exist in the literature based on different theoretical approaches (a detailed summary may be found for instance in [146]). Although there is still not a clear consensus, design codes are increasingly being based on mechanical models [48, 49], replacing empirical formulae which have traditionally governed shear design [45, 147]. Such change of paradigm in design models has been possible to a large extent by the better understanding of the mechanics of shear transfer, which have been confirmed or revised according to detailed experimental measurements (see for instance [148, 149]).

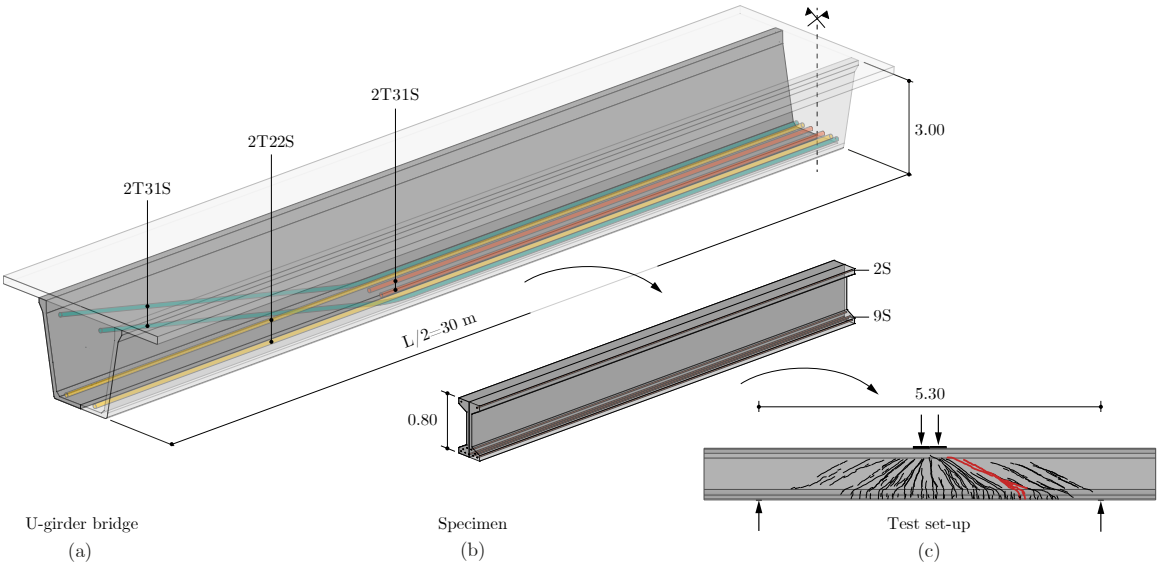

Figure 7.1: Research visual abstract: (a) Proposal of a HPFRC U-girder bridge with a span of 60 m, (b) laboratory specimen prestressed beam, and (c) test set-up with crack pattern.

With respect to shear design formulations for prestressed members cast in Fibre-Reinforced Concrete (FRC) and without stirrups, they have traditionally been inspired by physical models of reinforced or prestressed concrete beams. This is for instance the case of the formulation by König and Fisher [62] provisioned in EN1992-1-1:2004 (Eurocode 2) [45] which was later adapted by Minelli [65] for FRC beams (with or without prestressing) for the MC2010 [49]. Another example is the Modified Compression Field Theory (MCFT) [150] and its simplified version [64], currently considered in the commentary of fib's Model Code 2010 for FRC beams [151]. These formulations (as well as that of FprEN1992-1-1:2023 [45]) still show in some cases a relatively high level of conservatism when compared to available databases. In order to provide more consistent design approaches or to tailor the previous mechanical models for prestressed FRC beams, it is advisable to better understand the mechanics of

shear failure. This requires performing tests at realistic scales (Figure 1 (b) and (c)), and to implement detailed measurements on the crack development and kinematics.

In order to take a step forward in this direction, an experimental programme is presented in this paper aimed at investigating the shear resistance of prestressed HPFRC beams without stirrups. The experimental programme comprises eight HPFRC beams of 80 cm height, six specimens with high levels of prestressing and two without prestressing. Based on the surface measurements, the contribution of the various potential shear-transfer actions (namely aggregate interlock [152–160], dowel action [161–166], tensile strength of FRC [167, 168] and the contribution of the inclined compression chord [169]) will be investigated, following previously established methodologies [148, 149, 170–172]. On that basis, an unbiased discussion on the role of the different actions and influencing parameters is presented, highlighting their differences with respect to reinforced concrete members failing in shear.

7.2 Experimental programme

7.2.1 Specimen description

The experimental programme comprises eight prefabricated beams cast at the factory Pretersa and Prenavisa in Teruel (Spain). All specimens were later transported and tested at the Structural Engineering Laboratory of Universidad Politécnica de Madrid (Spain).

All beams presented identical dimensions, with a length of 7 m and an I-shaped cross-section, see Figure 7.2. The beams were 800 mm high and the web thickness was 100 mm. The flanges were 400 mm wide and had a total height of 160 mm (80 mm of constant width plus 80 mm of variable width). Six beams contained only prestressing strands (150 mm^2 of cross-sectional area each) as longitudinal reinforcement, with nine strands arranged in the bottom flange and two in the top flange. The remaining two beams, had identical dimensions, but had no prestressing strands and the longitudinal reinforcement on the bottom flange consisted of 5 rebars diameter 25 mm and 2 rebars diameter 20 mm.

The variables investigated within this programme included the level of prestressing and the bond conditions between concrete and the strands. To that aim, the arrangement of the strands was kept identical, but ducts were installed around the strands at specific locations as shown in Figure 7.2 (c) for a prestressed specimen (bottom flange of specimen BR-B13-5). In the same figure, the layout of the rebars for the reference specimens (without prestressing,

specimens BR-B0-1, and -2) is also shown. The ducts installed around the strands were single flexible plastic tubes (Figure 7.2 (a)), which is a typical solution used in practice. The tubes were closed and secured to the strands using the same metal wires for reinforcement positioning. Despite the efforts devoted to the placing of the ducts as debonding system of the strands, the system did not always disable the transfer of prestressing. In fact, after testing the specimens, the strands were inspected at regions where bond shall be disabled, and cement grout was found inside the ducts. This was attributed to deficient sealing of the ducts and allowed for partial transfer of prestressing in several cases. The actual level of prestressing was in any case assessed in detail as it will be explained later.

As it can be noted (refer to Figure 7.2 (b)), one side of the span was shear-reinforced while the other not. This was performed to promote shear failures in a restrained area so that DIC measurements could be performed in a precise manner.

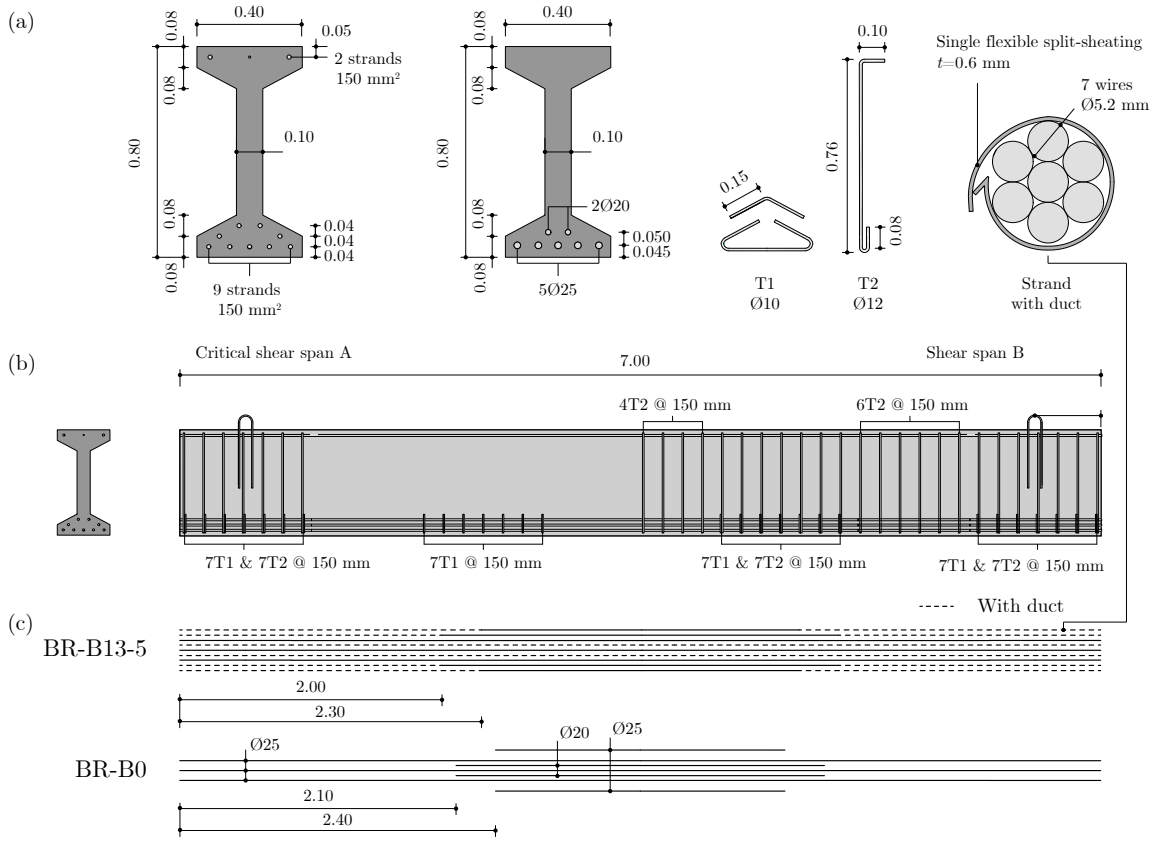

Figure 7.2: Geometry and reinforcement layout: (a) Cross sections, stirrup detailing, and cross section of a strand with duct, (b) longitudinal specimen view; and (c) regions of strands with ducts and layout of ordinary reinforcement.

7.2.2 Specimens casting and material properties

Figure 7.3 illustrates the arrangement of prestressing and passive reinforcement in beams BR-B13-1 and BR-B13-2 within the prestressing bed. Specifically, Figure 7.3 (a) presents the steel plate covering of the formwork, the strands, sheathing, and stirrups type T1 and T2. Furthermore, for the purpose of documenting the positioning of the sheathing along the strands, Figure 7.3 (b) portrays the utilization of a measuring tape alongside the strands to capture in photographs the prestressing sheath position along the strands.

(a) (b)

Figure 7.3: Preparation of the reinforcement in the prestressing bed: (a) Beam BR-B13-1 and BR-B13-2 formworks and reinforcement in the prestressing bed, and (b) documenting of the exact location of the passive reinforcement and the sheaths in BR-B13-1.

As an initial trial with an HPFRC in this precast plant, a prestressing rectangular cross-section beam was successfully cast. During this experience, it was observed that the HPFRC demanded substantial energy for mixing due to its significant content of long steel fibres. Accordingly, it was decided to use the 2.5 m^3 capacity planetary mixer at 25% of its capacity. The casting procedure for each beam involved three layers: the first focused on the lower flange, without covering the two strands in the third row. This choice prevented any reduction in tensile strength of the HPFRC due to the appearance of a weak plane between the bottom flange and the web. The second layer encompassed the web and a portion of the upper flange, followed by the third layer covering the remaining portion. To facilitate the casting, the quantity of fibres within the lower flange was reduced to 40 kg/m^3.

In Figure 7.4 (a), the concrete container, which was equipped with an external vibration apparatus, is depicted. This instrument allows the precise and controlled pouring of concrete layers to the designated height. Figure 7.4 (b) shows the first layer completely cast, and

the two strands of the third layer can be detected. Figure 7.4 (c) provides insight into the compaction method using a poker vibrator. This aligns with the authors prior experiences, emphasizing the need to vibrate across the discontinuity planes between layers to allow fibres to stitch it. Furthermore, this HPFRC requires the introduction of energy to correctly fill the formwork.

To ensure the desired workability, all concrete batches underwent rigorous assessment via a flow table test. Figure 7.4 (d) captures the result of one test, showing a homogeneous distribution and with a diameter measuring 550 mm, sourced from a BR-B13-1 concrete batch.

(a) (b) (c) (d)

Figure 7.4: Casting of the beam BR-B13-1 (a) pouring from the container, (b) surface of the first layer of concrete with two uncovered strands, (c) compaction with a poker vibrator, (d) the result of the flow table test with a diameter equal to 550 mm.

The HPFRC mix contained 500 kg/m^3 of cement (CEM I 52.5R) and 50 kg/m^3 of silica fume with 150 kg/m^3 of water (water-to-cement ratio equal to 0.3). Quartzite sand was used (0-6 mm) as per 978 kg/m^3 as well as 796 kg/m^3 of quartzite aggregates (6-12 mm). In addition, 3.75 kg/m^3 of plasticizer were used (Sikament 3003 NG) together with 8.5 kg/m^3 of superplasticizer (Sikaviscocrete 90 NG).

Regarding fibres, the batches of the web and top flange contained 80 kg/m^3 of 4D-fibres (Bekaert 4D Plus 80/60) with a length of 60 mm, an aspect ratio (l_f/d_f) equal to 80 and a nominal tensile strength of 2200 MPa. To enhance the workability of the mix in the bottom flange, this amount was reduced to 40 kg/m^3 for the corresponding batch. In addition, concrete was vibrated with poker vibrators at the interfaces of different batches.

Characterization of the concrete properties was performed by means of conventional material

testing in compression and tension. In compression, cube specimens (150 × 150 × 150 mm) were continuously tested, namely at 28 days and at the end of the testing programme (610 days). The results are shown in Figure 7.5 together with the prediction of strength development with time according to fib's Model Code 2010. The corresponding values for each specimen on the day of testing (ranging between 118 and 135 MPa) are presented in Table 7.1. In addition, cylinders of the same dimensions were cast in the laboratory to obtain the modulus of elasticity according to EN12390-13 [173]. The results, obtained at 14 and 35 days, were 40.3 and 46.3 GPa, respectively.

Concerning the response of concrete in tension, 3-point notched bending tests were performed at 28 days on prisms of dimensions 150 × 150 × 550 mm and according to EN14651 [4]. The results are presented in Figures 7.5 (b,c) for the fibre contents of 80 kg/m3 and 40 kg/m^3 respectively. Each individual test is represented by a light grey line, while the average of all tests is depicted as a solid line. Additionally, a dashed line denotes the direct tensile law, which has been derived through inverse analysis, considering the constitutive laws provided in Model Code 2010 [49]. The results show a higher resistance for the highest content of fibres, with a tensile strength $f_{ct0.5}$=5.39 MPa and $f_{ct2.5}$=5.15 MPa for 80 kg/m^3 while $f_{ct0.5}$=3.45 MPa and $f_{ct2.5}$=3.84 MPa for 40 kg/m^3. For both contents of fibres, the average tensile strength of the concrete (first cracking) was f_{ct}=4.62 MPa.

With respect to the strands, their tensile strength was f_{pu}=1934 MPa, with a conventional yield limit (at 0.2% of residual strain) equal to f_{py}=1744 MPa and a modulus of elasticity equal to E_p=196.6 GPa. The ordinary reinforcement was grade B500 (ductility class B, with f_y = 500 MPa).

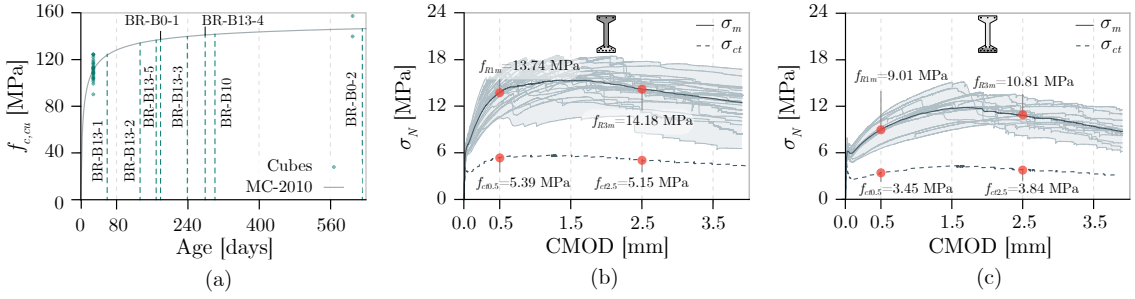

Figure 7.5: Characterization of HPFRC: (a) compressive strength measured in cube; and stress-CMOD curves from the three-point notched tests according to EN14651 (σ_m represents the average curve) and direct tensile law (σ_{ct}) for the HPFRC containing: (b) 80 kg/m^3; (c) 40 kg/m^3.

After casting, the beams underwent a protective measure by being covered with plastic sheeting. Subsequently, a span of 10 hours elapsed prior to the removal of the formwork. Figure 7.6 (a) shows the final surface of the beam, affirming the accurate execution of the casting process and the effective formwork filling. Notably, the visual inspection attests the continuity achieved throughout the different layers. To accurately ascertain the influence of prestressing, a total of 68 steel pins, depicted in Figure 7.6 (b) were positioned to measure with a handheld extensometer the longitudinal strains by conducting measurements both before and after the prestressing transfer.

(a) (b)

Figure 7.6: Beam B7 after demoulding (a) surface of the beam and (b) the beam prepared for the transfer of the prestressing force.

To avoid nonlinear creep effects, a decision was made to establish the required f_{cm} value at 70 MPa for prestress transfer. As per protocol, six concrete cubes per beam were subjected to testing after 30 hours, successfully meeting the stipulated criterion.

Table 7.1: Characteristics of the HPFRC beams tested.

Beams	σ_{cp} [MPa]	f_{cm} [MPa]	V_{cr} [kN]	V_{sh} [kN]	$V_{u,test}$ [kN]
BR-B0-1	0.00	130	83	-	376
BR-B0-2	0.00	138	113	-	371
BR-B10	10.7	135	316	481	548
BR-B13-1	13.7	118	389	456	621
BR-B13-2	13.7	128	388	-	615
BR-B13-3	13.5	133	384	450	599
BR-B13-4	13.6	134	386	453	486
BR-B13-5	13.7	130	389	554	583

7.2.3 Test set-up and measurements

Figure 7.7 shows the test set-up. The specimens were simply supported spanning 5.30 m with two cantilevers of 0.85 m (to avoid local failures due to prestress transfer). The load was introduced by means of two hydraulic jacks with a maximum capacity of 1000 kN each (at a distance of 300 mm between axes). The supports consisted of rollers allowing for free rotations, supported on load cells to continuously track the reactions. The dimensions of all steel plates at supports and load application are indicated in Figure 7.7.

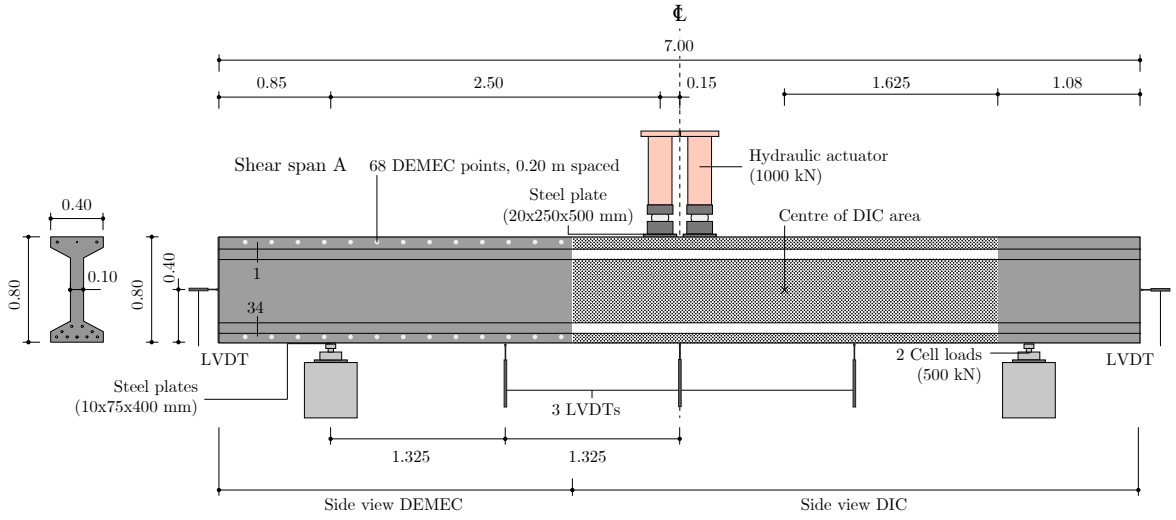

Figure 7.7: Side view of the test set-up: (left side) DEMEC measurements; and (right side) DIC area.

The test set-up allowed for a constant geometrical shear slenderness (ratio between shear span and effective depth, a/d) equal to approximately 3.5. The load was applied by selected load increments. At each load step, visual examination and tracking of the cracks were performed, as well as manual DEMEC measurements in the top and bottom chords. The deflections were continuously monitored through three LVDTs with a maximum range of 200 mm, located at midspan and at quarters of the span (see Figure 7.7, left side). Two additional LVDTs were also arranged horizontally to measure the elongation of the specimen. Furthermore, the reactions at the supports were captured using four load cells, with two load cells at each support. Each of these load cells presents a maximum capacity of 500 kN.

Details of the general set-up of the laboratory are provided in Figure 7.8 (a-c). Furthermore, the applied loads and supports are defined in Figure 7.8 (d-e).

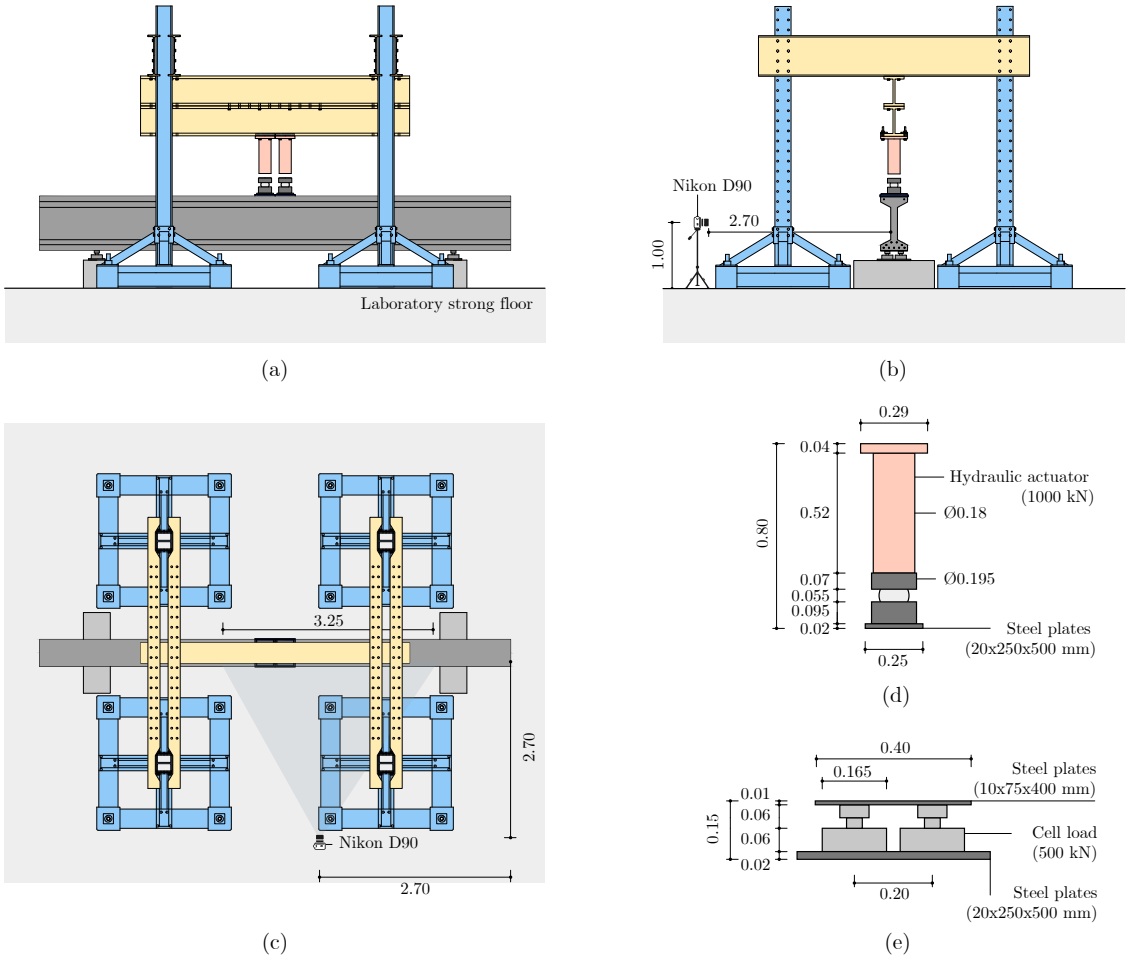

Figure 7.8: Test Setup (a) front view, (b) side view, (c) top view, (d) detailed of the hydraulic actuator, and (e) detailed of the cell loads at the supports.

In addition to the LVDTs and DEMEC measurements, two-dimensional Digital Image Correlation (DIC) was also used to track the crack development and kinematics. To that aim, a random speckle pattern was sprayed in the web and flanges (according to the Speckle Kit from Correlated Solutions). A Nikon D90 camera was used, featuring a CMOS sensor measuring 23.6×15.8 mm^2 and equipped with a resolution of 4288×2848 pixels. This camera was paired with Nikon lens boasting a focal length range from 18 to 200 mm. Positioned at 2.70 metres from the beam web, it captured a measuring width of around 3.25 metres with an image resolution equal to 1.24 pixels per millimetre. Two dot patterns of 2.54 and 5.08 mm were tested under zero displacement tests (ZDT). The latter was preferred due to its reduced noise when measuring displacement on a stationary surface in the ZDT. The final pattern density was achieved through two passes, ensuring the desired density of dots (≈50%). The frequency of photography was manually adjusted between 1/30 to 1 Hz via

the DigiCamControl software, increasing in frequency as the load of failure approached. To ensure consistent lighting conditions, two spotlights were positioned at a distance of 2.70 metres from the camera on both sides and 1.40 metres from the beam. Furthermore, black cloths were arranged behind the specimen to create a shield against external light, preventing direct illumination on the specimen. For post-processing of DIC, the software NCORR [174] was used. A size subset of 10 and a subset spacing of 2 were configured for the analysis. Subsequently, the deformations derived from the designated area of interest underwent further assessment using the refined Automated Crack Detection and Measurement (ACDM) [175, 176].

7.2.4 Level of prestressing at the time of testing

Due to the uncertainties in the conditions of the ducts around the strands and the potential transfer of prestress, the level of prestressing was analysed in detail on the basis of the DEMEC measurements on the top and bottom flanges (refer to Figure 7.7) and the material properties. To that aim, DEMEC readings were performed before and after the transfer of the prestress in the beam.

Figure 7.9 shows the average measured strains recorded in the chords with the DEMEC measurements for the various prestressed specimens (lines with dots at the left hand-side of the plots). In the same figure, the theoretical strains expected are also depicted (solid lines at the right hand-side of the plot). In order to avoid uncertainties related to the value of the modulus of elasticity of concrete, the vertical axis of the theoretical strains has been normalized by the theoretical maximum strain of the specimens considering all strands as bonded.

As it can be noted, in case the ducts efficiently disabled the transfer of prestress, the theoretical development of longitudinal strains should have been relatively different for the different specimens (right hand-side of Figure 7.9). This was however not observed, and all beams depicted similar patterns of longitudinal strains with comparable transfer lengths (left hand-side of Figure 7.9).

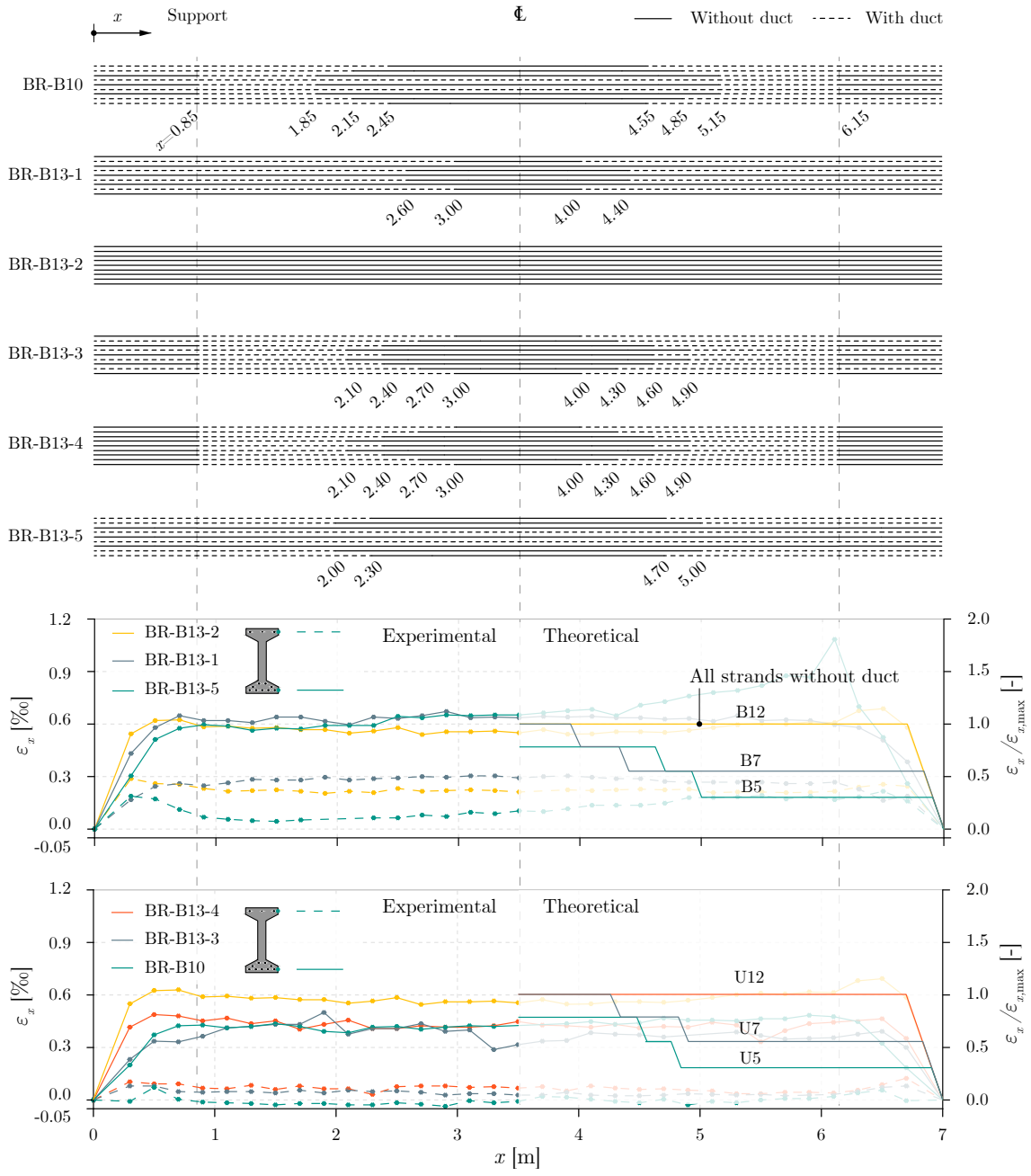

Figure 7.9: Analysis of the longitudinal strains of the specimens after transfer of prestress: (top) location of ducts in the bottom flange; and (bottom) experimental longitudinal strains compared to theoretical values in case of full debonding in presence of ducts.

In order to get a direct confirmation of this phenomenon (ducts were not disabling bond of the strands), the strands of beam BR-B13-5 were investigated after testing, extracting four samples drilled at different locations. The inspection of the strands, as shown Figure 7.10,

showed clear deficiencies in the covering by the ducts, revealing infiltration of mortar and even small aggregates inside the ducts (in fact entirely filling the space between the strand and the duct).

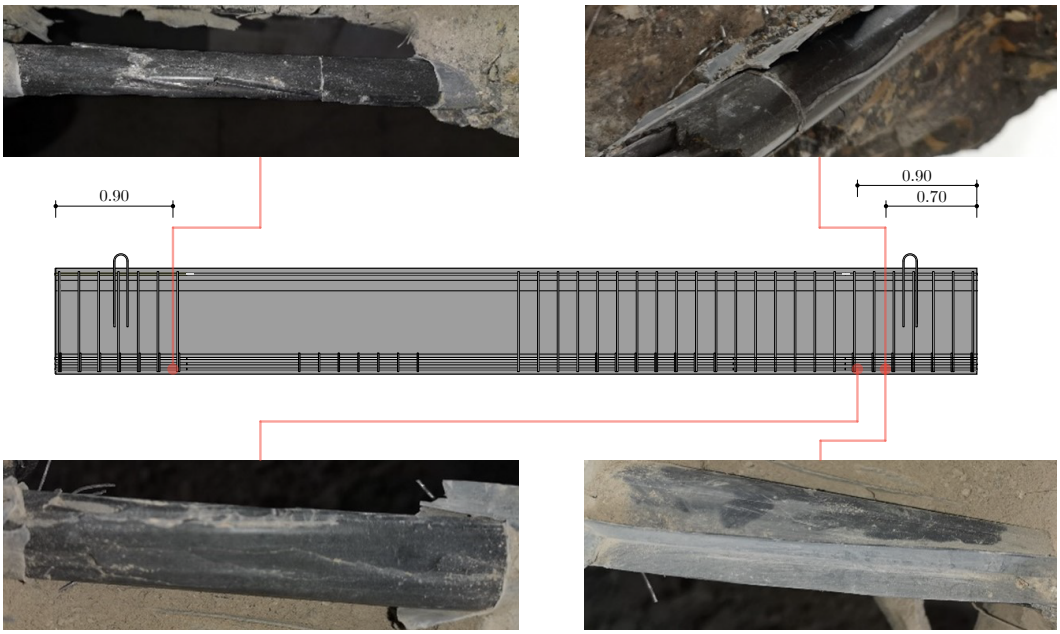

Figure 7.10: Location of the drills at the bottom surface of the bottom flange of beam BR-B13-5 and images of the strands.

The measurement of the strains was eventually not used to estimate the level of prestressing to avoid potential deviations in the modulus of elasticity of the concrete. The prestressing level was thus determined based on the flexural cracking load of the beams. This was performed assuming plane sections to remain plane in bending, the detection of cracks based on the DIC measurements and the value of the tensile strength of the concrete (development of first tension crack, accounting for the tensile strength reported in Table 7.1 and considering the effect of restrained shrinkage evaluated as 0.17 MPa). The obtained values for the prestressing levels σ_{cp} are reported in Table 7.1, ranging between 10.7 and 13.7 MPa, which and are in fine agreement with the DEMEC measurements. It can also be noted that the calculated value of $\sigma_{cp}\approx$13.7 MPa is consistent with the theoretical prestressing level of the member.

7.2.5 Main results

All tested beams failed in shear. For the prestressed specimens, quasi-vertical flexural cracking was first observed, followed by development of inclined shear cracks in the webs.

Eventually, one of the shear cracks localized the strains and governed failure. For one of the prestressed beams, specimen BR-B13-4, failure was originated by a new shear crack appearing at the moment of failure. For the non-prestressed specimens, flexural cracks developed first and progressed later as inclined shear cracks, with one crack again localizing the strains and governing failure. Details on the shear forces associated to first flexural cracking (V_{cr}), first shear cracking (V_{sh}) and failure ($V_{u,test}$) are reported in Table 1. When no value of V_{sh} is reported, all cracks developing in the webs were originated from flexural cracks. Details on the crack widths of the critical cracks are also presented for all beams. As it can be noted, fairly large crack widths were recorded at failure in the shear cracks, with values even above 10 mm.

Figure 7.11 (a) presents the deflection at mid-span measured with LVDT versus the applied shear force at the support. As it can be noted, the beams without prestressing (BR-B0-1 and BR-B0-2) developed flexural cracking at lower shear levels than the prestressed specimens, and both presented similar experimental shear strengths (difference equal to 1.6%). For the prestressed members, the cracking load was similar except for specimen BR-B10, where it was lower. This can be explained by a lower level of prestressing in that member, meaning that bond was at least partly disabled for this beam (the estimated average compression level was 10.7 MPa in this case). It is also worth mentioning that despite the higher tension-stiffening of specimen BR-B13-5, first flexural cracks appeared at a similar level of shear force than the other BR-B13 specimens.

The average shear stress at failure (τ_u=$V_u/(b_w \cdot z)$ where z≈$0.8h$) of the different members is depicted in Figure 7.11 b as a function of the average prestressing level (σ_{cp}=P/A, where P refers to the prestressing force including strands both in the top and bottom flanges and A to the gross cross-sectional area). One test is identified in this plot as an outlier, named BR-B13-4. Although this specimen was nominally comparable to the other three of the series BR-B13, it presented a sudden and unstable propagation of a shear crack which led to the instant failure of the specimen at a lower level of load. For the remaining beams, the shear resistance increased consistently with the level of prestressing in a rather linear manner (as confirmed by a correlation coefficient R^2=0.99).

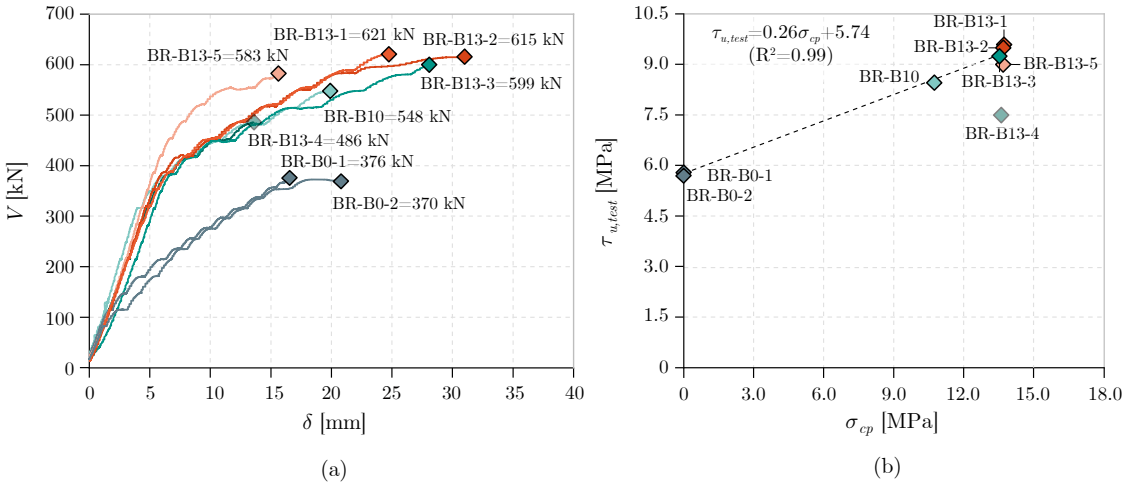

Figure 7.11: Experimental results: (a) deflection at mid-span versus shear at the support; and (b) shear resistance versus average compression stress in the concrete.

7.2.6 Cracking patterns

The cracking patterns obtained through DIC analysis are depicted in Figure 7.12, where cracks with significant strain localization are highlighted in red. In contrast to prestressed beams, the non-prestressed specimens (BR-B0-1 and BR-B0-2) exhibited smaller crack spacing in the bottom flange. This allowed smearing strains and several cracks increased their opening until failure. Both non-prestressed specimens developed curved shear cracks with flatter angles close to the top flange.

Concerning the prestressed members, the shear cracks have a rather linear shape. The crack spacing was also neatly higher than for the non-prestressed specimens, although it allowed to smear the strains in general in two or more cracks (except for specimen BR-B13-1). This indicates potential differences on the kinematics at failure as well as on the transfer of shear forces, as it will be discussed later.

Regarding the onset of initial shear cracking, the following observations can be made:

- For the prestressed beams (BR-B10, BR-B13-1, BR-B13-3, BR-B13-4 and BR-B13-5), shear cracking originates in the web. Typically, these cracks have an approximate inclination of 30º.
- The critical shear crack of beam BR-B13-2 developed closer to the loading plate. In

fact, its tip is located under the loading plate and allowed for the development of a direct strut action, contrary to the other specimens (where the tip of the critical shear crack was located in the shear span). This specimen experienced, accordingly, a higher shear resistance.

- Beam BR-B13-4 showed a controlled propagation of the shear cracks in the web until reaching a shear force of 486 kN. At that load level, suddenly, another shear crack developed closer to the support with an inclination of 24º, progressing in an unstable manner and leading to failure.
- Beam BR-B13-5 exhibited the largest crack spacing in the bottom flange. The cracked portion of the bottom flange was also smaller than for the rest of the specimens. At a shear force of 553 kN, three shear cracks appeared in the web, with the one closest to the loading plate eventually becoming the critical one.

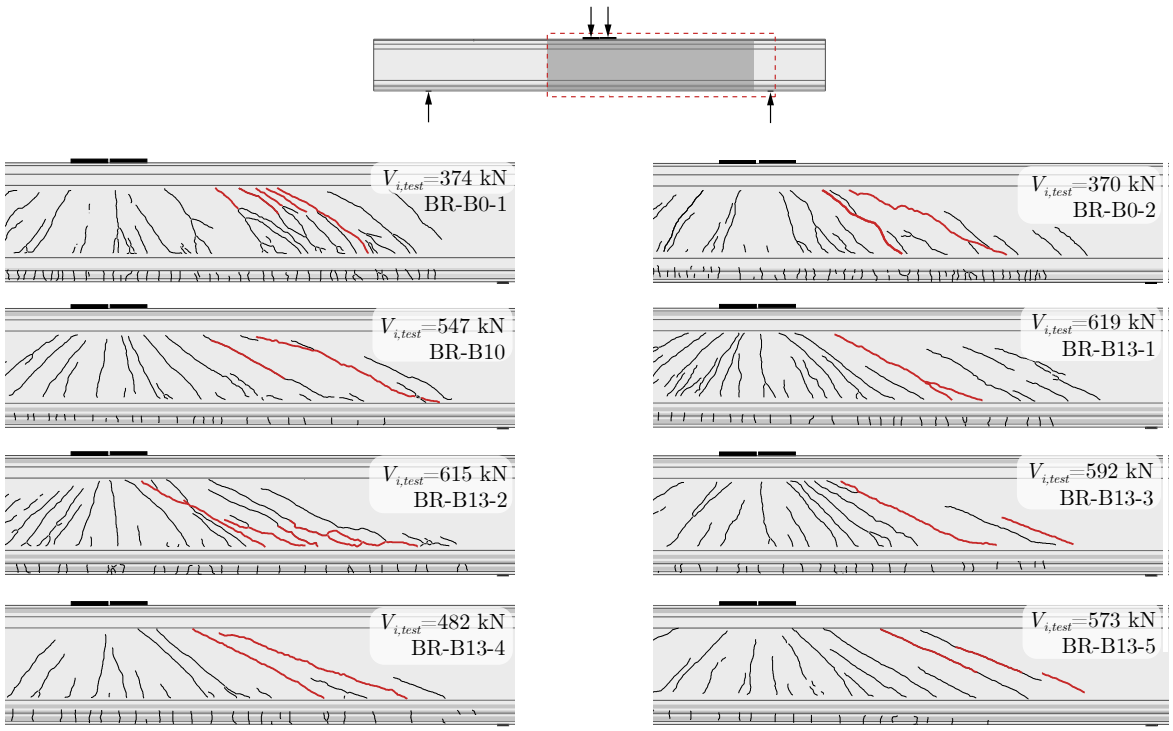

Figure 7.12: Observed cracking patterns for the tests (length represented=3.60 m; cracks with significant localization in red).

7.3 Analysis of shear-transfer actions

7.3.1 Introduction

This section describes the fundamentals and expressions used to assess the contributions of the different shear-transfer actions based on the measured crack kinematics and constitutive laws for the materials. As shown in Figure 7.13 for a general case, the shear resistance (V) is assumed to be composed by the action of the inclined component of the compression chord (V_{cc}), aggregate interlock (V_{agg}), the contribution of fibres in tension crossing the crack (V_{cF}) and the dowel effect (V_{dow}). These components ensure the equilibrium of vertical forces and shall also serve to ensure the equilibrium of moments considering also their components in the longitudinal direction, the external actions and the forces in the chords including prestressing. Concerning the latter, it shall be noted that, in the present case, prestressing acts both on the bottom and top flanges (F_{p0}, $F_{p0,t}$ respectively) as well the increase of force in the tension flange due to flexural deformation (ΔF_p). In the following, the different contributions will be examined in detail.

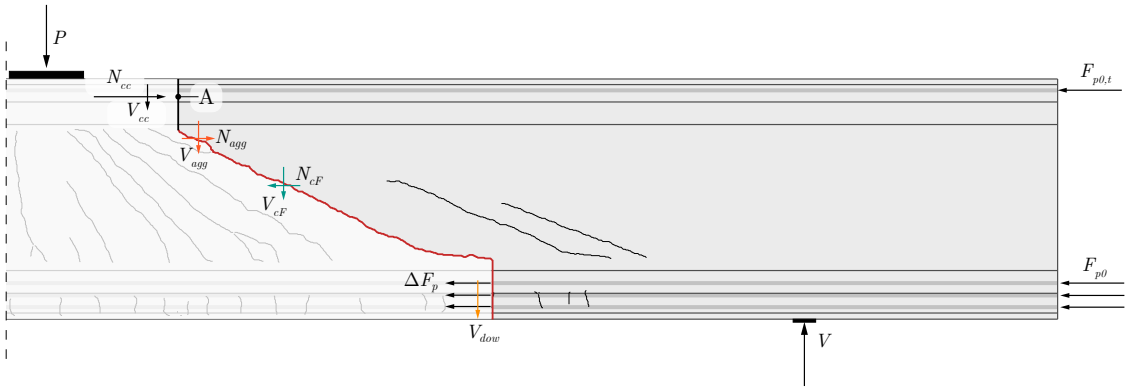

Figure 7.13: Internal forces along the investigated free-body.

7.3.2 Aggregate interlock

The capacity of cracked concrete to transfer shear by aggregate interlock has been investigated in detail in the past [152, 156, 160, 177]. Accounting for the range of crack openings recorded during the experimental programme (from approximately 2 mm for the non-prestressed beam to more than 10 mm in some prestressed specimens), the mechanical approach presented by Fernández Ruiz will be used in the following [160]. This model considers the crack as a potential yield line and allows describing both concrete crushing and crack disengagement for

a wide range of crack openings (covering the ranges of the current experimental programme).

The fundamentals of this model are summarized in Figure 7.14 (a). Provided that a plastic band experiences the combined effects of normal stress (σ_n) and shear stress (τ), its response can be characterized by its kinematics (opening angle α, Figure 7.14 (b) which, in turn, allows determining the internal stress state within the plastic band (Figure 7.14 (c). Several cases may be identified concerning both unconfined (regimes A and B in Figure 7.14 (d,e) or confined conditions (regime C in Figure 7.14 (d,e). In the present case, unconfined conditions were governing (consistent with the large crack openings observed).

According to Fernández Ruiz [160], a reduced plastic strength shall be considered to account for the fact that some regions may be in their softening regime while others have still not attained their maximum resistance. For calculation of the plastic compressive strength (f_{cp}) the conventional brittleness factor used for ordinary and high-strength concrete will be considered here (η_{f_c}) as given in Eq. 7.2 [178]:

$$f_{cp} = f_c \cdot \eta_{fc} \cdot \eta_w \tag{7.1}$$

$$\eta_{cp} = \left(\frac{f_{c0}}{f_c}\right)^{1/3} \leq 1 \tag{7.2}$$

Additionally, the efficiency factor associated to crack opening (η_w, refer also to Figure 7.14 (e) is also applied [160], as given in Eq. 7.3. The latter factor is affected by the crack opening (w) and by the surface roughness parameter (r), refer to Eq. 7.4.

$$\eta_w = \frac{1}{1 + 100\frac{w}{r}} \tag{7.3}$$

$$r = d_{g0} + D_{Max} \cdot min((60/f_c)^2, 1) \tag{7.4}$$

Concerning the dilatancy angle (ϕ accounting for the actual loading path [160]), it is estimated consistently with the recommendations of [160] as:

$$\phi \approx 10 \cdot \left(1.1 + 20\sqrt{\frac{w_0}{r}}\right) \tag{7.5}$$

On that basis, the resulting stresses transferred by aggregate interlock are evaluated by the expressions given in Eqs. 7.6 and 7.7 for the unconfined regime (blue lines in Figure 7.14 (e).

$$-\sigma_n = \frac{1}{2} f_{cp} \left(1 - sin(\alpha + \phi)\right) \tag{7.6}$$

$$\tau = \frac{1}{2} f_{cp} cos(\alpha + \phi) \tag{7.7}$$

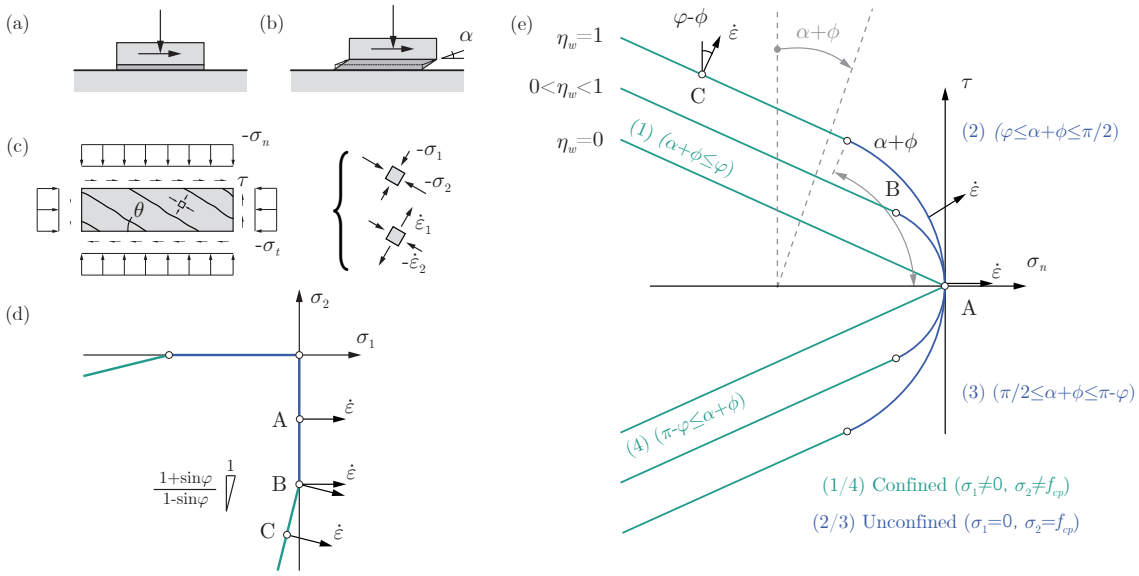

Figure 7.14: Analysis of transfer of forces through cracked concrete: (a) case investigated; (b) kinematics, (c) stress and strain state; (d) yield conditions; and (e) yield surface considering dilatancy angle and efficiency factor (adapted from [160]).

7.3.3 Dowel action

The dowel effect is activated by shearing of the reinforcement (due to displacement perpendicular to the reinforcement axis). This contribution is typically of moderate or low significance in elements without stirrups [161–163, 166]. However, in elements with shear reinforcement, the stirrups can efficiently resist the dowelling forces and significantly increase the contribution of this action [148, 172]. In the present experimental programme, although no stirrups are arranged within the section, the steel fibres could resist the dowelling forces, and this action was thus analysed in detail.

To that aim, the contribution of the dowel effect (V_{dow}) is determined using the displacements measured at the concrete surface with DIC, following the methodology described and applied in Cavagnis [171] and Monserrat et al. [170]. As shown in Figure 7.15 for a given case (beam BR-B13-1), the shape of the longitudinal reinforcement (reinforcement rebars or strands) is approximated using a polynomial of third order (considering the outer points located at a distance x_{dow}=2ϕ). For the longitudinal rebars at the height of the inclined plane (not monitored by DIC) an interpolation between the two analysed lines was performed. The curvature of the section is thus calculated by taking the second derivative of the deflection with respect to the x-coordinate [170, 171] allowing to estimate the bending moments and, on that basis, the associated shear force (V_{dow}, derivative of the bending moment).

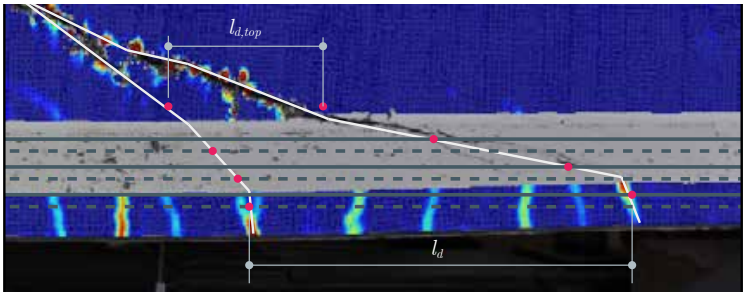

Figure 7.15: Application of the dowel effect for beam BR-B13-1.

7.3.4 Contribution of fibres

The steel fibres in tension contribute to the shear resistance in a similar manner as conventional stirrups, but with a peculiar activation as a function of the crack kinematics. To determine the total contribution of the fibres, it is necessary to define their stress-crack opening law as a function of the crack kinematics and orientation factor. In this paper, the model used is the one suggested by Kaufmann et al. [168] (based on Pfyl [167]) as depicted in Figures 7.16 (a,b). According to this model, the fibres are assumed to have no bending stiffness and, thus, the forces associated to the fibres develop parallel to them. The fibres are also assumed to be pulled at the side of shorter length (l_{fb}), while remaining completely anchored in the other. During the activation phase (Figure 7.16 (c), the bond stresses increase, until reaching a maximum value when the fibre is pulled-out. The softening response involves the pull-out of the fibre, where the anchored force decreases with crack opening as the embedded length is reduced (see Figure 7.16 (a)). It shall be noted that the bond stress is assumed to remain constant during this stage (see Figure 7.16 (d)), and that the stress will reach zero when the displacement equals the initial embedded length.

The behaviour of cracked HPFRC, specifically concerning orthogonally opening cracks in concrete reinforced with uniformly distributed and randomly oriented fibres, is determined by integrating the behaviour of all individual fibres that cross the crack. The resulting (integrated) FRC constitutive law is shown in Figure 7.16 (b) [167], which is described by the activation phase of the FRC (Eq. 7.8), the maximum stress (Eq. 7.9), and the pull-out phase of the fibres (Eq. 7.10):

$$\sigma_{cf} = \sigma_{cf0}\left(2\sqrt{\frac{w}{w_{cp}}} - \frac{w}{w_{cp}}\right) \tag{7.8}$$

$$\sigma_{cf0} = K_f \rho_f \frac{\tau_{bf}}{d_f} l_f \tag{7.9}$$

$$\sigma_{cf} = \sigma_{cf0}\left(1 - \frac{2w}{l_f}\right)^2 \tag{7.10}$$

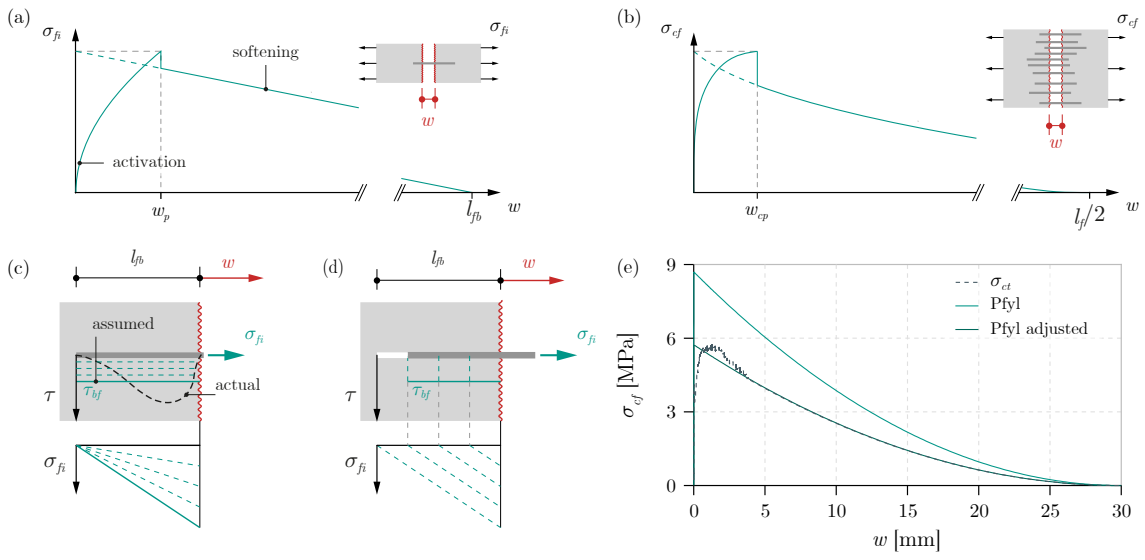

Figure 7.16: Fibre engagement [167, 168]: (a) constitutive law for a single fibre, (b) constitutive law for FRC; (c) fibre activation; (d) fibre pull-out; and (e) FRC activation and pullout phases adapted from tensile law of the HPFRC (80 kg/m^3 of fibres).

As this approach is based on a mechanical model, the value of its physical parameters can be tailored to available specific data on the materials. In the present case, this was used to adjust the bond strength of the fibres (τ_{bf}) to match tensile response of the HPFRC (as presented in

section 2). As shown in Figure 7.16 (e), the default value suggested by Pfyl [167] (τ_{bf}=$2f_{ct}$) overestimates the tensile capacity of the concrete and a reduced bond strength needs to be accounted for (τ_{bf}=$1.34f_{ct}$, for example, for BR-B13-1).

Other effects were also addressed according to Kauffman et al. [168]:

- Considering skew displacements of the crack in the stress components.
- Orientation of fibres, disregarding the contribution of fibres in compression
- Interaction between fibres and aggregate interlock.

With respect to the latter, Kauffman et al. [168] state that deviation forces caused by fibres not perpendicular to the crack develop stresses in the concrete and potentially reduce aggregate interlocking. To address this effect, a simplified reduction coefficient named η_{int} (varying between 0 and 1) was considered:

$$\eta_{int} = 1 + \frac{\frac{\sigma_{fcdn}}{2} - \sqrt{\frac{\sigma_{cfdn}^2}{4} + \tau_{cfdtn}^2}}{f_c} \tag{7.11}$$

This coefficient yields a reduction in the concrete strength due to the stresses originated by fibres which are non-orthogonal to the crack. This effect is in any case limited and was roughly 0.95 for the performed tests.

7.3.5 Contribution of compression chord

The contribution of the compression chord to the shear resistance is governed by both its force and angle (refer to Figure 7.13). For beams in shear without shear reinforcement and without prestressing, this contribution depends to a large extent on the shear slenderness [171], but it is moderate or low in many cases, particularly for slender beams. For the investigated specimens, this contribution may however have a significant relevance. This is largely justified by the fact that the forces of the compression chord are high due to the levels of prestressing, but also due to the location of the critical shear cracks and the height of the top flange.

In general, two cases shall be distinguished with respect to the contribution of the compression chord. The first one (Figure 7.17 (a)) relates to beams where the tip of the shear crack is

located in the shear span, which is a typical case of slender members. In such case, the inclination of the compression chord is relatively flat and governed by the position of the tip of the crack with respect to the loading plate. The second case (Figure 7.17 (b)) relates to members where the location of the critical shear crack does not disturb a potential transfer of the shear force by direct strut action. This is typically the case of squat members but may also occur when high compression forces are present. In particular, in the second case, higher levels of shear force may be transferred by direct strut action (inclined compression strut) [171].

The methodology applied to evaluate the contribution of the first case is based on that developed by Cavagnis et al. [171] and has been used in recent works, such as that of Monserrat et al. [170]. It relies on the stress field presented in Figure 7.17 (c), where the resultant force (F_{cc}) is defined by its horizontal (N_{cc}) and vertical components (V_{cc}). The horizontal component is calculated through the global equilibrium of horizontal forces (see Figure 7.13), while the vertical component is determined from the previous one by considering the inclination of the strut (α_{cc}). Such angle is eventually estimated by assuming a constant stress distribution under the loading plate (with a stress equal to the concrete plastic strength f_{cp}) as well as in the section at the tip of the crack (with a stress constant in the whole compression flange), see Figure 7.17 (c). Consequently, the angle of the compression strut results:

$$tan(\alpha_{cc}) = \frac{c_n - c_m/2}{r_T} = \frac{V_{cc}}{N_{cc}} \tag{7.12}$$

In the case of direct strut (governing in the performed tests for specimen BR-B13-2) the angle α_{cc} is directly obtained through the geometry of the strut (Figure 7.17 (b)), while the component N_{cc} results equal to the prestressing force F_{p0}.

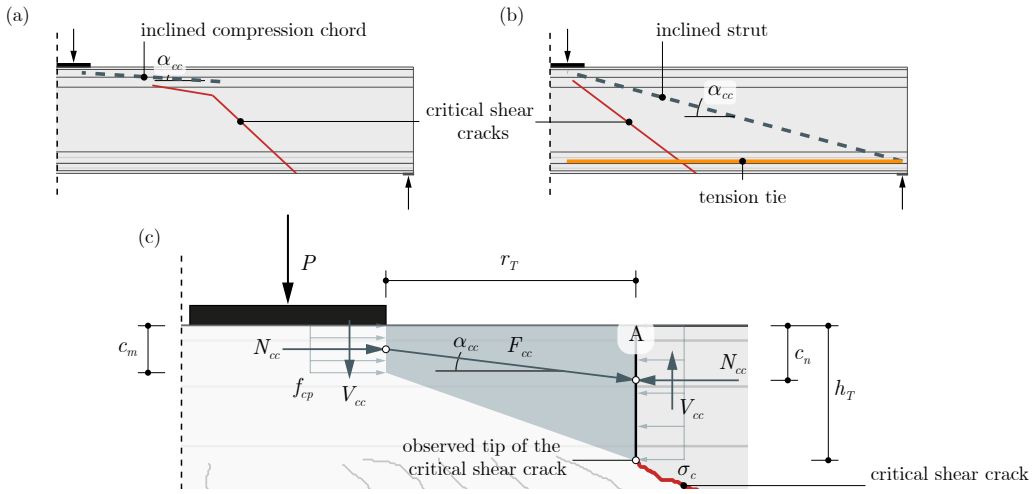

Figure 7.17: Analysis of the compression chord contribution: (a) tip of critical shear crack located in the shear span; (b) tip of critical shear crack located under the loading plate; and (c) calculation of contribution of the compression chord.

7.4 Analysis of the contributions of the shear-transfer actions to the shear strength

Based on the previous considerations, the crack kinematics obtained from the DIC and the physical models presented can be used to calculate the various shear contributions. Such analysis can furthermore be performed at different load levels, allowing for a detailed tracking of their evolution.

The figures present the relative displacement of the crack lips at different load levels according to DIC. For test BR-B13-3 it can be noted relatively large crack openings at failure (close to 10 mm) as well as the fact that the opening was mostly perpendicular to the crack, with low levels of sliding. Such kinematics limited the development of aggregate interlock stresses, but also reduced the contribution of fibres as they enter in their softening phase. Details on the evolution of the shear transfer actions are also shown (bottom right plot), where it can be noted that the contribution of the compression chord was governing at failure, for example, for test BR-B13-3, with low (almost negligible) contributions of aggregate interlock and dowel action. The contributions of fibres were also significant, but decaying gradually as the crack opened progressively (softening response).

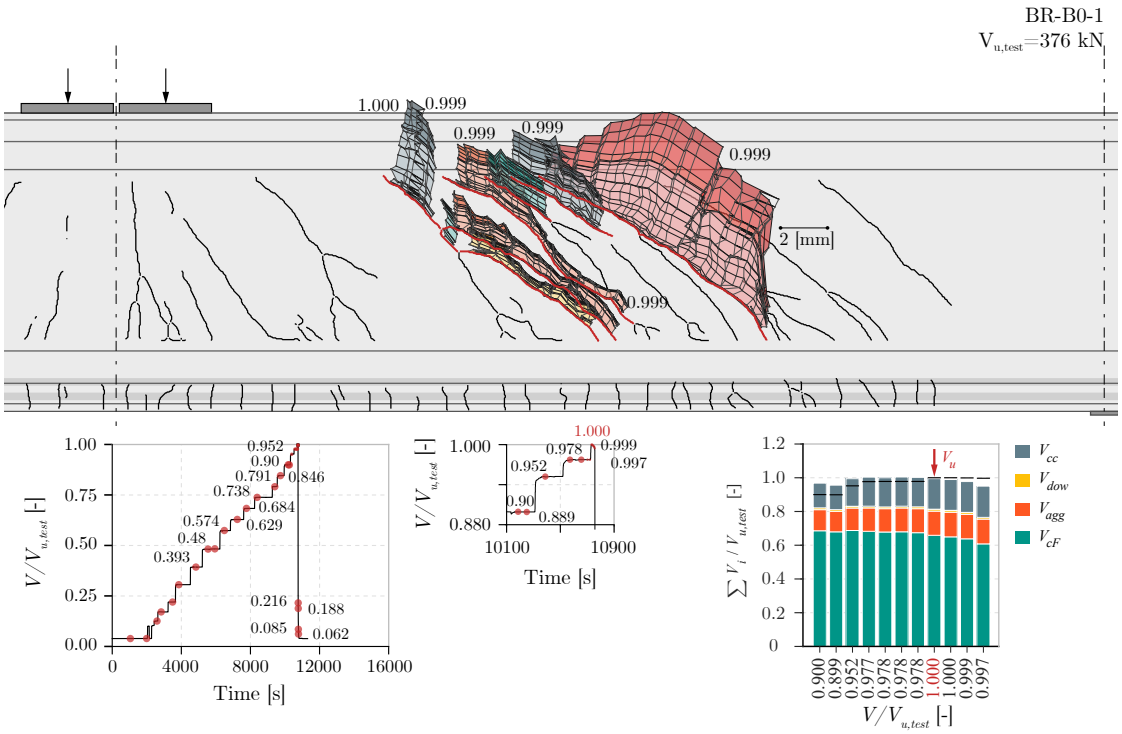

Figure 7.18: Test BR-B0-1: development of the cracking at selected load steps (shear failure at the step 0.997) and the corresponding contribution of the various shear-transfer actions.

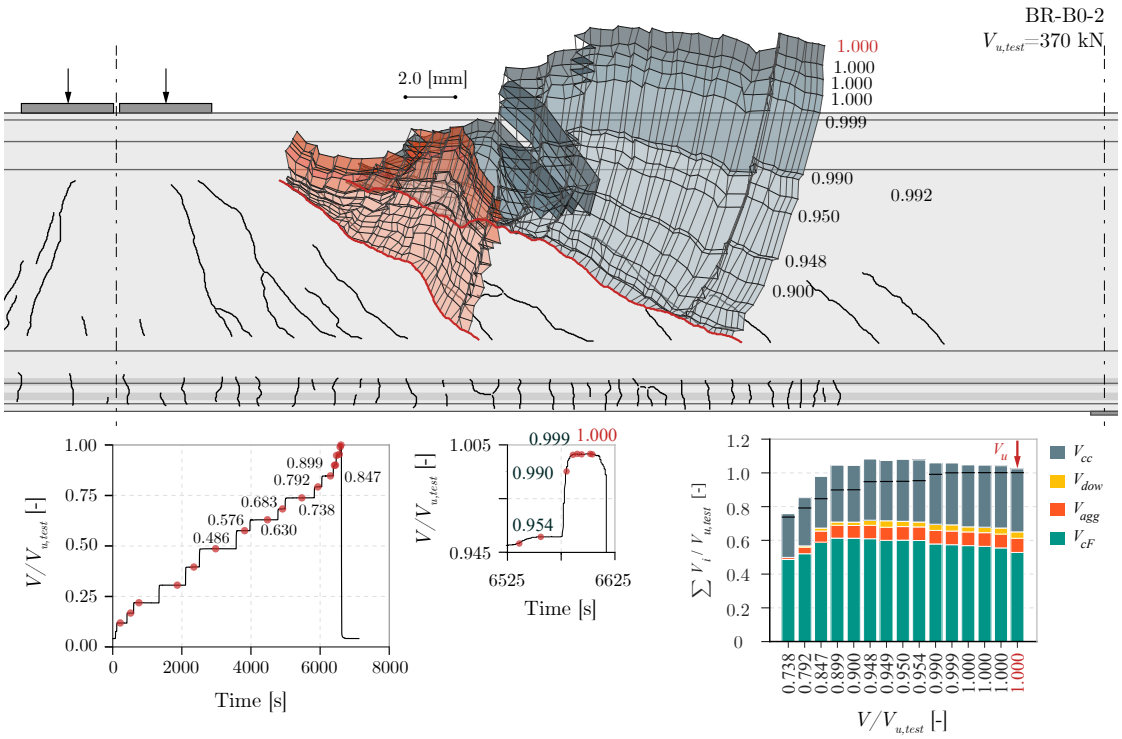

Figure 7.19: Test BR-B0-2: development of the cracking at selected load steps (shear failure at the step 1.000) and the corresponding contribution of the various shear-transfer actions.

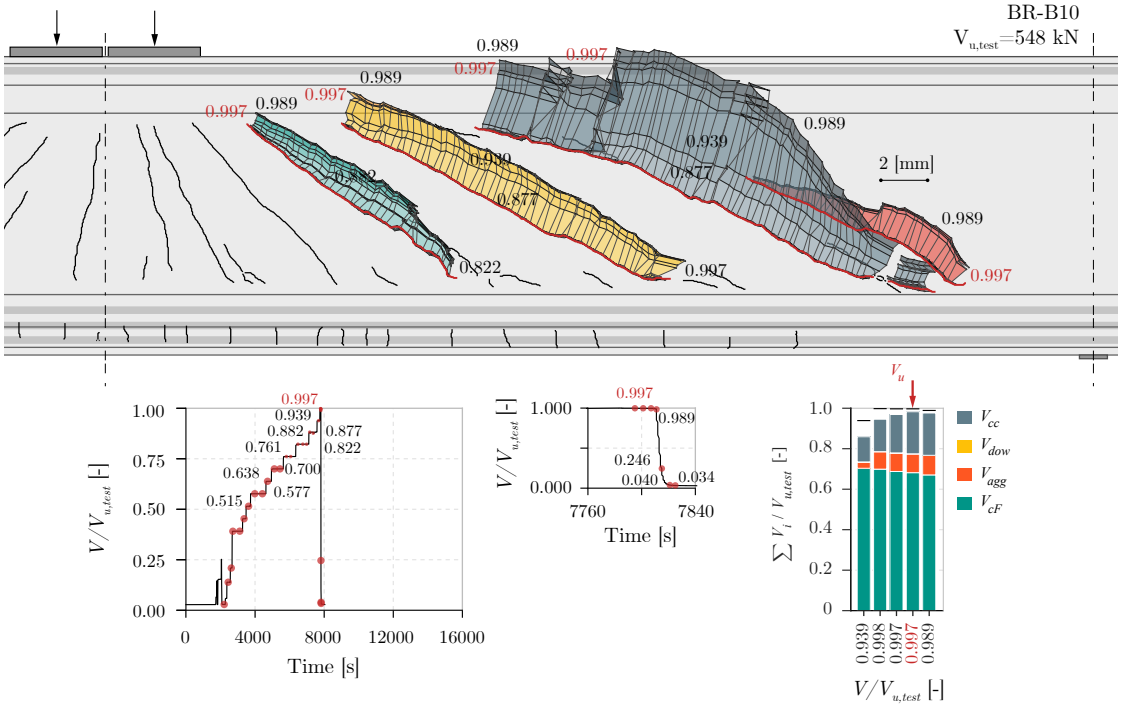

Figure 7.20: Test BR-B10: development of the cracking at selected load steps (shear failure at the step 0.997) and the corresponding contribution of the various shear-transfer actions.

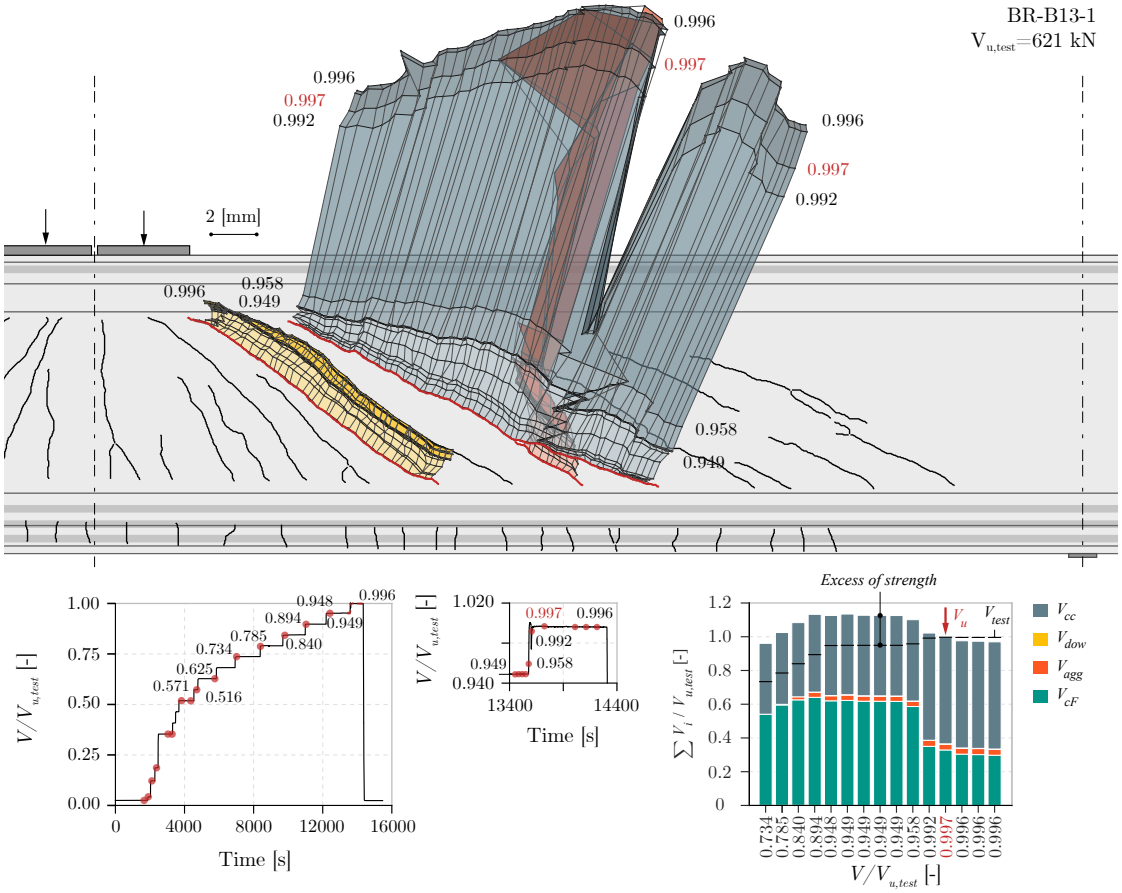

Figure 7.21: Test BR-B13-1: development of the cracking at selected load steps (shear failure at the step 0.997) and the corresponding contribution of the various shear-transfer actions.

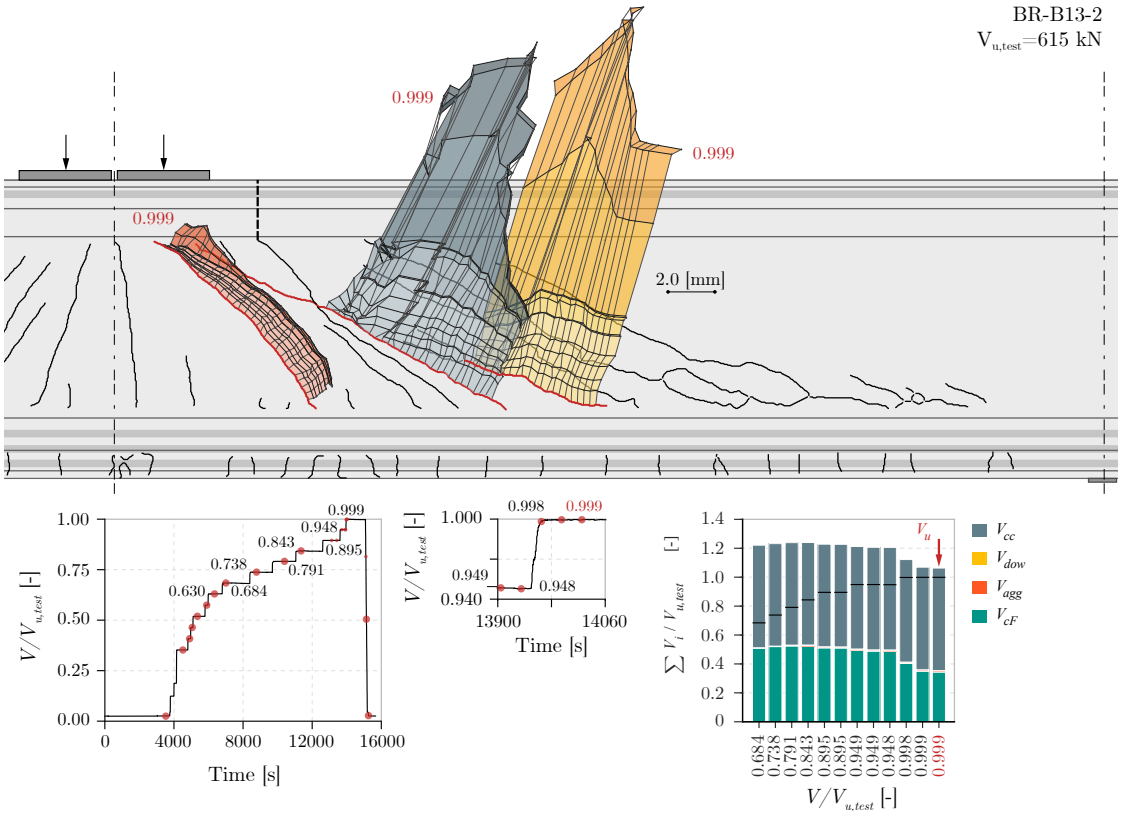

Figure 7.22: Test BR-B13-2: development of the cracking at selected load steps (shear failure at the step 0.999) and the corresponding contribution of the various shear-transfer actions.

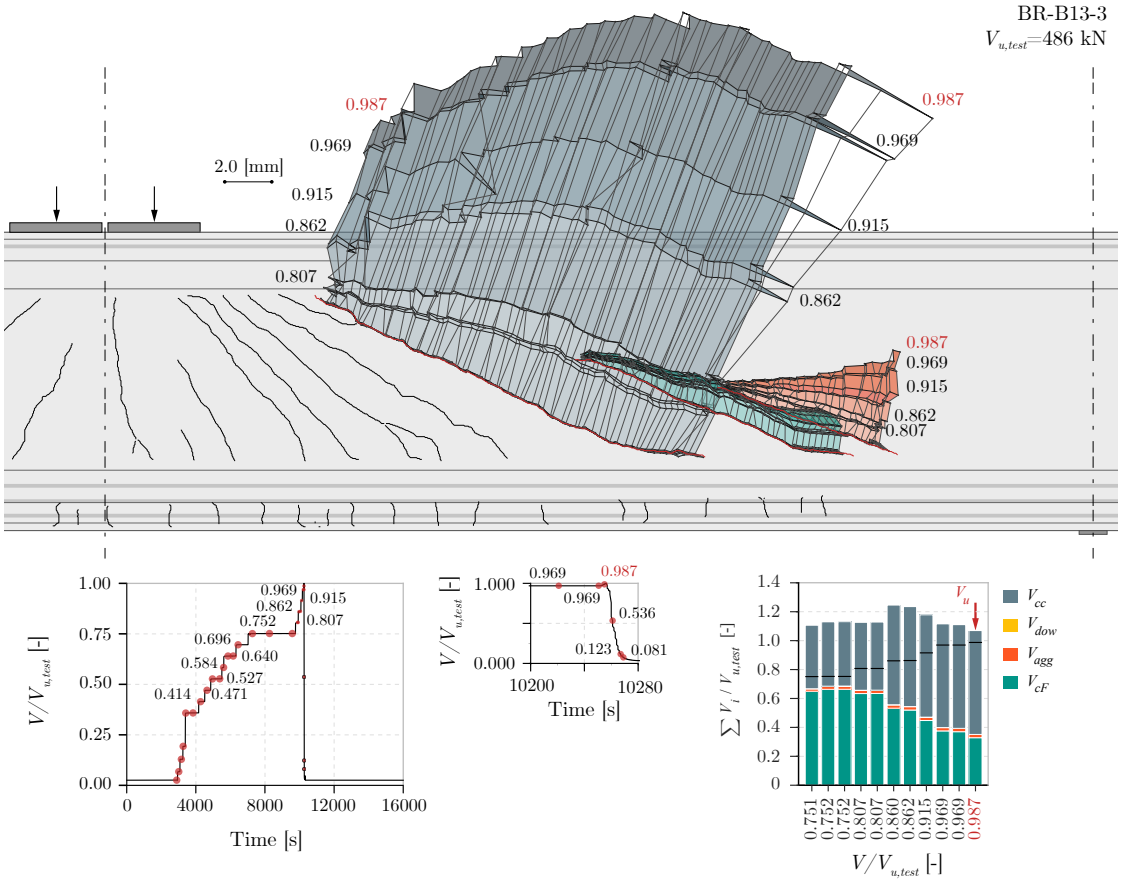

Figure 7.23: Test BR-B13-3: development of the cracking at selected load steps (shear failure at the step 0.987) and the corresponding contribution of the various shear-transfer actions.

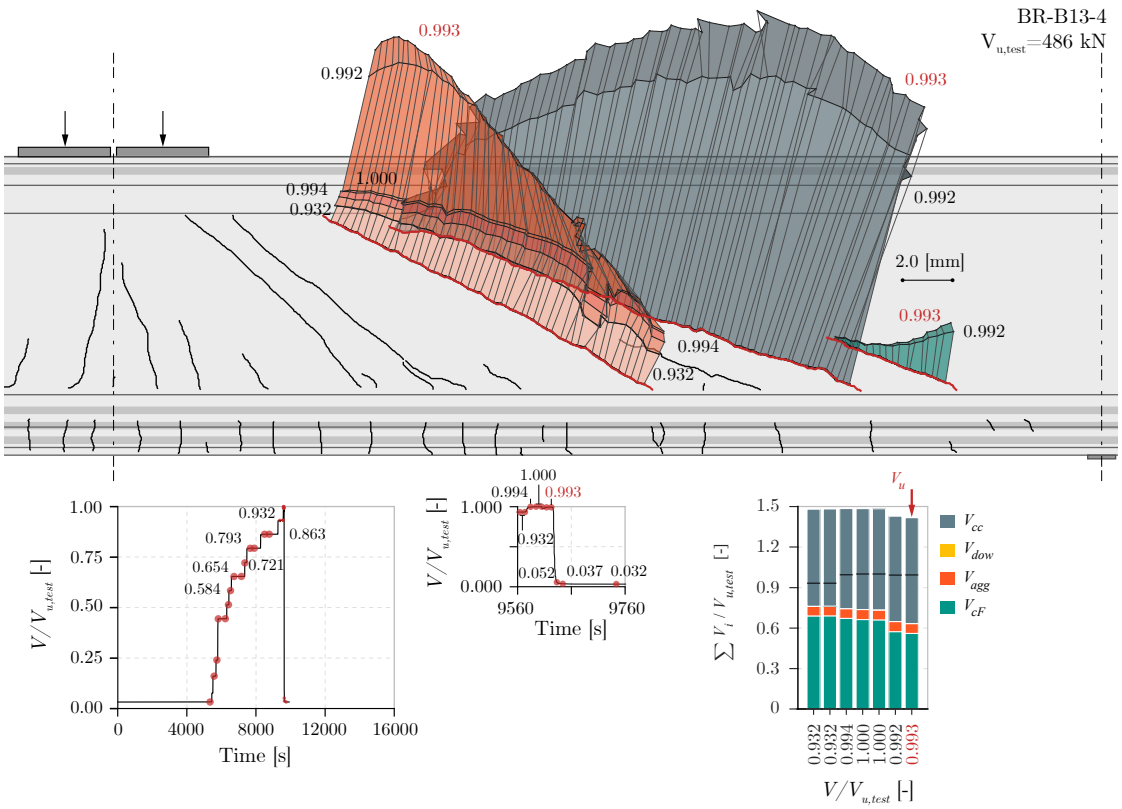

Figure 7.24: Test BR-B13-4: development of the cracking at selected load steps (shear failure at the step 0.993) and the corresponding contribution of the various shear-transfer actions.

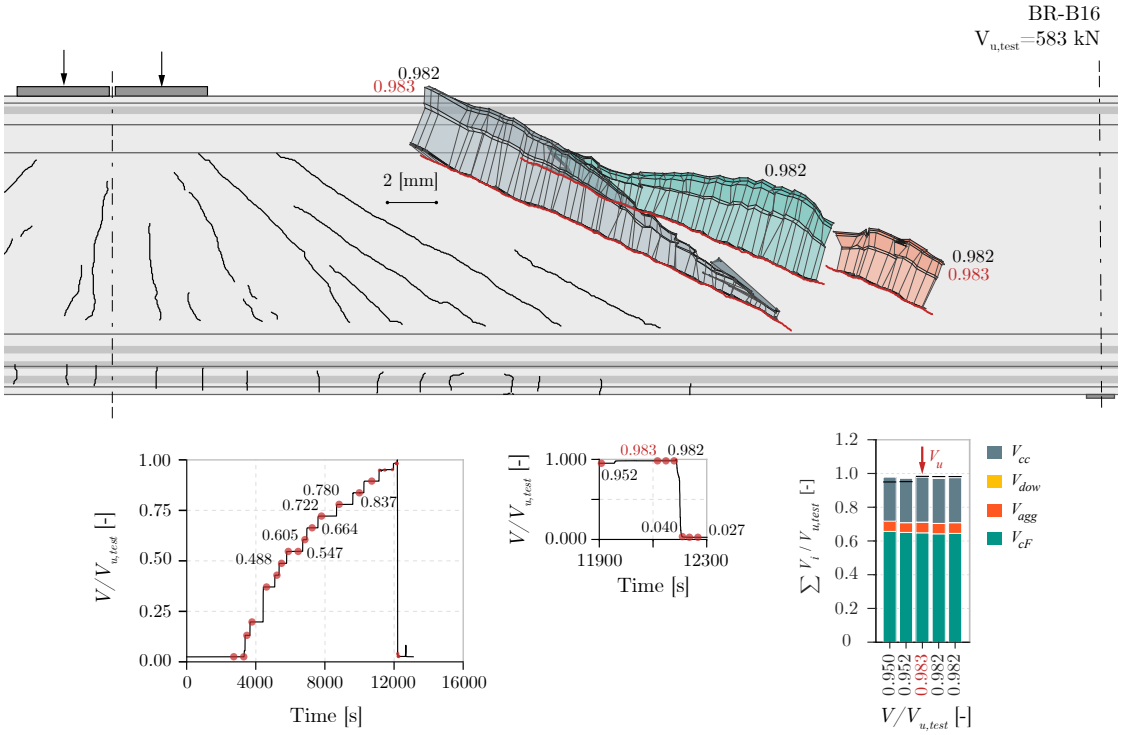

Figure 7.25: Test BR-B16: development of the cracking at selected load steps (shear failure at the step 0.993) and the corresponding contribution of the various shear-transfer actions.

The results for all specimens at failure, in terms of (τ_u=V_u/(b_w·z)), are presented in Table 7.2. The table includes the fraction of each shear-transfer action at failure, as well as the comparison between the experimental shear strength and the calculated shear strength ($\tau_{u,test}/\tau_{u,cal}$. As it can be noted, for the prestressed members, the contribution of the compression chord is governing followed by the contribution of fibres, while aggregate interlock and dowel action can be neglected.

Depending on the cracking pattern, for some specimens such as BR-B10 or BR-B13-5, the governing contribution was the one associated to the fibres. This was associated to a lower contribution of the compression chord and a more significant contribution of aggregate interlock. For these beams, it can be noted that the crack openings were relatively low (2-4 millimetres) when compared to the others (exceeding 10 mm in most cases). For the beam without prestressing BR-B0-1 (with crack opening of approximately 2 mm at failure), the response was comparable to that of prestressed beams with low crack openings. However, the aggregate interlock played a more significant role, which is due to the shape of the cracks (steeper close to the tension chord and flatter close to the compression chord). On the contrary, BR-B0-2 critical shear crack developed closer to the load plate, allowing a higher

contribution of the inclined compression chord, and wider cracks openings.

Table 7.2: Contribution of the various shear-transfer actions to the shear strength.

Beams	τ_{ucF} [MPa] (%)	τ_{uagg} [MPa] (%)	τ_{udow} [MPa] (%)	τ_{ucc} [MPa] (%)	$\tau_{u,cal}$ [MPa]	$\tau_{u,test}$ [MPa]	$\tau_{u,test}/\tau_{u,cal}$ [-]
BR-B0-1	3.82 (66)	0.83 (14)	0.07 (1)	1.05 (18)	5.77	5.80	1.01
BR-B0-2	3.02 (53)	0.48 (8)	0.22 (4)	2.14 (37)	5.85	5.72	0.98
BR-B10	5.78 (68)	0.79 (9)	0.00 (0)	1.76 (21)	8.33	8.46	1.02
BR-B13-1	3.15 (33)	0.34 (4)	0.01 (0)	6.09 (64)	9.59	9.58	1.00
BR-B13-2	3.26 (34)	0.09 (1)	0.00 (0)	6.73 (71)	10.08	9.49	0.94
BR-B13-3	3.04 (33)	0.21 (2)	0.00 (0)	6.64 (72)	9.89	9.24	0.93
BR-B13-4	4.95 (66)	0.56 (7)	0.00 (0)	5.61 (75)	11.12	7.50	0.67
BR-B13-5	5.84 (65)	0.57 (6)	0.00 (0)	2.36 (26)	8.77	9.04	1.03

Note: values in parentheses refer to the ratio of the estimated shear-transfer action with respect to the experimental shear strength $\tau_{u,test}$

The results at failure are also presented in Figure 7.26 as a function of the average level of prestressing (σ_{cp}) using a bar chart to indicate the calculated strength ($\tau_{u,cal}$) and black dots for the experimental one ($\tau_{u,test}$). Beam BR-B13-4 is depicted in light colours as the failure crack developed instantly and the strength calculations were thus performed on the wider crack at that moment, but that was not the shear-critical one. For the others, sound agreement is found for the range of prestressing level investigated and the various cracking patterns and kinematics observed, with a ratio of measured-to-calculated shear resistance equal to 0.99 and a Coefficient of Variation equal to 4%.

In addition, several observations can be made relating the activation of the shear transfer actions with respect to the observed cracking patterns and kinematics:

- Activation of dowelling action requires that the critical shear crack develops through the longitudinal reinforcement and that its kinematics is associated to a transverse slip. In the tested specimens, such component was in all cases low when compared to others (notably contribution of compression chord and fibres). For some prestressed beams, as BR-B13-5, the critical shear crack did not develop through the bottom flange and this contribution was thus negligible.
- While the effect of aggregate interlock is relatively low in most of the specimens due to the kinematics of the cracks (high perpendicular opening with low sliding), its contribution to the shear resistance is not negligible for three specimens (BR-B0-1,

BR-B10, and BR-B13-5). These cases are associated, as previously explained, to lower openings of the critical shear crack at failure.

- The contribution of fibres is one of the most relevant shear transfer actions (33% to 68% of the shear resistance). The results show that this contribution was softening (decreasing contribution for increasing levels of deformation), particularly for beams BR-B13-1 and BR-B13-3 with high crack openings. Additionally, the length and inclination of the crack significantly influence the contribution of fibres to the shear resistance (as can be observed for instance by comparison of beam BR-B0-1 with respect to the prestressed specimens).

- Regarding the contribution of the force in the inclined compression chord, there is a notable difference between the non-prestressed beams (as BR-B0-1) or prestressed beams with low crack openings (BR-B10 and BR-B13-5) and the prestresses specimens with high crack openings (BR-B13-1, BR-B13-2, and BR-B13-3), see Table 4. The latter specimens had a much higher significance of the compression chord. Other than the detrimental effect of crack openings for the fibre and aggregate interlock contributions, the beams with higher crack openings presented a location of the tip of the crack that was neatly closer to the loading plate. This enhanced the possibility of transferring shear through the inclination of the compression chord or even direct strut action (as for specimen BR-B13-2).

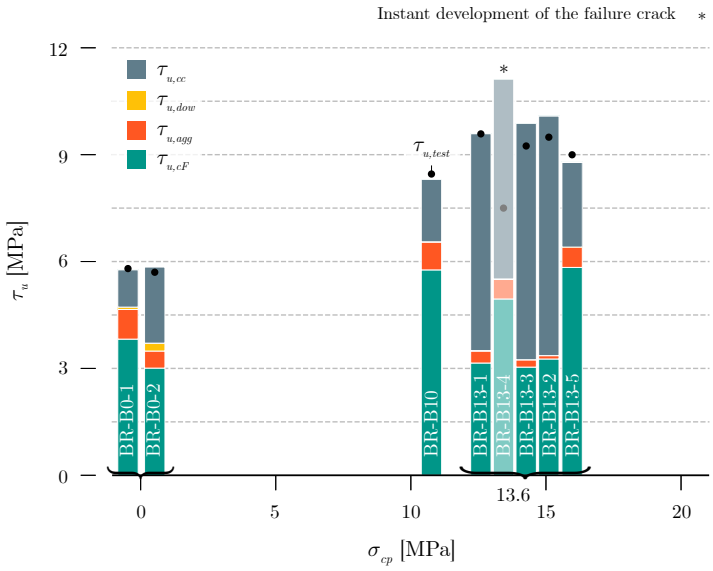

Figure 7.26: Ultimate shear stress, the columns represent the addition of the shear contributions with the model, and the black dots the results from the tests, the horizontal axis shows the compressive stress in the bottom flange.

7.5 Conclusions

This paper investigates on the shear resistance and associated shear transfer actions of High Performance Fibre Reinforced Concrete (HPFRC) beams. To that aim, the results of an experimental programme on eight full-scale beams is presented, with high contents of fibres in the web (80 kg/m^3) and high levels of prestressing. Its main conclusions are summarized below:

- The shear resistance of the tested girders is significantly influenced by the level of prestressing. For the non-prestressed beams, BR-B0-1, and -2, the shear resistance resulted equal to 5.80 and 5.72 MPa, while for the prestressed specimens (with average compressive stresses ranging between 10.7 and 13.7 MPa), it increased to values between 7.50 a 9.58 MPa.
- The addition of fibres allowed smearing cracking in the web. This influence was particularly notable for the non-prestressed members. For the prestressed beams, the shear cracks were more spaced, but still allowing in general to localize strains at failure in more than one crack. The shape of the cracks was also different, being flatter and

rather linear for the prestressed beams, while it was curved for the non-prestressed ones. For one specimen, failure was associated to a sudden propagation of a new shear crack developing in the web.

- Amongst the prestressed beams, five exhibited the formation of shear cracks in the web (not originating from flexural cracks). In contrast, in the non-prestressed beams, a flexural crack initiated and subsequently propagates into a shear crack. This highly influenced the cracking pattern and associated kinematics.

- The critical shear crack of one prestressed beam located its tip under the loading plates. Thus, direct strut action was possible for that member despite the geometrical slenderness of the specimens.

- The shear resistance and contributions of the potential shear-transfer actions can be efficiently assessed on the basis of detailed surface measurements (based on Digital Image Correlation) and using suitable mechanical laws describing the transfer of shear forces.

- The governing shear transfer actions identified from the analyses performed are the contribution of the inclined component of the compression chord as well as the contribution of fibres. The former governs for higher crack openings while the latter governs for lower crack openings (non-prestressed member and some of the prestressed specimens). With this respect, it is identified that the contribution of fibres was in its softening regime accounting for the relatively large crack openings experienced.

- The contribution of aggregate interlock has in general a secondary influence on the shear strength. This is due to the relatively high crack openings (ranging between 2 and 10 mm in general) and also the observed kinematics of the cracks (with relatively low slip).

8

Conclusions

8.1 Conclusions

This thesis conducted a comprehensive study on the feasibility of applying HPFRC and UHPFRC in road bridge girders. This work considers several relevant aspects as: design of material-efficient structural solutions, development of a tailor-made material, testing at material- and structural-scale, comparison with code provisions.

The following conclusions are derived from the design stage of alternatives for road bridges.

- International applications of UHPFRC and HPFRC in girders of road bridges demonstrate the potential use of these materials into the construction sector. In fact, the collaborative efforts between the construction company, proprietary administration, and designers working on the development of tailor-made HPFRC specifically designed for the structure under consideration can result in significant material savings. Despite these potential advantages, the use of these materials in road bridges is still uncommon.
- As a general rule, fibre contribution can be neglected at the calculation of the resistant moment for prestressed girders. This contribution should be accounted for only specific cases. Furthermore, in contrast to common practice, when working with HPFRC I-girders of a single segment the fulfilment of ULS conditions is generally more restrictive than the ones at SLS for the dimensioning of the prestressing. This is because higher values of the tensile strength associated to HPFRC are more effective at SLS than ULS, where its contribution is almost negligible. On the contrary, fibres can account for a relevant part of the ultimate shear strength.

- Concrete and prestressing consumption can be reduced, respectively, by 50% and 30% when adopting an optimized UHPFRC decked I-girder solution for a 40-metre-span compared with a conventional concrete alternative.
- From the design of different U-girder alternatives for road bridges, it was found that the location of the tendons outside the concrete cross-section achieved great concrete savings. In addition, by deviating two tendons at L/6 from the extremes of the girder, the applied shear load was considerably reduced, hence reducing the residual flexural strength requirement for the HPFRC. In addition, by placing the joints between segments far from the section with maximum bending moments, a reduction in the prestressed quantity was found.
- The shear strength of these girders was estimated using different standard provisions. Results showed a relevant degree of variability, motivating a further investigation on the topic.
- When comparing the proposed girders with two conventional box girders, a 48% reduction in concrete consumption and a 66% reduction in passive steel in the beams were observed. A comparison of the material cost of the HPFRC U-girders with the reference girders shows the competitiveness of the proposed solution, with a reduction in cost ranging between 5-20% when compared with the box-girder solutions.
- Furthermore, a comparison with a conventional U-girder of similar features, but with a span of 44.25 m, reveals that the reduction in self-weight, together with the polygonal profile of the tendons of the proposed solution, reduces significantly the prestressed required for this typology.

The following conclusions are derived from mix development, material characterization, and constructability aspects.

- There is a strong difference between UHPFRC and HPFRC mix designs and mechanical properties, which may cause the UHPFRC to be around four times more expensive than HPFRC.
- It is possible to develop a cost-affordable HPFRC (with a cost only 2.5-3.0 times higher than a C70/85) that reaches strength class C100/115 (f_{ck}=100 MPa) using a cement content of 500 kg/m^3 and 50 kg/m^3 silica fume with a maximum aggregate size of 12 mm. Furthermore, the selected fibre content was 80 kg/m^3 of 4D+60 leading to a 13a

class post-cracking strength and a workability class F5 without any sign of segregation or fibre balls.

- Minimum variations from conventional casting techniques will ease the adoption of novel HPFRC by precasters. Specifically, the formwork remains opened at top face of the bottom slab.
- From the casting of two real-scale L-shaped panels it was concluded that a waiting time of 90 minutes between casting successive layers can be considered adequate for real-scale production.
- From the test of the extracted prismatic specimens from the two rectangular-shaped panels it was concluded: (i) no difference was detected between the specimens located horizontally or vertically in the panel, (ii) the potential cold joints characterised by a waiting time of 90 minutes do not cause a strength reduction of the prismatic specimens, attributed to the layers stitching of by means of poker vibration.
- Digital image analysis and inductance measurements were used on the elements extracted from the panels to assess the distribution of fibres. These endorsed that there is no reduction in the number of fibres crossing the notched sections affected by the discontinuity between pours. This proved that the methods of pouring and vibration avoided any cold joint.

The following conclusions are derived from the analysis of the database of shear tests.

- All shear strength obtained through the use of formulations provided by standards yielded clear conservative results.
- In the design expressions of the MC-2010 SMCFT and MC-2020 draft, there are pronounced trends for the model safety factor with respect to ρ_{pw}, and σ_{cp}. Therefore, the conservatism of these shear models can be improved by increasing the effect of these two factors.
- The comparison of the results with other databases with similar beams but without prestress proved a pronounced conservativeness of the shear models when dealing with prestress beams.

The following conclusions are derived from the experimental campaign of shear tests and the analysis of the shear-transfer contributions to shear strength.

- The shear resistance of the tested girders is significantly influenced by the level of prestressing. For the non-prestressed beams, the shear resistance resulted 5.77 MPa, while for the prestressed specimens (with average compressive stresses ranging between 10.7 and 13.7 MPa), it increased to values between 7.50 a 9.58 MPa.

- The addition of fibres allowed smearing cracking in the web. This influence was particularly notable for the non-prestressed members, where low shear crack spacing was observed. For the prestressed beams, the shear cracks were more spaced, but still allowing in general to localize strains at failure in more than one crack. The shape of the cracks was also different, being flatter and rather linear for the prestressed beams, while it was curved for the non-prestressed one. For one specimen, failure was associated to a sudden propagation of a new shear crack developing in the web.

- Amongst the prestressed beams, five exhibited the formation of shear cracks in the web (not originating from flexural cracks). In contrast, in the non-prestressed beams, a flexural crack initiated and subsequently propagates into a shear crack. This highly influenced the cracking pattern and associated kinematics.

- The governing shear transfer actions identified from the analyses based on Digital Image Correlation performed are the contribution of the inclined component of the compression chord as well as the contribution of fibres. The former governs for higher crack openings while the latter governs for lower crack openings (non-prestressed member and some of the prestressed specimens). With this respect, it is identified that the contribution of fibres was in its softening regime accounting for the relatively large crack openings experienced.

- The contribution of aggregate interlock has in general a secondary influence on the shear strength. This is due to the relatively high crack openings (ranging between 2 and 10 mm in general) and also the observed kinematics of the cracks (with relatively low slip).

8.2 Further studies

A forthcoming work to obtain more optimized results should consider the following:

- In order to implement bonded external prestressing in the proposed U-beams, a study should be conducted to analyze the number and typology of blisters required.
- The estimation of the time-dependant effects; to perform individual calculations of the prestressing losses for each case and to obtain more reliable stresses for the SLS. This would require the calibration of creep and shrinkage models for the selected HPFRC material.
- The in-depth study of the discontinuity regions of the girders such as the prestressing anchorages and deviators, considering the effects of the introduction of the prestressing.
- Further bridge typologies such as bridges with continuous prestressing on the supports, or the study of lightened decks made with the developed HPFRC.
- HPFRC is not fully covered by the standards; hence, a better characterisation of its tensile behaviour, rheological and durability properties will allow optimisation of current beam designs.
- The implementation of vibrators placed within the formwork of structural elements could potentially eliminate the need for poker vibrators. Nonetheless, there is a concern that the steel fibres may align parallel to the formwork walls and the top free surface, which could result in the appearance of planes of weakness. A comprehensive study on casting structural elements would be necessary to determine the feasibility of using vibrators within the formwork.
- The use of a high-precision camera, closer and focused on the load application zone, will allow for the application of more sophisticated methods of analysing the inclined compression chord based on the principal strains obtained through DIC.
- Two other beams have been already cast, and ready for testing, featuring unbonded and bonded strands characterized by σ_{cp} values of 5 MPa.
- Two additional experimental campaigns are suggested. The first campaign aims to investigate the behaviour of segmental beams, with a specific focus on analyzing the joint's influence on the shear behaviour of prestressed beams. The second campaign involves casting a conventional concrete top slab onto the precast HPFRC beams to study the effects of a composite section cast in two phases.

- A stress-field-based mechanical model, aligned with established standards, should be developed to capture and represent the observed behaviour of beams with similar characteristics. An adaptation of the formulation presented in the draft of FprEN1992-1-1:2023 for beams reinforced with stirrups is worth considering, with the substitution of stirrup contribution for fibre contribution. This approach facilitates the consideration of concrete strain levels independently of the type of longitudinal reinforcement, making it applicable to the cases examined in this thesis.

A

Technical drawings for the HPFRC U-girder road bridge

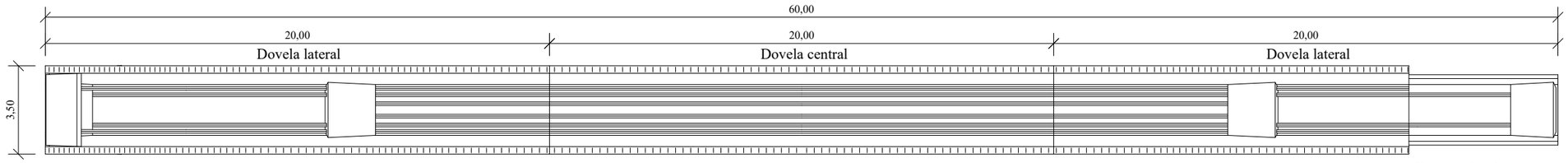

Planta

Corte A-A

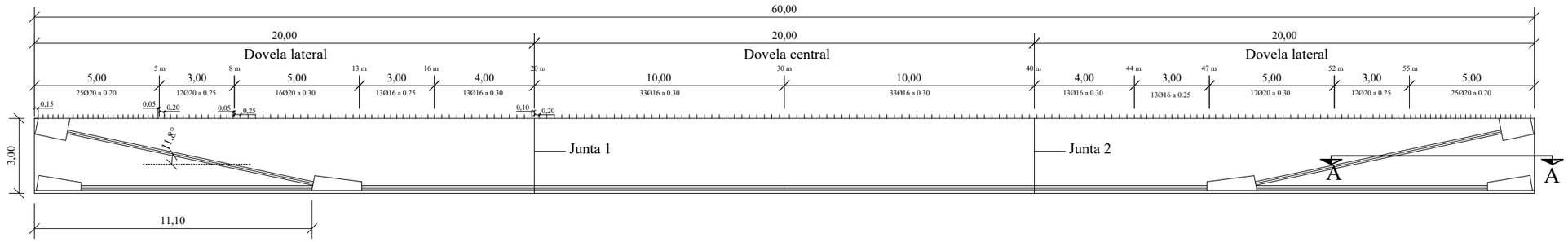

Perfil longitudinal

Escala de detalles 1:200
Todas las cotas están en metros

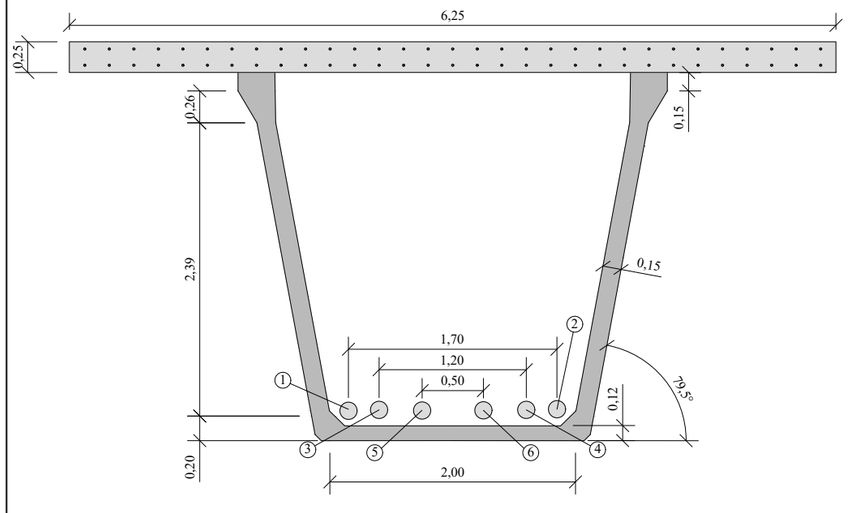

Sección transversal centro de vano

Escala de detalles 1:50
Todas las cotas están en metros

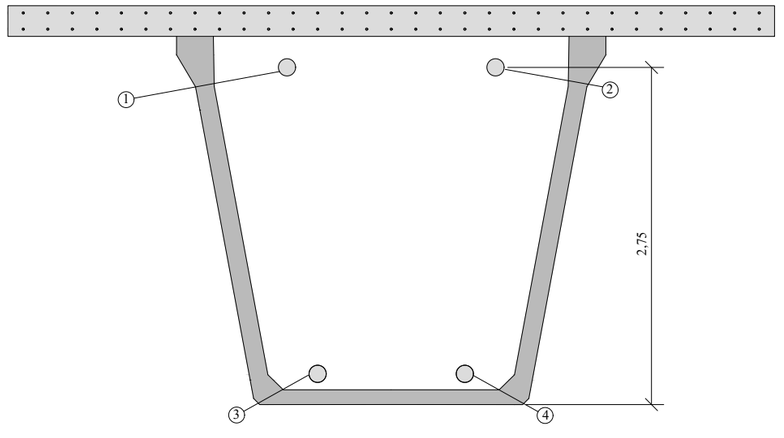

Sección transversal apoyo

Escala de detalles 1:50
Todas las cotas están en metros

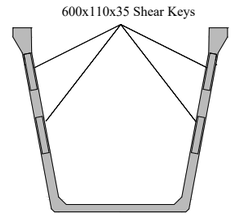

Sección junta entre dovelas

Escala de detalles 1:100
Todas las cotas están en metros

Pretensado						
	Tendón	Tesado 1 [%]	Tesado 2 [%]	Cordones	Diámetro de cordones [mm]	Fuerza de tesado [kN]
Viga artesa	1	100	-	31	150	209
	2	100	-	31	150	209
	3	100	-	22	150	209
	4	100	-	22	150	209
	5	30	70	31	150	209
	6	30	70	31	150	209

Título del Proyecto

ALTERNATIVAS DE VIGAS ARTESA
CON HORMIGÓN DE MUY ALTAS PRESTACIONES REFORZADO CON FIBRAS

Investigadores principales

D. Hugo Corres D. Leonardo Todisco

Autor

D. Rafael Ruiz Maestre

Título del plano

3 DOVELAS 20 m VERSIÓN 2
Perfil longitudinal y secciones transversales

Fecha **10/2020**

Plano nº **1**

Escala A3: **Varias Especificadas en plano**

Hoja 1 de 5

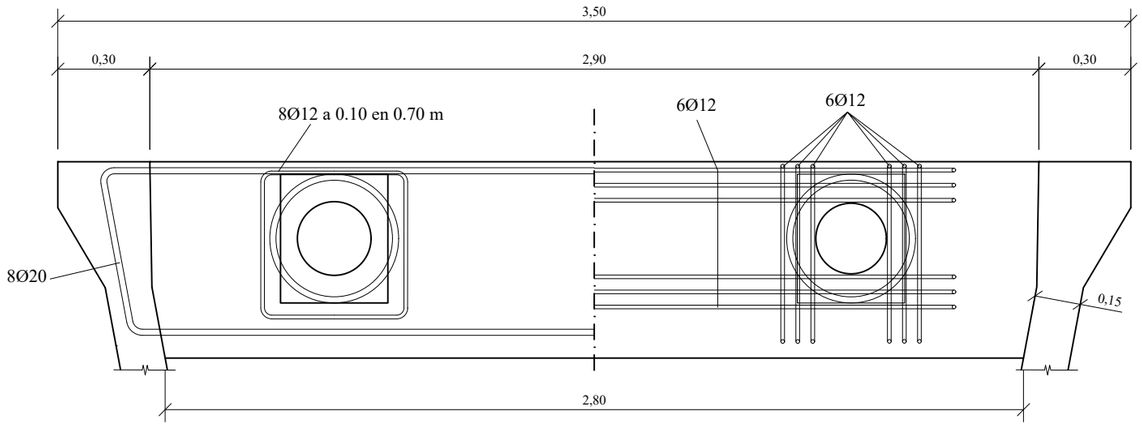

Detalle del anclaje superior de 2T31C sobre el apoyo

Vista A-A

Escala de detalles 1:20
Todas las cotas están en metros

Detalle del armado de piel del anclaje superior de 2T31C sobre el apoyo

Vista A-A

Escala de detalles 1:20
Todas las cotas están en metros

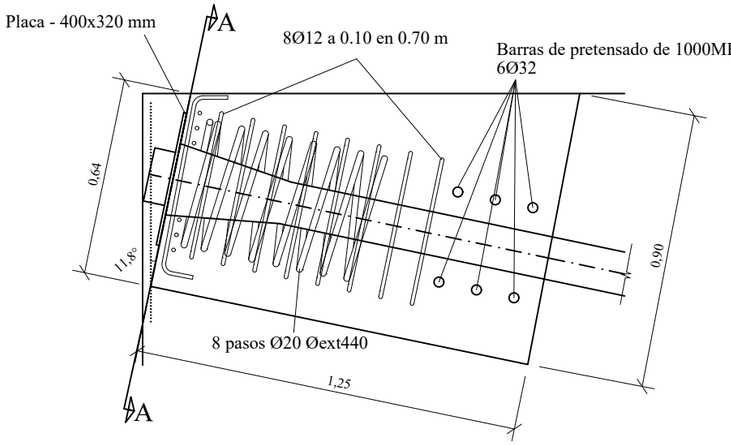

Detalle del anclaje de los 2T31C sobre el apoyo

Escala de detalles 1:20
Todas las cotas están en metros

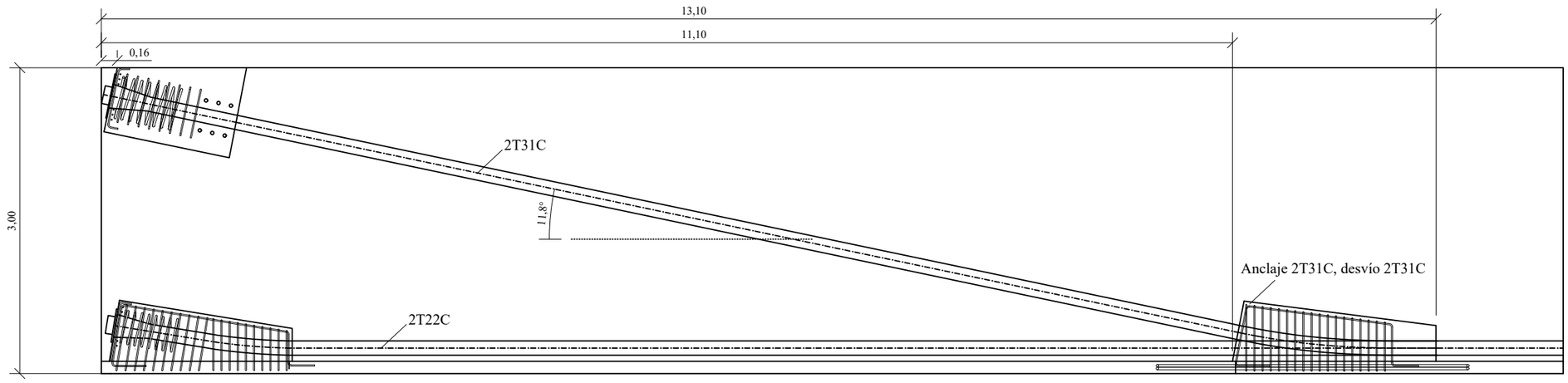

Perfil de los tendones entre el apoyo y la desviación y anclaje

Escala de detalles 1:50
Todas las cotas están en metros

Título del Proyecto **ALTERNATIVAS DE VIGAS ARTESA CON HORMIGÓN DE MUY ALTAS PRESTACIONES REFORZADO CON FIBRAS**	Investigadores principales D. Hugo Corres D. Leonardo Todisco	Autor D. Rafael Ruiz Maestre	Título del plano **3 DOVELAS 20 m VERSIÓN 2 Zona de anclajes y anclaje superior**	Fecha **10/2020** Escala A3: **Varias Especificadas en plano**	Plano nº **2** Hoja 2 de 5

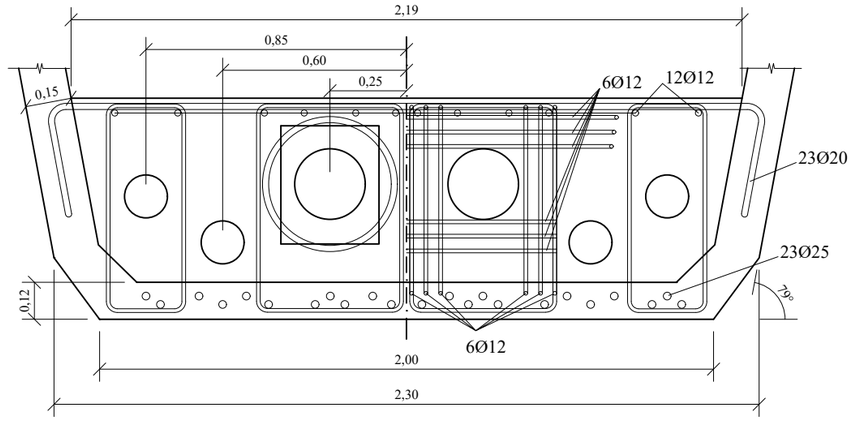

Detalle del anclaje de los 2T31C a 12m del apoyo
Vista A-A
Escala de detalles 1:20
Todas las cotas están en metros

Detalle del armado de piel del anclaje 2T31C a 12m del apoyo
Vista A-A
Escala de detalles 1:20
Todas las cotas están en metros

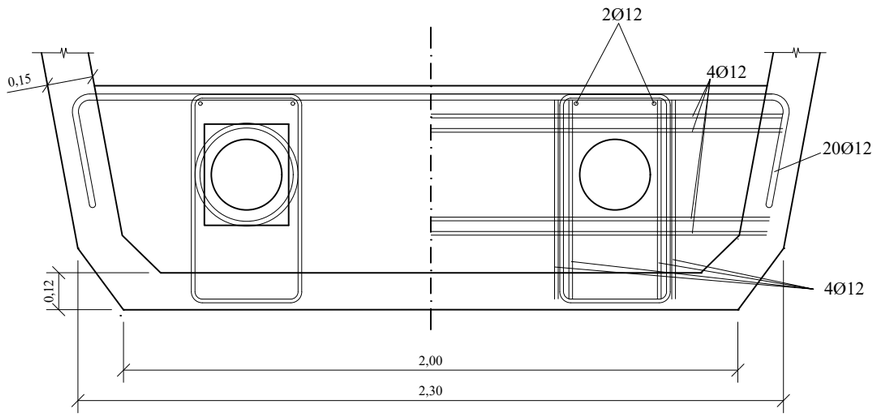

Detalle del anclaje de los 2T22C sobre el apoyo
Vista B-B
Escala de detalles 1:20
Todas las cotas están en metros

Detalle del armado de piel del anclaje 2T22C sobre el apoyo
Vista B-B
Escala de detalles 1:20
Todas las cotas están en metros

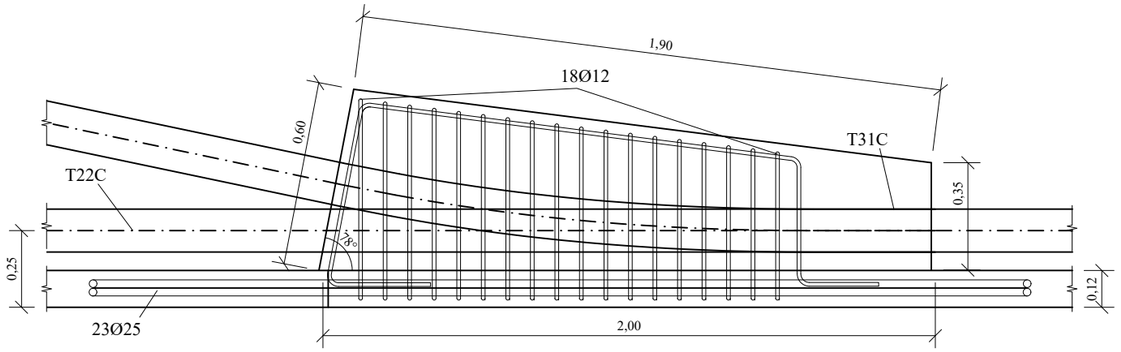

Detalle del desvío de los 2T31C a 12m del apoyo
Escala de detalles 1:20
Todas las cotas están en metros

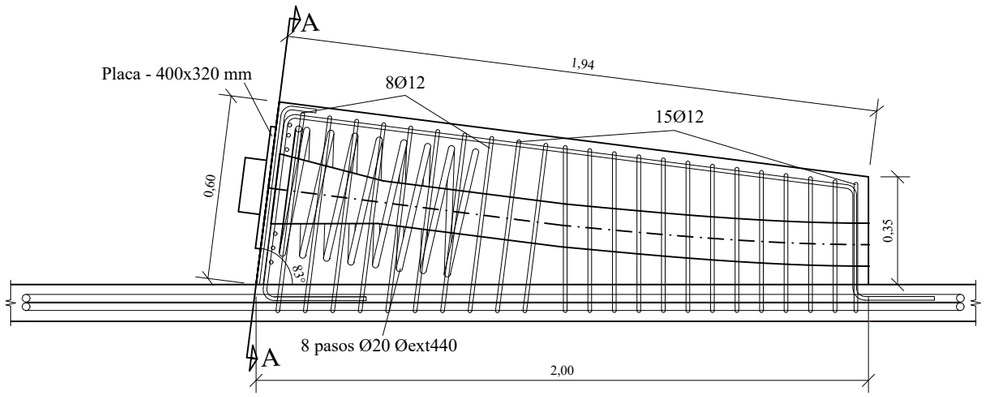

Detalle del anclaje de los 2T31C a 12m del apoyo
Escala de detalles 1:20
Todas las cotas están en metros

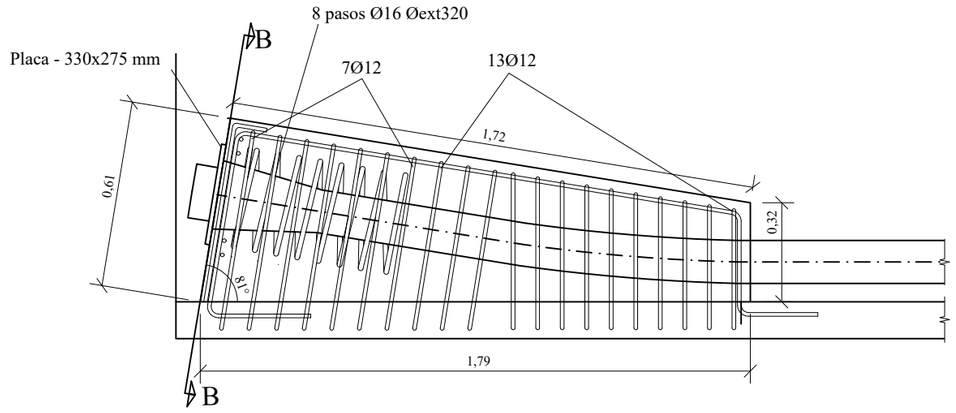

Detalle del anclaje de los 2T22C a 0m del apoyo
Escala de detalles 1:20
Todas las cotas están en metros

Título del Proyecto	Investigadores principales	Autor	Título del plano	Fecha	Plano nº
ALTERNATIVAS DE VIGAS ARTESA CON HORMIGÓN DE MUY ALTAS PRESTACIONES REFORZADO CON FIBRAS	D. Hugo Corres D. Leonardo Todisco	D. Rafael Ruiz Maestre	**3 DOVELAS 20 m VERSIÓN 2 Anclajes y desviadores**	**10/2020**	**3**
				Escala A3: **Varias Especificadas en plano**	Hoja **3 de 5**

Armadura rasante entre la viga y el tablero

SITUACIÓN	DIAMETRO [mm]	DIAGRAMA DE DOBLADO [m]	LONGITUD UNITARIA [m]	NUMERO DE BARRAS	LONGITUD TOTAL [m]	PESO [kg/m]	PESO PARCIAL [kg]
1	20		1.30	212.00	275.60	2.47	680.73
2	16			242.00	314.60	1.58	497.07

Total kg ... 1177.80

Resumen total por diámetros

Ø [mm]	Longitud [m]	Peso [kg]
16	314.60	497.07
20	275.60	680.73

Armadura de un anclaje de 2T22C sobre el apoyo de viga

SITUACIÓN	DIAMETRO [mm]	DIAGRAMA DE DOBLADO [m]	LONGITUD UNITARIA [m]	NUMERO DE BARRAS	LONGITUD TOTAL [m]	PESO [kg/m]	PESO PARCIAL [kg]
3	12	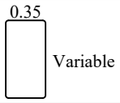	1.90	14	26.60	0.89	23.60
4	12	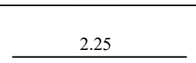	2.25	4	9.00	0.89	8.00
5	16		8.00	2	16.00	1.58	25.26
6	12	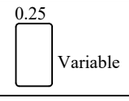	1.47	26	38.22	0.89	34.00
7	12	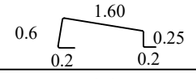	2.85	4	11.40	0.89	10.15
8	12		0.65	8	5.20	0.89	4.60
9	20	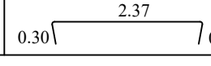	2.97	20	59.40	2.47	146.00

Total kg ... 251.61

Resumen total por diámetros

Ø [mm]	Longitud [m]	Peso [kg]
12	90.42	80.47
16	16	25.28
20	59.40	146.00

Armadura de anclaje de 2T31C y del desvío de 2T31C en x=12 m

SITUACIÓN	DIAMETRO [mm]	DIAGRAMA DE DOBLADO [m]	LONGITUD UNITARIA [m]	NUMERO DE BARRAS	LONGITUD TOTAL [m]	PESO [kg/m]	PESO PARCIAL [kg]
10	12	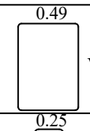	2.20	16	35.20	0.89	31.33
11	12		1.55	30	46.50	0.89	41.39
12	12	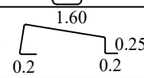	2.85	8	22.80	0.89	20.30
13	20	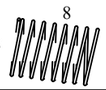	11.04	2	22.08	2.47	54.55
14	20	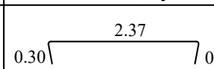	2.97	23	68.31	2.47	168.73
15	12	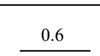	0.60	12	7.20	0.89	6.41
16	12	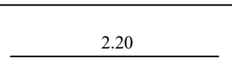	2.20	6	13.20	0.89	11.75
17	25	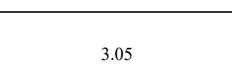	3.05	23	70.15	3.85	270.10
18	12	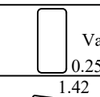	1.56	36	56.16	0.89	49.98
19	12	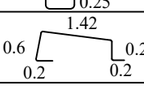	2.67	4	10.67	0.89	9.50

Total kg ... 664.04

Resumen total por diámetros

Ø [mm]	Longitud [m]	Peso [kg]
12	191.73	170.66
20	90.39	223.28
25	70.15	270.10

Título del Proyecto

ALTERNATIVAS DE VIGAS ARTESA
CON HORMIGÓN DE MUY ALTAS PRESTACIONES REFORZADO CON FIBRAS

Investigadores principales

D. Hugo Corres D. Leonardo Todisco

Autor

D. Rafael Ruiz Maestre

Título del plano

3 DOVELAS 20 m VERSIÓN 2
Tablas de despiece 001

Fecha **10/2020**

Plano nº **4**

Escala A3: **Varias Especificadas en plano**

Hoja **4 de 5**

Armadura de un anclaje de 2T31C en la zona superior de la sección sobre el apoyo

SITUACIÓN	DIAMETRO [mm]	DIAGRAMA DE DOBLADO [m]	LONGITUD UNITARIA [m]	NUMERO DE BARRAS	LONGITUD TOTAL [m]	PESO [kg/m]	PESO PARCIAL [kg]
20	12	0.46	1.84	12	22.08	0.89	19.65
21	12	0.24 0.46	1.40	4	5.60	0.89	4.98
22	20	8 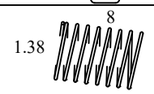 1.38	11.04	2	22.08	2.47	54.55
23	20	3.31 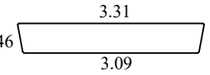 0.46 3.09	7.32	8	58.56	2.47	144.64
24	12	0.70	0.70	12	8.40	0.89	7.48
25	12	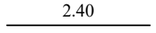 2.40	2.40	6	14.40	0.89	12.82

Total kg ... 244.12

Resumen total por diámetros

Ø [mm]	Longitud [m]	Peso [kg]
12	131.12	44.93
20	80.64	199.19

Armadura pasiva total de una viga

Tipo	nº elementos	Peso/elemento [kg]	Peso [kg]
Rasante	1	1177.80	1177.80
Anclaje 2T22C	2	251.61	503.22
Anclaje superior 2T31C	2	244.12	488.24
Anclaje y desviador	2	664.04	1328.08

Total kg 1 viga ... 3497.34

Total kg 2 viga ... 6994.68

Título del Proyecto

ALTERNATIVAS DE VIGAS ARTESA
CON HORMIGÓN DE MUY ALTAS PRESTACIONES REFORZADO CON FIBRAS

Investigadores principales

D. Hugo Corres D. Leonardo Todisco

Autor

D. Rafael Ruiz Maestre

Título del plano

3 DOVELAS 20 m VERSIÓN 2
Tablas de despiece 002

Fecha **10/2020**

Plano nº **5**

Escala A3: **Varias Especificadas en plano**

Hoja **5** de **5**

APPENDIX A. TECHNICAL DRAWINGS FOR THE HPFRC U-GIRDER ROAD BRIDGE 184

B

Database of fibre reinforced concrete mixes

Table B.1: Database of FRC mixes. Aggregate information 1/5

Id	Ref.	Mix ref.	Year	Agg1 inf. -	Agg1 q. [kg/m^3]	Agg2 inf.	Agg2 quant. [kg/m^3]	Agg3 inf.	Agg3 quant. [kg/m^3]	Agg4 inf.	Agg4 quant. [kg/m^3]	Agg. total [kg/m^3]	D_{Max} [mm]
1	[94]	TC-0-0	2015	Sand 0/1	202	Sand 0/4	674	Crushed limestone 2/7	257	Crushed limestone 7/14	566	1699	14
2	[94]	TC-20S-0	2015	Sand 0/1	202	Sand 0/4	674	Crushed limestone 2/7	257	Crushed limestone 7/14	566	1699	14
3	[94]	TC-40S-0	2015	Sand 0/1	202	Sand 0/4	674	Crushed limestone 2/7	257	Crushed limestone 7/14	566	1699	14
4	[94]	TC-60S-0	2015	Sand 0/1	202	Sand 0/4	674	Crushed limestone 2/7	257	Crushed limestone 7/14	566	1699	14
5	[94]	SCC-0-0	2015	Limestone filler	240	Sand 0/4	816	Crushed limestone 2/7	346	Crushed limestone 7/14	388	1790	14
6	[94]	SCC-20L-0	2015	Limestone filler	240	Sand 0/4	816	Crushed limestone 2/7	346	Crushed limestone 7/14	388	1790	14
7	[94]	SCC-40L-0	2015	Limestone filler	240	Sand 0/4	816	Crushed limestone 2/7	346	Crushed limestone 7/14	388	1790	14
8	[94]	SCC-60L-0	2015	Limestone filler	240	Sand 0/4	816	Crushed limestone 2/7	346	Crushed limestone 7/14	388	1790	14
9	[94]	SCC-20S-0	2015	Limestone filler	240	Sand 0/4	816	Crushed limestone 2/7	346	Crushed limestone 7/14	388	1790	14
10	[94]	SCC-40S-0	2015	Limestone filler	240	Sand 0/4	816	Crushed limestone 2/7	346	Crushed limestone 7/14	388	1790	14
11	[94]	SCC-60S-0	2015	Limestone filler	240	Sand 0/4	816	Crushed limestone 2/7	346	Crushed limestone 7/14	388	1790	14
12	[94]	SCC-20L-5	2015	Limestone filler	240	Sand 0/4	816	Crushed limestone 2/7	346	Crushed limestone 7/14	388	1790	14
13	[94]	SCC-20L-10	2015	Limestone filler	240	Sand 0/4	816	Crushed limestone 2/7	346	Crushed limestone 7/14	388	1790	14
14	[94]	SCC-40L-5	2015	Limestone filler	240	Sand 0/4	816	Crushed limestone 2/7	346	Crushed limestone 7/14	388	1790	14
15	[94]	SCC-40L-10	2015	Limestone filler	240	Sand 0/4	816	Crushed limestone 2/7	346	Crushed limestone 7/14	388	1790	14
16	[94]	SCC-40L-25	2015	Limestone filler	240	Sand 0/4	816	Crushed limestone 2/7	346	Crushed limestone 7/14	388	1790	14
17	[94]	REF	2015	Sand 0/1	202	Sand 0/4	674	Crushed limestone 2/6	257	Crushed limestone 6/14	566	1699	14
18	[94]	20	2015	Sand 0/1	202	Sand 0/4	674	Crushed limestone 2/6	257	Crushed limestone 6/14	566	1699	14
19	[94]	40	2015	Sand 0/1	202	Sand 0/4	674	Crushed limestone 2/6	257	Crushed limestone 6/14	566	1699	14
20	[94]	20+20	2015	Sand 0/1	202	Sand 0/4	674	Crushed limestone 2/6	257	Crushed limestone 6/14	566	1699	14
21	[94]	60	2015	Sand 0/1	202	Sand 0/4	674	Crushed limestone 2/6	257	Crushed limestone 6/14	566	1699	14
22	[13]	SB1	2006	Sydney sand 150-400 μm	928	-	-	-	-	-	-	928	0.4
23	[13]	SB2	2006	Sydney sand 150-400 μm	920	-	-	-	-	-	-	920	0.4
24	[13]	SB3	2006	Sydney sand 150-400 μm	911	-	-	-	-	-	-	911	0.4
25	[13]	SB4	2006	Sydney sand 150-400 μm	939	-	-	-	-	-	-	939	0.4
26	[13]	SB5	2006	Sydney sand 150-400 μm	937	-	-	-	-	-	-	937	0.4
27	[13]	SB6	2006	Sydney sand 150-400 μm	911	-	-	-	-	-	-	911	0.4
28	[13]	SB7	2006	Sydney sand 150-400 μm	920	-	-	-	-	-	-	920	0.4
29	[65]	I-BEAM 1	2005	-	-	-	-	-	-	-	-	-	15
30	[65]	I-BEAM 2	2005	-	-	-	-	-	-	-	-	-	15
31	[65]	I-BEAM 3	2005	-	-	-	-	-	-	-	-	-	15
32	[65]	I-BEAM 4	2005	-	-	-	-	-	-	-	-	-	15
33	[65]	I-BEAM 5	2005	-	-	-	-	-	-	-	-	-	15
34	[65]	I-BEAM 6	2005	-	-	-	-	-	-	-	-	-	15
35	[87]	NS00	2017	Sand 125-250 μm	171	Sand 250-500 μm	217	Sand 500 μm-1 mm	296	Sand 1/2 mm	456	1140	2
36	[87]	WS00	2017	Sand 125-250 μm	171	Sand 250-500 μm	217	Sand 500 μm-1 mm	296	Sand 1/2 mm	456	1140	2
37	[87]	NS08	2017	Sand 125-250 μm	168	Sand 250-500 μm	212	Sand 500 μm-1 mm	291	Sand 1/2 mm	447	1118	2
38	[87]	WS08	2017	Sand 125-250 μm	168	Sand 250-500 μm	212	Sand 500 μm-1 mm	291	Sand 1/2 mm	447	1118	2
39	[87]	SN16	2017	Sand 125-250 μm	165	Sand 250-500 μm	208	Sand 500 μm-1 mm	285	Sand 1/2 mm	439	1097	2
40	[87]	WS16	2017	Sand 125-250 μm	165	Sand 250-500 μm	208	Sand 500 μm-1 mm	285	Sand 1/2 mm	439	1097	2
41	[88]	X-B1	2010	Fine sand 100-1000 μm	1100	-	-	-	-	-	-	1100	1
42	[88]	X-B2	2010	Fine sand 100-1000 μm	1100	-	-	-	-	-	-	1100	1
43	[88]	X-B3	2010	Fine sand 100-1000 μm	1100	-	-	-	-	-	-	1100	1
44	[88]	X-B4	2010	Fine sand 100-1000 μm	1100	-	-	-	-	-	-	1100	1
45	[88]	X-B5	2010	Fine sand 100-1000 μm	1100	-	-	-	-	-	-	1100	1
46	[88]	X-B6	2010	Fine sand 100-1000 μm	1100	-	-	-	-	-	-	1100	1
47	[88]	X-B7	2010	Fine sand 100-1000 μm	1100	-	-	-	-	-	-	1100	1
48	[88]	X-B8	2010	Fine sand 100-1000 μm	1100	-	-	-	-	-	-	1100	1

Table B.2: Database of FRC mixes. Aggregate information 2/5

Id	Ref.	Mix ref.	Year	Agg1 inf. -	Agg1 q. [kg/m^3]	Agg2 inf.	Agg2 quant. [kg/m^3]	Agg3 inf.	Agg3 quant. [kg/m^3]	Agg4 inf.	Agg4 quant. [kg/m^3]	Agg. total [kg/m^3]	D_{Max} [mm]
49	[89]	HF600TR/1	2015	Filler	50	Sand 500 μm-1 mm	985	Agg. 7/12	721	-	-	1756	12
50	[89]	HF600TR/2	2015	Filler	50	Sand 500 μm-1 mm	985	Agg. 7/12	721	-	-	1756	12
51	[89]	H600TR/3	2015	Filler	41	Sand 500 μm-1 mm	924	Agg. 7/12	846	-	-	1811	12
52	[89]	HF600/4	2015	Filler	50	Sand 500 μm-1 mm	985	Agg. 7/12	721	-	-	1756	12
53	[89]	HF600/5	2015	Filler	50	Sand 500 μm-1 mm	985	Agg. 7/12	721	-	-	1756	12
54	[89]	HF400h/6a	2015	Filler	50	Sand 500 μm-1 mm	985	Agg. 7/12	721	-	-	1756	12
55	[89]	HF400/7	2015	Filler	50	Sand 500 μm-1 mm	985	Agg. 7/12	721	-	-	1756	12
56	[89]	HF400TR/8	2015	Filler	50	Sand 500 μm-1 mm	985	Agg. 7/12	721	-	-	1756	12
57	[89]	HF260TR/9	2015	Filler	50	Sand 500 μm-1 mm	985	Agg. 7/12	721	-	-	1756	12
58	[89]	PC	2015	Sand 0/4	1073	Coarse Agg. 4/16	645	-	-	-	-	1718	16
59	[89]	FRC50	2015	Sand 0/4	1073	Coarse Agg. 4/16	645	-	-	-	-	1718	16
60	[89]	FRC75	2015	Sand 0/4	1073	Coarse Agg. 4/16	645	-	-	-	-	1718	16
61	[89]	M-65/40BN-a	2015	Filler	125	Sand	954	Agg. 7/12 mm	731	-	-	1810	12
62	[89]	M-80/40BP	2015	Filler	125	Sand	954	Agg. 7/12 mm	731	-	-	1810	12
63	[89]	L-80/50BN-a	2015	Filler	180	Sand	954	Agg. 7/12 mm	658	-	-	1792	12
64	[89]	L-65/40BN	2015	Filler	180	Sand	954	Agg. 7/12 mm	658	-	-	1792	12
65	[89]	M-80/50BN	2015	Filler	125	Sand	954	Agg. 7/12 mm	731	-	-	1810	12
66	[89]	H-65/40BN	2015	Filler	0	Sand	1075	Agg. 7/12 mm	610	-	-	1685	12
67	[89]	H-80/40BP	2015	Filler	0	Sand	1075	Agg. 7/12 mm	610	-	-	1685	12
68	[89]	M-0	2015	Filler	125	Sand	954	Agg. 7/12 mm	731	-	-	1810	12
69	[89]	M-45/50BN	2015	Filler	125	Sand	954	Agg. 7/12 mm	731	-	-	1810	12
70	[89]	L-80/40BP	2015	Filler	180	Sand	954	Agg. 7/12 mm	658	-	-	1792	12
71	[89]	M-ϕ8	2015	Filler	125	Sand	954	Agg. 7/12 mm	731	-	-	1810	12
72	[89]	M-80/30BP	2015	Filler	125	Sand	954	Agg. 7/12 mm	731	-	-	1810	12
73	[89]	H-0	2015	Filler	0	Sand	1075	Agg. 7/12 mm	610	-	-	1685	12
74	[89]	H-80/50BN	2015	Filler	0	Sand	1075	Agg. 7/12 mm	610	-	-	1685	12
75	[89]	H-45/50BN	2015	Filler	0	Sand	1075	Agg. 7/12 mm	610	-	-	1685	12
76	[89]	H-80/30BP	2015	Filler	0	Sand	1075	Agg. 7/12 mm	610	-	-	1685	12
77	[89]	H-ϕ8	2015	Filler	0	Sand	1075	Agg. 7/12 mm	610	-	-	1685	12
78	[89]	M-ϕ6	2015	Filler	125	Sand	954	Agg. 7/12 mm	731	-	-	1810	12
79	[89]	H-ϕ6	2015	Filler	0	Sand	1075	Agg. 7/12 mm	610	-	-	1685	12
80	[89]	L-ϕ6	2015	Filler	180	Sand	954	Agg. 7/12 mm	658	-	-	1792	12
81	[89]	M-65/40BN-b	2015	Filler	125	Sand	954	Agg. 7/12 mm	731	-	-	1810	12
82	[89]	L-80/50BN-b	2015	Filler	180	Sand	954	Agg. 7/12 mm	658	-	-	1792	12
83	[89]	TC	2015	Sand 0/4 mm	690	Sand 0/6 mm	311	Coarse agg. 6/10 mm	843	-	-	1844	10
84	[89]	FRC-50	2015	Sand 0/4 mm	690	Sand 0/6 mm	311	Coarse agg. 6/10 mm	843	-	-	1844	10
85	[89]	FRC-70	2015	Sand 0/4 mm	690	Sand 0/6 mm	311	Coarse agg. 6/10 mm	843	-	-	1844	10
86	[90]	M2Q	2001	Quartz powder, fine	207	Quartz powder, coarse	-	Quartz sand 0.125/0.5 mm	975	-	-	1182	0.5
87	[91, 179]	M3Q	2012	Quartz powder, fine	193	Quartz powder, coarse	-	Quartz sand 0.125/0.5 mm	946	-	-	1139	0.5
88	[92]	B5Q	2010	Quartz powder, fine	325	Quartz powder, coarse	135	Quartz sand 0.125/0.5 mm	354	Basalt 2/8 mm	598	1412	8
89	[93]	0.45NC	2013	Siliceous sand	356	Crushed sand 0/4 mm	507	Crushed stone 4/16 mm	626	Crushed stone 16/32 mm	273	1762	20
90	[93]	0.45A55VO.26	2013	Siliceous sand	354	Crushed sand 0/4 mm	502	Crushed stone 4/16 mm	621	Crushed stone 16/32 mm	271	1748	20
91	[93]	0.45A55VO.51	2013	Siliceous sand	356	Crushed sand 0/4 mm	505	Crushed stone 4/16 mm	624	Crushed stone 16/32 mm	272	1757	20
92	[93]	0.45A55VO.78	2013	Siliceous sand	356	Crushed sand 0/4 mm	506	Crushed stone 4/16 mm	625	Crushed stone 16/32 mm	273	1760	20
93	[93]	0.45A65VO.26	2013	Siliceous sand	354	Crushed sand 0/4 mm	504	Crushed stone 4/16 mm	623	Crushed stone 16/32 mm	272	1753	20
94	[93]	0.45A65VO.51	2013	Siliceous sand	358	Crushed sand 0/4 mm	509	Crushed stone 4/16 mm	630	Crushed stone 16/32 mm	275	1772	20
95	[93]	0.45A65VO.78	2013	Siliceous sand	358	Crushed sand 0/4 mm	508	Crushed stone 4/16 mm	628	Crushed stone 16/32 mm	274	1768	20
96	[93]	0.45A80VO.26	2013	Siliceous sand	360	Crushed sand 0/4 mm	510	Crushed stone 4/16 mm	631	Crushed stone 16/32 mm	275	1776	20
97	[93]	0.45A80VO.51	2013	Siliceous sand	360	Crushed sand 0/4 mm	510	Crushed stone 4/16 mm	631	Crushed stone 16/32 mm	275	1776	20

Table B.3: Database of FRC mixes. Aggregate information 3/5

Id	Ref.	Mix ref.	Year	Agg1 inf. -	Agg1 q. [kg/m^3]	Agg2 inf.	Agg2 quant. [kg/m^3]	Agg3 inf.	Agg3 quant. [kg/m^3]	Agg4 inf.	Agg4 quant. [kg/m^3]	Agg. total [kg/m^3]	D_{Max} [mm]
98	[93]	0.45A80VO.78	2013	Siliceous sand	356	Crushed sand 0/4 mm	506	Crushed stone 4/16 mm	625	Crushed stone 16/32 mm	273	1760	20
99	[93]	O.70NC	2013	Siliceous sand	352	Crushed sand 0/4 mm	499	Crushed stone 4/16 mm	617	Crushed stone 16/32 mm	270	1738	20
100	[93]	O.70A55VO.26	2013	Siliceous sand	354	Crushed sand 0/4 mm	503	Crushed stone 4/16 mm	621	Crushed stone 16/32 mm	271	1749	20
101	[93]	O.70A55VO.51	2013	Siliceous sand	356	Crushed sand 0/4 mm	505	Crushed stone 4/16 mm	625	Crushed stone 16/32 mm	273	1759	20
102	[93]	O.70A55VO.78	2013	Siliceous sand	354	Crushed sand 0/4 mm	504	Crushed stone 4/16 mm	623	Crushed stone 16/32 mm	272	1753	20
103	[93]	O.70A65VO.26	2013	Siliceous sand	364	Crushed sand 0/4 mm	516	Crushed stone 4/16 mm	638	Crushed stone 16/32 mm	279	1797	20
104	[93]	O.70A65VO.51	2013	Siliceous sand	360	Crushed sand 0/4 mm	513	Crushed stone 4/16 mm	634	Crushed stone 16/32 mm	277	1784	20
105	[93]	0.70A65VO.78	2013	Siliceous sand	360	Crushed sand 0/4 mm	511	Crushed stone 4/16 mm	632	Crushed stone 16/32 mm	276	1779	20
106	[93]	O.70A80VO.26	2013	Siliceous sand	358	Crushed sand 0/4 mm	509	Crushed stone 4/16 mm	629	Crushed stone 16/32 mm	275	1771	20
107	[93]	O.70A80VO.51	2013	Siliceous sand	354	Crushed sand 0/4 mm	504	Crushed stone 4/16 mm	624	Crushed stone 16/32 mm	272	1754	20
108	[93]	O.70A80VO.78	2013	Siliceous sand	356	Crushed sand 0/4 mm	506	Crushed stone 4/16 mm	625	Crushed stone 16/32 mm	273	1760	20
109	[29]	Precaster B	2021	Sand	1069	Limestone	84	-	-	-	-	1153	0.76
110	[29]	Precaster C	2021	Sand	911	-	-	-	-	-	-	911	0.76
111	[29]	Precaster D	2021	Sand	945	Limestone	150	-	-	-	-	1095	0.76
112	[29]	Precaster E	2021	Sand	999	Slag	358	-	-	-	-	1357	0.76
113	[86]	0	2020	Artificial sand $\leq$ 2.36 mm	856	Coarse Agg.	957	-	-	-	-	1813	12.5
114	[86]	0.5S	2020	Artificial sand $\leq$ 2.36 mm	856	Coarse Agg.	941	-	-	-	-	1797	12.5
115	[86]	1S	2020	Artificial sand $\leq$ 2.36 mm	856	Coarse Agg.	929	-	-	-	-	1785	12.5
116	[86]	1L	2020	Artificial sand $\leq$ 2.36 mm	856	Coarse Agg.	929	-	-	-	-	1785	12.5
117	[95]	Mix A	2010	Sand	626	Lightweight sand	0	Coarse agg.	1061	Lightweight coarse agg.	0	1687	-
118	[95]	Mix B	2010	Sand	643	Lightweight sand	-	Coarse agg.	1139	Lightweight coarse agg.	-	1782	-
119	[95]	Mix C	2010	Sand	554	Lightweight sand	-	Coarse agg.	1050	Lightweight coarse agg.	-	1604	-
120	[95]	Mix D	2010	Sand	643	Lightweight sand	-	Coarse agg.	1174	Lightweight coarse agg.	-	1817	-
121	[95]	Mix E	2010	Sand	321	Lightweight sand	231	Coarse agg.	359	Lightweight coarse agg.	413	1324	-
122	[95]	Mix F	2010	Sand	611	Lightweight sand	-	Coarse agg.	1109	Lightweight coarse agg.	-	1720	-
123	[95]	Mix G	2010	Sand	610	Lightweight sand	-	Coarse agg.	1137	Lightweight coarse agg.	-	1747	-
124	[96]	3FI8-NF Mix 1	2016	Crushed sand	954	Gravel 7/12 mm	401	Gravel 12/20 mm	568	-	-	1923	20
125	[96]	2FI8-NF Mix 2	2016	Crushed sand	954	Gravel 7/12 mm	969	Gravel 12/20 mm	0	-	-	1923	12
126	[96]	2FI8-NF Mix 3	2016	Crushed sand	1220	Gravel 7/12 mm	690	Gravel 12/20 mm	0	-	-	1910	12
127	[96]	3FI8-NF Mix 4	2016	Crushed sand	1220	Gravel 7/12 mm	690	Gravel 12/20 mm	0	-	-	1910	12
128	[96]	0FI8-NF Mix 5	2016	Crushed sand	1220	Gravel 7/12 mm	690	Gravel 12/20 mm	0	-	-	1910	12
129	[97]	PC-SNR	2008	Sand	804	Gravel 10 mm MSA	579	Gravel 20 mm MSA	464	-	-	1847	20
130	[97]	Dramix 1%	2008	Sand	804	Gravel 10 mm MSA	579	Gravel 20 mm MSA	464	-	-	1847	20
131	[97]	Novotex 1050 1%	2008	Sand	804	Gravel 10 mm MSA	579	Gravel 20 mm MSA	464	-	-	1847	20
132	[98]	UM-5	2014	Quartz powder $\leq$40 μm	397	Quartz sand 0.1/0.5 mm	833	-	-	-	-	1230	0.5
133	[98]	UM-5-FA	2014	Quartz powder $\leq$40 μm	397	Quartz sand 0.1/0.5 mm	833	-	-	-	-	1230	0.5
134	[98]	UM-5-GBSf	2014	Quartz powder $\leq$40 μm	397	Quartz sand 0.1/0.5 mm	833	-	-	-	-	1230	0.5
135	[98]	UM-5-GBSef	2014	Quartz powder $\leq$40 μm	397	Quartz sand 0.1/0.5 mm	833	-	-	-	-	1230	0.5
136	[77]	N1-S1-0	2011	-	-	Natural quartz sand	1110	Basalt coarse agg.	872	-	-	1982	22
137	[77]	H1-S1-0-1	2011	-	-	Natural quartz sand	704	Basalt coarse agg.	1082	-	-	1786	22
138	[77]	H1-S1-0-2	2011	-	-	Natural quartz sand	704	Basalt coarse agg.	1082	-	-	1786	22
139	[77]	H2-S1-1-1	2011	-	-	Natural quartz sand	704	Basalt coarse agg.	1082	-	-	1786	22
140	[77]	H2-S1-1-2	2011	-	-	Natural quartz sand	704	Basalt coarse agg.	1082	-	-	1786	22
141	[77]	H3-S0-1-35	2011	-	-	Natural quartz sand	704	Basalt coarse agg.	1082	-	-	1786	22
142	[77]	H3-S0-1-60	2011	-	-	Natural quartz sand	704	Basalt coarse agg.	1082	-	-	1786	22
143	[77]	H9-S0-0-1	2011	-	-	Natural quartz sand	704	Basalt coarse agg.	1082	-	-	1786	22
144	[77]	H9-S0-0-2	2011	-	-	Natural quartz sand	704	Basalt coarse agg.	1082	-	-	1786	22
145	[78]	T30	2003	-	-	Natural quartz sand	704	Basalt coarse agg.	1082	-	-	1786	22
146	[78]	T60	2003	-	-	Natural quartz sand	704	Basalt coarse agg.	1082	-	-	1786	22

Table B.4: Database of FRC mixes. Aggregate information 4/5

Id	Ref.	Mix ref.	Year	Agg1 inf. -	Agg1 q. [kg/m^3]	Agg2 inf.	Agg2 quant. [kg/m^3]	Agg3 inf.	Agg3 quant. [kg/m^3]	Agg4 inf.	Agg4 quant. [kg/m^3]	Agg. total [kg/m^3]	D_{Max} [mm]
147	[79]	A0-0	2008	-	-	Limestone fines 0/4 mm	835	Crushed limestone 4/12 mm	665	Crushed limestone 12/19 mm	382	1882	19
148	[79]	A0650.5	2008	-	-	Limestone fines 0/4 mm	835	Crushed limestone 4/12 mm	665	Crushed limestone 12/19 mm	382	1882	19
149	[79]	A0651	2008	-	-	Limestone fines 0/4 mm	835	Crushed limestone 4/12 mm	665	Crushed limestone 12/19 mm	382	1882	19
150	[79]	A0800.5	2008	-	-	Limestone fines 0/4 mm	835	Crushed limestone 4/12 mm	665	Crushed limestone 12/19 mm	382	1882	19
151	[79]	A0801	2008	-	-	Limestone fines 0/4 mm	835	Crushed limestone 4/12 mm	665	Crushed limestone 12/19 mm	382	1882	19
152	[79]	B0-0	2008	-	-	Limestone fines 0/4 mm	835	Crushed limestone 4/12 mm	665	Crushed limestone 12/19 mm	382	1882	19
153	[79]	B0650.5	2008	-	-	Limestone fines 0/4 mm	835	Crushed limestone 4/12 mm	665	Crushed limestone 12/19 mm	382	1882	19
154	[79]	B0651	2008	-	-	Limestone fines 0/4 mm	835	Crushed limestone 4/12 mm	665	Crushed limestone 12/19 mm	382	1882	19
155	[79]	B0800.5	2008	-	-	Limestone fines 0/4 mm	835	Crushed limestone 4/12 mm	665	Crushed limestone 12/19 mm	382	1882	19
156	[79]	B0801	2008	-	-	Limestone fines 0/4 mm	835	Crushed limestone 4/12 mm	665	Crushed limestone 12/19 mm	382	1882	19
157	[79]	C0-0	2008	-	-	Limestone fines 0/4 mm	835	Crushed limestone 4/12 mm	665	Crushed limestone 12/19 mm	382	1882	19
158	[79]	C0650.5	2008	-	-	Limestone fines 0/4 mm	835	Crushed limestone 4/12 mm	665	Crushed limestone 12/19 mm	382	1882	19
159	[79]	C0651	2008	-	-	Limestone fines 0/4 mm	835	Crushed limestone 4/12 mm	665	Crushed limestone 12/19 mm	382	1882	19
160	[79]	C0800.5	2008	-	-	Limestone fines 0/4 mm	835	Crushed limestone 4/12 mm	665	Crushed limestone 12/19 mm	382	1882	19
161	[79]	C0801	2008	-	-	Limestone fines 0/4 mm	835	Crushed limestone 4/12 mm	665	Crushed limestone 12/19 mm	382	1882	19
162	[79]	D0-0	2008	-	-	Limestone fines 0/4 mm	835	Crushed limestone 4/12 mm	665	Crushed limestone 12/19 mm	382	1882	19
163	[79]	D0650.5	2008	-	-	Limestone fines 0/4 mm	835	Crushed limestone 4/12 mm	665	Crushed limestone 12/19 mm	382	1882	19
164	[79]	D0651	2008	-	-	Limestone fines 0/4 mm	835	Crushed limestone 4/12 mm	665	Crushed limestone 12/19 mm	382	1882	19
165	[79]	D0800.5	2008	-	-	Limestone fines 0/4 mm	835	Crushed limestone 4/12 mm	665	Crushed limestone 12/19 mm	382	1882	19
166	[79]	D0801	2008	-	-	Limestone fines 0/4 mm	835	Crushed limestone 4/12 mm	665	Crushed limestone 12/19 mm	382	1882	19
167	[80]	HPC0	2004	-	-	River sand	739	Crushed basalt	1052	-	-	1791	19
168	[80]	HPC0.5	2004	-	-	River sand	740	Crushed basalt	1052	-	-	1792	19
169	[80]	HPC1.0	2004	-	-	River sand	741	Crushed basalt	1052	-	-	1793	19
170	[80]	HPC1.5	2004	-	-	River sand	742	Crushed basalt	1052	-	-	1794	19
171	[80]	HPC2.0	2004	-	-	River sand	743	Crushed basalt	1052	-	-	1795	19
172	[81]	A0-0	1997	-	-	Fine agg.	710	Medium agg.	622	Coarse agg.	444	1776	13
173	[81]	A0600.5	1997	-	-	Fine agg.	710	Medium agg.	622	Coarse agg.	444	1776	13
174	[81]	A0601.0	1997	-	-	Fine agg.	710	Medium agg.	622	Coarse agg.	444	1776	13
175	[81]	A0602.0	1997	-	-	Fine agg.	710	Medium agg.	622	Coarse agg.	444	1776	13
176	[81]	A0750.5	1997	-	-	Fine agg.	710	Medium agg.	622	Coarse agg.	444	1776	13
177	[81]	A0751.0	1997	-	-	Fine agg.	710	Medium agg.	622	Coarse agg.	444	1776	13
178	[81]	A0752.0	1997	-	-	Fine agg.	710	Medium agg.	622	Coarse agg.	444	1776	13
179	[81]	A0830.5	1997	-	-	Fine agg.	710	Medium agg.	622	Coarse agg.	444	1776	13
180	[81]	A0831.0	1997	-	-	Fine agg.	710	Medium agg.	622	Coarse agg.	444	1776	13
181	[81]	A0832.0	1997	-	-	Fine agg.	710	Medium agg.	622	Coarse agg.	444	1776	13
182	[81]	B5-0	1997	-	-	Fine agg.	710	Medium agg.	622	Coarse agg.	444	1776	13
183	[81]	B5600.5	1997	-	-	Fine agg.	710	Medium agg.	622	Coarse agg.	444	1776	13
184	[81]	B5601.0	1997	-	-	Fine agg.	710	Medium agg.	622	Coarse agg.	444	1776	13
185	[81]	B5602.0	1997	-	-	Fine agg.	710	Medium agg.	622	Coarse agg.	444	1776	13
186	[81]	B5750.5	1997	-	-	Fine agg.	710	Medium agg.	622	Coarse agg.	444	1776	13
187	[81]	B5751.0	1997	-	-	Fine agg.	710	Medium agg.	622	Coarse agg.	444	1776	13
188	[81]	B5752.0	1997	-	-	Fine agg.	710	Medium agg.	622	Coarse agg.	444	1776	13
189	[81]	B5830.5	1997	-	-	Fine agg.	710	Medium agg.	622	Coarse agg.	444	1776	13
190	[81]	B5831.0	1997	-	-	Fine agg.	710	Medium agg.	622	Coarse agg.	444	1776	13
191	[81]	B5832.0	1997	-	-	Fine agg.	710	Medium agg.	622	Coarse agg.	444	1776	13
192	[81]	C10-0	1997	-	-	Fine agg.	710	Medium agg.	622	Coarse agg.	444	1776	13
193	[81]	C10600.5	1997	-	-	Fine agg.	710	Medium agg.	622	Coarse agg.	444	1776	13
194	[81]	C10601.0	1997	-	-	Fine agg.	710	Medium agg.	622	Coarse agg.	444	1776	13
195	[81]	C10602.0	1997	-	-	Fine agg.	710	Medium agg.	622	Coarse agg.	444	1776	13

Table B.5: Database of FRC mixes. Aggregate information 5/5

Id	Ref.	Mix ref.	Year	Agg1 inf. -	Agg1 q. [kg/m^3]	Agg2 inf.	Agg2 quant. [kg/m^3]	Agg3 inf.	Agg3 quant. [kg/m^3]	Agg4 inf.	Agg4 quant. [kg/m^3]	Agg. total [kg/m^3]	D_{Max} [mm]
196	[81]	C10750.5	1997	-	-	Fine agg.	710	Medium agg.	622	Coarse agg.	444	1776	13
197	[81]	C10751.0	1997	-	-	Fine agg.	710	Medium agg.	622	Coarse agg.	444	1776	13
198	[81]	C10752.0	1997	-	-	Fine agg.	710	Medium agg.	622	Coarse agg.	444	1776	13
199	[81]	C10830.5	1997	-	-	Fine agg.	710	Medium agg.	622	Coarse agg.	444	1776	13
200	[81]	C10831.0	1997	-	-	Fine agg.	710	Medium agg.	622	Coarse agg.	444	1776	13
201	[81]	C10832.0	1997	-	-	Fine agg.	710	Medium agg.	622	Coarse agg.	444	1776	13
202	[82]	30	2010	Limestone filler	312	Fine river sand	108	Coarse river sand	709	Crushed granite 5/12	665	1795	12
203	[82]	45	2010	Limestone filler	344	Fine river sand	102	Coarse river sand	666	Crushed granite 5/12	625	1737	12
204	[83]	0-0-0	2008	-	-	-	-	River sand	-	Coarse agg.	-	0	12.5
205	[83]	100-0-1	2008	-	-	-	-	River sand	-	Coarse agg.	-	0	12.5
206	[83]	65-35-1	2008	-	-	-	-	River sand	-	Coarse agg.	-	0	12.5
207	[83]	50-50-1	2008	-	-	-	-	River sand	-	Coarse agg.	-	0	12.5
208	[83]	35-65-1	2008	-	-	-	-	River sand	-	Coarse agg.	-	0	12.5
209	[83]	0-100-1	2008	-	-	-	-	River sand	-	Coarse agg.	-	0	12.5
210	[83]	100-0-1.5	2008	-	-	-	-	River sand	-	Coarse agg.	-	0	12.5
211	[83]	65-35-1.5	2008	-	-	-	-	River sand	-	Coarse agg.	-	0	12.5
212	[83]	50-50-1.5	2008	-	-	-	-	River sand	-	Coarse agg.	-	0	12.5
213	[83]	35-56-1.5	2008	-	-	-	-	River sand	-	Coarse agg.	-	0	12.5
214	[83]	0-100-1.5	2008	-	-	-	-	River sand	-	Coarse agg.	-	0	12.5
215	[83]	100-0-2	2008	-	-	-	-	River sand	-	Coarse agg.	-	0	12.5
216	[83]	65-35-2	2008	-	-	-	-	River sand	-	Coarse agg.	-	0	12.5
217	[83]	50-50-2	2008	-	-	-	-	River sand	-	Coarse agg.	-	0	12.5
218	[83]	35-65-2	2008	-	-	-	-	River sand	-	Coarse agg.	-	0	12.5
219	[83]	0-100-2	2008	-	-	-	-	River sand	-	Coarse agg.	-	0	12.5
220	[180]	UM-2-NF	2015	Quartz powder	17	Quartz sand 0.4 mm	36	-	-	-	-	53	0.4
221	[180]	UM-2-2	2015	Quartz powder	17	Quartz sand 0.4 mm	36	-	-	-	-	53	0.4
222	[180]	UM-3-1	2015	Quartz powder	11	Quartz sand 0.4 mm	37	-	-	-	-	48	0.4
223	[180]	UM-3-2	2015	Quartz powder	11	Quartz sand 0.4 mm	37	-	-	-	-	48	0.4
224	[58]	SCHPFRC	2021	Sand 0/4 mm	757	Porphyry 2/6 mm	634	-	-	-	-	1391	6
225	[85]	Mix 1	2001	Sand 0/3 mm	110	Sand 0/12 mm	960	Grave 8-15 mm	810	-	-	1880	15
226	[85]	Mix 2	2001	Sand 0/5 mm	869	Grave 5/12 mm	869	-	-	-	-	1738	12

Table B.6: Database of FRC mixes. Paste phase information 1/5

Id	Ref.	Cem1 inf.	Cem1 q. [kg/m^3]	Cem2 inf. -	Cem2 q. [kg/m^3]	Cem. total [kg/m^3]	Sil. fume [kg/m^3]	Fly ash [kg/m^3]	Micro-sil. [kg/m^3]	Add. total [kg/m^3]	Water [kg/m^3]	Supl. info	Supl. q.	w/c
1	[94]	CEM 52.5 R	390	-	-	390	-	-	-	0	190	-	2.20	0.49
2	[94]	CEM 52.5 R	390	-	-	390	-	-	-	0	190	-	2.20	0.49
3	[94]	CEM 52.5 R	390	-	-	390	-	-	-	0	190	-	2.20	0.49
4	[94]	CEM 52.5 R	390	-	-	390	-	-	-	0	190	-	2.20	0.49
5	[94]	CEM 52.5 N	360	-	-	360	-	-	-	0	165	-	3.50	0.46
6	[94]	CEM 52.5 N	360	-	-	360	-	-	-	0	165	-	3.50	0.46
7	[94]	CEM 52.5 N	360	-	-	360	-	-	-	0	165	-	3.50	0.46
8	[94]	CEM 52.5 N	360	-	-	360	-	-	-	0	165	-	3.50	0.46
9	[94]	CEM 52.5 N	360	-	-	360	-	-	-	0	165	-	3.50	0.46
10	[94]	CEM 52.5 N	360	-	-	360	-	-	-	0	165	-	3.50	0.46
11	[94]	CEM 52.5 N	360	-	-	360	-	-	-	0	165	-	3.50	0.46
12	[94]	CEM 52.5 N	360	-	-	360	-	-	-	0	165	-	3.50	0.46
13	[94]	CEM 52.5 N	360	-	-	360	-	-	-	0	165	-	3.50	0.46
14	[94]	CEM 52.5 N	360	-	-	360	-	-	-	0	165	-	3.50	0.46
15	[94]	CEM 52.5 N	360	-	-	360	-	-	-	0	165	-	3.50	0.46
16	[94]	CEM 52.5 N	360	-	-	360	-	-	-	0	165	-	3.50	0.46
17	[94]	CEM I 52.5 R/HES	390	-	-	390	-	60	-	60	190	-	2.61	0.49
18	[94]	CEM I 52.5 R/HES	390	-	-	390	-	60	-	60	190	-	2.61	0.49
19	[94]	CEM I 52.5 R/HES	390	-	-	390	-	60	-	60	190	-	2.61	0.49
20	[94]	CEM I 52.5 R/HES	390	-	-	390	-	60	-	60	190	-	2.61	0.49
21	[94]	CEM I 52.5 R/HES	390	-	-	390	-	60	-	60	190	-	2.61	0.49
22	[13]	Kandos T1 Portland	928	-	-	928	223	-	-	223	186	Glenium 51 [kg/m^3]	39.0	0.16
23	[13]	Kandos T1 Portland	920	-	-	920	221	-	-	221	193	Glenium 51 [kg/m^3]	39.0	0.16
24	[13]	Kandos T1 Portland	911	-	-	911	219	-	-	219	200	Glenium 51 [kg/m^3]	38.0	0.16
25	[13]	Kandos T1 Portland	939	-	-	939	225	-	-	225	188	Glenium 51 [kg/m^3]	39.0	0.16
26	[13]	Kandos T1 Portland	937	-	-	937	225	-	-	225	178	Glenium 51 [kg/m^3]	39.0	0.16
27	[13]	Kandos T1 Portland	911	-	-	911	219	-	-	219	200	Glenium 51 [kg/m^3]	38.0	0.16
28	[13]	Kandos T1 Portland	920	-	-	920	221	-	-	221	193	Glenium 51 [kg/m^3]	39.0	0.16
29	[65]	CEM I 52.5R	380	-	-	380	-	-	-	0	118	-	2.75	0.31
30	[65]	CEM I 52.5R	380	-	-	380	-	-	-	0	118	-	2.75	0.31
31	[65]	CEM I 52.5R	380	-	-	380	-	-	-	0	118	-	3.67	0.31
32	[65]	CEM I 52.5R	380	-	-	380	-	-	-	0	118	-	3.67	0.31
33	[65]	CEM I 52.5R	380	-	-	380	-	-	-	0	118	-	3.67	0.31
34	[65]	CEM I 52.5R	380	-	-	380	-	-	-	0	118	-	3.67	0.31
35	[87]	CEM III 52.5/A	558	CEM I 52.5R	390	948	-	-	102	102	138	-	33.0	0.23
36	[87]	CEM III 52.5/A	558	CEM I 52.5R	390	948	-	-	102	102	138	-	33.0	0.23
37	[87]	CEM III 52.5/A	558	CEM I 52.5R	390	948	-	-	102	102	138	-	33.0	0.23
38	[87]	CEM III 52.5/A	558	CEM I 52.5R	390	948	-	-	102	102	138	-	33.0	0.23
39	[87]	CEM III 52.5/A	558	CEM I 52.5R	390	948	-	-	102	102	138	-	33.0	0.23
40	[87]	CEM III 52.5/A	558	CEM I 52.5R	390	948	-	-	102	102	138	-	33.0	0.23
41	[88]	Lafarge T1 Portland	742	-	-	742	149	-	-	149	151	ViscoCrete-2044	40.0	0.17
42	[88]	Lafarge T1 Portland	742	-	-	742	149	-	-	149	151	ViscoCrete-2044	40.0	0.17
43	[88]	Lafarge T1 Portland	742	-	-	742	149	-	-	149	151	ViscoCrete-2044	40.0	0.17
44	[88]	Lafarge T1 Portland	740	-	-	740	148	-	-	148	160	ViscoCrete-2044	40.0	0.18
45	[88]	Lafarge T1 Portland	776	-	-	776	155	-	-	155	163	ViscoCrete-2044	41.0	0.18
46	[88]	Lafarge T1 Portland	776	-	-	776	155	-	-	155	163	ViscoCrete-2044	41.0	0.18
47	[88]	Lafarge T1 Portland	780	-	-	780	156	-	-	156	140	ViscoCrete-2044	40.0	0.15
48	[88]	Lafarge T1 Portland	740	-	-	740	148	-	-	148	160	ViscoCrete-2044	40.0	0.18

Table B.7: Database of FRC mixes. Paste phase information 2/5

Id	Ref.	Cem1 inf.	Cem1 q. [kg/m^3]	Sil. fume [kg/m^3]	Water [kg/m^3]	Supl. info [kg/m^3]	Supl. q.	w/c
49	[89]	CEM I 52.5R	460	-	205	[kg/m^3]	12.8	0.45
50	[89]	CEM I 52.5R	460	-	205	[kg/m^3]	12.8	0.45
51	[89]	CEM I 52.5R	440	-	198	[kg/m^3]	11.1	0.45
52	[89]	CEM I 52.5R	460	-	205	[kg/m^3]	12.8	0.45
53	[89]	CEM I 52.5R	460	-	205	[kg/m^3]	12.8	0.45
54	[89]	CEM I 52.5R	460	-	205	[kg/m^3]	12.8	0.45
55	[89]	CEM I 52.5R	460	-	205	[kg/m^3]	12.8	0.45
56	[89]	CEM I 52.5R	460	-	205	[kg/m^3]	12.8	0.45
57	[89]	CEM I 52.5R	460	-	205	[kg/m^3]	12.8	0.45
58	[89]	CEM I 42.5R	410	-	168	[l/m^3]	4.1	0.41
59	[89]	CEM I 42.5R	410	-	168	[l/m^3]	4.8	0.41
60	[89]	CEM I 42.5R	410	-	168	[l/m^3]	5.7	0.41
61	[89]	CEM 52.5R	340	-	210	[kg/m^3]	7.45	0.62
62	[89]	CEM 52.5R	340	-	210	[kg/m^3]	7.45	0.62
63	[89]	CEM 52.5R	290	-	210	[kg/m^3]	5.2	0.72
64	[89]	CEM 52.5R	290	-	210	[kg/m^3]	5.2	0.72
65	[89]	CEM 52.5R	340	-	210	[kg/m^3]	7.45	0.62
66	[89]	CEM 52.5R	450	50	175	[kg/m^3]	26.7	0.39
67	[89]	CEM 52.5R	450	50	175	[kg/m^3]	26.7	0.39
68	[89]	CEM 52.5R	340	-	210	[kg/m^3]	7.45	0.62
69	[89]	CEM 52.5R	340	-	210	[kg/m^3]	7.45	0.62
70	[89]	CEM 52.5R	290	-	210	[kg/m^3]	5.2	0.72
71	[89]	CEM 52.5R	340	-	210	[kg/m^3]	7.45	0.62
72	[89]	CEM 52.5R	340	-	210	[kg/m^3]	7.45	0.62
73	[89]	CEM 52.5R	450	50	175	[kg/m^3]	26.7	0.39
74	[89]	CEM 52.5R	450	50	175	[kg/m^3]	26.7	0.39
75	[89]	CEM 52.5R	450	50	175	[kg/m^3]	26.7	0.39
76	[89]	CEM 52.5R	450	50	175	[kg/m^3]	26.7	0.39
77	[89]	CEM 52.5R	450	50	175	[kg/m^3]	26.7	0.39
78	[89]	CEM 52.5R	340	-	210	[kg/m^3]	7.45	0.62
79	[89]	CEM 52.5R	450	50	175	[kg/m^3]	26.7	0.39
80	[89]	CEM 52.5R	290	-	210	[kg/m^3]	5.2	0.72
81	[89]	CEM 52.5R	340	-	210	[kg/m^3]	7.45	0.62
82	[89]	CEM 52.5R	290	-	210	[kg/m^3]	5.2	0.72
83	[89]	CEM I 52.5R	411	-	198	Liters	1.5	0.48
84	[89]	CEM I 52.5R	411	-	198	Liters	1.5	0.48
85	[89]	CEM I 52.5R	411	-	198	Liters	1.6	0.48
86	[90]	CEM I 52.5R	832	135	166	FMW/b [% by mass]	1.1	0.2
87	[91, 179]	CEM I 52.5R	775	164	183	[kg/m^3]	23.5	0.24
88	[92]	CEM I 52.5R	650	177	158	[kg/m^3]	30.3	0.24
89	[93]	CEM I 42.5	403	-	181	[%]	1.3	0.45
90	[93]	CEM I 42.5	401	-	180	[%]	1.52	0.45
91	[93]	CEM I 42.5	405	-	182	[%]	1.73	0.45
92	[93]	CEM I 42.5	409	-	184	[%]	2.20	0.45
93	[93]	CEM I 42.5	402	-	181	[%]	1.5	0.45
94	[93]	CEM I 42.5	409	-	184	[%]	1.71	0.45
95	[93]	CEM I 42.5	410	-	184	[%]	1.85	0.45
96	[93]	CEM I 42.5	407	-	183	[%]	1.47	0.45
97	[93]	CEM I 42.5	410	-	184	[%]	1.73	0.45

Table B.8: Database of FRC mixes. Paste phase information 3/5

Id	Ref.	Cem1 inf.	Cem1 q. [kg/m^3]	Microsil. [kg/m^3]	Sil. fume [kg/m^3]	Fly ash [kg/m^3]	Slag [kg/m^3]	Add. total [kg/m^3]	Water [kg/m^3]	Supl. info	Supl. q.	w/c
98	[93]	CEM I 42.5	408	-	-	-	-	0	184	[%]	1.96	0.45
99	[93]	CEM I 42.5	295	-	-	-	-	0	206	[%]	-	0.7
100	[93]	CEM I 42.5	298	-	-	-	-	0	208	[%]	-	0.7
101	[93]	CEM I 42.5	301	-	-	-	-	0	210	[%]	-	0.7
102	[93]	CEM I 42.5	301	-	-	-	-	0	211	[%]	-	0.7
103	[93]	CEM I 42.5	306	-	-	-	-	0	214	[%]	-	0.7
104	[93]	CEM I 42.5	305	-	-	-	-	0	213	[%]	-	0.7
105	[93]	CEM I 42.5	305	-	-	-	-	0	214	[%]	-	0.7
106	[93]	CEM I 42.5	301	-	-	-	-	0	211	[%]	-	0.7
107	[93]	CEM I 42.5	300	-	-	-	-	0	210	[%]	-	0.7
108	[93]	CEM I 42.5	302	-	-	-	-	0	211	[%]	-	0.7
109	[29]	Type III	737	-	184	-	-	184	189	MaterGrenium 7920	23	0.21
110	[29]	Type I/II	933	-	234	-	-	234	205	MaterGlenium 7920	18	0.2
111	[29]	White Type I/II	829	-	181	-	-	181	188	Superflo 2040RM	17	0.18
112	[29]	Type I/II	737	-	95	-	-	95	172	Premia 150	16	0.16
113	[86]	CEM II	412	-	-	-	-	0	185	HRWRA [kg/m^3]	8.24	0.45
114	[86]	CEM II	412	-	-	-	-	0	185	HRWRA [kg/m^3]	12.4	0.45
115	[86]	CEM II	412	-	-	-	-	0	185	HRWRA [kg/m^3]	12.4	0.45
116	[86]	CEM II	412	-	-	-	-	0	185	HRWRA [kg/m^3]	12.4	0.45
117	[95]	-	418	-	-	-	-	0	160	[l/m^3]	0.7	0.38
118	[95]	-	418	-	-	-	-	0	169	[l/m^3]	1.6	0.4
119	[95]	-	504	-	-	-	-	0	178	[l/m^3]	0.9	0.36
120	[95]	-	445	-	-	-	-	0	136	[l/m^3]	0	0.26
121	[95]	-	267	-	-	-	178	178	151	[l/m^3]	0.7	0.34
122	[95]	-	445	-	56	-	-	56	136	[l/m^3]	0.3	0.31
123	[95]	-	398	-	-	187	-	187	146	[l/m^3]	0	0.25
124	[96]	CEM II/B-V 42.5 N	300	-	0	0	0	0	177	[kg/m^3]	0	0.59
125	[96]	CEM II/B-V 42.5 N	300	-	0	0	0	0	177	[kg/m^3]	1.5	0.59
126	[96]	CEM II/B-V 42.5 N	300	-	0	0	0	0	177	[kg/m^3]	3	0.59
127	[96]	CEM II/B-V 42.5 N	300	-	0	0	0	0	177	[kg/m^3]	3	0.59
128	[96]	CEM II/B-V 42.5 N	300	-	0	0	0	0	177	[kg/m^3]	3.55	0.59
129	[97]	-	363	-	-	-	-	0	181	[l/m^3]	2	0.5
130	[97]	-	363	-	-	-	-	0	181	[l/m^3]	2	0.5
131	[97]	-	363	-	-	-	-	0	181	[l/m^3]	2	0.5
132	[98]	CEM I 42.5 R	729	124	-	-	-	124	200	SKI [kg/m^3]	30	0.23
133	[98]	CEM I 42.5 R	401	124	-	328	-	452	200	SKI [kg/m^3]	30	0.23
134	[98]	CEM I 42.5 R	401	124	-	-	328	452	200	SKI [kg/m^3]	30	0.23
135	[98]	CEM I 42.5 R	401	124	-	-	328	452	200	SKI [kg/m^3]	30	0.23
136	[77]	CEM I 42.5N	246	-	0	-	-	0	150	Rheobuild 2000 [l/m^3]	4.8	0.61
137	[77]	CEM I 52.5N	461	-	65	-	-	65	159	Rheobuild 2000 [l/m^3]	14.9	0.35
138	[77]	CEM I 52.5N	461	-	66	-	-	66	159	Rheobuild 2000 [l/m^3]	14.9	0.35
139	[77]	CEM I 52.5N	461	-	67	-	-	67	159	Rheobuild 2000 [l/m^3]	14.9	0.35
140	[77]	CEM I 52.5N	461	-	68	-	-	68	159	Rheobuild 2000 [l/m^3]	14.9	0.35
141	[77]	CEM I 52.5N	461	-	69	-	-	69	159	Rheobuild 2000 [l/m^3]	14.9	0.35
142	[77]	CEM I 52.5N	461	-	70	-	-	70	159	Rheobuild 2000 [l/m^3]	14.9	0.35
143	[77]	CEM I 52.5N	461	-	71	-	-	71	159	Rheobuild 2000 [l/m^3]	14.9	0.35
144	[77]	CEM I 52.5N	461	-	72	-	-	72	159	Rheobuild 2000 [l/m^3]	14.9	0.35
145	[78]	CEM I 52.5 N	461	-	65	-	-	65	159	Rheobuild 2000 [l/m^3]	14.9	0.35
146	[78]	CEM I 52.5 N	461	-	65	-	-	65	159	Rheobuild 2000 [l/m^3]	14.9	0.35

Table B.9: Database of FRC mixes. Paste phase information 4/5

Id	Ref.	Cem1 inf.	Cem1 q. [kg/m^3]	Sil. fume [kg/m^3]	Water [kg/m^3]	Pl. info [kg/m^3]	Pl. q.	Supl. info	Supl. q.	w/c
147	[79]	CEM I 42.5 R Portland	400	0	152	[kg/m^3]	4	-	-	0.38
148	[79]	CEM I 42.5 R Portland	400	0	152	[kg/m^3]	4	-	-	0.38
149	[79]	CEM I 42.5 R Portland	400	0	152	[kg/m^3]	4	-	-	0.38
150	[79]	CEM I 42.5 R Portland	400	0	152	[kg/m^3]	4	-	-	0.38
151	[79]	CEM I 42.5 R Portland	400	0	152	[kg/m^3]	4	-	-	0.38
152	[79]	CEM I 42.5 R Portland	400	20	152	[kg/m^3]	4	-	-	0.38
153	[79]	CEM I 42.5 R Portland	400	20	152	[kg/m^3]	4	-	-	0.38
154	[79]	CEM I 42.5 R Portland	400	20	152	[kg/m^3]	4	-	-	0.38
155	[79]	CEM I 42.5 R Portland	400	20	152	[kg/m^3]	4	-	-	0.38
156	[79]	CEM I 42.5 R Portland	400	20	152	[kg/m^3]	4	-	-	0.38
157	[79]	CEM I 42.5 R Portland	400	40	152	[kg/m^3]	4	-	-	0.38
158	[79]	CEM I 42.5 R Portland	400	40	152	[kg/m^3]	4	-	-	0.38
159	[79]	CEM I 42.5 R Portland	400	40	152	[kg/m^3]	4	-	-	0.38
160	[79]	CEM I 42.5 R Portland	400	40	152	[kg/m^3]	4	-	-	0.38
161	[79]	CEM I 42.5 R Portland	400	40	152	[kg/m^3]	4	-	-	0.38
162	[79]	CEM I 42.5 R Portland	400	60	152	[kg/m^3]	4	-	-	0.38
163	[79]	CEM I 42.5 R Portland	400	60	152	[kg/m^3]	4	-	-	0.38
164	[79]	CEM I 42.5 R Portland	400	60	152	[kg/m^3]	4	-	-	0.38
165	[79]	CEM I 42.5 R Portland	400	60	152	[kg/m^3]	4	-	-	0.38
166	[79]	CEM I 42.5 R Portland	400	60	152	[kg/m^3]	4	-	-	0.38
167	[80]	Type I	430	43	133	-	-	-	9	0.31
168	[80]	Type I	431	43	133	-	-	-	9	0.31
169	[80]	Type I	432	43	133	-	-	-	9	0.31
170	[80]	Type I	433	43	133	-	-	-	9	0.31
171	[80]	Type I	434	43	133	-	-	-	9	0.31
172	[81]	Blast-furnace slag	550	-	191	-	-	[kg/m^3]	16.5	0.35
173	[81]	Blast-furnace slag	550	-	191	-	-	[kg/m^3]	16.5	0.35
174	[81]	Blast-furnace slag	550	-	191	-	-	[kg/m^3]	16.5	0.35
175	[81]	Blast-furnace slag	550	-	191	-	-	[kg/m^3]	16.5	0.35
176	[81]	Blast-furnace slag	550	-	191	-	-	[kg/m^3]	16.5	0.35
177	[81]	Blast-furnace slag	550	-	191	-	-	[kg/m^3]	16.5	0.35
178	[81]	Blast-furnace slag	550	-	191	-	-	[kg/m^3]	16.5	0.35
179	[81]	Blast-furnace slag	550	-	191	-	-	[kg/m^3]	16.5	0.35
180	[81]	Blast-furnace slag	550	-	191	-	-	[kg/m^3]	16.5	0.35
181	[81]	Blast-furnace slag	550	-	191	-	-	[kg/m^3]	16.5	0.35
182	[81]	Blast-furnace slag	550	-	191	-	-	[kg/m^3]	16.5	0.35
183	[81]	Blast-furnace slag	550	-	191	-	-	[kg/m^3]	16.5	0.35
184	[81]	Blast-furnace slag	550	-	191	-	-	[kg/m^3]	16.5	0.35
185	[81]	Blast-furnace slag	550	-	191	-	-	[kg/m^3]	16.5	0.35
186	[81]	Blast-furnace slag	550	-	191	-	-	[kg/m^3]	16.5	0.35
187	[81]	Blast-furnace slag	550	-	191	-	-	[kg/m^3]	16.5	0.35
188	[81]	Blast-furnace slag	550	-	191	-	-	[kg/m^3]	16.5	0.35
189	[81]	Blast-furnace slag	550	-	191	-	-	[kg/m^3]	16.5	0.35
190	[81]	Blast-furnace slag	550	-	191	-	-	[kg/m^3]	16.5	0.35
191	[81]	Blast-furnace slag	550	-	191	-	-	[kg/m^3]	16.5	0.35
192	[81]	Blast-furnace slag	550	-	191	-	-	[kg/m^3]	16.5	0.35
193	[81]	Blast-furnace slag	550	-	191	-	-	[kg/m^3]	16.5	0.35
194	[81]	Blast-furnace slag	550	-	191	-	-	[kg/m^3]	16.5	0.35
195	[81]	Blast-furnace slag	550	-	191	-	-	[kg/m^3]	16.5	0.35

Table B.10: Database of FRC mixes. Paste phase information 5/5

Id	Ref.	Cem1 inf.	Cem1 q. [kg/m^3]	Microsil. [kg/m^3]	Sil. fume [kg/m^3]	Fly ash [kg/m^3]	Slag [kg/m^3]	Add. total [kg/m^3]	Water [kg/m^3]	Supl. info	Supl. q.	w/c
196	[81]	Blast-furnace slag	550	-	-	-	-	0	191	[kg/m^3]	16.5	0.35
197	[81]	Blast-furnace slag	550	-	-	-	-	0	191	[kg/m^3]	16.5	0.35
198	[81]	Blast-furnace slag	550	-	-	-	-	0	191	[kg/m^3]	16.5	0.35
199	[81]	Blast-furnace slag	550	-	-	-	-	0	191	[kg/m^3]	16.5	0.35
200	[81]	Blast-furnace slag	550	-	-	-	-	0	191	[kg/m^3]	16.5	0.35
201	[81]	Blast-furnace slag	550	-	-	-	-	0	191	[kg/m^3]	16.5	0.35
202	[82]	CEM I 42.5R	359	-	-	-	-	0	97	Glenium 77SCC [kg/m^3]	6.9	0.29
203	[82]	CEM I 42.5R	402	-	-	-	-	0	108	Glenium 77SCC [kg/m^3]	7.6	0.29
204	[83]	-	-	-	-	-	-	0	-	-	-	0.35
205	[83]	-	-	-	-	-	-	0	-	-	-	0.35
206	[83]	-	-	-	-	-	-	0	-	-	-	0.35
207	[83]	-	-	-	-	-	-	0	-	-	-	0.35
208	[83]	-	-	-	-	-	-	0	-	-	-	0.35
209	[83]	-	-	-	-	-	-	0	-	-	-	0.35
210	[83]	-	-	-	-	-	-	0	-	-	-	0.35
211	[83]	-	-	-	-	-	-	0	-	-	-	0.35
212	[83]	-	-	-	-	-	-	0	-	-	-	0.35
213	[83]	-	-	-	-	-	-	0	-	-	-	0.35
214	[83]	-	-	-	-	-	-	0	-	-	-	0.35
215	[83]	-	-	-	-	-	-	0	-	-	-	0.35
216	[83]	-	-	-	-	-	-	0	-	-	-	0.35
217	[83]	-	-	-	-	-	-	0	-	-	-	0.35
218	[83]	-	-	-	-	-	-	0	-	-	-	0.35
219	[83]	-	-	-	-	-	-	0	-	-	-	0.35
220	[180]	Portland CEM I 42.5 R	-	-	-	-	-	0	-	-	-	0.25
221	[180]	Portland CEM I 42.5 R	-	-	-	-	-	0	-	-	-	0.25
222	[180]	Portland CEM I 42.5 R	-	-	-	-	-	0	-	-	-	0.2
223	[180]	Portland CEM I 42.5 R	-	-	-	-	-	0	-	-	-	0.2
224	[58]	CEM I 52.5R	567	-	40	-	170	210	192	BASF Glennium 51	6.2	0.34
225	[85]	CEM I 52.5R	405	45	-	-	-	45	125	Acrilics	12	0.31
226	[85]	CEM I 52.5R	457	46	-	-	-	46	143	Acrilics	17.8	0.31

Table B.11: Database of FRC mixes. Fibres information 1/5

Id	Ref.	F1 info.	$\lambda_f 1$ [-]	$l_f 1$ [mm]	$d_f 1$ [mm]	$\sigma_{fu} 1$ [MPa]	F1 q. [kg/m^3]	F2 info.	$\lambda_f 2$ [-]	$l_f 2$ [mm]	$d_f 2$ [mm]	$\sigma_{fu} 2$ [MPa]	F2 q. [kg/m^3]	V_f [%]
1	[94]	None	-	-	-	-	0	-	-	-	-	-	-	0
2	[94]	Hooked end DRAMIX cold drawn	-	30	-	2100	20	-	-	-	-	-	-	0.25
3	[94]	Hooked end DRAMIX cold drawn	-	30	-	2100	40	-	-	-	-	-	-	0.51
4	[94]	Hooked end DRAMIX cold drawn	-	30	-	2100	60	-	-	-	-	-	-	0.76
5	[94]	None	-	-	-	-	0	-	-	-	-	-	-	0
6	[94]	Hooked end DRAMIX cold drawn	-	60	-	2100	20	-	-	-	-	-	-	0.25
7	[94]	Hooked end DRAMIX cold drawn	-	60	-	2100	40	-	-	-	-	-	-	0.51
8	[94]	Hooked end DRAMIX cold drawn	-	60	-	2100	60	-	-	-	-	-	-	0.76
9	[94]	Hooked end DRAMIX cold drawn	-	30	-	2100	20	-	-	-	-	-	-	0.25
10	[94]	Hooked end DRAMIX cold drawn	-	30	-	2100	40	-	-	-	-	-	-	0.51
11	[94]	Hooked end DRAMIX cold drawn	-	30	-	2100	60	-	-	-	-	-	-	0.76
12	[94]	Hooked end DRAMIX cold drawn	-	60	-	2100	20	-	-	-	-	-	-	0.25
13	[94]	Hooked end DRAMIX cold drawn	-	60	-	2100	20	-	-	-	-	-	-	0.25
14	[94]	Hooked end DRAMIX cold drawn	-	60	-	2100	40	-	-	-	-	-	-	0.51
15	[94]	Hooked end DRAMIX cold drawn	-	60	-	2100	40	-	-	-	-	-	-	0.51
16	[94]	Hooked end DRAMIX cold drawn	-	60	-	2100	40	-	-	-	-	-	-	0.51
17	[94]	None	-	-	-	-	0	-	-	-	-	-	-	0
18	[94]	RC-80/30-CP	79	30	0.38	3000	20	-	-	-	-	-	-	0.30
19	[94]	RC-80/30-CP	79	30	0.38	3000	40	-	-	-	-	-	-	0.50
20	[94]	RC-80/60-BP + RC-80/30-CP	79	30	0.38	3000	40	-	-	-	-	-	-	0.50
21	[94]	RC-80/30-CP	79	30	0.38	3000	60	-	-	-	-	-	-	0.80
22	[13]	Type I	65	13	0.2	1800	176	-	-	-	-	-	0	2.2
23	[13]	Type I	65	13	0.2	1800	175	-	-	-	-	-	0	2.2
24	[13]	Type I	65	13	0.2	1800	173	-	-	-	-	-	0	2.2
25	[13]	Type I	65	13	0.2	1800	89	-	-	-	-	-	0	1.1
26	[13]	Both Types	65	13	0.2	1800	107	-	60	30	0.5	1000	71	2.3
27	[13]	Type II	-	-	-	-	0	-	60	30	0.5	1000	173	2.2
28	[13]	Both Types	65	13	0.2	1800	131	-	60	30	0.5	1000	43	2.2
29	[65]	0	0	0	0	0	0	-	-	-	-	-	-	0
30	[65]	0	0	0	0	0	0	-	-	-	-	-	-	0
31	[65]	RC-45/30-CN	48	30	0.62	1250	50	-	-	-	-	-	-	0.64
32	[65]	RC-80/30-BP	86	30	0.38	2300	50	-	-	-	-	-	-	0.64
33	[65]	RC-45/30-CN	48	30	0.62	1250	50	-	-	-	-	-	-	0.64
34	[65]	RC-80/30-BP	86	30	0.38	2300	50	-	-	-	-	-	-	0.64
35	[87]	0	0	0	0	0	0	-	-	-	-	-	-	0
36	[87]	0	0	0	0	0	0	-	-	-	-	-	-	0
37	[87]	Dramix OL 13/0.20	65	13	0.2	2000	63	-	-	-	-	-	-	0.8
38	[87]	Dramix OL 13/0.20	65	13	0.2	2000	63	-	-	-	-	-	-	0.8
39	[87]	Dramix OL 13/0.20	65	13	0.2	2000	125	-	-	-	-	-	-	1.6
40	[87]	Dramix OL 13/0.20	65	13	0.2	2000	125	-	-	-	-	-	-	1.6
41	[88]	Type I-SS0215	75	15	0.2	2300	78.8	-	-	-	-	-	-	1
42	[88]	Type I-SS0215	75	15	0.2	2300	78.8	-	-	-	-	-	-	1
43	[88]	Type I-SS0215	75	15	0.2	2300	78.8	-	-	-	-	-	-	1
44	[88]	Type I-SS0215	75	15	0.2	2300	78.8	-	-	-	-	-	-	1
45	[88]	Type III-SS0225	125	25	0.2	2300	78.8	-	-	-	-	-	-	1
46	[88]	Type III-SS0225	125	25	0.2	2300	78.8	-	-	-	-	-	-	1
47	[88]	Type II-SS0220	100	20	0.2	2300	117.75	-	-	-	-	-	-	1.5
48	[88]	Type I-SS0215	75	15	0.2	2300	78.8	-	-	-	-	-	-	1

Table B.12: Database of FRC mixes. Fibres information 2/5

Id	Ref.	F1 info.	$\lambda_f 1$ [-]	$l_f 1$ [mm]	$d_f 1$ [mm]	$\sigma_{fu} 1$ [MPa]	F1 q. [kg/m^3]	V_f [%]
49	[89]	RC65/40BN	65	40	0.62	1225	60	0.8
50	[89]	RC65/40BN	65	40	0.62	1225	60	0.8
51	[89]	None	-	-	-	-	0	0
52	[89]	RC65/40BN	65	40	0.62	1225	60	0.8
53	[89]	RC65/40BN	65	40	0.62	1225	60	0.8
54	[89]	RC65/40BN	65	40	0.62	1225	60	0.8
55	[89]	RC65/40BN	65	40	0.62	1225	60	0.8
56	[89]	RC65/40BN	65	40	0.62	1225	60	0.8
57	[89]	RC65/40BN	65	40	0.62	1225	60	0.8
58	[89]	None	-	-	-	-	0	0
59	[89]	Carbon Hooked 50/0.80	63	50	0.8	1100	50	0.6
60	[89]	Carbon Hooked 50/0.80	63	50	0.8	1100	75	1
61	[89]	65/40 BN	65	40	0.62	1225	50	0.6
62	[89]	80/40 BP	80	40	0.5	3070	50	0.6
63	[89]	80/50 BN	80	50	0.63	1225	50	0.6
64	[89]	65/40 BN	65	40	0.63	1225	50	0.6
65	[89]	80/50 BN	80	50	0.63	1225	50	0.6
66	[89]	65/40 BN	65	40	0.63	1225	50	0.6
67	[89]	80/40 BP	80	40	0.5	3070	50	0.6
68	[89]	None	-	-	-	-	0	0
69	[89]	45/50 BN	45	50	1.11	1225	50	0.6
70	[89]	80/40 BP	80	40	0.5	3070	50	0.6
71	[89]	None	-	-	-	-	0	0
72	[89]	80/30 BP	80	30	0.38	3070	50	0.6
73	[89]	None	-	-	-	-	0	0
74	[89]	80/50 BN	80	50	0.63	1225	50	0.6
75	[89]	45/50 BN	45	50	1.11	1225	50	0.6
76	[89]	80/30 BP	80	30	0.38	3070	50	0.6
77	[89]	None	-	-	-	-	0	0
78	[89]	None	-	-	-	-	0	0
79	[89]	None	-	-	-	-	0	0
80	[89]	None	-	-	-	-	0	0
81	[89]	65/40 BN	65	45	0.69	1225	50	0.6
82	[89]	80/50 BN	80	50	0.63	1225	50	0.6
83	[89]	Low carbon steel with hooked-end (RC 65/40 BN)	65	40	0.62	1225	0	0
84	[89]	Low carbon steel with hooked-end (RC 65/40 BN)	65	40	0.62	1225	50	0.6
85	[89]	Low carbon steel with hooked-end (RC 65/40 BN)	65	40	0.62	1225	70	0.9
86	[90]	Micro-wire steel fibres	40-60	6-9	0.15	-	192	2.5
87	[91, 179]	Micro-wire steel fibres	-	-	0.19	-	196	2.5
88	[92]	Micro-wire steel fibres	-	-	0.19	-	196	2.5
89	[93]	None	-	-	-	-	0	0
90	[93]	Cold-drawn steel fibres with hooked ends	55	60	0.75	1050	21	0.3
91	[93]	Cold-drawn steel fibres with hooked ends	55	60	0.75	1050	40	0.5
92	[93]	Cold-drawn steel fibres with hooked ends	55	60	0.75	1050	62	0.8
93	[93]	Cold-drawn steel fibres with hooked ends	65	60	0.9	1000	21	0.3
94	[93]	Cold-drawn steel fibres with hooked ends	65	60	0.9	1000	40	0.5
95	[93]	Cold-drawn steel fibres with hooked ends	65	60	0.9	1000	62	0.8
96	[93]	Cold-drawn steel fibres with hooked ends	80	30	0.55	1150	21	0.3
97	[93]	Cold-drawn steel fibres with hooked ends	80	30	0.55	1150	40	0.5

Table B.13: Database of FRC mixes. Fibres information 3/5

Id	Ref.	F1 info.	$\lambda_f 1$ [-]	$l_f 1$ [mm]	$d_f 1$ [mm]	$\sigma_{fu} 1$ [MPa]	F1 q. [kg/m^3]	V_f [%]
98	[93]	Cold-drawn steel fibres with hooked ends	80	30	0.55	1150	62	0.8
99	[93]	None	-	-	-	-	0	0
100	[93]	Cold-drawn steel fibres with hooked ends	55	60	0.75	1050	21	0.3
101	[93]	Cold-drawn steel fibres with hooked ends	55	60	0.75	1050	40	0.5
102	[93]	Cold-drawn steel fibres with hooked ends	55	60	0.75	1050	62	0.8
103	[93]	Cold-drawn steel fibres with hooked ends	65	60	0.9	1000	21	0.3
104	[93]	Cold-drawn steel fibres with hooked ends	65	60	0.9	1000	40	0.5
105	[93]	Cold-drawn steel fibres with hooked ends	65	60	0.9	1000	62	0.8
106	[93]	Cold-drawn steel fibres with hooked ends	80	30	0.55	1150	21	0.3
107	[93]	Cold-drawn steel fibres with hooked ends	80	30	0.55	1150	40	0.5
108	[93]	Cold-drawn steel fibres with hooked ends	80	30	0.55	1150	62	0.8
109	[29]	-	-	20/25	-	20/25	153	1.9
110	[29]	-	-	13	-	13	157	2
111	[29]	-	-	20	-	20	159	2
112	[29]	-	-	13	-	13	161	2
113	[86]	None	-	-	-	-	0	0
114	[86]	Dramix hooked-end RL 45/30 BN	45	30	0.67	1100	39.3	0.5
115	[86]	Dramix hooked-end RL 45/30 BN	45	30	0.67	1100	78.5	1
116	[86]	Dramix hooked-end RC 80/60 BN	80	60	0.75	1100	78.5	1
117	[95]	-	-	-	-	-	-	0
118	[95]	-	-	-	-	-	-	0
119	[95]	-	-	-	-	-	-	0
120	[95]	-	-	-	-	-	-	0
121	[95]	-	-	-	-	-	-	0
122	[95]	-	-	-	-	-	-	0
123	[95]	-	-	-	-	-	-	0
124	[96]	None	-	-	-	-	0	0
125	[96]	None	-	-	-	-	0	0
126	[96]	Low carbon steel hooked-end steel	64	35	0.55	1100	50	0.6
127	[96]	Low carbon steel hooked-end steel	64	35	0.55	1100	50	0.6
128	[96]	Low carbon steel hooked-end steel	64	35	0.55	1100	50	0.6
129	[97]	None	-	-	-	-	0	0
130	[97]	Dramix RL 45/50 BN	-	50	-	-	78.8	1
131	[97]	Novotex 1050	-	50	-	-	78.8	1
132	[98]	Stratec Steel 15/0.20	75	15	0.2	2000	155	2
133	[98]	Stratec Steel 15/0.20	75	15	0.2	2000	155	2
134	[98]	Stratec Steel 15/0.20	75	15	0.2	2000	155	2
135	[98]	Stratec Steel 15/0.20	75	15	0.2	2000	155	2
136	[77]	None	0	0	0	0	0	0
137	[77]	None	0	0	0	0	0	0
138	[77]	None	0	0	0	0	0	0
139	[77]	Dramix RC-BN 35/65	64	35	0.55	1000	60	0.8
140	[77]	None	0	0	0	0	0	0
141	[77]	Dramix RC-65/60-BN	67	60	0.9	1000	60	0.8
142	[77]	Dramix RC-65/60-BN	67	60	0.9	1000	60	0.8
143	[77]	None	0	0	0	0	0	0
144	[77]	None	0	0	0	0	0	0

Table B.14: Database of FRC mixes. Fibres information 4/5

Id	Ref.	F1 info.	$\lambda_f 1$ [-]	$l_f 1$ [mm]	$d_f 1$ [mm]	$\sigma_{fu} 1$ [MPa]	F1 q. [kg/m^3]	V_f [%]
145	[78]	Dramix ZP 30/0.5	60	30	0.5	1000	60	0.8
146	[78]	Dramix RC-BN 65/60	67	60	0.9	1000	60	0.8
147	[79]	None	-	-	-	-	0	0
148	[79]	Dramix RC 65/40 CN	65	40	0.615	1100	39	0.5
149	[79]	Dramix RC 65/40 CN	65	40	0.615	1100	78	1
150	[79]	Dramix RC 80/60 BN	80	60	0.75	1100	39	0.5
151	[79]	Dramix RC 80/60 BN	80	60	0.75	1100	78	1
152	[79]	None	-	-	-	-	0	0
153	[79]	Dramix RC 65/40 CN	65	40	0.615	1100	39	0.5
154	[79]	Dramix RC 65/40 CN	65	40	0.615	1100	78	1
155	[79]	Dramix RC 80/60 BN	80	60	0.75	1100	39	0.5
156	[79]	Dramix RC 80/60 BN	80	60	0.75	1100	78	1
157	[79]	None	-	-	-	-	0	0
158	[79]	Dramix RC 65/40 CN	65	40	0.615	1100	39	0.5
159	[79]	Dramix RC 65/40 CN	65	40	0.615	1100	78	1
160	[79]	Dramix RC 80/60 BN	80	60	0.75	1100	39	0.5
161	[79]	Dramix RC 80/60 BN	80	60	0.75	1100	78	1
162	[79]	None	-	-	-	-	0	0
163	[79]	Dramix RC 65/40 CN	65	40	0.615	1100	39	0.5
164	[79]	Dramix RC 65/40 CN	65	40	0.615	1100	78	1
165	[79]	Dramix RC 80/60 BN	80	60	0.75	1100	39	0.5
166	[79]	Dramix RC 80/60 BN	80	60	0.75	1100	78	1
167	[80]	None	-	-	-	-	0	0
168	[80]	Hooked steel	64	35	0.55	-	39.25	0.5
169	[80]	Hooked steel	64	35	0.55	-	78.5	1
170	[80]	Hooked steel	64	35	0.55	-	117.75	1.5
171	[80]	Hooked steel	64	35	0.55	-	157	2
172	[81]	None	0	0	0	0	0	0
173	[81]	Hooked steel	60	30	0.5	1250	39.25	0.5
174	[81]	Hooked steel	60	30	0.5	1250	78.5	1
175	[81]	Hooked steel	60	30	0.5	1250	157	2
176	[81]	Hooked steel	75	60	0.8	1100	39.25	0.5
177	[81]	Hooked steel	75	60	0.8	1100	78.5	1
178	[81]	Hooked steel	75	60	0.8	1100	157	2
179	[81]	Hooked steel	83	50	0.6	1200	39.25	0.5
180	[81]	Hooked steel	83	50	0.6	1200	78.5	1
181	[81]	Hooked steel	83	50	0.6	1200	157	2
182	[81]	None	0	0	0	0	0	0
183	[81]	Hooked steel	60	30	0.5	1250	39.25	0.5
184	[81]	Hooked steel	60	30	0.5	1250	78.5	1
185	[81]	Hooked steel	60	30	0.5	1250	157	2
186	[81]	Hooked steel	75	60	0.8	1100	39.25	0.5
187	[81]	Hooked steel	75	60	0.8	1100	78.5	1
188	[81]	Hooked steel	75	60	0.8	1100	157	2
189	[81]	Hooked steel	83	50	0.6	1200	39.25	0.5
190	[81]	Hooked steel	83	50	0.6	1200	78.5	1
191	[81]	Hooked steel	83	50	0.6	1200	157	2
192	[81]	None	0	0	0	0	0	0
193	[81]	Hooked steel	60	30	0.5	1250	39.25	0.5
194	[81]	Hooked steel	60	30	0.5	1250	78.5	1
195	[81]	Hooked steel	60	30	0.5	1250	157	2

Table B.15: Database of FRC mixes. Fibres information 5/5

Id	Ref.	F1 info.	$\lambda_f 1$ [-]	$l_f 1$ [mm]	$d_f 1$ [mm]	$\sigma_{fu} 1$ [MPa]	F1 q. [kg/m^3]	F2 info.	$\lambda_f 2$ [-]	$l_f 2$ [mm]	$d_f 2$ [mm]	$\sigma_{fu} 2$ [MPa]	F2 q. [kg/m^3]	V_f [%]
196	[81]	Hooked steel	75	60	0.8	1100	39.25	-	-	-	-	-	-	0.5
197	[81]	Hooked steel	75	60	0.8	1100	78.5	-	-	-	-	-	-	1
198	[81]	Hooked steel	75	60	0.8	1100	157	-	-	-	-	-	-	2
199	[81]	Hooked steel	83	50	0.6	1200	39.25	-	-	-	-	-	-	0.5
200	[81]	Hooked steel	83	50	0.6	1200	78.5	-	-	-	-	-	-	1
201	[81]	Hooked steel	83	50	0.6	1200	157	-	-	-	-	-	-	2
202	[82]	Type A hooked end steel fibres	80	60	0.75	1100	30	-	-	-	-	-	-	0.4
203	[82]	Type A hooked end steel fibres	80	60	0.75	1100	30	-	-	-	-	-	-	0.4
204	[83]	None	-	-	-	-	-	None	-	-	-	-	-	0
205	[83]	Fibre size 0.6x2.0x50	40	50	-	801	78.8	Fibre size 0.6x2.0x25	20	25	-	826	0	1
206	[83]	Fibre size 0.6x2.0x50	40	50	-	801	51.22	Fibre size 0.6x2.0x25	20	25	-	826	27.58	1
207	[83]	Fibre size 0.6x2.0x50	40	50	-	801	39.4	Fibre size 0.6x2.0x25	20	25	-	826	39.4	1
208	[83]	Fibre size 0.6x2.0x50	40	50	-	801	27.58	Fibre size 0.6x2.0x25	20	25	-	826	51.22	1
209	[83]	Fibre size 0.6x2.0x50	40	50	-	801	0	Fibre size 0.6x2.0x25	20	25	-	826	78.8	1
210	[83]	Fibre size 0.6x2.0x50	40	50	-	801	118.2	Fibre size 0.6x2.0x25	20	25	-	826	0	1.5
211	[83]	Fibre size 0.6x2.0x50	40	50	-	801	76.83	Fibre size 0.6x2.0x25	20	25	-	826	41.37	1.5
212	[83]	Fibre size 0.6x2.0x50	40	50	-	801	59.1	Fibre size 0.6x2.0x25	20	25	-	826	59.1	1.5
213	[83]	Fibre size 0.6x2.0x50	40	50	-	801	41.37	Fibre size 0.6x2.0x25	20	25	-	826	76.83	1.5
214	[83]	Fibre size 0.6x2.0x50	40	50	-	801	0	Fibre size 0.6x2.0x25	20	25	-	826	118.2	1.5
215	[83]	Fibre size 0.6x2.0x50	40	50	-	801	157.6	Fibre size 0.6x2.0x25	20	25	-	826	0	2
216	[83]	Fibre size 0.6x2.0x50	40	50	-	801	102.44	Fibre size 0.6x2.0x25	20	25	-	826	55.16	2
217	[83]	Fibre size 0.6x2.0x50	40	50	-	801	78.8	Fibre size 0.6x2.0x25	20	25	-	826	78.8	2
218	[83]	Fibre size 0.6x2.0x50	40	50	-	801	55.16	Fibre size 0.6x2.0x25	20	25	-	826	102.44	2
219	[83]	Fibre size 0.6x2.0x50	40	50	-	801	0	Fibre size 0.6x2.0x25	20	25	-	826	157.6	2
220	[180]	None	-	-	-	-	0	-	-	-	-	-	-	0
221	[180]	Straight and smooth steel wire fibers	75	15	0.2	2000	155	-	-	-	-	-	-	2
222	[180]	Straight and smooth steel wire fibers	75	15	0.2	2000	77.5	-	-	-	-	-	-	1
223	[180]	Straight and smooth steel wire fibers	75	15	0.2	2000	155	-	-	-	-	-	-	2
224	[58]	Steel fibers l/d=30/0.38	79	30	0.38	-	61.8	-	-	-	-	-	-	0.8
225	[85]	Low-carbon steel fibre 30/0.6	50	30	0.6	-	50	-	-	-	-	-	-	0.6
226	[85]	High-carbon steel fibre 30/0.5	60	30	0.5	-	80	-	-	-	-	-	-	1

Table B.16: Database of FRC mixes. Testing information 1/5

Id	Ref.	Comp. Spec.	f_{cm} [MPa]	f_{1cm} [MPa]	Elast. Spec.	E_c [GPa]	Ind. Tens. Spec.	f_{ct} [MPa]	Bend. Spec.	f_{Rm} [MPa]	Tens. Spec.	f_{ct} [MPa]	Workability test	Slump [mm]	Flow [mm]
1	[94]	Cyl. 150x300	58	55	-	-	-	-	-	-	-	-	-	160	-
2	[94]	Cyl. 150x300	66	63	-	-	-	-	-	-	-	-	-	210	-
3	[94]	Cyl. 150x300	60	57	-	-	-	-	-	-	-	-	-	210	-
4	[94]	Cyl. 150x300	58	55	-	-	-	-	-	-	-	-	-	180	-
5	[94]	Cyl. 150x300	65	62	-	-	-	-	-	-	-	-	-	-	825
6	[94]	Cyl. 150x300	64	60	-	-	-	-	-	-	-	-	-	-	745
7	[94]	Cyl. 150x300	63	60	-	-	-	-	-	-	-	-	-	-	805
8	[94]	Cyl. 150x300	60	57	-	-	-	-	-	-	-	-	-	-	825
9	[94]	Cyl. 150x300	64	61	-	-	-	-	-	-	-	-	-	-	740
10	[94]	Cyl. 150x300	58	55	-	-	-	-	-	-	-	-	-	-	770
11	[94]	Cyl. 150x300	61	58	-	-	-	-	-	-	-	-	-	-	650
12	[94]	Cyl. 150x300	65	62	-	-	-	-	-	-	-	-	-	-	705
13	[94]	Cyl. 150x300	65	62	-	-	-	-	-	-	-	-	-	-	705
14	[94]	Cyl. 150x300	70	67	-	-	-	-	-	-	-	-	-	-	725
15	[94]	Cyl. 150x300	71	67	-	-	-	-	-	-	-	-	-	-	656
16	[94]	Cyl. 150x300	72	69	-	-	-	-	-	-	-	-	-	-	790
17	[94]	Cyl. 150x300	69	65	-	-	-	-	-	-	-	-	-	-	-
18	[94]	Cyl. 150x300	53	50	-	-	-	3.97	EN 14651	4.37	-	-	-	-	-
19	[94]	Cyl. 150x300	65	61	-	-	-	4.63	EN 14651	7.37	-	-	-	-	-
20	[94]	Cyl. 150x300	56	53	-	-	-	5.50	EN 14651	9.07	-	-	-	-	-
21	[94]	Cyl. 150x300	67	63	-	-	-	5.90	EN 14651	10.11	-	-	-	-	-
22	[13]	Cyl. 100x200	161	153	Cyl. 100x200	44.0	Split cyl. 100x200	19.20	ASTM C1018	29.80	-	-	ASTM C230-03	-	170
23	[13]	Cyl. 100x200	160	152	Cyl. 100x200	45.0	Split cyl. 100x200	20.90	ASTM C1018	26.40	-	-	ASTM C230-03	-	180
24	[13]	Cyl. 100x200	149	142	Cyl. 100x200	43.0	Split cyl. 100x200	21.90	ASTM C1018	23.20	-	-	ASTM C230-03	-	210
25	[13]	Cyl. 100x200	164	156	Cyl. 100x200	43.0	Split cyl. 100x200	18.00	ASTM C1018	14.80	-	-	ASTM C230-03	-	170
26	[13]	Cyl. 100x200	171	163	Cyl. 100x200	49.0	Split cyl. 100x200	22.40	ASTM C1018	26.30	-	-	ASTM C230-03	-	150
27	[13]	Cyl. 100x200	157	149	Cyl. 100x200	40.0	Split cyl. 100x200	18.30	ASTM C1018	25.20	-	-	ASTM C230-03	-	210
28	[13]	Cyl. 100x200	169	161	Cyl. 100x200	46.0	Split cyl. 100x200	23.50	ASTM C1018	23.80	-	-	ASTM C230-03	-	180
29	[65]	Cube 100	85	57	Cyl. 80x240	41.4	Cyl. 80x240	4.43	0	0	-	-	-	-	-
30	[65]	Cube 100	86	58	Cyl. 80x240	41.6	Cyl. 80x240	3.69	0	0	-	-	-	-	-
31	[65]	Cube 100	82	56	Cyl. 80x240	44.2	Cyl. 80x240	4.65	UNI 11039	2.18	-	-	-	-	-
32	[65]	Cube 100	93	63	Cyl. 80x240	43.1	Cyl. 80x240	5.18	UNI 11039	8.61	-	-	-	-	-
33	[65]	Cube 100	84	56	Cyl. 80x240	42.3	Cyl. 80x240	4.43	UNI 11039	2.18	-	-	-	-	-
34	[65]	Cube 100	84	57	Cyl. 80x240	43.5	Cyl. 80x240	4.72	UNI 11039	8.61	-	-	-	-	-
35	[87]	Cube 100	141	134	-	-	Cube 100	11.53	-	-	Dog-Bone 180x160	3.66	Slump flow, (H 30 cm, UD20 LD10)	1050	-
36	[87]	Cube 100	137	130	-	-	Cube 100	10.38	-	-	Dog-Bone 180x160	3.66	Slump flow, (H 30 cm, UD20 LD10)	820	-
37	[87]	Cube 100	148	140	-	-	Cube 100	16.27	-	-	Dog-Bone 180x160	6.20	Slump flow, (H 30 cm, UD20 LD10)	775	-
38	[87]	Cube 100	144	137	-	-	Cube 100	13.69	-	-	Dog-Bone 180x160	6.20	Slump flow, (H 30 cm, UD20 LD10)	970	-
39	[87]	Cube 100	147	139	-	-	Cube 100	17.00	-	-	Dog-Bone 180x160	9.10	Slump flow, (H 30 cm, UD20 LD10)	995	-
40	[87]	Cube 100	147	140	-	-	Cube 100	15.80	-	-	Dog-Bone 180x160	9.10	Slump flow, (H 30 cm, UD20 LD10)	930	-
41	[88]	Cyl. 100x200	125	119	Cyl. 100x200	40.0	-	-	ASTM C1018	13.00	-	-	ASTM C230M, 2003	-	210
42	[88]	Cyl. 100x200	126	120	Cyl. 100x200	40.0	-	-	ASTM C1018	15.60	-	-	ASTM C230M, 2003	-	210
43	[88]	Cyl. 100x200	135	128	Cyl. 100x200	42.3	-	-	ASTM C1018	13.60	-	-	ASTM C230M, 2003	-	210
44	[88]	Cyl. 100x200	122	116	Cyl. 100x200	42.3	-	-	ASTM C1018	13.60	-	-	ASTM C230M, 2003	-	210
45	[88]	Cyl. 100x200	140	133	Cyl. 100x200	45.0	-	-	ASTM C1018	19.70	-	-	ASTM C230M, 2003	-	200
46	[88]	Cyl. 100x200	140	133	Cyl. 100x200	45.0	-	-	ASTM C1018	19.70	-	-	ASTM C230M, 2003	-	200
47	[88]	Cyl. 100x200	122	116	Cyl. 100x200	41.0	-	-	ASTM C1018	13.60	-	-	ASTM C230M, 2003	-	225
48	[88]	Cyl. 100x200	122	116	Cyl. 100x200	42.3	-	-	ASTM C1018	13.60	-	-	ASTM C230M, 2003	-	210

Table B.17: Database of FRC mixes. Testing information 2/5

Id	Ref.	Comp. Spec.	f_{cm} [MPa]	f_{1cm} [MPa]	Elast. Spec.	E_c [GPa]	Ind. Tens. Spec.	f_{ct} [MPa]	Bend. Spec.	f_{Rm} [MPa]	Tens. Spec.	f_{ct} [MPa]	Workability test	Slump [mm]	Flow [mm]
49	[89]	Cyl. 150x300	61	58	-	-	EN 14651	3.36	EN 14651	5.26	-	-	Slump flow EN 12350-8	-	550-710
50	[89]	Cyl. 150x300	66	62	-	-	EN 14651	4.39	EN 14651	8.13	-	-	Slump flow EN 12350-8	-	550-710
51	[89]	Cyl. 150x300	52	50	-	-	EN 14651	3.64	-	-	-	-	Slump flow EN 12350-8	-	550-710
52	[89]	Cyl. 150x300	65	62	-	-	EN 14651	4.70	EN 14651	8.35	-	-	Slump flow EN 12350-8	-	550-710
53	[89]	Cyl. 150x300	66	63	-	-	EN 14651	4.20	EN 14651	7.05	-	-	Slump flow EN 12350-8	-	550-710
54	[89]	Cyl. 150x300	60	57	-	-	EN 14651	4.45	EN 14651	7.46	-	-	Slump flow EN 12350-8	-	550-710
55	[89]	Cyl. 150x300	63	60	-	-	EN 14651	4.08	EN 14651	5.71	-	-	Slump flow EN 12350-8	-	550-710
56	[89]	Cyl. 150x300	70	67	-	-	EN 14651	4.33	EN 14651	6.39	-	-	Slump flow EN 12350-8	-	550-710
57	[89]	Cyl. 150x300	65	62	-	-	EN 14651	3.11	EN 14651	6.45	-	-	Slump flow EN 12350-8	-	550-710
58	[89]	Cyl. 150x300	39	37	EN 12390-3	33.5	EN 14651	3.00	-	-	-	-	Slump flow EN 12350-8	-	-
59	[89]	Cyl. 150x300	32	31	EN 12390-3	30.8	EN 14651	2.40	EN 14651	5.20	-	-	Slump flow EN 12350-8	-	-
60	[89]	Cyl. 150x300	33	31	EN 12390-3	32.1	EN 14651	2.50	EN 14651	6.00	-	-	Slump flow EN 12350-8	-	-
61	[89]	Cyl. 150x300	67	63	-	-	-	-	EN 14651	5.49	-	-	-	-	-
62	[89]	Cyl. 150x300	71	68	-	-	-	-	EN 14651	8.80	-	-	-	-	-
63	[89]	Cyl. 150x300	34	33	-	-	-	-	EN 14651	4.42	-	-	-	-	-
64	[89]	Cyl. 150x300	34	32	-	-	-	-	EN 14651	4.57	-	-	-	-	-
65	[89]	Cyl. 150x300	62	59	-	-	-	-	EN 14651	4.67	-	-	-	-	-
66	[89]	Cyl. 150x300	96	91	-	-	-	-	EN 14651	3.82	-	-	-	-	-
67	[89]	Cyl. 150x300	88	84	-	-	-	-	EN 14651	11.40	-	-	-	-	-
68	[89]	Cyl. 150x300	51	48	-	-	-	-	-	-	-	-	-	-	-
69	[89]	Cyl. 150x300	51	49	-	-	-	-	EN 14651	4.31	-	-	-	-	-
70	[89]	Cyl. 150x300	41	39	-	-	-	-	EN 14651	8.00	-	-	-	-	-
71	[89]	Cyl. 150x300	51	48	-	-	-	-	-	-	-	-	-	-	-
72	[89]	Cyl. 150x300	50	47	-	-	-	-	EN 14651	7.03	-	-	-	-	-
73	[89]	Cyl. 150x300	86	81	-	-	-	-	-	-	-	-	-	-	-
74	[89]	Cyl. 150x300	96	92	-	-	-	-	EN 14651	4.31	-	-	-	-	-
75	[89]	Cyl. 150x300	85	81	-	-	-	-	EN 14651	6.61	-	-	-	-	-
76	[89]	Cyl. 150x300	84	79	-	-	-	-	EN 14651	8.11	-	-	-	-	-
77	[89]	Cyl. 150x300	86	81	-	-	-	-	-	-	-	-	-	-	-
78	[89]	Cyl. 150x300	48	46	-	-	-	-	-	-	-	-	-	-	-
79	[89]	Cyl. 150x300	75	71	-	-	-	-	-	-	-	-	-	-	-
80	[89]	Cyl. 150x300	42	40	-	-	-	-	-	-	-	-	-	-	-
81	[89]	Cyl. 150x300	45	43	-	-	-	-	EN 14651	5.88	-	-	-	-	-
82	[89]	Cyl. 150x300	40	37	-	-	-	-	EN 14651	7.01	-	-	-	-	-
83	[89]	Cyl. 150x300	44	42	-	-	-	-	-	-	-	-	-	-	-
84	[89]	Cyl. 150x300	38	36	-	-	-	-	EN 14651	4.48	-	-	-	-	-
85	[89]	Cyl. 150x300	36	34	-	-	-	-	EN 14651	5.77	-	-	-	-	-
86	[90]	Cyl. 150x300 C 7d	189	180	-	-	-	-	-	-	-	-	DIN 1048	650	-
87	[91, 179]	Cyl. 100x200	180-200	-	-	45-50	-	-	-	-	-	-	-	-	-
88	[92]	Cyl. 100x200	180-200	-	-	45-50	-	-	-	-	-	-	-	-	-
89	[93]	Cyl. 150x300	62	58	Cyl. 150x300	47.7	Disc 150x60	-	-	-	-	-	Slump	130	-
90	[93]	Cyl. 150x300	57	54	Cyl. 150x300	44.0	Disc 150x60	-	-	-	-	-	Slump	100	-
91	[93]	Cyl. 150x300	61	58	Cyl. 150x300	41.7	Disc 150x60	-	-	-	-	-	Slump	110	-
92	[93]	Cyl. 150x300	61	58	Cyl. 150x300	45.4	Disc 150x60	-	-	-	-	-	Slump	110	-
93	[93]	Cyl. 150x300	57	54	Cyl. 150x300	43.9	Disc 150x60	-	-	-	-	-	Slump	110	-
94	[93]	Cyl. 150x300	63	60	Cyl. 150x300	45.3	Disc 150x60	-	-	-	-	-	Slump	120	-
95	[93]	Cyl. 150x300	61	58	Cyl. 150x300	44.9	Disc 150x60	-	-	-	-	-	Slump	130	-
96	[93]	Cyl. 150x300	59	56	Cyl. 150x300	46.6	Disc 150x60	-	-	-	-	-	Slump	120	-
97	[93]	Cyl. 150x300	64	60	Cyl. 150x300	45.2	Disc 150x60	-	-	-	-	-	Slump	120	-

Table B.18: Database of FRC mixes. Testing information 3/5

Id	Ref.	Comp. Spec.	f_{cm} [MPa]	f_{1cm} [MPa]	Elast. Spec.	E_c [GPa]	Ind. Tens. Spec.	f_{ct} [MPa]	Bend. Spec.	f_{Rm} [MPa]	Tens. Spec.	f_{ct} [MPa]	Workability test	Slump [mm]	Flow [mm]
98	[93]	Cyl. 150x300	63	60	Cyl. 150x300	46.0	Disc 150x60	-	-	-	-	-	Slump	120	-
99	[93]	Cyl. 150x300	32	30	Cyl. 150x300	37.2	Disc 150x60	-	-	-	-	-	Slump	120	-
100	[93]	Cyl. 150x300	31	29	Cyl. 150x300	35.5	Disc 150x60	-	-	-	-	-	Slump	130	-
101	[93]	Cyl. 150x300	32	31	Cyl. 150x300	34.1	Disc 150x60	-	-	-	-	-	Slump	110	-
102	[93]	Cyl. 150x300	31	30	Cyl. 150x300	34.4	Disc 150x60	-	-	-	-	-	Slump	100	-
103	[93]	Cyl. 150x300	32	31	Cyl. 150x300	36.1	Disc 150x60	-	-	-	-	-	Slump	120	-
104	[93]	Cyl. 150x300	31	30	Cyl. 150x300	37.9	Disc 150x60	-	-	-	-	-	Slump	110	-
105	[93]	Cyl. 150x300	34	33	Cyl. 150x300	38.0	Disc 150x60	-	-	-	-	-	Slump	110	-
106	[93]	Cyl. 150x300	32	30	Cyl. 150x300	38.7	Disc 150x60	-	-	-	-	-	Slump	120	-
107	[93]	Cyl. 150x300	33	31	Cyl. 150x300	37.6	Disc 150x60	-	-	-	-	-	Slump	110	-
108	[93]	Cyl. 150x300	31	30	Cyl. 150x300	35.7	Disc 150x60	-	-	-	-	-	Slump	100	-
109	[29]	Cyl. 75x150	125	119	-	-	-	-	C1609	22.27	-	-	-	-	-
110	[29]	Cyl. 75x150	137	131	-	-	-	-	C1609	22.06	-	-	-	-	-
111	[29]	Cyl. 75x150	125	118	-	-	-	-	C1609	18.41	-	-	-	-	-
112	[29]	Cyl. 75x150	124	117	-	-	-	-	C1609	18.51	-	-	-	-	-
113	[86]	Cyl. 100x200	38	35	-	-	ASTM C496/C496M	2.88	-	-	-	-	-	-	-
114	[86]	Cyl. 100x200	37	34	-	-	-	-	EN 14651	2.20	Cardoso et al.	2.51	-	-	-
115	[86]	Cyl. 100x200	41	38	-	-	-	-	EN 14651	6.57	Cardoso et al.	3.34	-	-	-
116	[86]	Cyl. 100x200	40	37	-	-	-	-	EN 14651	8.23	Cardoso et al.	3.15	-	-	-
117	[95]	PCI	39	37	-	-	-	-	-	-	-	-	-	-	-
118	[95]	PCI	44	42	-	-	-	-	-	-	-	-	-	-	-
119	[95]	PCI	55	52	-	-	-	-	-	-	-	-	-	-	-
120	[95]	PCI	65	62	-	-	-	-	-	-	-	-	-	-	-
121	[95]	PCI	56	53	-	-	-	-	-	-	-	-	-	-	-
122	[95]	PCI	72	68	-	-	-	-	-	-	-	-	-	-	-
123	[95]	PCI	96	91	-	-	-	-	-	-	-	-	-	-	-
124	[96]	Eq 150x300	33	31	-	-	-	-	-	-	-	-	-	-	-
125	[96]	Eq 150x300	36	35	-	-	-	-	-	-	-	-	-	-	-
126	[96]	Eq 150x300	30	28	-	-	-	-	EN 14651	4.05	-	-	-	-	-
127	[96]	Eq 150x300	34	32	-	-	-	-	EN 14651	4.51	-	-	-	-	-
128	[96]	Eq 150x300	31	29	-	-	-	-	EN 14651	4.77	-	-	-	-	-
129	[97]	JSCE-SF5	52	49	-	-	-	-	ASTM C1018	-	-	-	-	-	-
130	[97]	JSCE-SF5	50	48	-	-	-	-	ASTM C1018	-	-	-	-	-	-
131	[97]	JSCE-SF5	49	46	-	-	-	-	ASTM C1018	-	-	-	-	-	-
132	[98]	Cube 100	166	158	-	-	-	-	-	-	-	-	-	-	-
133	[98]	Cube 100	125	119	-	-	-	-	-	-	-	-	-	-	-
134	[98]	Cube 100	139	132	-	-	-	-	-	-	-	-	-	-	-
135	[98]	Cube 100	164	155	-	-	-	-	-	-	-	-	-	-	-
136	[77]	Cube 100	47	32	-	-	-	-	-	-	-	-	-	-	-
137	[77]	Cube 100	121	81	-	-	-	-	-	-	-	-	-	-	-
138	[77]	Cube 100	115	77	-	-	-	-	-	-	-	-	-	-	-
139	[77]	Cube 100	124	84	-	-	-	-	-	-	-	-	-	-	-
140	[77]	Cube 100	124	84	-	-	-	-	-	-	-	-	-	-	-
141	[77]	Cube 100	129	88	-	-	-	-	-	-	-	-	-	-	-
142	[77]	Cube 100	124	83	-	-	-	-	-	-	-	-	-	-	-
143	[77]	Cube 100	119	80	-	-	-	-	-	-	-	-	-	-	-
144	[77]	Cube 100	119	80	-	-	-	-	-	-	-	-	-	-	-
145	[78]	Cube 150	117	88	-	-	Spl. prism. 150x150x600	6.70	ASTM C1018	9.20	-	-	No	-	-
146	[78]	Cube 150	114	85	-	-	Spl. prism. 150x150x600	5.60	ASTM C1018	10.10	-	-	No	-	-

Table B.19: Database of FRC mixes. Testing information 4/5

Id	Ref.	Comp. Spec.	f_{cm} [MPa]	f_{1cm} [MPa]	Elast. Spec.	E_c [GPa]	Ind. Tens. Spec.	f_{ct} [MPa]	Bend. Spec.	f_{Rm} [MPa]	Tens. Spec.	f_{ct} [MPa]	Workability test	Slump [mm]	Flow [mm]
147	[79]	Cyl. 150x300	32	31	Cyl. 150x300	33.8	Split. test ϕ 100xE60	3.48	ASTM C1018	5.70	-	-	Slump	120	-
148	[79]	Cyl. 150x300	33	32	Cyl. 150x300	32.0	Split. test ϕ 100xE60	3.75	ASTM C1018	5.90	-	-	Slump	100	-
149	[79]	Cyl. 150x300	37	35	Cyl. 150x300	31.6	Split. test ϕ 100xE60	4.59	ASTM C1018	6.69	-	-	Slump	80	-
150	[79]	Cyl. 150x300	34	32	Cyl. 150x300	32.6	Split. test ϕ 100xE60	3.70	ASTM C1018	6.10	-	-	Slump	100	-
151	[79]	Cyl. 150x300	39	37	Cyl. 150x300	31.7	Split. test ϕ 100xE60	6.60	ASTM C1018	10.10	-	-	Slump	70	-
152	[79]	Cyl. 150x300	36	35	Cyl. 150x300	39.4	Split. test ϕ 100xE60	3.82	ASTM C1018	6.10	-	-	Slump	120	-
153	[79]	Cyl. 150x300	38	36	Cyl. 150x300	37.8	Split. test ϕ 100xE60	4.05	ASTM C1018	7.20	-	-	Slump	100	-
154	[79]	Cyl. 150x300	48	46	Cyl. 150x300	34.9	Split. test ϕ 100xE60	8.98	ASTM C1018	8.70	-	-	Slump	70	-
155	[79]	Cyl. 150x300	41	39	Cyl. 150x300	38.1	Split. test ϕ 100xE60	4.40	ASTM C1018	7.60	-	-	Slump	90	-
156	[79]	Cyl. 150x300	46	43	Cyl. 150x300	35.9	Split. test ϕ 100xE60	6.90	ASTM C1018	10.3	-	-	Slump	40	-
157	[79]	Cyl. 150x300	56	53	Cyl. 150x300	42.5	Split. test ϕ 100xE60	5.36	ASTM C1018	8.08	-	-	Slump	110	-
158	[79]	Cyl. 150x300	60	57	Cyl. 150x300	39.1	Split. test ϕ 100xE60	6.91	ASTM C1018	8.50	-	-	Slump	80	-
159	[79]	Cyl. 150x300	67	64	Cyl. 150x300	38.2	Split. test ϕ 100xE60	9.56	ASTM C1018	9.66	-	-	Slump	50	-
160	[79]	Cyl. 150x300	60	57	Cyl. 150x300	39.6	Split. test ϕ 100xE60	7.30	ASTM C1018	8.98	-	-	Slump	70	-
161	[79]	Cyl. 150x300	64	61	Cyl. 150x300	38.4	Split. test ϕ 100xE60	9.70	ASTM C1018	11.30	-	-	Slump	50	-
162	[79]	Cyl. 150x300	60	57	Cyl. 150x300	48.6	Split. test ϕ 100xE60	6.54	ASTM C1018	9.35	-	-	Slump	80	-
163	[79]	Cyl. 150x300	67	63	Cyl. 150x300	43.3	Split. test ϕ 100xE60	8.40	ASTM C1018	9.52	-	-	Slump	50	-
164	[79]	Cyl. 150x300	69	66	Cyl. 150x300	40.6	Split. test ϕ 100xE60	10.01	ASTM C1018	10.28	-	-	Slump	40	-
165	[79]	Cyl. 150x300	63	60	Cyl. 150x300	46.4	Split. test ϕ 100xE60	7.50	ASTM C1018	9.58	-	-	Slump	50	-
166	[79]	Cyl. 150x300	71	67	Cyl. 150x300	41.3	Split. test ϕ 100xE60	10.00	ASTM C1018	12.80	-	-	Slump	30	-
167	[80]	Cyl. 150x300 (ASTM C39)	85	81	-	-	ASTM C496	5.80	ASTM C1018	6.40	-	-	-	-	-
168	[80]	Cyl. 150x300 (ASTM C39)	91	87	-	-	ASTM C496	6.90	ASTM C1018	8.20	-	-	-	-	-
169	[80]	Cyl. 150x300 (ASTM C39)	95	90	-	-	ASTM C496	8.70	ASTM C1018	10.10	-	-	-	-	-
170	[80]	Cyl. 150x300 (ASTM C39)	98	93	-	-	ASTM C496	10.80	ASTM C1018	12.30	-	-	-	-	-
171	[80]	Cyl. 150x300 (ASTM C39)	96	91	-	-	ASTM C496	11.50	ASTM C1018	14.50	-	-	-	-	-
172	[81]	Cubes 150 (BS 1881)	56	42	-	-	Cubes 150	4.58	-	-	-	-	-	-	-
173	[81]	Cubes 150 (BS 1881)	49	37	-	-	Cubes 150	5.91	-	-	-	-	-	-	-
174	[81]	Cubes 150 (BS 1881)	36	27	-	-	Cubes 150	6.34	-	-	-	-	-	-	-
175	[81]	Cubes 150 (BS 1881)	36	27	-	-	Cubes 150	6.61	-	-	-	-	-	-	-
176	[81]	Cubes 150 (BS 1881)	34	26	-	-	Cubes 150	6.33	-	-	-	-	-	-	-
177	[81]	Cubes 150 (BS 1881)	37	28	-	-	Cubes 150	6.17	-	-	-	-	-	-	-
178	[81]	Cubes 150 (BS 1881)	33	25	-	-	Cubes 150	5.18	-	-	-	-	-	-	-
179	[81]	Cubes 150 (BS 1881)	47	35	-	-	Cubes 150	5.92	-	-	-	-	-	-	-
180	[81]	Cubes 150 (BS 1881)	49	37	-	-	Cubes 150	6.37	-	-	-	-	-	-	-
181	[81]	Cubes 150 (BS 1881)	45	34	-	-	Cubes 150	5.16	-	-	-	-	-	-	-
182	[81]	Cubes 150 (BS 1881)	61	46	-	-	Cubes 150	5.62	-	-	-	-	-	-	-
183	[81]	Cubes 150 (BS 1881)	57	43	-	-	Cubes 150	6.54	-	-	-	-	-	-	-
184	[81]	Cubes 150 (BS 1881)	49	37	-	-	Cubes 150	6.41	-	-	-	-	-	-	-
185	[81]	Cubes 150 (BS 1881)	49	37	-	-	Cubes 150	6.40	-	-	-	-	-	-	-
186	[81]	Cubes 150 (BS 1881)	52	39	-	-	Cubes 150	6.28	-	-	-	-	-	-	-
187	[81]	Cubes 150 (BS 1881)	64	48	-	-	Cubes 150	7.51	-	-	-	-	-	-	-
188	[81]	Cubes 150 (BS 1881)	48	36	-	-	Cubes 150	6.06	-	-	-	-	-	-	-
189	[81]	Cubes 150 (BS 1881)	54	40	-	-	Cubes 150	6.54	-	-	-	-	-	-	-
190	[81]	Cubes 150 (BS 1881)	57	43	-	-	Cubes 150	6.27	-	-	-	-	-	-	-
191	[81]	Cubes 150 (BS 1881)	58	43	-	-	Cubes 150	5.60	-	-	-	-	-	-	-
192	[81]	Cubes 150 (BS 1881)	70	52	-	-	Cubes 150	4.96	-	-	-	-	-	-	-
193	[81]	Cubes 150 (BS 1881)	72	54	-	-	Cubes 150	6.67	-	-	-	-	-	-	-
194	[81]	Cubes 150 (BS 1881)	72	54	-	-	Cubes 150	7.55	-	-	-	-	-	-	-
195	[81]	Cubes 150 (BS 1881)	72	54	-	-	Cubes 150	10.53	-	-	-	-	-	-	-

Table B.20: Database of FRC mixes. Testing information 5/5

Id	Ref.	Comp. Spec.	f_{cm} [MPa]	f_{1cm} [MPa]	Elast. Spec.	E_c [GPa]	Ind. Tens. Spec.	f_{ct} [MPa]	Bend. Spec.	f_{Rm} [MPa]	Tens. Spec.	f_{ct} [MPa]	Workability test	Slump [mm]	Flow [mm]
196	[81]	Cubes 150 (BS 1881)	71	53	-	-	Cubes 150	7.07	-	-	-	-	-	-	-
197	[81]	Cubes 150 (BS 1881)	71	53	-	-	Cubes 150	7.52	-	-	-	-	-	-	-
198	[81]	Cubes 150 (BS 1881)	64	48	-	-	Cubes 150	10.06	-	-	-	-	-	-	-
199	[81]	Cubes 150 (BS 1881)	59	44	-	-	Cubes 150	6.51	-	-	-	-	-	-	-
200	[81]	Cubes 150 (BS 1881)	61	46	-	-	Cubes 150	6.17	-	-	-	-	-	-	-
201	[81]	Cubes 150 (BS 1881)	60	45	-	-	Cubes 150	5.85	-	-	-	-	-	-	-
202	[82]	Cyl. 150x300	70	66	-	41.5	-	-	3P 150x150x600	5.66	-	-	Yes	-	-
203	[82]	Cyl. 150x300	56	53	-	34.5	-	-	3P 150X150X600	10.34	-	-	Yes	-	-
204	[83]	Cubes 150	58	43	-	-	Cyl. 150x300	3.83	4P 100x100x500	5.35	-	-	Yes	-	-
205	[83]	Cubes 150	60	45	-	-	Cyl. 150x300	4.82	4P 100x100x500	7.50	-	-	Yes	-	-
206	[83]	Cubes 150	62	47	-	-	Cyl. 150x300	4.88	4P 100x100x500	7.61	-	-	Yes	-	-
207	[83]	Cubes 150	63	47	-	-	Cyl. 150x300	4.65	4P 100x100x500	7.45	-	-	Yes	-	-
208	[83]	Cubes 150	65	49	-	-	Cyl. 150x300	4.63	4P 100x100x500	7.49	-	-	Yes	-	-
209	[83]	Cubes 150	70	52	-	-	Cyl. 150x300	4.58	4P 100x100x500	7.16	-	-	Yes	-	-
210	[83]	Cubes 150	64	48	-	-	Cyl. 150x300	5.78	4P 100x100x500	9.44	-	-	Yes	-	-
211	[83]	Cubes 150	67	51	-	-	Cyl. 150x300	5.55	4P 100x100x500	9.05	-	-	Yes	-	-
212	[83]	Cubes 150	66	49	-	-	Cyl. 150x300	5.21	4P 100x100x500	8.44	-	-	Yes	-	-
213	[83]	Cubes 150	69	52	-	-	Cyl. 150x300	5.06	4P 100x100x500	7.98	-	-	Yes	-	-
214	[83]	Cubes 150	72	54	-	-	Cyl. 150x300	4.83	4P 100x100x500	7.73	-	-	Yes	-	-
215	[83]	Cubes 150	62	47	-	-	Cyl. 150x300	5.97	4P 100x100x500	10.72	-	-	Yes	-	-
216	[83]	Cubes 150	67	50	-	-	Cyl. 150x300	6.09	4P 100x100x500	10.05	-	-	Yes	-	-
217	[83]	Cubes 150	65	49	-	-	Cyl. 150x300	5.40	4P 100x100x500	8.92	-	-	Yes	-	-
218	[83]	Cubes 150	69	51	-	-	Cyl. 150x300	5.17	4P 100x100x500	8.44	-	-	Yes	-	-
219	[83]	Cubes 150	73	55	-	-	Cyl. 150x300	4.98	4P 100x100x500	8.11	-	-	Yes	-	-
220	[180]	Cube 100	148	141	Cyl. 100x200	48.7	Split. cyl. 100x200	8.05	4P 150x150x700	-	-	-	-	-	-
221	[180]	Cube 100	162	154	Cyl. 100x200	48.7	Split. cyl. 100x200	12.49	4P 150x150x700	-	-	-	-	-	-
222	[180]	Cube 100	165	156	Cyl. 100x200	48.7	Split. cyl. 100x200	12.32	4P 150x150x700	-	-	-	-	-	-
223	[180]	Cube 100	167	159	Cyl. 100x200	48.7	Split. cyl. 100x200	15.83	4P 150x150x700	-	-	-	-	-	-
224	[58]	Cube 150	111	106	-	-	-	-	EN 14651	12.31	-	-	-	-	-
225	[85]	Cubic 150	110	83	-	-	RILEM 2000b	5.60	RILEM 2000b	5.89	-	-	-	-	-
226	[85]	Cubic 150	75	56	-	-	RILEM 2000b	5.70	RILEM 2000b	12.05	-	-	-	-	-

C

Database of shear tests for prestressed FRC beams without vertical stirrups

Table C.1: Database of shear tests. Geometry of beams 1/2

Id	Ref.	Beam	Units	b [mm]	b_w [mm]	h [mm]	h_f [mm]	h_{htop} [mm]	h_w [mm]	h_{ft} [mm]	h_{hbot} [mm]	b_{ft} [mm]	A_c [mm^2]	z_{c2} [mm]	I [mm^4]	S [mm^3]	d [mm]	z [mm]
1	[89]	HF400 h/6	SI	400	100	800	86	84	400	130	100	400	168608	421	1.36E+10	2.21E+07	725	653
2	[89]	HF600/4	SI	600	100	750	86	84	350	130	100	400	182220	359	1.35E+10	2.32E+07	675	608
3	[89]	HF600/5	SI	600	100	750	86	84	350	130	100	400	182220	359	1.35E+10	2.32E+07	675	608
4	[89]	HF400/7	SI	400	100	750	86	84	350	130	100	400	163608	395	1.15E+10	2.01E+07	675	608
5	[89]	HF400/8	SI	400	100	750	86	84	350	130	100	400	163608	395	1.15E+10	2.01E+07	675	608
6	[89]	HF260/9	SI	260	100	750	86	84	350	130	100	400	148900	429	9.59E+09	1.72E+07	675	608
7	[130]	V105	SI		114	270			152	118		156	35736	146	2.17E+08	1.21E+06	212	191
8	[130]	V106	SI		114	270			152	118		156	35736	146	2.17E+08	1.21E+06	209	188
9	[130]	V108	SI		114	270			152	118		156	35736	146	2.17E+08	1.21E+06	211	190
10	[130]	V109	SI		114	270			152	118		156	35736	146	2.17E+08	1.21E+06	210	189
11	[130]	V105-2	SI		114	270			152	118		156	35736	146	2.17E+08	1.21E+06	212	191
12	[130]	V106-2	SI		114	270			152	118		156	35736	146	2.17E+08	1.21E+06	209	188
13	[130]	V108-2	SI		114	270			152	118		156	35736	146	2.17E+08	1.21E+06	211	190
14	[130]	V109-2	SI		114	270			152	118		156	35736	146	2.17E+08	1.21E+06	210	189
15	[131]	H-P1	SI/A	711	76	889	118	73	406	127	165	711	272538	478	3.11E+10	4.37E+07	787	708
16	[131]	H-P2	SI/A	737	102	889	118	73	406	127	165	737	295285	476	3.26E+10	4.63E+07	787	708
17	[131]	H-P3	SI/A	711	76	1092	118	73	610	127	165	711	288083	589	5.17E+10	5.78E+07	990	891
18	[131]	J-P1	SI/A	711	76	889	118	73	406	127	165	711	272538	478	3.11E+10	4.37E+07	787	708
19	[131]	J-P1S	SI/A	711	76	889	118	73	406	127	165	711	272538	478	3.11E+10	4.37E+07	787	708
20	[13]	SB2	SI	400	50	650	100	25	400	100	25	250	94375	277	5.45E+09	1.06E+07	620	558
21	[13]	SB3	SI	400	50	650	100	25	400	100	25	250	94375	277	5.45E+09	1.06E+07	620	558
22	[13]	SB4	SI	400	50	650	100	25	400	100	25	250	94375	277	5.45E+09	1.06E+07	620	558
23	[13]	SB5	SI	400	50	650	100	25	400	100	25	250	94375	277	5.45E+09	1.06E+07	620	558
24	[13]	SB6	SI	400	50	650	100	25	400	100	25	250	94375	277	5.45E+09	1.06E+07	620	558
25	[13]	SB7	SI	400	50	650	100	25	400	100	25	250	94375	277	5.45E+09	1.06E+07	620	558
26	[88]	XB1	SI	500	50	650	50	50	450	50	50	500	100000	325	6.71E+09	1.23E+07	620	558
27	[88]	XB2	SI	500	50	650	50	50	450	50	50	500	100000	325	6.71E+09	1.23E+07	620	558
28	[88]	XB3	SI	500	50	650	50	50	450	50	50	500	100000	325	6.71E+09	1.23E+07	620	558
29	[88]	XB4	SI	500	50	650	50	50	450	50	50	500	100000	325	6.71E+09	1.23E+07	620	558
30	[88]	XB5	SI	500	50	650	50	50	450	50	50	500	100000	325	6.71E+09	1.23E+07	620	558
31	[88]	XB6	SI	500	50	650	50	50	450	50	50	500	100000	325	6.71E+09	1.23E+07	620	558
32	[88]	XB7	SI	500	50	650	50	50	450	50	50	500	100000	325	6.71E+09	1.23E+07	620	558
33	[88]	XB8	SI	500	50	650	50	50	450	50	50	500	100000	325	6.71E+09	1.23E+07	620	558
34	[129]	S25-F10-PS	SI	500	50	700	100	50	400	110	40	500	149750	353	1.09E+10	2.03E+07	630	567
35	[129]	S25-F15-PS	SI	500	50	700	100	50	400	110	40	500	149750	352	1.09E+10	2.03E+07	630	567
36	[129]	S25-F20-PS	SI	500	50	700	100	50	400	110	40	500	149750	351	1.09E+10	2.03E+07	630	567
37	[129]	S34-F10-PS	SI	500	50	700	100	50	400	110	40	500	149750	350	1.09E+10	2.03E+07	630	567
38	[129]	S34-F15-PS	SI	500	50	700	100	50	400	110	40	500	149750	349	1.09E+10	2.03E+07	630	567
39	[129]	S34-F20-PS	SI	500	50	700	100	50	400	110	40	500	149750	348	1.09E+10	2.03E+07	630	567
40	[122]	PC-0.2-0.30	SI	200	70	400	40	0	240	50	30	300	50850	207	9.79E+08	3.22E+06	350	315

Table C.2: Database of shear tests. Geometry of beams 2/2

Id	Ref.	Beam	Units	b [mm]	b_w [mm]	h [mm]	h_f [mm]	h_{htop} [mm]	h_w [mm]	h_{ft} [mm]	h_{hbot} [mm]	b_{ft} [mm]	A_c [mm^2]	z_{c2} [mm]	I [mm^4]	S [mm^3]	d [mm]	z [mm]
41	[122]	PC-0.2-0.46	SI	200	70	400	40		240	50	30	300	50850	207	9.79E+08	3.22E+06	350	315
42	[122]	PC-0.2-0.65	SI	200	70	400	40		240	50	30	300	50850	207	9.79E+08	3.22E+06	350	315
43	[127]	T1a		200	60	400	50	10	155	145	40	165	49025	214	8.19E+08	2.82E+06	316	284
44	[127]	T1b		200	60	400	50	10	155	145	40	165	49025	214	8.19E+08	2.82E+06	316	284
45	[127]	T3a		200	60	400	50	10	155	145	40	165	49025	214	8.19E+08	2.82E+06	316	284
46	[127]	T3b		200	60	400	50	10	155	145	40	165	49025	214	8.19E+08	2.82E+06	316	284
47	[127]	T4a		200	60	400	50	10	155	145	40	165	49025	214	8.19E+08	2.82E+06	316	284
48	[127]	T4b		200	60	400	50	10	155	145	40	165	49025	214	8.19E+08	2.82E+06	316	284
49	[127]	T6a		200	60	400	50	10	155	145	40	165	49025	214	8.19E+08	2.82E+06	316	284
50	[127]	T6b		200	60	400	50	10	155	145	40	165	49025	214	8.19E+08	2.82E+06	316	284
51	[127]	T7a		200	60	400	50	10	155	145	40	165	49025	214	8.19E+08	2.82E+06	316	284
52	[127]	T7b		200	60	400	50	10	155	145	40	165	49025	214	8.19E+08	2.82E+06	316	284
53	[65]	I beam-3-DZ		600	120	700	120	52.5	355	120	53	600	224400	350	1.44E+10	2.67E+07	630	567
54	[65]	I beam-4-DZ		600	120	700	120	52.5	355	120	53	600	224400	350	1.44E+10	2.67E+07	630	567
55	[65]	I beam-5-DZ I		600	120	700	120	52.5	355	120	53	600	224400	350	1.44E+10	2.67E+07	630	567
56	[65]	I beam-5-DZ II		600	120	700	120	52.5	355	120	53	600	224400	350	1.44E+10	2.67E+07	630	567
57	[65]	I beam-6-DZ I		600	120	700	120	52.5	355	120	53	600	224400	350	1.44E+10	2.67E+07	630	567
58	[65]	I beam-6-DZ II		600	120	700	120	52.5	355	120	53	600	224400	350	1.44E+10	2.67E+07	630	567
59	[132]	28S		300	148	910	152	76	381	152	152	460	234228	513	2.07E+10	3.15E+07	819	737
60	[132]	24S		300	148	910	152	76	381	152	152	460	234228	513	2.07E+10	3.15E+07	819	737
61	[132]	14S		300	148	910	152	76	381	152	152	460	234228	513	2.07E+10	3.15E+07	819	737
62	[94]	1-2,5-20A		400	100	1000	100	50	620	135	95	400	192250	531	2.46E+10	3.16E+07	900	810
63	[94]	2-2,5-20A		400	100	1000	100	50	620	135	95	400	192250	531	2.46E+10	3.16E+07	900	810
64	[94]	3-2,5-20A		400	100	1000	100	50	620	135	95	400	192250	531	2.46E+10	3.16E+07	900	810
65	[94]	1-2,5-20B		400	100	1000	100	50	620	135	95	400	192250	531	2.46E+10	3.16E+07	900	810
66	[94]	2-2,5-20B		400	100	1000	100	50	620	135	95	400	192250	531	2.46E+10	3.16E+07	900	810
67	[94]	1-2,5-40A		400	100	1000	100	50	620	135	95	400	192250	531	2.46E+10	3.16E+07	900	810
68	[94]	2-2,5-40A		400	100	1000	100	50	620	135	95	400	192250	531	2.46E+10	3.16E+07	900	810
69	[94]	3-2,5-40A		400	100	1000	100	50	620	135	95	400	192250	531	2.46E+10	3.16E+07	900	810
70	[94]	1-2,5-40B		400	100	1000	100	50	620	135	95	400	192250	531	2.46E+10	3.16E+07	900	810
71	[94]	2-2,5-40B		400	100	1000	100	50	620	135	95	400	192250	531	2.46E+10	3.16E+07	900	810
72	[94]	1-2,5-20+20		400	100	1000	100	50	620	135	95	400	192250	531	2.46E+10	3.16E+07	900	810
73	[94]	2-3,0-20+20		400	100	1000	100	50	620	135	95	400	192250	531	2.46E+10	3.16E+07	900	810
74	[94]	1-2,5-60		400	100	1000	100	50	620	135	95	400	192250	531	2.46E+10	3.16E+07	900	810
75	[94]	3-2,5-60		400	100	1000	100	50	620	135	95	400	192250	531	2.46E+10	3.16E+07	900	810
76	[60]	UHPFRC-A-PC-NS	SI/A	270	65	380	45	45	140	105	45	270	64675	208	1.07E+09	3.54E+06	305	274
77	[60]	UHPFRC-A-PC-NS (2)	SI/A	270	65	380	45	45	140	105	45	270	64675	208	1.07E+09	3.54E+06	305	274
78	[60]	UHPFRC-B-PC-NC	SI/A	270	65	380	45	45	140	105	45	270	64675	208	1.07E+09	3.54E+06	305	274
79	[128]	Beam 3	SI	300	80	900	100	50	490	150	100	300	144600	484	1.44E+10	2.09E+7	810	729
80	[128]	Beam 4	SI	300	80	900	100	50	490	150	100	300	144600	484	1.44E+10	2.09E+7	810	729

Table C.3: Database of shear tests. Test set-up and material characterization 1/2

Id	Ref.	a_a [mm]	a_f [mm]	b_a [mm]	L [mm]	c_p [mm]	a [mm]	κ [-]	c_c [mm]	$V_{u,test}$ [kN]	Test	V_f [%]	D_{low} [mm]	D_{Max} [mm]	f_{R1} [MPa]	f_{R3} [MPa]	f_R [MPa]	$f_{c,cyl}$ [MPa]	$f_{c,cu}$ [MPa]	f_{1c} [MPa]
1	[89]		500		5000	950	2025	2.8	0	420	4p	0.75	7	12	8.96	5.96		60	0	57
2	[89]		500		5000	950	2025	3	0	392	4p	0.75	7	12	10.46	6.24		65	0	62
3	[89]		500		5000	950	2025	3	0	347	4p	0.75	7	12	8.55	5.55		66	0	63
4	[89]		500		5000	950	2025	3	0	390	4p	0.75	7	12	6.64	4.77		64	0	60
5	[89]		500		5000	950	2025	3	0	428	4p	0.75	7	12	8.1	4.68		70	0	67
6	[89]		500		5000	950	2025	3	0	326	4p	0.75	7	12	6.45	5.68		65	0	62
7	[130]	150	200	250	1900	0	740	3.49	34	145	3p	1	5	8	8.5	3.5		0	175	118
8	[130]	150	200	250	1900	0	740	3.54	34	198	3p	1	5	8	8.5	3.5		0	175	118
9	[130]	150	200	250	1900	0	740	3.51	34	160	3p	1	5	8	17.5	6.8		0	184	124
10	[130]	150	200	250	1900	0	740	3.52	34	218	3p	1	5	8	8.5	3.5		0	184	124
11	[130]	150	200	250	2000	0	840	3.96	34	146	3p	2	5	8	8.5	3.5		0	175	118
12	[130]	150	200	250	2000	0	840	4.02	34	218	3p	2	5	8	17.5	6.8		0	175	118
13	[130]	150	200	250	2000	0	840	3.98	34	158	3p	2	5	8	17.5	6.8		0	184	124
14	[130]	150	200	250	2000	0	840	4	34	204	3p	2	5	8	17.5	6.8		0	184	124
15	[131]	152	152	914	8200	914	2740	3.48	42	1242	4p	2						137	0	123
16	[131]	152	152	914	8200	914	2740	3.48	42	1491	4p	2						140	0	125
17	[131]	152	152	914	10000	914	3350	3.38	42	1410	4p	2						160	0	143
18	[131]	152	152	914	8200	914	2740	3.48	42	1265	4p	2						158	0	142
19	[131]	152	152	914	8200	914	2740	3.48	42	1236	4p	2						152	0	136
20	[13]	200	200	250	4000	0	2000	3.23	22	994	3p	2.5	0.15	0.4			5.2	0	178	152
21	[13]	200	200	250	4000	0	2000	3.23	22	856	3p	2.5	0.15	0.4			5.2	0	166	142
22	[13]	200	200	250	4000	0	2000	3.23	22	673	3p	2.5	0.15	0.4			2.7	0	180	156
23	[13]	200	200	250	4000	0	2000	3.23	22	880	3p	2.5	0.15	0.4			4.3	0	187	162
24	[13]	200	200	250	4000	0	2000	3.23	22	660	3p	2.5	0.15	0.4			3.1	0	168	149
25	[13]	200	200	250	4000	0	2000	3.23	22	880	3p	2.5	0.15	0.4			4.7	0	185	161
26	[88]	200	200	4300	4000	0	2000	3.23	22	660	3p	1	0.1	1			1.64	0	100	119
27	[88]	200	200	2300	4000	0	2000	3.23	22	710	3p	1	0.1	1			1.65	0	101	120
28	[88]	200	200	6300	4000	0	2000	3.23	22	483	3p	1	0.1	1			1.7	0	108	128
29	[88]	200	200	2750	3100	0	1550	2.5	22	911	3p	1	0.1	1			1.62	0	98	116
30	[88]	200	200	2130	4340	0	2170	3.5	22	845	3p	1	0.1	1			3.03	0	112	133
31	[88]	200	200	1510	5580	0	2790	4.5	22	781	3p	1	0.1	1			3.03	0	112	133
32	[88]	200	200	2750	3100	0	1550	2.5	22	1043	3p	1.5	0.1	1			3.33	0	98	116
33	[88]	200	200	3215	2170	0	1085	1.75	22	1164	3p	1	0.1	1			1.62	0	98	116
34	[129]				3200	0	1600	2.5	0	590	3P	1		0.5			9.4	181	0	167
35	[129]				3200	0	1600	2.5	0	712	3P	1.5		0.5			14.2	184	0	169
36	[129]				3200	0	1600	2.5	0	717	3P	2		0.5			17.2	190	0	175
37	[129]				4400	0	2200	3.4	0	374	3P	1		0.5			9.2	167	0	154
38	[129]				4400	0	2200	3.4	0	437	3P	1.5		0.5			14.4	189	0	174
39	[129]				4400	0	2200	3.4	0	477	3P	2		0.5			16.8	182	0	168
40	[122]				2000		700	2	50	237	3p	0.78		32				0	120	81

Table C.4: Database of shear tests. Test set-up and material characterization 2/2

Id	Ref.	a_a [mm]	a_f [mm]	b_a [mm]	L [mm]	c_p [mm]	a [mm]	κ [-]	c_c [mm]	$V_{u,test}$ [kN]	Test	V_f [%]	D_{low} [mm]	D_{Max} [mm]	f_{R1} [MPa]	f_{R3} [MPa]	f_R [MPa]	$f_{c,cyl}$ [MPa]	$f_{c,cu}$ [MPa]	f_{1c} [MPa]
41	[122]				2000		700	1.94	50	254	3p	0.78		32				0	118	80
42	[122]				2000		700	1.94	50	316	3p	0.78		32				0	125	84
43	[127]			150	1200		1201	3.8	0	234	3p	0.9	2	8	1.73	2.8		0	151	102
44	[127]			150	1200		1201	3.8	0	267	3p	0.9	2	8	1.73	2.8		0	174	117
45	[127]			150	1200		1201	3.8	0	0	3p	2.5	2	8	4.37	5.39		0	162	109
46	[127]			150	1200		1201	3.8	0	408	3p	2.5	2	8	4.37	5.39		0	170	115
47	[127]			150	1200		1390	4.4	0	344	3p	0.9	2	8	5.61	5.64		0	176	119
48	[127]			150	1200		1390	4.4	0	291	3p	0.9	2	8	5.61	5.64		0	183	124
49	[127]			150	1200		1201	3.8	0	266	3p	0.9	2	8	5.61	5.64		0	142	96
50	[127]			150	1200		1201	3.8	0	226	3p	0.9	2	8	1.73	2.8		0	155	105
51	[127]			150	1200		1201	3.8	0	234	3p	0.9	2	8	1.73	2.8		0	192	130
52	[127]			150	1200		1201	3.8	0	232	3p	0.9	2	8	4.37	5.39		0	183	124
53	[65]			2325	5650	0	2200	3.49	50	574	3p	0.64		15	4.37	3.18		0	82	56
54	[65]			2325	5650	0	2200	3.49	50	709	3p	0.64		15	5.61	8.61		0	93	63
55	[65]			3225	5650	0	2200	3.49	50	579	3p	0.64		15	5.61	3.18		0	84	56
56	[65]			3225	5650	0	2200	3.49	50	542	3p	0.64		15	5.61	3.18		0	84	56
57	[65]			3225	5650	0	2200	3.49	50	573	3p	0.64		15	1.73	8.61		0	84	57
58	[65]			3225	5650	0	2200	3.49	50	608	3p	0.64		15	1.73	8.61		0	84	57
59	[132]			1220	8530		1990	2.43	42	1710	3p	1.99	0.15	0.6	4.37	5.39		193	0	174
60	[132]			1220	7310		2290	2.8	42	2230	3p	1.99	0.15	0.6	4.37	5.39		193	0	174
61	[132]			160	4270		1840	2.25	42	1950	3p	1.99	0.15	0.6	5.61	5.64		193	0	174
62	[94]						2250	2.5	42	756	3p	0.3	6	14	2.59	4.09		41	0	50
63	[94]						2250	2.5	0	781	3p	0.3	6	14	2.59	4.09		41	0	50
64	[94]						2250	2.5	0	609	3p	0.3	6	14	2.59	4.09		41	0	50
65	[94]						2250	2.5	42	786	3p	0.3	6	14	4.82	4.89		65	0	50
66	[94]						2250	2.5	0	570	3p	0.3	6	14	4.815	4.89		65	0	50
67	[94]						2250	2.5	42	799	3p	0.5	6	14	7.59	8.15		70	0	61
68	[94]						2250	2.5	0	809	3p	0.5	6	14	7.59	8.15		70	0	61
69	[94]						2250	2.5	0	737	3p	0.5	6	14	7.59	8.15		70	0	61
70	[94]						2250	2.5	42	744	3p	0.5	6	14	6.66	7.08		59	0	61
71	[94]						2250	2.5	0	599	3p	0.5	6	14	6.66	7.08		59	0	61
72	[94]						2250	2.5	42	696	3p	0.5	6	14	8.07	9.69		56	0	53
73	[94]						2700	3	0	595	3p	0.5	6	14	8.07	9.69		56	0	53
74	[94]						2250	2.5	0	672	3p	0.8	6	14	10.37	9.85		67	0	63
75	[94]						2250	2.5	42	721	3p	0.8	6	14	10.37	9.85		67	0	63
76	[60]						0	2.5	0	430	4P	2.5					34.5	0	198	134
77	[60]						0	2.5	0	431	4P	2.5					34.5	0	198	134
78	[60]						0	2.5	0	507	4P	2					28.5	0	212	143
79	[128]						2750	3.4	0	740	3P	0.5			5.22		6.35	0	62	47
80	[128]						2750	3.4	0	695	3P	0.75			4.52		4.82	0	56	42

Table C.5: Database of shear tests. Prestressing information 1/2

Id	Ref.	d_{pbot} [mm]	d_{pweb} [mm]	d_{ptop} [mm]	Pre/Post	ϕ [mm]	A_{pbot} [mm^2]	A_{pweb} [mm^2]	A_{ptop} [mm^2]	A_p [mm^2]	E_p [GPa]	f_{py} [MPa]	ε_{py} [‰]	f_{pu} [MPa] [kN]	P_{bot} [kN]	P_{web} [kN]	P_{top} [mm]	z_{pbot} [mm]	z_{pweb} [mm]	z_{ptop} [MPa]	σ_{cp} [-]	σ_{cp} / f_{1c} [MPa]	σ_{pp}
1	[89]	725		50	Pre	15.2	1260	0	280	1540	200	1691	8.46	1860	1758	0	391	304	0	371	12.7	0.22	1395
2	[89]	675		50	Pre	15.2	1260	0	280	1540	200	1691	8.46	1860	1758	0	391	316	0	309	11.8	0.19	1395
3	[89]	675		50	Pre	15.2	1260	0	280	1540	200	1691	8.46	1860	1758	0	391	316	0	309	11.8	0.19	1395
4	[89]	675		50	Pre	15.2	1260	0	280	1540	200	1691	8.46	1860	1758	0	391	280	0	345	13.1	0.22	1395
5	[89]	675		50	Pre	15.2	1260	0	280	1540	200	1691	8.46	1860	1758	0	391	280	0	345	13.1	0.2	1395
6	[89]	675		50	Pre	15.2	1260	0	280	1540	200	1691	8.46	1860	1758	0	391	246	0	379	14.4	0.23	1395
7	[130]	211	40		Pre	12.5	558	93	0	651	200	1691	8.46	1860	389	65	0	65	84	0	12.8	0.11	700
8	[130]	211	40		Pre	12.5	558	93	0	651	200	1691	8.46	1860	778	130	0	65	84	0	26.2	0.22	1441
9	[130]	211	40		Pre	12.5	558	93	0	651	200	1691	8.46	1860	389	65	0	65	84	0	12.8	0.1	700
10	[130]	211	40		Pre	12.5	558	93	0	651	200	1691	8.46	1860	778	130	0	65	84	0	26.2	0.21	1441
11	[130]	211	40		Pre	12.5	558	93	0	651	200	1691	8.46	1860	389	65	0	65	84	0	12.8	0.11	700
12	[130]	211	40		Pre	12.5	558	93	0	651	200	1691	8.46	1860	778	130	0	65	84	0	26.2	0.22	1441
13	[130]	211	40		Pre	12.5	558	93	0	651	200	1691	8.46	1860	389	65	0	65	84	0	12.8	0.1	700
14	[130]	211	40		Pre	12.5	558	93	0	651	200	1691	8.46	1860	778	130	0	65	84	0	26.2	0.21	1441
15	[131]	787.4		50.8	Pre	17.8	4553	0	379	4932	200	1691	8.46	1860	6351	0	529	309	0	427	25.3	0.21	1397
16	[131]	787.4		50.8	Pre	17.8	4553	0	379	4932	200	1691	8.46	1860	6351	0	529	311	0	425	23.3	0.19	1397
17	[131]	990.4		50.8	Pre	17.8	4553	0	379	4932	200	1691	8.46	1860	6351	0	529	401	0	538	23.9	0.17	1397
18	[131]	787.4		50.8	Pre	17.8	4553	0	379	4932	200	1691	8.46	1860	6351	0	529	309	0	427	25.3	0.18	1397
19	[131]	787.4		50.8	Pre	17.8	3415	0	379	3794	200	1691	8.46	1860	4763	0	529	309	0	427	19.4	0.14	1397
20	[13]	585		50	Pre	15.2	1716	0	858	2574	200	1591	7.96	1750	2252	0	1126	308	0	227	35.8	0.24	1312
21	[13]	585		50	Pre	15.2	1716	0	858	2574	200	1591	7.96	1750	2252	0	1126	308	0	227	35.8	0.25	1312
22	[13]	585		50	Pre	15.2	1716	0	858	2574	200	1591	7.96	1750	2252	0	1126	308	0	227	35.8	0.23	1312
23	[13]	585		50	Pre	15.2	1716	0	858	2574	200	1591	7.96	1750	2252	0	1126	308	0	227	35.8	0.22	1312
24	[13]	585		50	Pre	15.2	1716	0	858	2574	200	1591	7.96	1750	2252	0	1126	308	0	227	35.8	0.24	1312
25	[13]	585	0	50	Pre	15.2	1716	0	858	2574	200	1591	7.96	1750	2252	0	1126	308	0	227	35.8	0.22	1312
26	[88]	620	0	30	Pre	15.2	858	0	858	1716	200	1591	7.96	1750	1126	0	1126	295	0	295	22.5	0.19	1312
27	[88]	620	0	30	Pre	15.2	858	0	858	1716	200	1591	7.96	1750	1126	0	1126	295	0	295	22.5	0.19	1312
28	[88]	620	0	30	Pre	15.2	858	0	858	1716	200	1591	7.96	1750	1126	0	1126	295	0	295	22.5	0.18	1312
29	[88]	620	0	30	Pre	15.2	858	0	858	1716	200	1591	7.96	1750	1126	0	1126	295	0	295	22.5	0.19	1312
30	[88]	620	0	30	Pre	15.2	858	0	858	1716	200	1591	7.96	1750	1126	0	1126	295	0	295	22.5	0.17	1312
31	[88]	620	0	30	Pre	15.2	858	0	858	1716	200	1591	7.96	1750	1126	0	1126	295	0	295	22.5	0.17	1312
32	[88]	620	0	30	Pre	15.2	858	0	858	1716	200	1591	7.96	1750	1126	0	1126	295	0	295	22.5	0.19	1312
33	[88]	620	0	30	Pre	15.2	858	0	858	1716	200	1591	7.96	1750	1126	0	1126	295	0	295	22.5	0.19	1312
34	[129]	645			Pre	15.2	1716	0	0	1716	200	1691	8.46	1860	2394	0	0	292	0	0	16	0.1	1395
35	[129]	645			Pre	15.2	1716	0	0	1716	200	1691	8.46	1860	2394	0	0	0	0	0	16	0.09	1395
36	[129]	645			Pre	15.2	1716	0	0	1716	200	1691	8.46	1860	2394	0	0	0	0	0	16	0.09	1395
37	[129]	645			Pre	15.2	1716	0	0	1716	200	1691	8.46	1860	2394	0	0	0	0	0	16	0.1	1395
38	[129]	645			Pre	15.2	1716	0	0	1716	200	1691	8.46	1860	2394	0	0	0	0	0	16	0.09	1395
39	[129]	645			Pre	15.2	1716	0	0	1716	200	1691	8.46	1860	2394	0	0	0	0	0	16	0.1	1395
40	[122]	350	0	0	Pre	15.2	363	0	0	363	200	1591	7.96	1750	476	0	0	350	0	0	9.4	0.12	1311

Table C.6: Database of shear tests. Prestressing information 2/2

Id	Ref.	d_{pbot} [mm]	d_{pweb} [mm]	d_{ptop} [mm]	Pre/Post	ϕ [mm]	A_{pbot} [mm^2]	A_{pweb} [mm^2]	A_{ptop} [mm^2]	A_p [mm^2]	E_p [GPa]	f_{py} [MPa]	ε_{py} [‰]	f_{pu} [MPa] [kN]	P_{bot} [kN]	P_{web} [kN]	P_{top} [mm]	z_{pbot} [mm]	z_{pweb} [mm]	z_{ptop} [MPa]	σ_{cp} [-]	σ_{cp} / f_{1c} [MPa]	σ_{pp}
41	[122]	350	0	0	Pre	15.2	363	0	0	363	200	1591	7.96	1750	476	0	0	350	0	0	9.4	0.12	1311
42	[122]	350	0	0	Pre	15.2	363	0	0	363	200	1591	7.96	1750	476	0	0	350	0	0	9.4	0.11	1311
43	[127]	316			Pre	12.7	700	0	200	900	200	1691	8.46	1860	875	0	250	0	0	0	22.9	0.22	1607
44	[127]	316			Pre	12.7	1100	0	200	1300	200	1691	8.46	1860	1125	0	250	0	0	0	28	0.24	1250
45	[127]	316			Pre	12.7	700	0	200	900	200	1691	8.46	1860	875	0	250	0	0	0	22.9	0.21	1607
46	[127]	316			Pre	12.7	1100	0	200	1300	200	1691	8.46	1860	1125	0	250	0	0	0	28	0.24	1250
47	[127]	316			Pre	12.7	1100	0	200	1300	200	1691	8.46	1860	1125	0	250	0	0	0	28	0.24	1250
48	[127]	316			Pre	12.7	1100	0	200	1300	200	1691	8.46	1860	1125	0	250	0	0	0	28	0.23	1250
49	[127]	316			Pre	12.7	1100	0	200	1300	200	1691	8.46	1860	1125	0	250	0	0	0	28	0.29	1250
50	[127]	316			Pre	12.7	1100	0	200	1300	200	1691	8.46	1860	1125	0	250	0	0	0	28	0.27	1250
51	[127]	316			Pre	12.7	1100	0	200	1300	200	1691	8.46	1860	1125	0	250	0	0	0	28	0.22	1250
52	[127]	316			Pre	12.7	1100	0	200	1300	200	1691	8.46	1860	1125	0	250	0	0	0	28	0.23	1250
53	[65]	625		50	Pre	15.2	2085	0	417	2502	200	1691	8.46	1860	2909	0	582	0	0	0	15.6	0.28	1395
54	[65]	625		50	Pre	15.2	2085	0	417	2502	200	1691	8.46	1860	2909	0	582	0	0	0	15.6	0.25	1395
55	[65]	625		50	Pre	15.2	2085	0	417	2502	200	1691	8.46	1860	2909	0	582	0	0	0	15.6	0.28	1395
56	[65]	625		50	Pre	15.2	2085	0	417	2502	200	1691	8.46	1860	2909	0	582	0	0	0	15.6	0.28	1395
57	[65]	625		50	Pre	15.2	2085	0	417	2502	200	1691	8.46	1860	2909	0	582	0	0	0	15.6	0.27	1395
58	[65]	625		50	Pre	15.2	2085	0	417	2502	200	1691	8.46	1860	2909	0	582	0	0	0	15.6	0.27	1395
59	[132]	808		51	Pre	12.7	1520	0	253	1773	200	1691	8.46	1860	2120	0	353	0	0	0	10.6	0.06	1395
60	[132]	808		51	Pre	12.7	1520	0	253	1773	200	1691	8.46	1860	2120	0	353	0	0	0	10.6	0.06	1395
61	[132]	808		51	Pre	12.7	1520	0	253	1773	200	1691	8.46	1860	2120	0	353	0	0	0	10.6	0.06	1395
62	[94]	882.5			Pre	12.5	1700	0	0	1700	200	1691	8.46	1860	2372	0	0	0	0	0	12.3	0.25	1395
63	[94]	882.5			Pre	12.5	1700	0	0	1700	200	1691	8.46	1860	2372	0	0	0	0	0	12.3	0.25	1395
64	[94]	882.5			Pre	12.5	1700	0	0	1700	200	1691	8.46	1860	2372	0	0	0	0	0	12.3	0.25	1395
65	[94]	882.5			Pre	12.5	1700	0	0	1700	200	1691	8.46	1860	2372	0	0	0	0	0	12.3	0.25	1395
66	[94]	882.5			Pre	12.5	1700	0	0	1700	200	1691	8.46	1860	2372	0	0	0	0	0	12.3	0.25	1395
67	[94]	882.5			Pre	12.5	1700	0	0	1700	200	1691	8.46	1860	2372	0	0	0	0	0	12.3	0.2	1395
68	[94]	882.5			Pre	12.5	1700	0	0	1700	200	1691	8.46	1860	2372	0	0	0	0	0	12.3	0.2	1395
69	[94]	882.5			Pre	12.5	1700	0	0	1700	200	1691	8.46	1860	2372	0	0	0	0	0	12.3	0.2	1395
70	[94]	882.5			Pre	12.5	1700	0	0	1700	200	1691	8.46	1860	2372	0	0	0	0	0	12.3	0.2	1395
71	[94]	882.5			Pre	12.5	1700	0	0	1700	200	1691	8.46	1860	2372	0	0	0	0	0	12.3	0.2	1395
72	[94]	882.5			Pre	12.5	1700	0	0	1700	200	1691	8.46	1860	2372	0	0	0	0	0	12.3	0.23	1395
73	[94]	882.5			Pre	12.5	1700	0	0	1700	200	1691	8.46	1860	2372	0	0	0	0	0	12.3	0.23	1395
74	[94]	882.5			Pre	12.5	1700	0	0	1700	200	1691	8.46	1860	2372	0	0	0	0	0	12.3	0.2	1395
75	[94]	882.5			Pre	12.5	1700	0	0	1700	200	1691	8.46	1860	2372	0	0	0	0	0	12.3	0.2	1395
76	[60]	304.5			Pre	15.7	900	0	0	900	200	1691	8.46	1860	709	0	0	0	0	0	11	0.08	788
77	[60]	304.5			Pre	15.7	900	0	0	900	200	1691	8.46	1860	709	0	0	0	0	0	11	0.08	788
78	[60]	304.5			Pre	15.7	900	0	0	900	200	1691	8.46	1860	689	0	0	0	0	0	10.7	0.07	766
79	[128]				Pre	12.5	651	0	0	651	200	1691	8.46	1860	945	0	0	0	0	0	6.5	0.14	1452
80	[128]				Pre	12.5	651	0	0	651	200	1692	8.46	1861	945	0	0	0	0	0	6.5	0.16	1452

D

Application of shear formulations to the Database of shear tests

The set-up and cross-section of the test "Beam HF400/8" with Id 5 from reference [89] are shown in Figure D.1. First, in this appendix the detailed calculation with the shear formulations described in this thesis are given for this example. Next, tables with the intermediate variables related with each calculation are given for the filtered database.

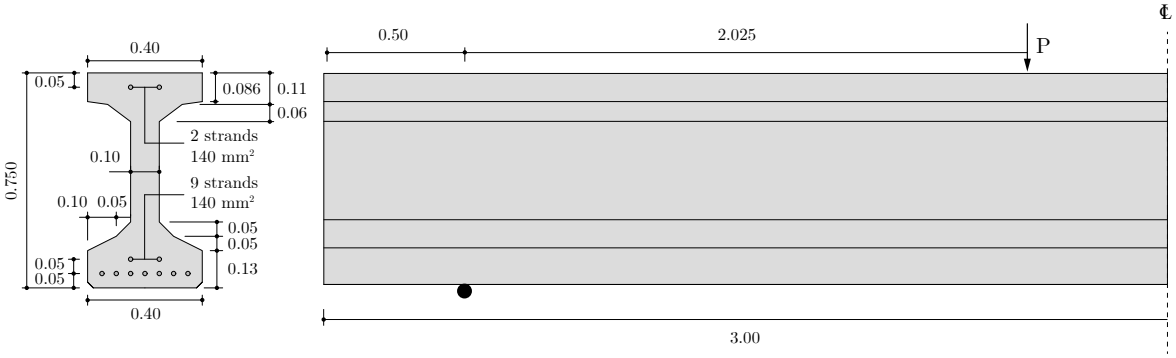

Figure D.1: Beam HF400/8 Id 5, Reference [89].

The following characteristics are used for the different formulations:

- shear force at failure with self-weight (from report): $V_{u,test}$=428 kN
- gross area of concrete section: A_c=1.636E+05 mm^2
- effective depth: d=675 mm
- internal lever arm: z=0.9·d=607.5 mm
- distance of CGS from top fibre: z_{c2}=394.72 mm
- width of web: b_w=100 mm
- shear span: a=2.025 m
- span: L=5.00 m
- prestressing stress: σ_{pp}=1395 MPa
- prestressing force of strands at top flange: P_{top}=σ_{pp}·140 mm^2·2=391 kN
- effective depth of top prestressing steel: d_{ptop}=50 mm
- prestressing force of strands at web: P_{web}=0
- effective depth of web prestressing steel: d_{pweb}=0

- prestressing force of strands at bottom flange: P_{bot}=σ_{pp}·140 mm^2·9=1758 kN
- effective depth of bottom prestressing steel: d_{pbot}=675 mm
- geometrical reinforcement ratio of prestressing steel under tension related to b_w:

$$\rho_{pw} = \frac{A_{pbot}}{b_w \cdot d} = \frac{140 \text{ mm}^2 \cdot 9}{100 \cdot 675} = 1.87\% \tag{D.1}$$

- mean concrete compressive stress due to prestressing force:

$$\sigma_{cp} = \frac{P_{bot} + P_{web} + P_{top}}{A_c} = \frac{(1758 + 391)}{1.636\text{E}+05} \cdot 1000 = 13.13 \text{ MPa} \tag{D.2}$$

- distributed load due to self-weight:

$$q_{sw} = A_c \cdot 25kN/m^3 = 1.636\text{E}+05 \text{ mm}^2 \cdot 25 \text{ kN/m}^3 \cdot 10^{-6} = 4.09 \text{ kN/m} \tag{D.3}$$

- mean compressive strength of the concrete: $f_{cm} = 66.50$ MPa
- ultimate post-cracking strength for fibre reinforced concrete:

$$f_{Ftu} = f_{R3}/3 = 4.68/3 = 1.56 \text{ MPa} \tag{D.4}$$

FprEN 1992-1-1:2022 (Issue date: 2022-09) [48]

The section under study, x=1.013 m from the support, is considered for the calculation as $a/2$. This formulation requires a non-linear analysis. Its implementation is performed in an Excel Spreadsheet using Solver with a GRG Nonlinear resolution method.

- effective depth considering all the prestressing strands:

$$\begin{aligned} d_{tot} &= \frac{d_{pbot}A_{pbot} + d_{pweb}A_{pweb} + d_{ptop}A_{ptop}}{A_{pbot} + A_{pweb} + A_{ptop}} = \frac{675 \cdot 140 \cdot 9 + 0 + 50 \cdot 140 \cdot 2}{140 \cdot 9 + 0 + 140 \cdot 2} \\ &= \frac{864500}{1540} = 561.36 \text{ mm} \end{aligned} \tag{D.5}$$

- eccentricity of the prestressing force or of the external load that produces the compressive axial force with respect to the centre of gravity of the cross-section considered as positive towards the tensile side:

$$e_p = d_{tot} - z_{c2} = 561.36 - 394.72 = 166.64 \text{ mm} \tag{D.6}$$

- calculated shear strength: $V_{u,cal}$=283.47 kN

- shear load by self-weight at different sections:

$$V_{sw}(L) = q_{sw}\frac{L^2}{8} = 4.09\frac{5^2}{8} = 12.78 \text{ kN} \tag{D.7}$$

$$V_{sw}(x) = q_{sw}\left(\frac{L}{2} - x\right) = 4.09\left(\frac{5}{2} - 1.013\right) = 6.08 \text{ kN} \tag{D.8}$$

- applied load by one jack: P=$V_{u,cal}$−$V_{sw,L}$=283.47-12.78=270.69 kN

- applied bending moment:

$$\begin{aligned} M_{u,cal} &= \frac{q_{sw}x}{2}(L-x) + Px \\ &= \frac{4.09 \cdot 1.013}{2}(5 - 1.013) + 270.69 \cdot 1.013 = 282.47 \text{ kNm} \end{aligned} \tag{D.9}$$

- effective shear span with respect to the control section:

$$a_{cs,0} = \left|\frac{M_{Ed}}{V_{Ed}}\right| \geq \ d = \left|\frac{282.47}{283.47}\right| \geq \ 0.675 = 0.996 \text{ m} \tag{D.10}$$

- factor multiplying the average compressive stress σ_{cp}: k_1

$$\begin{aligned} k_1 &= \frac{0.5}{a_{cs,0}}\left(e_p + \frac{d}{3}\right)\frac{A_c}{b_w z} \leq 0.18\frac{A_c}{b_w z} \\ &= \frac{0.5}{0.996}\left(0.166 + \frac{0.675}{3}\right)\frac{1.636\text{E}+0.5}{100 \cdot 607.5} = 0.529 \\ &\leq 0.18 \cdot \frac{1.636\text{E}+0.5}{100 \cdot 607.5} = 0.485 \end{aligned} \tag{D.11}$$

- size parameter describing the failure zone roughness: d_{dg}

$$d_{dg} = \begin{cases} 16 + D_{lower} \leq 40 \text{ mm for concrete with } f_{ck} \leq 60 \text{ MPa} \\ 16 + D_{lower}\,(60/f_{ck})^2 \leq 40 \text{ mm for concrete with } f_{ck} > 60 \text{ MPa} \end{cases} \tag{D.12}$$

$$16 + 7(60/66.50)^2 = 16 + 7(0.814) = 21.70 \leq 40 \text{ mm} \tag{D.13}$$

- Interaction coefficients between concrete and fibre shear contributions: η_{cF}

$$\begin{aligned} \eta_{cF} &= max\left\{1.2 - 0.5 f_{Ftuk}; 0.4\right\} \leq 1.0 \\ &= max\left\{1.2 - 0.5 \cdot 1.56; 0.4\right\} \leq 1.0 \\ &= max\left\{0.42; 0.4\right\} = 0.42 \leq 1.0 \\ \eta_F &= 1.0 \end{aligned} \tag{D.14}$$

$$\begin{aligned} V_{Rd,cf} &= \left(\eta_{cF}\left(\frac{0.66}{\gamma_V}\left(100\rho_l f_{ck}\frac{d_{dg}}{d}\right)^{1/3} - k_1\sigma_{cp}\right) + \ \eta_F f_{Ftud}\right) b_w z \\ &= \left(0.42\left(\frac{0.66}{1}\left(100\cdot 0.0187\cdot 66.50\frac{21.70}{675}\right)^{1/3} + 0.485\cdot 13.13\right) + 1\cdot 1.56\right) 100\cdot 607.5 = \\ &= 0.42\left(\left(0.66\cdot(4)^{1/3} + 6.37\right) + 1.56\right) 60750 = (0.42\,(1.05 + 6.37) + 1.56)\,60750 = \\ &= (3.12 + 1.56)\cdot 60750/1000 = \\ &= 4.68\cdot 60750/1000 = 283.47 \text{ kN} \end{aligned} \tag{D.15}$$

$$\begin{aligned} \tau_{Rd,min} &= \frac{11}{\gamma_V}\sqrt{\frac{f_{ck}}{f_{yd}}\frac{d_{dg}}{d}} = 11\sqrt{\frac{66.50}{1690.91}\frac{21.70}{675}} = \\ &= \frac{11}{1}\sqrt{0.039\cdot 0.032} = 11\cdot 0.035 = 0.385 \text{ MPa} \end{aligned} \tag{D.16}$$

$$\begin{aligned} V_{Rd,cf} \geq \ V_{Rd,min} &= (\eta_{cF}\tau_{Rdc,min} + \ \eta_F f_{Ftud})\, b_w z = \\ &= (0.42\cdot 0.385 + 1\cdot 1.56)\, 100\cdot 607.5 = \\ &= 1.72\cdot 60750/1000 = 104.49 \text{ kN} \end{aligned} \tag{D.17}$$

Spanish National Code [70]

- size effect coefficient:

$$\xi = 1 + \sqrt{\frac{200}{d}} = 1 + \sqrt{\frac{200}{675}} = 1.54 \leq 2 \tag{D.18}$$

- fibres shear contribution:

$$\tau_{fd} = 0.5 f_{ctR} = 0.5\cdot 0.33\cdot f_{R3} = 0.165\cdot 4.68 = 0.77 \text{ MPa} \tag{D.19}$$

- average compression level of the cross-section, limited:

$$\sigma_{cp} = min\,(\sigma_{cp}; 0.2 f_{ck}) = 13.13 \text{ MPa} \tag{D.20}$$

- longitudinal reinforcement ratio refered to the web, limited:

$$\rho_l = min\,(\rho_l; 2\%) = 1.87\% \tag{D.21}$$

- flange height: h_f=84 mm
- flange width: b_f=400 mm
- web width: b_w=100 mm
- flange coefficient for I-beams:

$$\begin{aligned} n &= \frac{b_f - b_w}{h_f} = \frac{400-100}{84} = 3.57 \leq 3 = \\ &= 3 \cdot b_w/h_f = 3 \cdot 100/84 = 3.57 \\ n &= 3 \end{aligned} \tag{D.22}$$

$$\begin{aligned} k_f &= 1 + n \cdot \frac{b_f}{b_w} dot \frac{h_f}{d} = 1 + 3\frac{400}{100} \cdot \frac{84}{675} = 2.49 \leq 1.5 \\ k_f &= 1.5 \end{aligned} \tag{D.23}$$

$$\begin{aligned} V_{cF} &= \left(0.7\xi k_f \tau_{fd} + \frac{0.18}{\gamma_c}\xi \left[100\rho_l f_{ck}\right]^{\frac{1}{3}} + 0.15\sigma_{cp}\right) b_w d = \\ &= \left(0.7 \cdot 1.54 \cdot 1.5 \cdot 0.77 + \frac{0.18}{1} 1.54 \left[100 \cdot 0.0187 \cdot 66.50\right]^{\frac{1}{3}} + 0.15 \cdot 13.13\right) 100 \cdot 675 \\ &= (1.25 + 1.38 + 1.97)\, 67500/1000 = 310.50 \text{ kN} \end{aligned} \tag{D.24}$$

MC-2010 [65]

- size effect coefficient:

$$k = 1 + \sqrt{\frac{200}{d}} = 1 + \sqrt{\frac{200}{675}} = 1.54 \leq 2 \tag{D.25}$$

$$\begin{aligned} V_{Rd,cf} &= \left(\frac{0.18}{\gamma_c} k \left[100\rho_l \left(1 + 7.5\frac{f_{Ftuk}}{f_{ctk}}\right) f_{ck}\right]^{\frac{1}{3}} + 0.15\sigma_{cp}\right) b_w d = \\ &= \left(\frac{0.18}{1} 1.54 \left[100 \cdot 0.0187 \left(1 + 7.5\frac{1.56}{3.29}\right) 66.50\right]^{\frac{1}{3}} + 0.15 \cdot 13.13\right) 100 \cdot 675 = \\ &= \left(0.277 \cdot \left[1.87 \cdot 4.56 \cdot 66.5\right]^{\frac{1}{3}} + 1.97\right) 100 \cdot 675 = \\ &= (0.277 \cdot 8.278 + 1.97)\, 100 \cdot 675/1000 = 287.8 \text{ kN} \end{aligned} \tag{D.26}$$

MC-2010 based on SMCFT [49]

As the formulation of the FprEN 1992-1-1:2022 (Issue date: 2022-09) [48], the calculation

is refered to the section under study, x=1.013 m from the support($a/2$). This formulation requires also a non-linear analysis. Its implementation is performed in an Excel Spreadsheet using Solver with a GRG Nonlinear resolution method.

- calculated shear strength: $V_{u,cal}$=288.82 kN
- applied load by one jack: P=$V_{u,cal}$−$V_{sw,L}$=288.82-12.78=276.04 kN
- applied bending moment:

$$\begin{aligned} M_{ext} &= \frac{q_{sw}x}{2}(L-x) + Px \\ &= \frac{4.09 \cdot 1.013}{2}(5-1.013) + 276 \cdot 1.013 = 287.85 \text{ kNm} \end{aligned} \tag{D.27}$$

- prestressing bending moment:

$$\begin{aligned} M_p &= P_{top} \cdot (z_{c2} - d_{ptop}) + P_{bot} \cdot (d_{pbot} - z_{c2}) = \\ &= 391 \cdot (394.7 - 50)/1000 - 1758 \cdot (675 - 394.7)/1000 = -357.99 \text{ kNm} \end{aligned} \tag{D.28}$$

- calculated bending moment:

$$M_{u,cal} = M_p + M_{ext} = -357.99 + 287.85 = -70 \text{ kN} \tag{D.29}$$

- calculated axial load:

$$N_{u,cal} = 1758 + 391 = 2149 \text{ kN} \tag{D.30}$$

- longitudinal strain at the centre of the lever arm:

$$\begin{aligned} \varepsilon_x &= \frac{\frac{M_{u,cal}}{z} + V_{u,cal} - N_{u,cal} \cdot \frac{z-e_p}{z}}{2 \cdot E_p \cdot A_p} = \\ &= \frac{\frac{-70}{0.607} + 288.85 - 2149 \cdot \frac{0.607-0.08}{0.607}}{2 \cdot 200 \cdot 9 \cdot 140} = \\ &= \frac{-115.77 + 288.85 - 1865.77}{504000} = -3.35\text{E-}03 \geq 0 = \\ &= 0 \end{aligned} \tag{D.31}$$

- angle of the compressive stress field:

$$\theta = 29 + 7000\varepsilon_x = 29 + 7000 \cdot 0 = 29^\circ \tag{D.32}$$

- aggregate size influence parameter:

$$k_{dg} = \frac{32}{16 + d_g} = \frac{32}{16 + 12} = 1.14 \tag{D.33}$$

- size and strain parameter:

$$k_v = \frac{0.4}{1+1500\cdot\varepsilon_x}\cdot\frac{1300}{1000+k_{dg}z} = \\ = \frac{0.4}{1+1500\cdot 0}\cdot\frac{1300}{1000+1.14\cdot 607.5} = 0.4\cdot 0.768 = 0.307 \tag{D.34}$$

$$V_{Rd,cf} = \frac{1}{\gamma_F}\left(k_v\sqrt{f_{ck}} + k_f f_{Ftuk} cot\theta\right) b_w z = \\ = \frac{1}{1}\left(0.307\sqrt{66.50} + 0.8\cdot 1.56\cdot \cot 29\right) 100\cdot 607.5 = \\ = (2.50+2.25)\,100\cdot 607.5/1000 = 288 \text{ kN} \tag{D.35}$$

MC-2020 [50]

Similar to the MC-2010 based on SMCFT, also requires referes to the section under study, x=1.013 m from the support($a/2$). This formulation requires also a non-linear analysis. Its implementation is performed in an Excel Spreadsheet using Solver with a GRG Nonlinear resolution method. Some parameters are not specified as are the same as for the MC-2010 based on SMCFT.

- calculated shear strength: $V_{u,cal}$=247.33 kN
- applied load by one jack: P=$V_{u,cal}$−$V_{sw,L}$=247.33-12.78=234.55 kN
- applied bending moment:

$$M_{ext} = \frac{q_{sw}x}{2}(L-x) + Px \\ = \frac{4.09\cdot 1.013}{2}(5-1.013) + 234.55\cdot 1.013 = 245.86 \text{ kNm} \tag{D.36}$$

- calculated bending moment:

$$M_{u,cal} = M_p + M_{ext} = -357.99 + 245.86 = -112.13 \text{ kN} \tag{D.37}$$

- longitudinal strain at the centre of the lever arm:

$$\varepsilon_x = \frac{\frac{M_{u,cal}}{z} + V_{u,cal} - N_{u,cal}\cdot\frac{z-e_p}{z}}{2\cdot E_p\cdot A_p} = \\ = \frac{\frac{-112.13}{0.607} + 247.33 - 2149\cdot\frac{0.607-0.08}{0.607}}{2\cdot 200\cdot 9\cdot 140} = \\ = \frac{-184.73 + 247.33 - 1865.77}{504000} = -3.57\text{E-}03 \geq 0 = \\ = 0 \tag{D.38}$$

- angle of the compressive stress field:

$$\theta = 29 + 7000\varepsilon_x = 29 + 7000 \cdot 0 = 29^\circ \tag{D.39}$$

- factor accounting for the ration between the tensile strength and the compressive strength of the concrete:

$$\begin{aligned} \xi &= (20 - 14000\varepsilon_x)\,\frac{K_s f_{Ftuk}}{f_{ck}} = (20 - 14000 \cdot 0)\,\frac{0.8 \cdot 1.56}{66.50} = \\ &= 20 \cdot 0.0188 = 0.376 \geq 0 \end{aligned} \tag{D.40}$$

- size and strain parameter:

$$\begin{aligned} k_v &= \frac{0.4}{1 + 1500\varepsilon_x + \xi}\,\frac{1300}{1000 + k_{dg} z} = \\ &= \frac{0.4}{1 + 1500 \cdot 0 + 0.376}\,\frac{1300}{1000 + 1.14 \cdot 607.5} = 0.291 \cdot 0.768 = 0.223 \end{aligned} \tag{D.41}$$

$$\begin{aligned} V_{Rd,cf} &= \frac{1}{\gamma_F}\left(k_v\sqrt{f_{ck}} + k_f f_{Ftuk} cot\theta\right) b_w z = \\ &= \frac{1}{1}\left(0.223\sqrt{66.50} + 0.8 \cdot 1.56 \cdot \cot 29\right) 100 \cdot 607.5/1000 = \\ &= (1.819 + 2.25)\,60.75 = 247.19 \text{ kN} \end{aligned} \tag{D.42}$$

Table D.1: Calculation of shear strength according to FprEN 1992-1-1:2023 [48] 1/2

Id	Ref.	Beam [kN]	$V_{u,test}$ [-]	ρ_{pw} [%]	d [mm]	b_w [mm]	z [mm]	A_c [mm^2]	a [m]	L [m]	$(L-a)$ [m]	x [m]	q_{sw} [kN/m]	σ_{cp} [MPa]	f_{R3} [MPa]	f_{Ftu} [MPa]	z_{c2} [mm]	d_{pbot} [mm]	d_{ptop} [mm]	A_{pbot} [mm^2]	A_{ptop} [mm^2]
1	[89]	HF400 h/6	420	1.74	725	100	652.5	1.69E+05	2.03	5.00	2.03	1.015	4.22	12.74	5.96	1.99	421	725	50	1260	280
2	[89]	HF600/4	392	1.87	675	100	607.5	1.82E+05	2.025	5.00	2.025	1.013	4.56	11.79	6.24	2.08	359	675	50	1260	280
3	[89]	HF600/5	347	1.87	675	100	607.5	1.82E+05	2.025	5.00	2.025	1.013	4.56	11.79	5.55	1.85	359	675	50	1260	280
4	[89]	HF400/7	390	1.87	675	100	607.5	1.64E+05	2.025	5.00	2.025	1.013	4.09	13.13	4.77	1.59	395	675	50	1260	280
5	[89]	HF400/8	428	1.87	675	100	607.5	1.64E+05	2.025	5.00	2.025	1.013	4.09	13.13	4.68	1.56	395	675	50	1260	280
6	[89]	HF260/9	326	1.87	675	100	607.5	1.49E+05	2.025	5.00	2.025	1.013	3.72	14.43	5.68	1.89	429	675	50	1260	280
49	[127]	T6a	266	5.8	316	60	284.4	4.90E+04	1.201	4.40	3.199	0.6	1.23	28.05	5.64	1.88	214	316	0	1100	200
53	[65]	I beam-3-DZ	574	2.76	630	120	567	2.24E+05	2.2	5.65	3.45	1.1	5.61	15.55	3.18	1.06	350	625	50	2085	417
54	[65]	I beam-4-DZ	709	2.76	630	120	567	2.24E+05	2.2	5.65	3.45	1.1	5.61	15.55	8.61	2.87	350	625	50	2085	417
55	[65]	I beam-5-DZ I	579	2.76	630	120	567	2.24E+05	2.2	5.65	3.45	1.1	5.61	15.55	3.18	1.06	350	625	50	2085	417
56	[65]	I beam-5-DZ II	542	2.76	630	120	567	2.24E+05	2.2	5.65	3.45	1.1	5.61	15.55	3.18	1.06	350	625	50	2085	417
57	[65]	I beam-6-DZ I	573	2.76	630	120	567	2.24E+05	2.2	5.65	3.45	1.1	5.61	15.55	8.61	2.87	350	625	50	2085	417
58	[65]	I beam-6-DZ II	608	2.76	630	120	567	2.24E+05	2.2	5.65	3.45	1.1	5.61	15.55	8.61	2.87	350	625	50	2085	417
62	[94]	1-2,5-20A	756	1.89	900	100	810	1.92E+05	2.25	17.45	15.2	1.125	4.81	12.34	4.09	1.36	531	883	0	1700	0
63	[94]	2-2,5-20A	781	1.89	900	100	810	1.92E+05	2.25	14.55	12.3	1.125	4.81	12.34	4.09	1.36	531	883	0	1700	0
64	[94]	3-2,5-20A	609	1.89	900	100	810	1.92E+05	2.25	12.15	9.9	1.125	4.81	12.34	4.09	1.36	531	883	0	1700	0
65	[94]	1-2,5-20B	786	1.89	900	100	810	1.92E+05	2.25	17.45	15.2	1.125	4.81	12.34	4.89	1.63	531	883	0	1700	0
66	[94]	2-2,5-20B	570	1.89	900	100	810	1.92E+05	2.25	14.55	12.3	1.125	4.81	12.34	4.89	1.63	531	883	0	1700	0
67	[94]	1-2,5-40A	799	1.89	900	100	810	1.92E+05	2.25	17.45	15.2	1.125	4.81	12.34	8.15	2.72	531	883	0	1700	0
68	[94]	2-2,5-40A	809	1.89	900	100	810	1.92E+05	2.25	14.55	12.3	1.125	4.81	12.34	8.15	2.72	531	883	0	1700	0
69	[94]	3-2,5-40A	737	1.89	900	100	810	1.92E+05	2.25	12.15	9.9	1.125	4.81	12.34	8.15	2.72	531	883	0	1700	0
70	[94]	1-2,5-40B	744	1.89	900	100	810	1.92E+05	2.25	17.45	15.2	1.125	4.81	12.34	7.08	2.36	531	883	0	1700	0
71	[94]	2-2,5-40B	599	1.89	900	100	810	1.92E+05	2.25	14.55	12.3	1.125	4.81	12.34	7.08	2.36	531	883	0	1700	0
72	[94]	1-2,5-20+20	696	1.89	900	100	810	1.92E+05	2.25	17.45	15.2	1.125	4.81	12.34	9.69	3.23	531	883	0	1700	0
73	[94]	2-3,0-20+20	595	1.89	900	100	810	1.92E+05	2.7	14.55	11.85	1.35	4.81	12.34	9.69	3.23	531	883	0	1700	0
74	[94]	1-2,5-60	672	1.89	900	100	810	1.92E+05	2.25	17.45	15.2	1.125	4.81	12.34	9.85	3.28	531	883	0	1700	0
75	[94]	3-2,5-60	721	1.89	900	100	810	1.92E+05	2.25	12.15	9.9	1.125	4.81	12.34	9.85	3.28	531	883	0	1700	0

Table D.2: Calculation of shear strength according to FprEN 1992-1-1:2023 [48] 2/2

Id	Ref.	Beam	e_p [mm]	k_1 [-]	$V_{u,test}$ [kN]	$M_{u,test}$ [kNm]	$a_{cs,0}$ [m]	η_{cF} [-]	f_c [MPa]	D_{Max} [mm]	d_{g0} [mm]	$\tau_{Rdc,0}$ [MPa]	τ_{Rdc} [MPa]	$\tau_{Rd,cF}$ [MPa]	f_{py} [MPa]	$\tau_{Rdc,min}$ [MPa]	$\tau_{RdcF,min}$ [MPa]	V_{Rd} [kN]	γ_{mod} [-]
1	[89]	HF400 h/6	181	0.47	309	309	1.00	0.4	57	12	23	0.96	6.89	4.74	1691	0.36	2.13	309	1.36
2	[89]	HF600/4	202	0.54	306	305	1.00	0.4	62	12	22.53	1.04	7.4	5.04	1691	0.39	2.23	306	1.28
3	[89]	HF600/5	202	0.54	292	291	0.99	0.4	63	12	22.43	1.04	7.4	4.81	1691	0.39	2.00	292	1.19
4	[89]	HF400/7	167	0.48	279	277	1.00	0.41	60	12	22.92	1.03	7.4	4.59	1691	0.38	1.75	279	1.40
5	[89]	HF400/8	167	0.48	283	282	1.00	0.42	67	12	21.7	1.05	7.41	4.67	1691	0.39	1.72	284	1.51
6	[89]	HF260/9	133	0.44	295	294	1.00	0.4	62	12	22.61	1.04	7.38	4.84	1691	0.38	2.05	294	1.11
49	[127]	T6a	53	0.52	145	40	0.32	0.4	96	8	16.78	2.04	16.54	8.5	1691	0.6	2.12	145	1.83
53	[65]	I beam-3-DZ	179	0.59	541	230	0.63	0.67	56	15	16	1.04	10.27	7.94	1691	0.32	1.27	541	1.06
54	[65]	I beam-4-DZ	179	0.59	476	404	0.85	0.4	63	15	16	1.08	10.32	7	1691	0.34	3.01	476	1.49
55	[65]	I beam-5-DZ I	179	0.59	541	230	0.63	0.67	56	15	16	1.04	10.27	7.94	1691	0.32	1.27	541	1.07
56	[65]	I beam-5-DZ II	179	0.59	541	230	0.63	0.67	56	15	16	1.04	10.27	7.94	1691	0.32	1.27	541	1.00
57	[65]	I beam-6-DZ I	179	0.59	475	403	0.85	0.4	57	15	16	1.05	10.28	6.98	1691	0.32	3	475	1.21
58	[65]	I beam-6-DZ II	179	0.59	475	403	0.85	0.4	57	15	16	1.05	10.28	6.98	1691	0.32	3	475	1.28
62	[94]	1-2,5-20A	352	0.43	368	251	0.90	0.52	50	14	22	0.87	6.14	4.54	1691	0.3	1.52	368	2.05
63	[94]	2-2,5-20A	352	0.43	368	251	0.90	0.52	50	14	22	0.87	6.14	4.54	1691	0.3	1.52	368	2.12
64	[94]	3-2,5-20A	352	0.43	368	251	0.90	0.52	50	14	22	0.87	6.14	4.54	1691	0.3	1.52	368	1.65
65	[94]	1-2,5-20B	352	0.43	331	259	0.90	0.4	50	14	22	0.87	6.14	4.09	1691	0.3	1.75	331	2.37
66	[94]	2-2,5-20B	352	0.43	331	259	0.90	0.4	50	14	22	0.87	6.14	4.09	1691	0.3	1.75	331	1.72
67	[94]	1-2,5-40A	352	0.43	421	411	0.98	0.4	61	14	21.8	0.93	6.2	5.2	1691	0.33	2.85	421	1.90
68	[94]	2-2,5-40A	352	0.43	421	411	0.98	0.4	61	14	21.8	0.93	6.2	5.2	1691	0.33	2.85	421	1.92
69	[94]	3-2,5-40A	352	0.43	421	411	0.98	0.4	61	14	21.8	0.93	6.2	5.2	1691	0.33	2.85	421	1.75
70	[94]	1-2,5-40B	352	0.43	392	362	0.92	0.4	61	14	21.8	0.93	6.2	4.84	1691	0.33	2.49	392	1.90
71	[94]	2-2,5-40B	352	0.43	392	444	1.13	0.4	61	14	21.8	0.93	6.2	4.84	1691	0.33	2.49	392	1.53
72	[94]	1-2,5-20+20	352	0.43	461	522	1.13	0.4	53	14	22	0.89	6.16	5.69	1691	0.3	3.35	461	1.51
73	[94]	2-3,0-20+20	352	0.43	461	627	1.36	0.4	53	14	22	0.89	6.16	5.69	1691	0.3	3.35	461	1.29
74	[94]	1-2,5-60	352	0.43	467	528	1.13	0.4	63	14	21.44	0.93	6.2	5.76	1691	0.33	3.41	467	1.44
75	[94]	3-2,5-60	352	0.43	467	528	1.13	0.4	63	14	21.44	0.93	6.2	5.76	1691	0.33	3.41	467	1.54
																		m	1.54
																		s	0.36
																		v	0.23

Table D.3: Calculation of shear strength according to Spanish National Code [70] 1/1

Id	Ref.	Beam	$V_{u,test}$ [kN]	κ [-]	d [mm]	k [-]	f_{R3} [MPa]	τ_f [MPa]	b_f [mm]	b_w [mm]	h_f [mm]	k_f [-]	V_{fu} [kN]	ρ [%]	ρ_{lim} [%]	f_{1cm} [MPa]	σ_{cp} [MPa]	$\sigma_{cp,lim}$ [MPa]	V_{cu} [kN]	V_{u2} [kN]	γ_{mod} [-]
1	[89]	HF400 h/6	420	2.8	725	1.53	5.96	0.98	400	100	84	1.5	114	1.74	1.74	57	12.7	11.3	215	329	1.28
2	[89]	HF600/4	392	3	675	1.54	6.24	1.03	600	100	84	1.5	113	1.87	1.87	62	11.8	11.8	211	324	1.21
3	[89]	HF600/5	347	3	675	1.54	5.55	0.92	600	100	84	1.5	100	1.87	1.87	63	11.8	11.8	211	311	1.12
4	[89]	HF400/7	390	3	675	1.54	4.77	0.79	400	100	84	1.5	86	1.87	1.87	60	13.1	12.1	213	299	1.30
5	[89]	HF400/8	428	3	675	1.54	4.68	0.77	400	100	84	1.5	85	1.87	1.87	67	13.1	13.1	227	311	1.38
6	[89]	HF260/9	326	3	675	1.54	5.68	0.94	260	100	84	1.5	103	1.87	1.87	62	14.4	12.4	216	319	1.02
53	[65]	I beam-3-DZ	574	3.49	630	1.56	3.18	0.52	600	120	52.5	1.5	65	2.76	2	56	15.6	11.2	230	295	1.95
54	[65]	I beam-4-DZ	709	3.49	630	1.56	8.61	1.42	600	120	52.5	1.5	176	2.76	2	63	15.6	12.6	250	426	1.66
55	[65]	I beam-5-DZ I	579	3.49	630	1.56	3.18	0.52	600	120	52.5	1.5	65	2.76	2	56	15.6	11.2	230	295	1.96
56	[65]	I beam-5-DZ II	542	3.49	630	1.56	3.18	0.52	600	120	52.5	1.5	65	2.76	2	56	15.6	11.2	230	295	1.84
57	[65]	I beam-6-DZ I	573	3.49	630	1.56	8.61	1.42	600	120	52.5	1.5	176	2.76	2	57	15.6	11.4	232	409	1.40
58	[65]	I beam-6-DZ II	608	3.49	630	1.56	8.61	1.42	600	120	52.5	1.5	176	2.76	2	57	15.6	11.4	232	409	1.49
62	[94]	1-2,5-20A	756	2.5	900	1.47	4.09	0.68	400	100	50	1.5	94	1.89	1.89	50	12.3	10	244	337	2.24
63	[94]	2-2,5-20A	781	2.5	900	1.47	4.09	0.68	400	100	50	1.5	94	1.89	1.89	50	12.3	10	244	337	2.31
64	[94]	3-2,5-20A	609	2.5	900	1.47	4.09	0.68	400	100	50	1.5	94	1.89	1.89	50	12.3	10	244	337	1.80
65	[94]	1-2,5-20B	786	2.5	900	1.47	4.89	0.81	400	100	50	1.5	112	1.89	1.89	50	12.3	10	244	356	2.21
66	[94]	2-2,5-20B	570	2.5	900	1.47	4.89	0.81	400	100	50	1.5	112	1.89	1.89	50	12.3	10	244	356	1.60
67	[94]	1-2,5-40A	799	2.5	900	1.47	8.15	1.34	400	100	50	1.5	187	1.89	1.89	61	12.3	12.2	281	468	1.71
68	[94]	2-2,5-40A	809	2.5	900	1.47	8.15	1.34	400	100	50	1.5	187	1.89	1.89	61	12.3	12.2	281	468	1.73
69	[94]	3-2,5-40A	737	2.5	900	1.47	8.15	1.34	400	100	50	1.5	187	1.89	1.89	61	12.3	12.2	281	468	1.58
70	[94]	1-2,5-40B	744	2.5	900	1.47	7.08	1.17	400	100	50	1.5	162	1.89	1.89	61	12.3	12.2	281	443	1.68
71	[94]	2-2,5-40B	599	2.5	900	1.47	7.08	1.17	400	100	50	1.5	162	1.89	1.89	61	12.3	12.2	281	443	1.35
72	[94]	1-2,5-20+20	696	2.5	900	1.47	9.69	1.6	400	100	50	1.5	222	1.89	1.89	53	12.3	10.6	254	476	1.46
73	[94]	2-3,0-20+20	595	3	900	1.47	9.69	1.6	400	100	50	1.5	222	1.89	1.89	53	12.3	10.6	254	476	1.25
74	[94]	1-2,5-60	672	2.5	900	1.47	9.85	1.62	400	100	50	1.5	226	1.89	1.89	63	12.3	12.3	284	510	1.32
75	[94]	3-2,5-60	721	2.5	900	1.47	9.85	1.62	400	100	50	1.5	226	1.89	1.89	63	12.3	12.3	284	510	1.41
																				m	1.59
																				s	0.35
																				v	0.22

Table D.4: Calculation of shear strength according to Model Code 2010 [49] 1/1

Id	Ref.	Beam	$V_{u,test}$ [kN]	κ [-]	f_{R3} [MPa]	f_{1cm} [MPa]	d [mm]	b_w [mm]	k [-]	ρ_l [%]	f_{Ftu} [MPa]	σ_{cp} [MPa]	f_{ctk} [MPa]	$V_{Rd,F}$ [kN]	γ_{mod} [-]
1	[89]	HF400 h/6	420	2.8	5.96	57	725	100	1.53	1.74	1.99	12.7	3.09	304	1.38
2	[89]	HF600/4	392	3	6.24	62	675	100	1.54	1.87	2.08	11.8	3.2	284	1.38
3	[89]	HF600/5	347	3	5.55	63	675	100	1.54	1.87	1.85	11.8	3.21	279	1.24
4	[89]	HF400/7	390	3	4.77	60	675	100	1.54	1.87	1.59	13.1	3.17	285	1.37
5	[89]	HF400/8	428	3	4.68	67	675	100	1.54	1.87	1.56	13.1	3.29	288	1.49
6	[89]	HF260/9	326	3	5.68	62	675	100	1.54	1.87	1.89	14.4	3.2	307	1.06
43	[127]	T1a	234	3.8	2.8	102	316	60	1.8	3.69	0.93	22.9	3.83	128	1.83
44	[127]	T1b	267	3.8	2.8	117	316	60	1.8	5.8	0.93	28	4.01	155	1.72
46	[127]	T3b	408	3.8	5.39	115	316	60	1.8	5.8	1.8	28	3.98	167	2.44
49	[127]	T6a	266	3.8	5.64	96	316	60	1.8	5.8	1.88	28	3.75	165	1.62
50	[127]	T6b	226	3.8	2.8	105	316	60	1.8	5.8	0.93	28	3.86	153	1.48
53	[65]	I beam-3-DZ	574	3.49	3.18	56	630	120	1.56	2.76	1.06	15.6	3.08	351	1.64
54	[65]	I beam-4-DZ	709	3.49	8.61	63	630	120	1.56	2.76	2.87	15.6	3.22	411	1.73
55	[65]	I beam-5-DZ I	579	3.49	3.18	56	630	120	1.56	2.76	1.06	15.6	3.08	351	1.65
56	[65]	I beam-5-DZ II	542	3.49	3.18	56	630	120	1.56	2.76	1.06	15.6	3.08	351	1.54
57	[65]	I beam-6-DZ I	573	3.49	8.61	57	630	120	1.56	2.76	2.87	15.6	3.1	405	1.41
58	[65]	I beam-6-DZ II	608	3.49	8.61	57	630	120	1.56	2.76	2.87	15.6	3.1	405	1.50
62	[94]	1-2,5-20A	756	2.5	4.09	50	900	100	1.47	1.89	1.36	12.3	2.95	345	2.19
63	[94]	2-2,5-20A	781	2.5	4.09	50	900	100	1.47	1.89	1.36	12.3	2.95	345	2.26
64	[94]	3-2,5-20A	609	2.5	4.09	50	900	100	1.47	1.89	1.36	12.3	2.95	345	1.76
65	[94]	1-2,5-20B	786	2.5	4.89	50	900	100	1.47	1.89	1.63	12.3	2.95	354	2.22
66	[94]	2-2,5-20B	570	2.5	4.89	50	900	100	1.47	1.89	1.63	12.3	2.95	354	1.61
67	[94]	1-2,5-40A	799	2.5	8.15	61	900	100	1.47	1.89	2.72	12.3	3.18	393	2.04
68	[94]	2-2,5-40A	809	2.5	8.15	61	900	100	1.47	1.89	2.72	12.3	3.18	393	2.06
69	[94]	3-2,5-40A	737	2.5	8.15	61	900	100	1.47	1.89	2.72	12.3	3.18	393	1.88
70	[94]	1-2,5-40B	744	2.5	7.08	61	900	100	1.47	1.89	2.36	12.3	3.18	384	1.94
71	[94]	2-2,5-40B	599	2.5	7.08	61	900	100	1.47	1.89	2.36	12.3	3.18	384	1.56
72	[94]	1-2,5-20+20	696	2.5	9.69	53	900	100	1.47	1.89	3.23	12.3	3.02	397	1.75
73	[94]	2-3,0-20+20	595	3	9.69	53	900	100	1.47	1.89	3.23	12.3	3.02	397	1.50
74	[94]	1-2,5-60	672	2.5	9.85	63	900	100	1.47	1.89	3.28	12.3	3.22	407	1.65
75	[94]	3-2,5-60	721	2.5	9.85	63	900	100	1.47	1.89	3.28	12.3	3.22	407	1.77
														m	1.70
														s	0.32
														v	0.19

Table D.5: Calculation of shear strength according to Model Code 2010 Comment section [49] 1/2

Id	Ref.	Beam	$V_{u,test}$ [kN]	κ [-]	b_w [mm]	z [mm]	f_{R3} [MPa]	f_{Ftu} [MPa]	f_{1cm} [MPa]	d_g [mm]	k_{dg} [-]	A_p [mm^2]	E_p [GPa]	e_p [mm]	A_c [mm^2]	Ensayo [-]	a [m]	L [m]	$(L-a)$ [m]	x [m]	q_{sw} [kN/m]
1	[89]	HF400 h/6	420	2.8	100	653	5.96	1.99	57	12	1.14	1260	200	84	1.69E+05	4	2.03	5.00	2.03	1.02	4.22
2	[89]	HF600/4	392	3	100	608	6.24	2.08	62	12	1.14	1260	200	47	1.82E+05	4	2.03	5.00	2.03	1.01	4.56
3	[89]	HF600/5	347	3	100	608	5.55	1.85	63	12	1.14	1260	200	47	1.82E+05	4	2.03	5.00	2.03	1.01	4.56
4	[89]	HF400/7	390	3	100	608	4.77	1.59	60	12	1.14	1260	200	82	1.64E+05	4	2.03	5.00	2.03	1.01	4.09
5	[89]	HF400/8	428	3	100	608	4.68	1.56	67	12	1.14	1260	200	82	1.64E+05	4	2.03	5.00	2.03	1.01	4.09
6	[89]	HF260/9	326	3	100	608	5.68	1.89	62	12	1.14	1260	200	116	1.49E+05	4	2.03	5.00	2.03	1.01	3.72
43	[127]	T1a	234	3.8	60	284	2.8	0.93	102	8	1.33	700	200	56	4.90E+04	3	1.2	4.40	3.2	0.6	1.23
44	[127]	T1b	267	3.8	60	284	2.8	0.93	117	8	1.33	1100	200	56	4.90E+04	3	1.2	2.40	1.2	0.6	1.23
46	[127]	T3b	408	3.8	60	284	5.39	1.8	115	8	1.33	1100	200	56	4.90E+04	3	1.2	2.40	1.2	0.6	1.23
49	[127]	T6a	266	3.8	60	284	5.64	1.88	96	8	1.33	1100	200	56	4.90E+04	3	1.2	4.40	3.2	0.6	1.23
50	[127]	T6b	226	3.8	60	284	2.8	0.93	105	8	1.33	1100	200	56	4.90E+04	3	1.2	2.40	1.2	0.6	1.23
53	[65]	I beam-3-DZ	574	3.49	120	567	3.18	1.06	56	15	1.03	2500	200	63	2.24E+05	3	2.2	5.65	3.45	1.1	5.61
54	[65]	I beam-4-DZ	709	3.49	120	567	8.61	2.87	63	15	1.03	2500	200	63	2.24E+05	3	2.2	5.65	3.45	1.1	5.61
55	[65]	I beam-5-DZ I	579	3.49	120	567	3.18	1.06	56	15	1.03	2500	200	63	2.24E+05	3	2.2	5.65	3.45	1.1	5.61
56	[65]	I beam-5-DZ II	542	3.49	120	567	3.18	1.06	56	15	1.03	2500	200	63	2.24E+05	3	2.2	5.65	3.45	1.1	5.61
57	[65]	I beam-6-DZ I	573	3.49	120	567	8.61	2.87	57	15	1.03	2500	200	63	2.24E+05	3	2.2	5.65	3.45	1.1	5.61
58	[65]	I beam-6-DZ II	608	3.49	120	567	8.61	2.87	57	15	1.03	2500	200	63	2.24E+05	3	2.2	5.65	3.45	1.1	5.61
62	[94]	1-2,5-20A	756	2.5	100	810	4.09	1.36	50	14	1.07	1700	200	89	1.92E+05	3	2.25	17.45	15.2	1.13	4.81
63	[94]	2-2,5-20A	781	2.5	100	810	4.09	1.36	50	14	1.07	1700	200	89	1.92E+05	3	2.25	14.55	12.3	1.13	4.81
64	[94]	3-2,5-20A	609	2.5	100	810	4.09	1.36	50	14	1.07	1700	200	89	1.92E+05	3	2.25	12.15	9.9	1.13	4.81
65	[94]	1-2,5-20B	786	2.5	100	810	4.89	1.63	50	14	1.07	1700	200	89	1.92E+05	3	2.25	17.45	15.2	1.13	4.81
66	[94]	2-2,5-20B	570	2.5	100	810	4.89	1.63	50	14	1.07	1700	200	89	1.92E+05	3	2.25	14.55	12.3	1.13	4.81
67	[94]	1-2,5-40A	799	2.5	100	810	8.15	2.72	61	14	1.07	1700	200	89	1.92E+05	3	2.25	17.45	15.2	1.13	4.81
68	[94]	2-2,5-40A	809	2.5	100	810	8.15	2.72	61	14	1.07	1700	200	89	1.92E+05	3	2.25	14.55	12.3	1.13	4.81
69	[94]	3-2,5-40A	737	2.5	100	810	8.15	2.72	61	14	1.07	1700	200	89	1.92E+05	3	2.25	12.15	9.9	1.13	4.81
70	[94]	1-2,5-40B	744	2.5	100	810	7.08	2.36	61	14	1.07	1700	200	89	1.92E+05	3	2.25	17.45	15.2	1.13	4.81
71	[94]	2-2,5-40B	599	2.5	100	810	7.08	2.36	61	14	1.07	1700	200	89	1.92E+05	3	2.25	14.55	12.3	1.13	4.81
72	[94]	1-2,5-20+20	696	2.5	100	810	9.69	3.23	53	14	1.07	1700	200	89	1.92E+05	3	2.25	17.45	15.2	1.13	4.81
73	[94]	2-3,0-20+20	595	3	100	810	9.69	3.23	53	14	1.07	1700	200	89	1.92E+05	3	2.7	14.55	11.85	1.35	4.81
74	[94]	1-2,5-60	672	2.5	100	810	9.85	3.28	63	14	1.07	1700	200	89	1.92E+05	3	2.25	17.45	15.2	1.13	4.81
75	[94]	3-2,5-60	721	2.5	100	810	9.85	3.28	63	14	1.07	1700	200	89	1.92E+05	3	2.25	12.15	9.9	1.13	4.81

Table D.6: Calculation of shear strength according to Model Code 2010 Comment section [49] 2/2

Id	Ref.	Beam	V_{sw} [kN]	V_{load} [kN]	P [kN]	M_{load} [kNm]	F_{pbot} [kN]	d_{pbot} [mm]	z_{c2} [mm]	F_{ptop} [kN]	d_{ptop} [mm]	M_p [kNm]	M_{Ed} [kNm]	N_{Ed} [kN]	ε_x [-]	θ [°]	k_v [-]	$V_{Rd,F}$ [kN]	γ_{mod} [-]
1	[89]	HF400 h/6	6.28	320	320	333	1758	725	421.3	390.6	50	-389	-55	2148	-3.22E-03	29	0.3	333	1.26
2	[89]	HF600/4	6.78	315	315	328	1758	675	359.2	390.6	50	-434	-106	2148	-3.63E-03	29	0.31	329	1.19
3	[89]	HF600/5	6.78	295	295	308	1758	675	359.2	390.6	50	-434	-126	2148	-3.73E-03	29	0.31	310	1.12
4	[89]	HF400/7	6.08	271	271	283	1758	675	394.7	390.6	50	-358	-75	2148	-3.37E-03	29	0.31	284	1.37
5	[89]	HF400/8	6.08	276	276	288	1758	675	394.7	390.6	50	-358	-70	2148	-3.34E-03	29	0.31	289	1.48
6	[89]	HF260/9	5.54	301	301	312	1758	675	428.5	390.6	50	-285	27	2148	-2.74E-03	29	0.31	313	1.04
43	[127]	T1a	1.96	86	118	53	875	316	214.3	250	0	-35	18	1125	-2.69E-03	29	0.38	88	2.66
44	[127]	T1b	0.74	92	184	56	1125	316	214.3	250	0	-61	-5	1375	-2.34E-03	29	0.38	93	2.88
46	[127]	T3b	0.74	112	225	68	1125	316	214.3	250	0	-61	7	1375	-2.19E-03	29	0.38	113	3.61
49	[127]	T6a	1.96	107	148	66	1125	316	214.3	250	0	-61	5	1375	-2.22E-03	29	0.38	109	2.43
50	[127]	T6b	0.74	88	176	54	1125	316	214.3	250	0	-61	-7	1375	-2.36E-03	29	0.38	89	2.55
53	[65]	I beam-3-DZ	9.68	261	428	302	2909	625	350	581.7	50	-625	-324	3490	-3.40E-03	29	0.33	271	2.12
54	[65]	I beam-4-DZ	9.68	449	736	508	2909	625	350	581.7	50	-625	-117	3490	-2.85E-03	29	0.33	459	1.54
55	[65]	I beam-5-DZ I	9.68	261	428	302	2909	625	350	581.7	50	-625	-324	3490	-3.40E-03	29	0.33	271	2.14
56	[65]	I beam-5-DZ II	9.68	261	428	302	2909	625	350	581.7	50	-625	-324	3490	-3.40E-03	29	0.33	271	2
57	[65]	I beam-6-DZ I	9.68	441	722	499	2909	625	350	581.7	50	-625	-127	3490	-2.88E-03	29	0.33	450	1.27
58	[65]	I beam-6-DZ II	9.68	441	722	499	2909	625	350	581.7	50	-625	-127	3490	-2.88E-03	29	0.33	450	1.35
62	[94]	1-2,5-20A	36.53	283	325	362	2372	882.5	530.6	0	0	-834	-472	2372	-3.49E-03	29	0.28	319	2.37
63	[94]	2-2,5-20A	29.56	290	343	362	2372	882.5	530.6	0	0	-834	-472	2372	-3.49E-03	29	0.28	319	2.45
64	[94]	3-2,5-20A	23.79	295	363	362	2372	882.5	530.6	0	0	-834	-472	2372	-3.49E-03	29	0.28	319	1.91
65	[94]	1-2,5-20B	36.53	314	360	397	2372	882.5	530.6	0	0	-834	-437	2372	-3.38E-03	29	0.28	350	2.24
66	[94]	2-2,5-20B	29.56	321	379	397	2372	882.5	530.6	0	0	-834	-437	2372	-3.38E-03	29	0.28	350	1.63
67	[94]	1-2,5-40A	36.53	457	525	559	2372	882.5	530.6	0	0	-834	-276	2372	-2.88E-03	29	0.28	494	1.62
68	[94]	2-2,5-40A	29.56	464	549	559	2372	882.5	530.6	0	0	-834	-276	2372	-2.88E-03	29	0.28	494	1.64
69	[94]	3-2,5-40A	23.79	470	577	559	2372	882.5	530.6	0	0	-834	-276	2372	-2.88E-03	29	0.28	494	1.49
70	[94]	1-2,5-40B	36.53	416	477	512	2372	882.5	530.6	0	0	-834	-322	2372	-3.02E-03	29	0.28	452	1.64
71	[94]	2-2,5-40B	29.56	423	500	512	2372	882.5	530.6	0	0	-834	-322	2372	-3.02E-03	29	0.28	452	1.32
72	[94]	1-2,5-20+20	36.53	506	580	613	2372	882.5	530.6	0	0	-834	-222	2372	-2.71E-03	29	0.28	542	1.28
73	[94]	2-3,0-20+20	28.48	514	631	736	2372	882.5	530.6	0	0	-834	-98	2372	-2.48E-03	29	0.28	542	1.1
74	[94]	1-2,5-60	36.53	527	605	637	2372	882.5	530.6	0	0	-834	-198	2372	-2.63E-03	29	0.28	563	1.19
75	[94]	3-2,5-60	23.79	539	662	637	2372	882.5	530.6	0	0	-834	-198	2372	-2.63E-03	29	0.28	563	1.28
																		m	1.78
																		s	0.62
																		v	0.35

Table D.7: Calculation of shear strength according to Model Code 2023 [50] 1/2

Id	Ref.	Beam	V_{test} [kN]	a/d [-]	f_{R3} [MPa]	f_{Ftu} [MPa]	f_{cm} [MPa]	k_{dg} [-]	A_p [mm^2]	E_p [GPa]	e_p [mm]	A_c [mm^2]	Ensayo [-]	a [m]	L [m]	$(L-a)$ [m]	x [m]	q_{sw} [kN/m]	V_{sw} [kN]	V_{load} [kN]
1	[89]	HF400 h/6	420	3	5.96	1.99	57	1.14	1260	200	84	1.69E+05	4	2.03	5.00	2.03	1.02	4.2	6.26	267
2	[89]	HF600/4	392	3	6.24	2.08	62	1.14	1260	200	47	1.82E+05	4	2.03	5.00	2.03	1.01	4.6	6.78	264
3	[89]	HF600/5	347	3	5.55	1.85	63	1.14	1260	200	47	1.82E+05	4	2.03	5.00	2.03	1.01	4.6	6.78	248
4	[89]	HF400/7	390	3	4.77	1.59	60	1.14	1260	200	82	1.64E+05	4	2.03	5.00	2.03	1.01	4.1	6.08	228
5	[89]	HF400/8	428	3	4.68	1.56	67	1.14	1260	200	82	1.64E+05	4	2.03	5.00	2.03	1.01	4.1	6.08	235
6	[89]	HF260/9	326	3	5.68	1.89	62	1.14	1260	200	116	1.49E+05	4	2.03	5.00	2.03	1.01	3.7	5.54	253
43	[127]	T1a	234	4	2.8	0.93	102	1.33	700	200	56	4.90E+04	3	1.2	4.4	3.2	0.6	1.2	2	78
44	[127]	T1b	267	4	2.8	0.93	117	1.33	1100	200	56	4.90E+04	3	1.2	2.4	1.2	0.6	1.2	0.7	84
46	[127]	T3b	408	4	5.39	1.8	115	1.33	1100	200	56	4.90E+04	3	1.2	2.4	1.2	0.6	1.2	0.7	99
49	[127]	T6a	266	4	5.64	1.88	96	1.33	1100	200	56	4.90E+04	3	1.2	4.4	3.2	0.6	1.2	2	92
50	[127]	T6b	226	4	2.8	0.93	105	1.33	1100	200	56	4.90E+04	3	1.2	2.4	1.2	0.6	1.2	0.7	80
53	[65]	I beam-3-DZ	574	3	3.18	1.06	56	1.03	2500	200	63	2.24E+05	3	2.2	5.65	3.45	1.1	5.6	9.7	223
54	[65]	I beam-4-DZ	709	3	8.61	2.87	63	1.03	2500	200	63	2.24E+05	3	2.2	5.65	3.45	1.1	5.6	9.7	375
55	[65]	I beam-5-DZ I	579	3	3.18	1.06	56	1.03	2500	200	63	2.24E+05	3	2.2	5.65	3.45	1.1	5.6	9.7	223
56	[65]	I beam-5-DZ II	542	3	3.18	1.06	56	1.03	2500	200	63	2.24E+05	3	2.2	5.65	3.45	1.1	5.6	9.7	223
57	[65]	I beam-6-DZ I	573	3	8.61	2.87	57	1.03	2500	200	63	2.24E+05	3	2.2	5.65	3.45	1.1	5.6	9.7	365
58	[65]	I beam-6-DZ II	608	3	8.61	2.87	57	1.03	2500	200	63	2.24E+05	3	2.2	5.65	3.45	1.1	5.6	9.7	365
62	[94]	1-2,5-20A	756	3	4.09	1.36	50	1.07	1700	200	89	1.92E+05	3	2.25	17.45	15.2	1.13	4.8	36.5	234
63	[94]	2-2,5-20A	781	3	4.09	1.36	50	1.07	1700	200	89	1.92E+05	3	2.25	14.55	12.3	1.13	4.8	29.6	241
64	[94]	3-2,5-20A	609	3	4.09	1.36	50	1.07	1700	200	89	1.92E+05	3	2.25	12.15	9.9	1.13	4.8	23.8	247
65	[94]	1-2,5-20B	786	3	4.89	1.63	50	1.07	1700	200	89	1.92E+05	3	2.25	17.45	15.2	1.13	4.8	36.5	259
66	[94]	2-2,5-20B	570	3	4.89	1.63	50	1.07	1700	200	89	1.92E+05	3	2.25	14.55	12.3	1.13	4.8	29.6	266
67	[94]	1-2,5-40A	799	3	8.15	2.72	61	1.07	1700	200	89	1.92E+05	3	2.25	17.45	15.2	1.13	4.8	36.5	384
68	[94]	2-2,5-40A	809	3	8.15	2.72	61	1.07	1700	200	89	1.92E+05	3	2.25	14.55	12.3	1.13	4.8	29.6	391
69	[94]	3-2,5-40A	737	3	8.15	2.72	61	1.07	1700	200	89	1.92E+05	3	2.25	12.15	9.9	1.13	4.8	23.8	397
70	[94]	1-2,5-40B	744	3	7.08	2.36	61	1.07	1700	200	89	1.92E+05	3	2.25	17.45	15.2	1.13	4.8	36.5	348
71	[94]	2-2,5-40B	599	3	7.08	2.36	61	1.07	1700	200	89	1.92E+05	3	2.25	14.55	12.3	1.13	4.8	29.6	355
72	[94]	1-2,5-20+20	696	3	9.69	3.23	53	1.07	1700	200	89	1.92E+05	3	2.25	17.45	15.2	1.13	4.8	36.5	424
73	[94]	2-3,0-20+20	595	3	9.69	3.23	53	1.07	1700	200	89	1.92E+05	3	2.7	14.55	11.85	1.35	4.8	28.5	432
74	[94]	1-2,5-60	672	3	9.85	3.28	63	1.07	1700	200	89	1.92E+05	3	2.25	17.45	15.2	1.13	4.8	36.5	445
75	[94]	3-2,5-60	721	3	9.85	3.28	63	1.07	1700	200	89	1.92E+05	3	2.25	12.15	9.9	1.13	4.8	23.8	458

Table D.8: Calculation of shear strength according to Model Code 2023 [50] 2/2

Id	Ref.	Beam	P_{load} [kN]	V_{Ed} [kN]	M_{load} [kNm]	F_{pbot} [kN]	d_{pbot} [mm]	z_{c2} [mm]	F_{ptop} [kN]	d_{ptop} [mm]	M_p [kNm]	M_{Ed} [kNm]	N_{Ed} [kN]	ε_x [-]	θ [°]	ξ [-]	k_v [-]	b_w [mm]	z [mm]	V_{Rd_F} [kN]	γ_{mod} [-]
1	[89]	HF400 h/6	267	281	280	1758	725	421.3	390.6	50	-389	-109	2148	-3.49E-03	29	0.56	0.19	100	653	281	1.5
2	[89]	HF600/4	264	278	276	1758	675	359.2	390.6	50	-434	-158	2148	-3.90E-03	29	0.54	0.2	100	608	278	1.41
3	[89]	HF600/5	248	262	260	1758	675	359.2	390.6	50	-434	-174	2148	-3.98E-03	29	0.47	0.21	100	608	262	1.32
4	[89]	HF400/7	228	241	240	1758	675	394.7	390.6	50	-358	-118	2148	-3.59E-03	29	0.42	0.22	100	608	241	1.62
5	[89]	HF400/8	235	247	246	1758	675	394.7	390.6	50	-358	-112	2148	-3.56E-03	29	0.38	0.22	100	608	247	1.73
6	[89]	HF260/9	253	264	263	1758	675	428.5	390.6	50	-285	-22	2148	-3.00E-03	29	0.49	0.21	100	608	264	1.23
43	[127]	T1a	107	80	48	875	316	214.3	250	0	-35	13	1125	-2.78E-03	29	0.15	0.33	60	284	80	2.94
44	[127]	T1b	168	85	51	1125	316	214.3	250	0	-61	-10	1375	-2.39E-03	29	0.13	0.33	60	284	85	3.15
46	[127]	T3b	197	99	60	1125	316	214.3	250	0	-61	-1	1375	-2.29E-03	29	0.25	0.3	60	284	99	4.11
49	[127]	T6a	127	94	57	1125	316	214.3	250	0	-61	-4	1375	-2.32E-03	29	0.31	0.29	60	284	94	2.82
50	[127]	T6b	160	81	49	1125	316	214.3	250	0	-61	-12	1375	-2.42E-03	29	0.14	0.33	60	284	81	2.8
53	[65]	I beam-3-DZ	365	232	259	2909	625	350	581.7	50	-625	-366	3490	-3.52E-03	29	0.3	0.25	120	567	232	2.47
54	[65]	I beam-4-DZ	613	384	426	2909	625	350	581.7	50	-625	-199	3490	-3.07E-03	29	0.73	0.19	120	567	384	1.84
55	[65]	I beam-5-DZ I	365	232	259	2909	625	350	581.7	50	-625	-366	3490	-3.52E-03	29	0.3	0.25	120	567	232	2.49
56	[65]	I beam-5-DZ II	365	232	259	2909	625	350	581.7	50	-625	-366	3490	-3.52E-03	29	0.3	0.25	120	567	232	2.33
57	[65]	I beam-6-DZ I	599	375	416	2909	625	350	581.7	50	-625	-209	3490	-3.10E-03	29	0.81	0.18	120	567	375	1.53
58	[65]	I beam-6-DZ II	599	375	416	2909	625	350	581.7	50	-625	-209	3490	-3.10E-03	29	0.81	0.18	120	567	375	1.62
62	[94]	1-2,5-20A	269	271	308	2372	882.5	530.6	0	0	-834	-527	2372	-3.66E-03	29	0.44	0.19	100	810	271	2.79
63	[94]	2-2,5-20A	285	271	308	2372	882.5	530.6	0	0	-834	-527	2372	-3.66E-03	29	0.44	0.19	100	810	271	2.88
64	[94]	3-2,5-20A	303	271	308	2372	882.5	530.6	0	0	-834	-527	2372	-3.66E-03	29	0.44	0.19	100	810	271	2.25
65	[94]	1-2,5-20B	297	296	335	2372	882.5	530.6	0	0	-834	-499	2372	-3.57E-03	29	0.52	0.18	100	810	296	2.66
66	[94]	2-2,5-20B	315	296	335	2372	882.5	530.6	0	0	-834	-499	2372	-3.57E-03	29	0.52	0.18	100	810	296	1.93
67	[94]	1-2,5-40A	441	421	476	2372	882.5	530.6	0	0	-834	-358	2372	-3.13E-03	29	0.71	0.16	100	810	421	1.9
68	[94]	2-2,5-40A	462	421	476	2372	882.5	530.6	0	0	-834	-358	2372	-3.13E-03	29	0.71	0.16	100	810	421	1.92
69	[94]	3-2,5-40A	487	421	476	2372	882.5	530.6	0	0	-834	-358	2372	-3.13E-03	29	0.71	0.16	100	810	421	1.75
70	[94]	1-2,5-40B	400	385	436	2372	882.5	530.6	0	0	-834	-398	2372	-3.26E-03	29	0.62	0.17	100	810	385	1.93
71	[94]	2-2,5-40B	420	385	436	2372	882.5	530.6	0	0	-834	-398	2372	-3.26E-03	29	0.62	0.17	100	810	385	1.56
72	[94]	1-2,5-20+20	487	461	521	2372	882.5	530.6	0	0	-834	-313	2372	-2.99E-03	29	0.97	0.14	100	810	461	1.51
73	[94]	2-3,0-20+20	531	461	626	2372	882.5	530.6	0	0	-834	-208	2372	-2.80E-03	29	0.97	0.14	100	810	461	1.29
74	[94]	1-2,5-60	511	482	545	2372	882.5	530.6	0	0	-834	-290	2372	-2.92E-03	29	0.83	0.15	100	810	482	1.4
75	[94]	3-2,5-60	562	482	545	2372	882.5	530.6	0	0	-834	-290	2372	-2.92E-03	29	0.83	0.15	100	810	482	1.5
																				m	2.07
																				s	0.69
																				v	0.33

E

Technical drawings for the HPFRC I-girders without stirrups of the experimental campaign

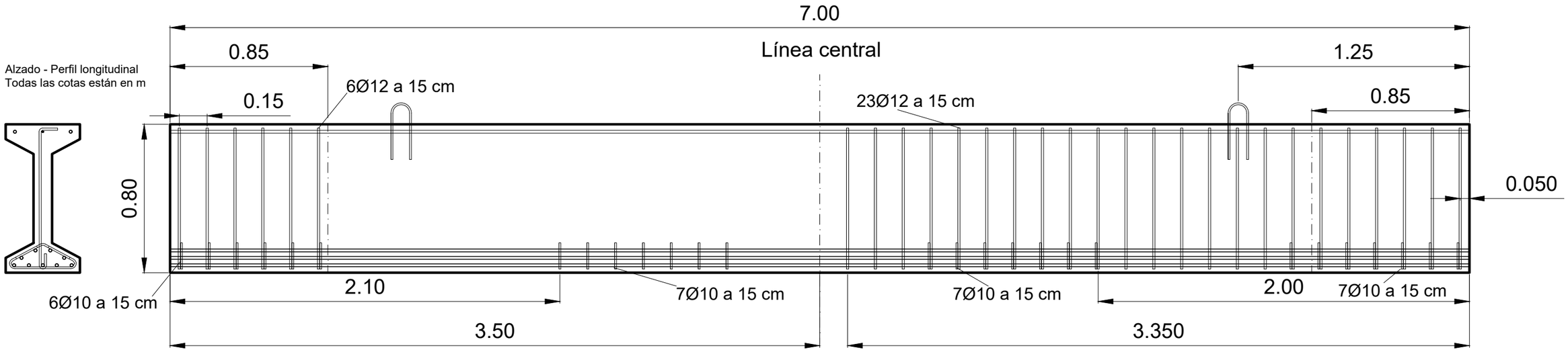

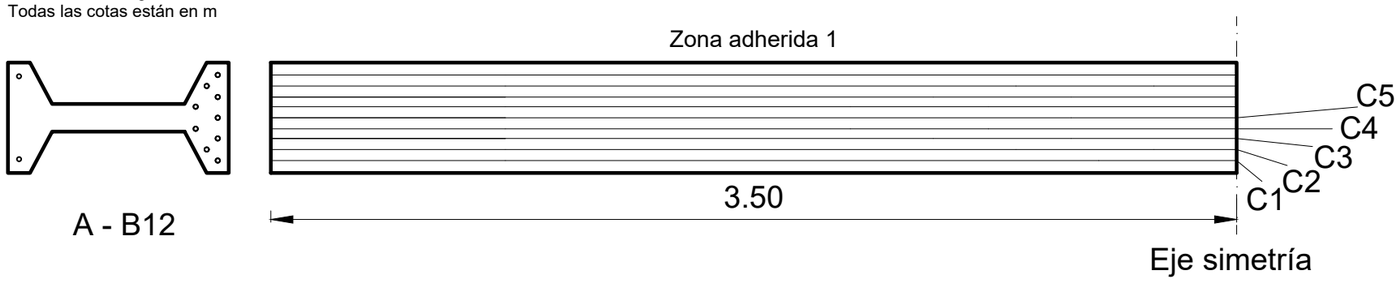

Cordón no envainado

Cordón envainado

Cordón de 150 mm2

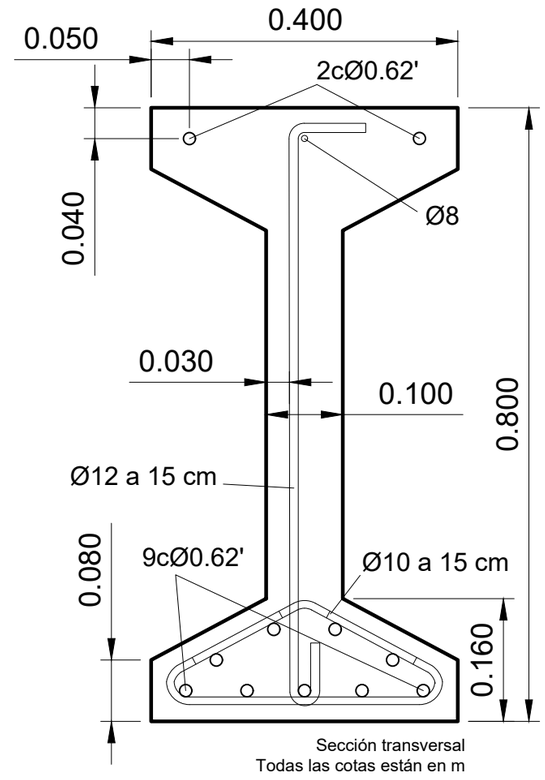

Detalle ala inferior
Todas las cotas están en m

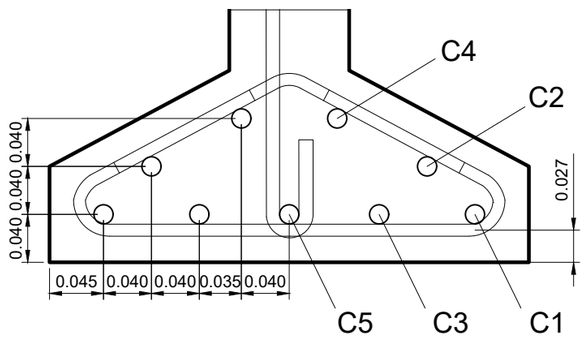

Tipo de cordón	Número cordones	Altura [cm]	Zona adherida 1 [m]	Zona envainada [m]	Zona adherida 2 [m]
C1	2	4.00	0-3.50	-	-
C2	2	8.00	0-3.50	-	-
C3	2	4.00	0-3.50	-	-
C4	2	12.00	0-3.50	-	-
C5	1	4.00	0-3.50	-	-

Elemento	Cantidad	Unidad
HPFRC	1.0640	m3
Cerco alma	29	
Cerco ala inferior	27	

Título del Proyecto

ENSAYOS A CORTANTE DE VIGAS PRETENSADAS DE HORMIGÓN DE ALTAS PRESTACIONES REFORZADO CON FIBRAS

Investigadores principales

D. Hugo Corres D. Leonardo Todisco

Autor

D. Rafael Ruiz Maestre

Título del plano

Prototipos vigas pretensadas B12

Fecha **11/2021**

Plano nº **1**

Escala A3: **Varias Especificadas en plano**

Hoja 1 de 7

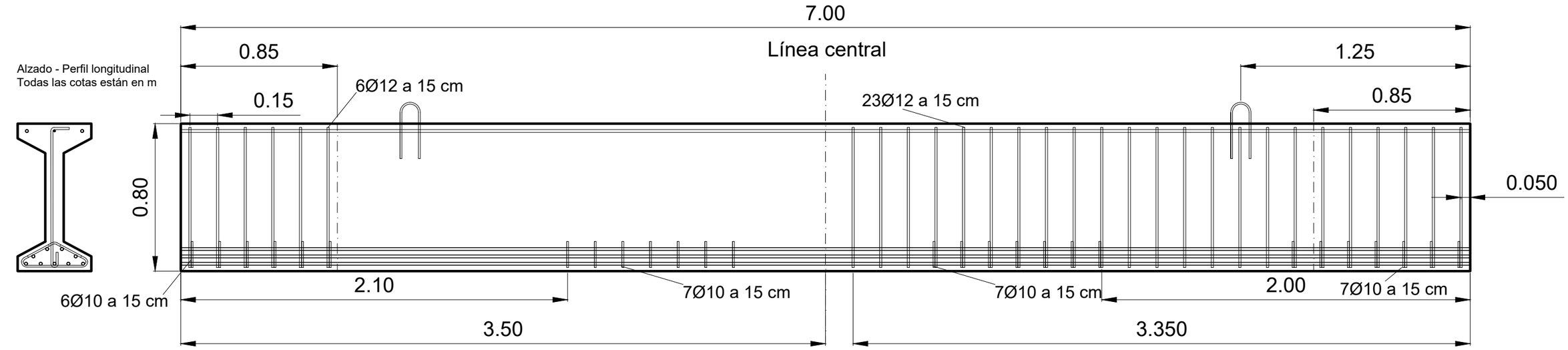

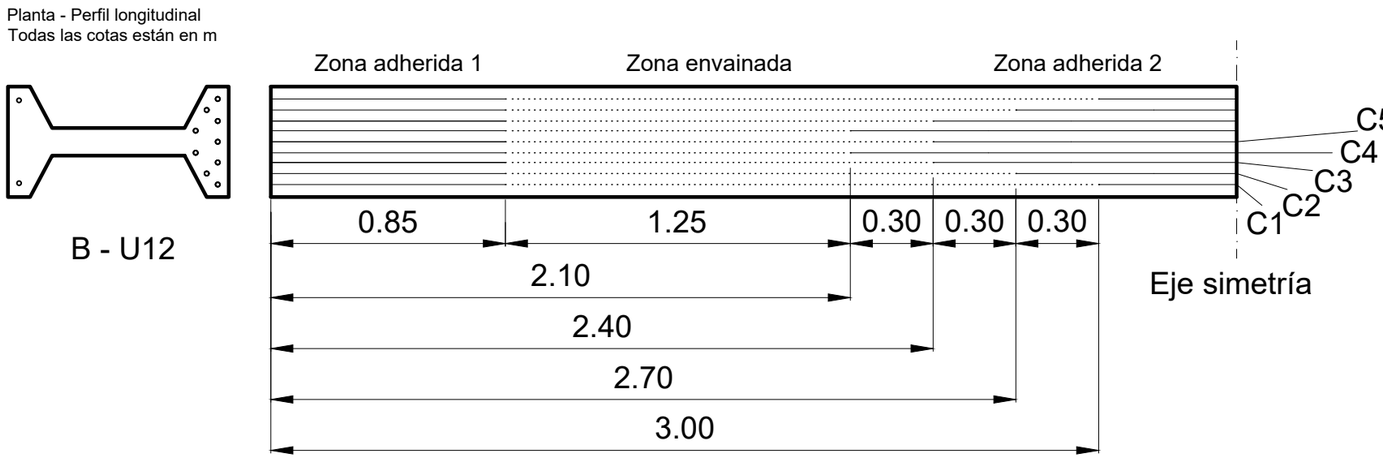

B - U12

Cordón no envainado

Cordón envainado

Cordón de 150 mm2

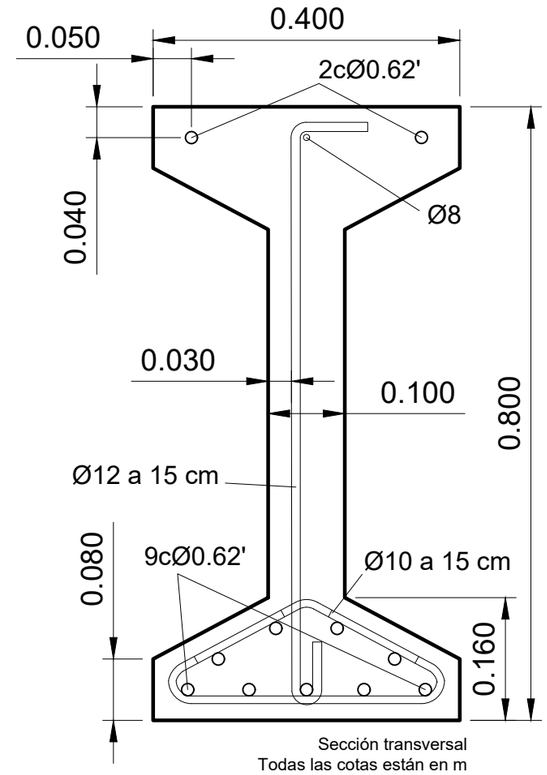

Sección transversal
Todas las cotas están en m

Detalle ala inferior
Todas las cotas están en m

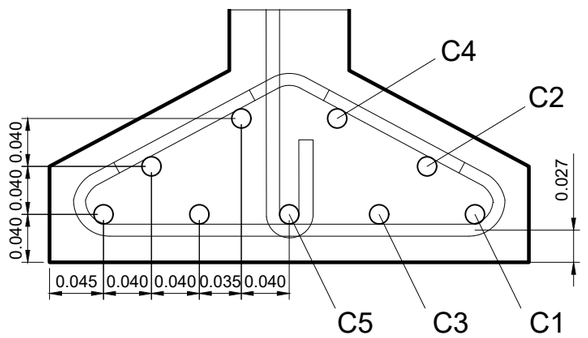

Tipo de cordón	Número cordones	Altura [cm]	Zona adherida 1 [m]	Zona envainada [m]	Zona adherida 2 [m]
C1	2	4.00	0-0.85	0.85-3.00	3.00-3.50
C2	2	8.00	0-0.85	0.85-2.70	2.70-3.50
C3	2	4.00	0-0.85	0.85-2.40	2.40-3.50
C4	2	12.00	0-0.85	0.85-2.10	2.10-3.50
C5	1	4.00	0-0.85	0.85-2.40	2.40-3.50

Elemento	Cantidad	Unidad
HPFRC	1.0640	m3
Cerco alma	29	
Cerco ala inferior	27	

Título del Proyecto

ENSAYOS A CORTANTE DE VIGAS PRETENSADAS DE HORMIGÓN DE ALTAS PRESTACIONES REFORZADO CON FIBRAS

Investigadores principales

D. Hugo Corres D. Leonardo Todisco

Autor

D. Rafael Ruiz Maestre

Título del plano

Prototipos vigas pretensadas U12

Fecha **11/2021**

Plano nº **2**

Escala A3: **Varias Especificadas en plano**

Hoja 2 de 7

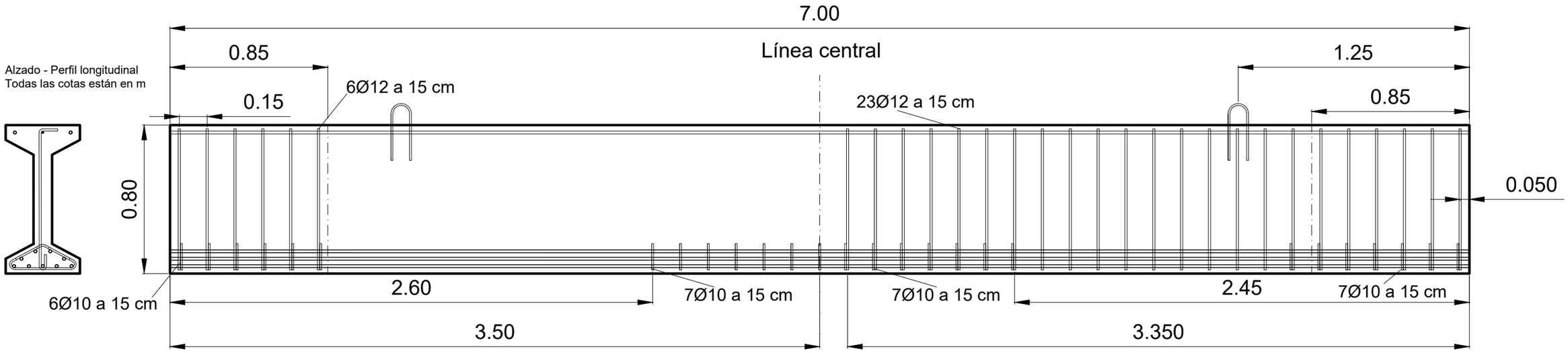

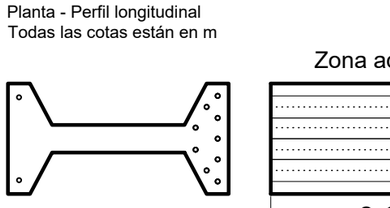

C - B7

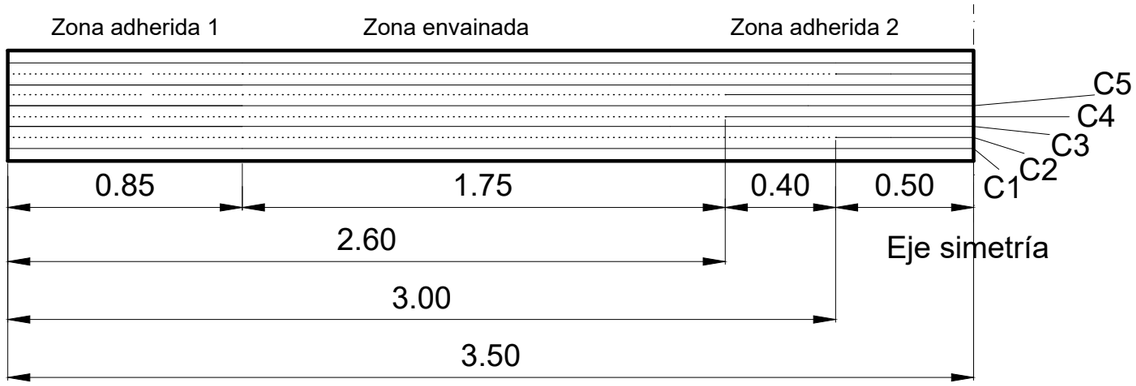

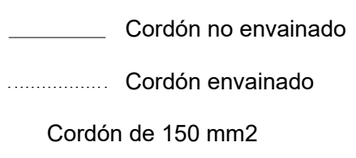

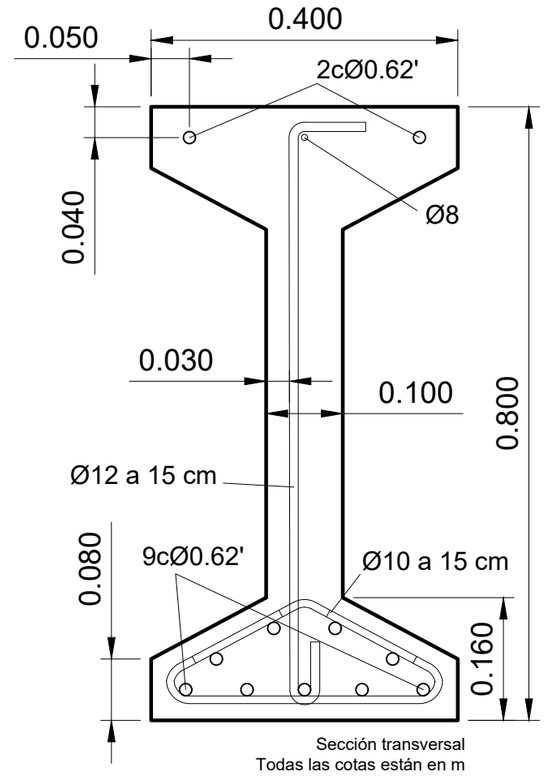

Detalle ala inferior
Todas las cotas están en m

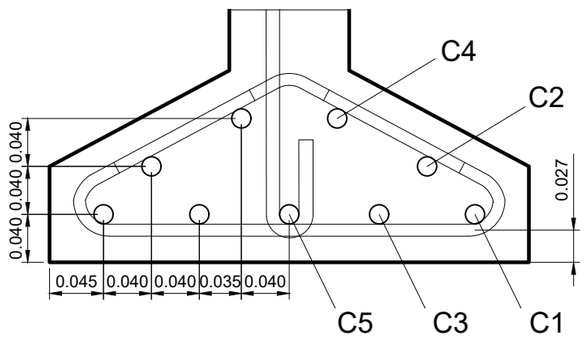

Tipo de cordón	Número cordones	Altura [cm]	Zona adherida 1 [m]	Zona envainada [m]	Zona adherida 2 [m]
C1	2	4.00	0-3.50	-	-
C2	2	8.00	-	0-3.00	3.00-3.50
C3	2	4.00	0-3.50	-	-
C4	2	12.00	-	0-2.60	2.60-3.50
C5	1	4.00	0-0.85	-	-

Elemento	Cantidad	Unidad
HPFRC	1.0640	m3
Cerco alma	29	
Cerco ala inferior	27	

Título del Proyecto

ENSAYOS A CORTANTE DE VIGAS PRETENSADAS DE HORMIGÓN DE ALTAS PRESTACIONES REFORZADO CON FIBRAS

Investigadores principales
D. Hugo Corres
D. Leonardo Todisco

Autor
D. Rafael Ruiz Maestre

Título del plano
Prototipos vigas pretensadas B7

Fecha **11/2021**

Plano nº **3**

Escala A3: **Varias Especificadas en plano**

Hoja 3 de 7

Alzado - Perfil longitudinal
Todas las cotas están en m

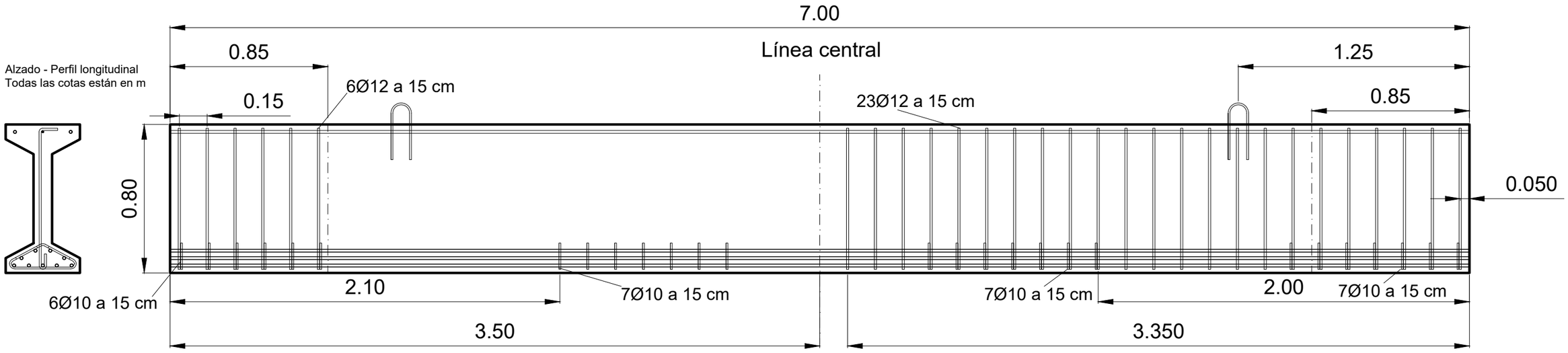

Planta - Perfil longitudinal
Todas las cotas están en m

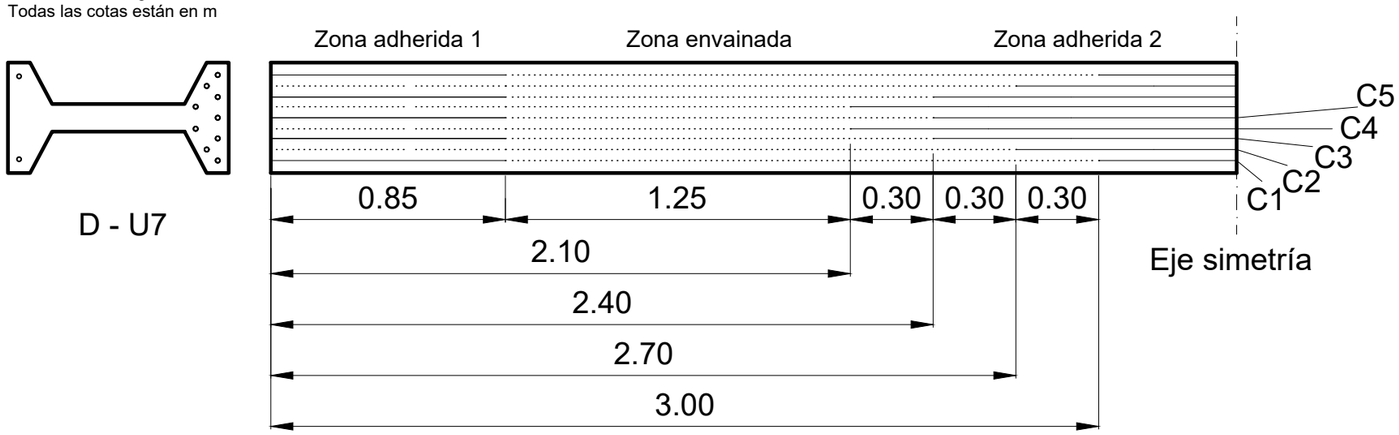

D - U7

Cordón no envainado
Cordón envainado
Cordón de 150 mm2

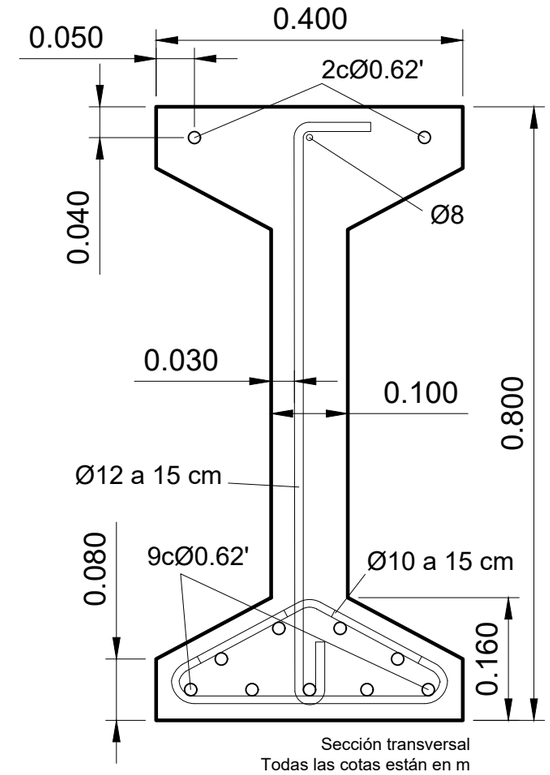

Sección transversal
Todas las cotas están en m

Detalle ala inferior
Todas las cotas están en m

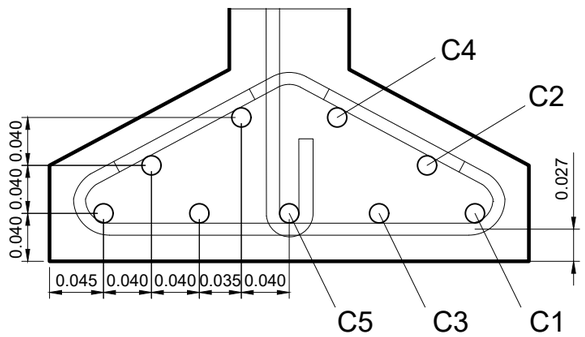

Tipo de cordón	Número cordones	Altura [cm]	Zona adherida 1 [m]	Zona envainada [m]	Zona adherida 2 [m]
C1	2	4.00	0-0.85	0.85-3.00	3.00-3.50
C2	2	8.00	-	0.00-2.70	2.70-3.50
C3	2	4.00	0-0.85	0.85-2.40	2.40-3.50
C4	2	12.00	-	0.00-2.10	2.10-3.50
C5	1	4.00	0-0.85	0.85-2.40	2.40-3.50

Elemento	Cantidad	Unidad
HPFRC	1.0640	m3
Cerco alma	29	
Cerco ala inferior	27	

Título del Proyecto

ENSAYOS A CORTANTE DE VIGAS PRETENSADAS DE HORMIGÓN DE ALTAS PRESTACIONES REFORZADO CON FIBRAS

Investigadores principales
D. Hugo Corres
D. Leonardo Todisco

Autor
D. Rafael Ruiz Maestre

Título del plano
Prototipos vigas pretensadas U7

Fecha **11/2021**

Plano nº **4**

Escala A3: **Varias Especificadas en plano**

Hoja 4 de 7

Alzado - Perfil longitudinal
Todas las cotas están en m

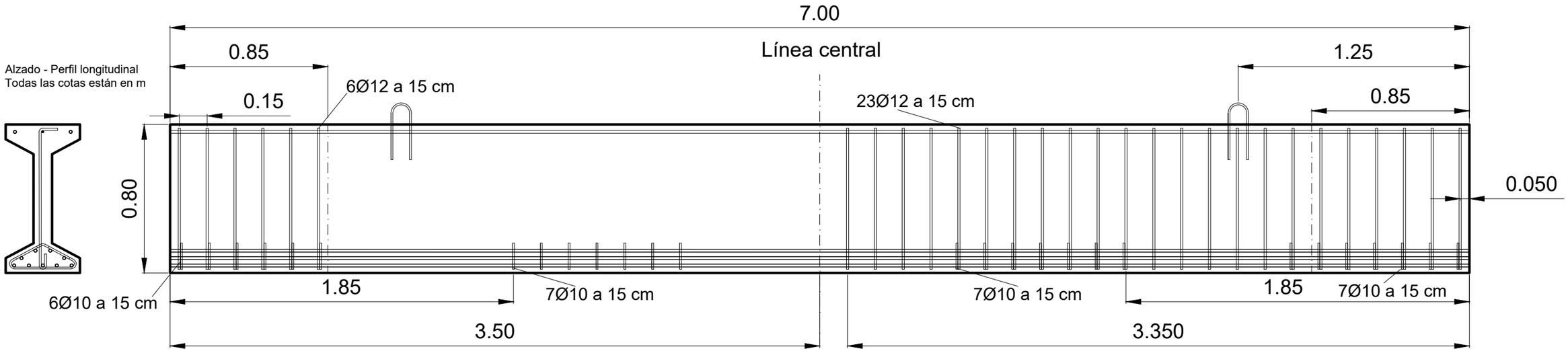

Planta - Perfil longitudinal
Todas las cotas están en m

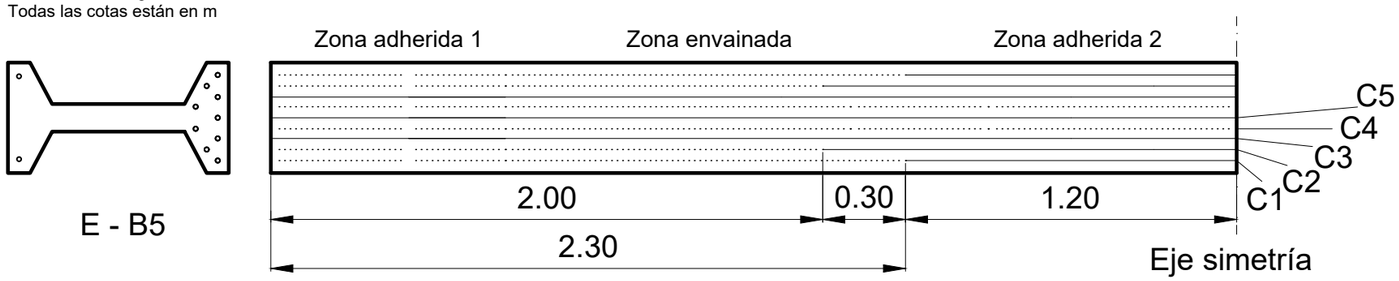

Cordón no envainado
Cordón envainado
Cordón de 150 mm2

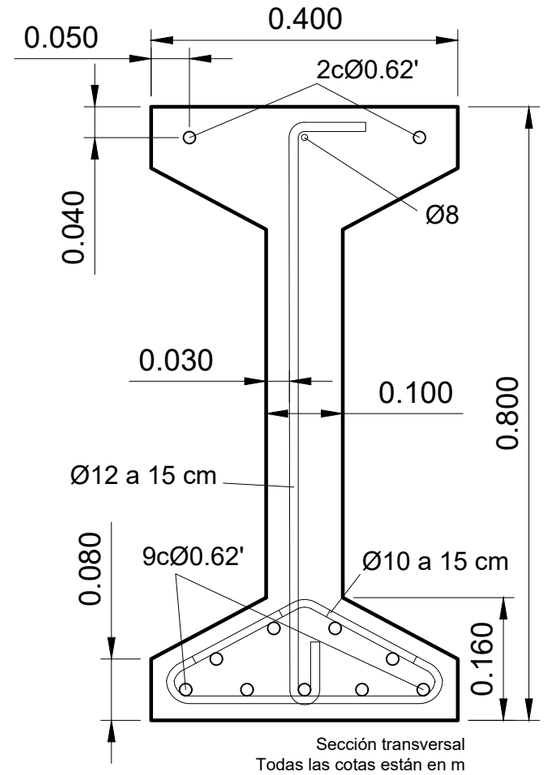

Sección transversal
Todas las cotas están en m

Detalle ala inferior
Todas las cotas están en m

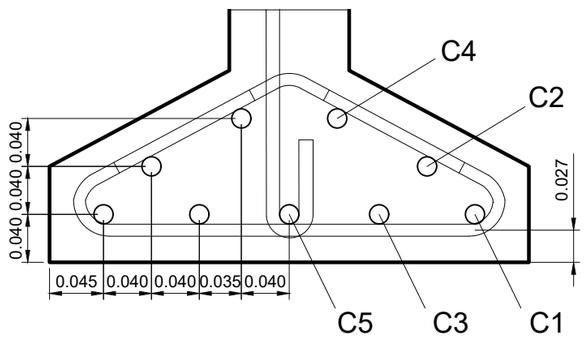

Tipo de cordón	Número cordones	Altura [cm]	Zona adherida 1 [m]	Zona envainada [m]	Zona adherida 2 [m]
C1	2	4.00	-	0-2.30	2.30-3.50
C2	2	8.00	-	0-2.00	2.00-3.50
C3	2	4.00	0-3.50	-	-
C4	2	12.00	-	-	-
C5	1	4.00	0-3.50	-	-

Elemento	Cantidad	Unidad
HPFRC	1.0640	m3
Cerco alma	29	
Cerco ala inferior	27	

Título del Proyecto

ENSAYOS A CORTANTE DE VIGAS PRETENSADAS DE HORMIGÓN DE ALTAS PRESTACIONES REFORZADO CON FIBRAS

Investigadores principales
D. Hugo Corres
D. Leonardo Todisco

Autor
D. Rafael Ruiz Maestre

Título del plano
Prototipos vigas pretensadas B7

Fecha **11/2021**

Plano nº **5**

Escala A3: **Varias Especificadas en plano**

Hoja 5 de 7

Alzado - Perfil longitudinal
Todas las cotas están en m

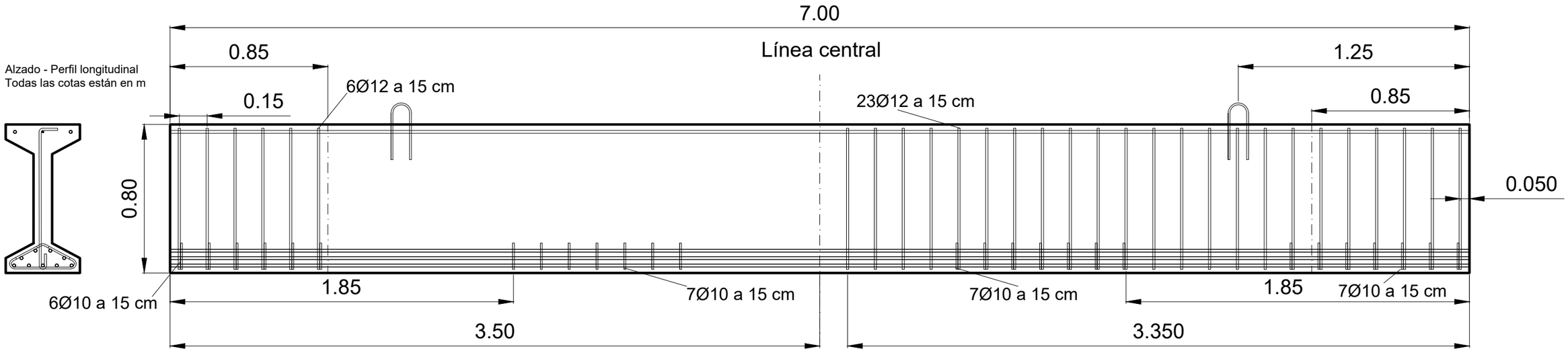

Planta - Perfil longitudinal
Todas las cotas están en m

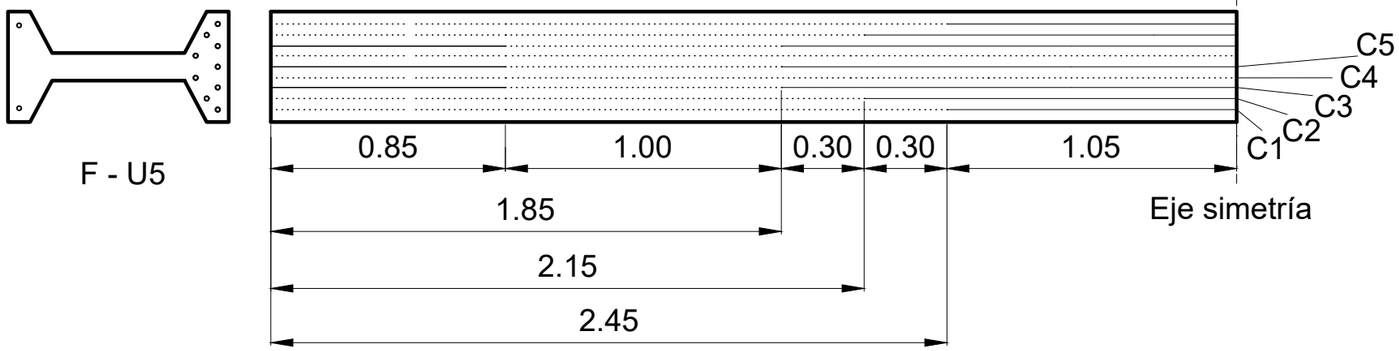

F - U5

Cordón no envainado
Cordón envainado
Cordón de 150 mm2

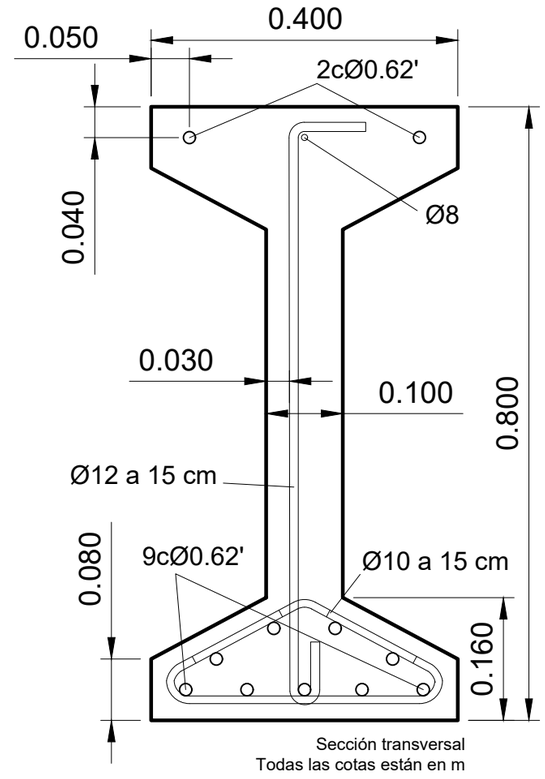

Sección transversal
Todas las cotas están en m

Detalle ala inferior
Todas las cotas están en m

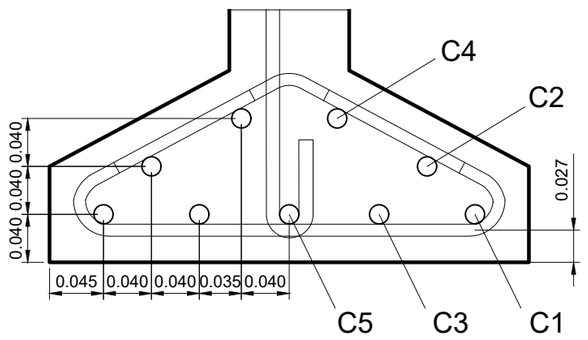

Tipo de cordón	Número cordones	Altura [cm]	Zona adherida 1 [m]	Zona envainada [m]	Zona adherida 2 [m]
C1	2	4.00	-	0.00-2.45	2.45-3.50
C2	2	8.00	-	0.00-2.15	2.15-3.50
C3	2	4.00	0.00-0.85	0.85-1.85	1.85-3.50
C4	2	12.00	-	-	-
C5	1	4.00	0.00-0.85	0.85-1.85	1.85-3.50

Elemento	Cantidad	Unidad
HPFRC	1.0640	m3
Cerco alma	29	
Cerco ala inferior	27	

Título del Proyecto

ENSAYOS A CORTANTE DE VIGAS PRETENSADAS DE HORMIGÓN DE ALTAS PRESTACIONES REFORZADO CON FIBRAS

Investigadores principales
D. Hugo Corres
D. Leonardo Todisco

Autor
D. Rafael Ruiz Maestre

Título del plano
Prototipos vigas pretensadas U5

Fecha
11/2021

Escala
A3: **Varias Especificadas en plano**

Plano nº
6

Hoja
6 de 7

Alzado - Perfil longitudinal
Todas las cotas están en m

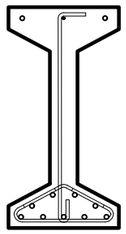

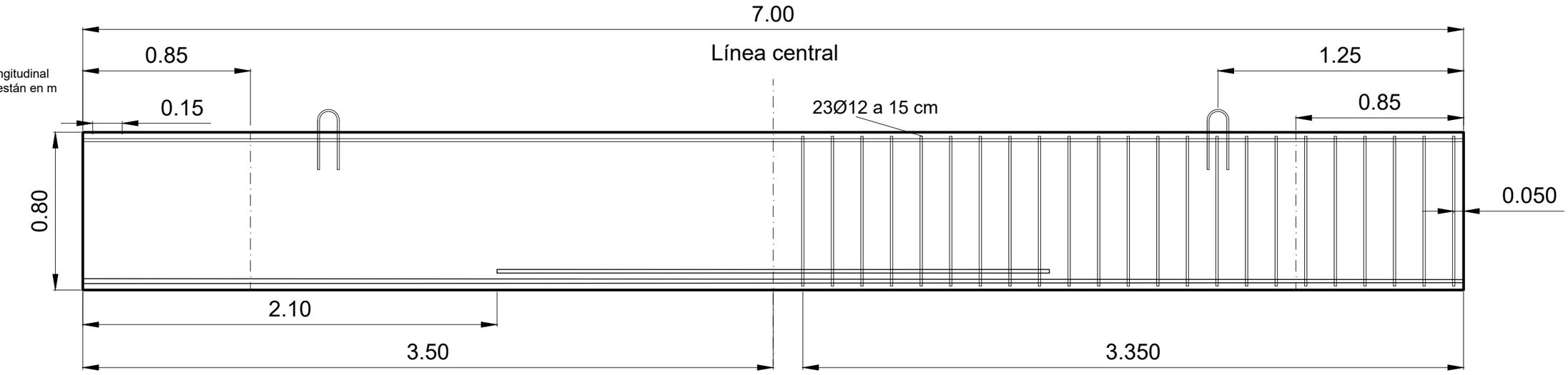

Planta - Perfil longitudinal
Todas las cotas están en m

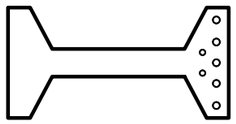

G - NP

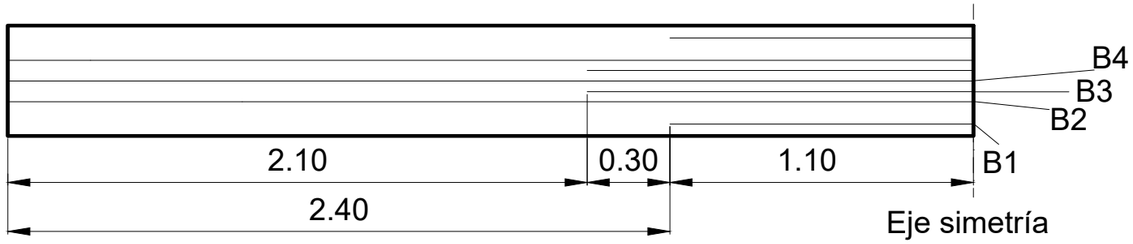

Eje simetría

Cordón no envainado
Cordón envainado
Cordón de 150 mm2

Detalle ala inferior
Todas las cotas están en m

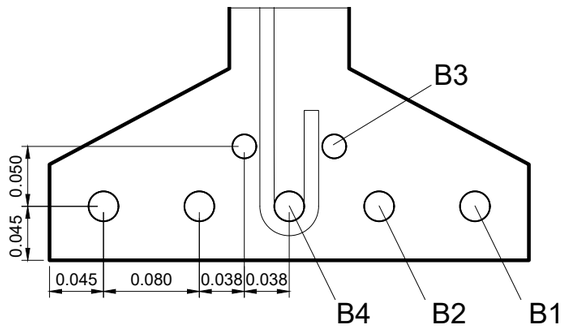

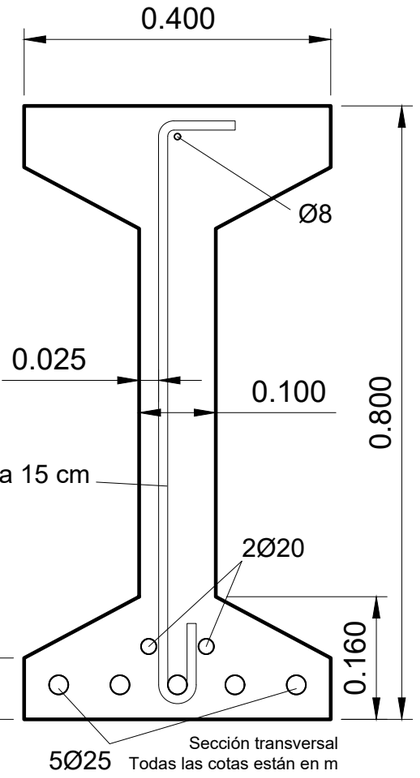

Tipo de cordón	Número cordones	Altura [cm]	Ubicación [m]
B1	2	4.50	2.40-3.50
B2	2	4.50	0.00-3.50
B3	2	9.50	2.10-3.50
B4	1	4.50	0.00-3.50

Elemento	Cantidad	Unidad
HPFRC	1.0640	m3
Cerco alma	23	8.00

Título del Proyecto

ENSAYOS A CORTANTE DE VIGAS PRETENSADAS DE HORMIGÓN DE ALTAS PRESTACIONES REFORZADO CON FIBRAS

Investigadores principales
D. Hugo Corres
D. Leonardo Todisco

Autor
D. Rafael Ruiz Maestre

Título del plano
Prototipos vigas pretensadas NP

Fecha **11/2021**

Plano nº **7**

Escala
A3: **Varias Especificadas en plano**

Hoja
7 de 7

APPENDIX E. TECHNICAL DRAWINGS FOR THE HPFRC I-GIRDERS WITHOUT STIRRUPS OF THE EXPERIMENTAL CAMPAIGN 242

F

Publications

The author, together with colleagues, has published a number of peer-reviewed papers and conference papers, dealing with aspects of the work herein:

- Ruiz, R.; Starchevich, G.B.; Todisco, L.; Corres, H.; (2023) "Parametric analysis of variables influencing the design of I-girder bridge decks made of high-performance fiber reinforced concrete", *Structural Concrete*, Vol. 4, Issue 4, 4606-4623. (doi: 10.1002/suco.202200477).
- Ruiz, R.; Todisco, L.; Corres, H.; (2023) "Application of high-performance fibre reinforced concrete to precast girders for road bridges: Conceptual considerations and numerical analyses", *Structural Concrete*, Vol. 4, Issue 4, 4645-4659. (doi: 10.1002/suco.202200907).
- Ruiz, R.; Doniak, L.O.; Todisco, L.; Corres, H.; (2023) "Database of shear tests for prestressed fibre reinforced concrete beams without vertical stirrups and comparison with code provisions", *Structural Concrete*, Vol. 4, Issue 4, 4565-4576. (doi: 10.1002/suco.202201130).
- Ruiz, R.; Todisco, L.; Corres, H.; (2023) "Application of high-performance fibre reinforced concrete to prestressed precast girders for road bridges", *Structural*, Vol. 243 October-December. (doi: 10.12917/STRU243.22).
- Ruiz, R.; Todisco, L.; Corres, H.; (2021) "Conceptual design of HPFRC and UHPFRC road girder bridges". *fib Symposium on Conceptual Design of Structures 2021*, Switzerland.

- Ruiz, R.; Todisco, L.; Corres, H.; (2022) "High performance-fibre reinforced concrete as a high performance and cost-effective solution for precast concrete bridges", *14th fib Symposium in Civil Engineering*, Rome. (Awarded with the Best Paper Award in the category of Steel Fibre Reinforced Concrete).

Additionally, the following paper has been submitted for publication and is currently under review:

- Ruiz, R.; Chozas-Ligero, V.; Todisco, L.; Jiménez-Vicaria, J. David; Corres, H.; "Experimental characterization of a cost-competitive tailor-made HPFRC mix design for wide application in precast girder of roadway bridges", *Structural Concrete* (submitted for publication in July 2023).

Bibliography

[1] United Nations. "UN General Assembly, Transforming our world: The 2030 agenda for sustainable development". In: *Resolution adopted by the General Assembly on 25 September 2015* 16301.October (2015), pp. 1–35. URL: https://www.refworld.org/docid/57b6e3e44.html.

[2] Paulo J.M. Monteiro, Sabbie A. Miller, and Arpad Horvath. "Towards sustainable concrete". In: *Nature Materials* 16.7 (2017), pp. 698–699. ISSN: 14764660. DOI: 10.1038/nmat4930. URL: http://dx.doi.org/10.1038/nmat4930.

[3] National Minerals Information Center. *USGS science for a changing world - Cement statistics and information*. 2023. URL: https://www.usgs.gov/centers/national-minerals-information-center/cement-statistics-and-information.

[4] Prefabricados de Cemento y de hormigón AEN/CTN 127. "UNE-EN 14651:2007+A1". In: *Norma española* (2008).

[5] Fehling E, Schmidt M, Walraven J, Leutbecher T, Fröhlichn S. *Ch 13. Ultra high-performance fibre reinforced concrete. fib bulletin 105. Fibre Reinforced Concrete State-of-the-Art report*. 2017, pp. 316–379. DOI: 10.35789/fib.BULL.0105.Ch13.

[6] Ekkehard Fehling et al. *Ultra-High Performance Concrete UHPC Fundamentals - Design - Examples*. 2014. ISBN: 9783433030004. DOI: 10.1002/9783433604076.

[7] Benjamin Graybeal et al. "International Perspective on UHPC in Bridge Engineering". In: *Journal of Bridge Engineering* 25.11 (Nov. 2020), p. 04020094. ISSN: 1084-0702. DOI: 10.1061/(ASCE)BE.1943-5592.0001630.

[8] AFGC. *Ultra High Performance Fibre-Reinforced Concretes Recommendations*. Ed. by AFGC. June. France: AFGC, 2013. URL: http://www.ductal.com/AFGC_Recommandations_BFUPJuin2013.pdf.

[9] Ziad Hajar et al. "Design and Construction of the world first Ultra-High Performance Concrete road bridges". In: *International Symposiun on Ultra High Performance Concrete*. 3. Kassel, 2004, pp. 39–48. ISBN: 3899580869.

[10] Olivier Delauzun et al. “Construction of the PS34 UHPFRC Bridge”. In: *Designing and Building with UHPFRC* January 2023 (2013), pp. 137–148. DOI: 10.1002/9781118557839.ch11.

[11] AFGC. *Ultra High Performance Fibre-Reinforced Concretes Recommendations*. Ed. by AFGC. June. France: AFGC, 2002. URL: http://www.ductal.com/AFGC_Recommandations_BFUPJuin2013.pdf.

[12] Nadarajah Gowripalan and R. Ian Gilbert. *Design Guidelines for Ductal Prestressed Concrete Beams*. Ed. by The University of New South Wales. Sydney, Australia, 2000.

[13] Yen Lei Voo, Stephen J. Foster, and R. Ian Gilbert. “Shear strength of fiber reinforced reactive powder concrete prestressed girders without stirrups”. In: *Journal of Advanced Concrete Technology* 4.1 (2006), pp. 123–132. ISSN: 13468014. DOI: 10.3151/jact.4.123.

[14] Mark Rebentrost and Gavin Wight. “UHPC Perspective from a Specialist Construction Company”. In: *fib UHPFRC 2009*. 2009, pp. 1–10.

[15] Zachary B. Haber, Igor De La Varga, and Benjamin A. Graybeal. *Properties and Behavior of UHPC - Class Materials*. Tech. rep. FHWA-HRT-18-036. Federal Highway Administration, 2018, p. 153.

[16] H. Russel, G and B. A. Graybeal. *Ultra-High Performance Concrete : A State-of-the-Art Report for the Bridge Community*. Tech. rep. No. FHWA-HRT-13-060. 2013, p. 171. DOI: FHWA-HRT-13-060.

[17] Federal Highways Administration. *North American Deployments of UHPC in Highway Bridge Construction*. 2023. URL: https://highways.dot.gov/research/structures/ultra-high-performance-concrete/deployments.

[18] Haena Kim. “Design and field construction of Hawkeye Bridge using ultra high performance concrete for accelerated bridge construction”. PhD thesis. Iowa City, IA, United States: University of Iowa, May 2016. DOI: 10.17077/etd.4b9futmh.

[19] American Association of State Highway and Transportation Officials. *AASHTO LRFD Bridge Design Specifications, Eighth Edition*. Vol. 280. 7. Washing, DC, Apr. 2017, pp. 1732–1732. ISBN: 978-1-56051-654-5. DOI: 10.1111/febs.12237. URL: https://onlinelibrary.wiley.com/doi/10.1111/febs.12237.

[20] Wayne A Endicott. “A whole new cast”. In: *ASPIRE* (2007), pp. 26–35.

[21] Holcim. *Ductal. Infrastructure*. 2023. URL: https://www.ductal.com/en/infrastructure.

[22] Benjamin Graybeal. “UHPC in the US Highway Infrastructure”. In: *Designing and Building with UHPFRC*. Ed. by Fib and AFGC. January. Marseille, France, 2009, pp. 221–234. ISBN: 9781848212718. DOI: 10.1002/9781118557839.ch15.

[23] Ministerio de Fomento. Dirección General de Carreteras. *Obras de paso de nueva construcción*. 2000, pp. 17–20.

[24] Brian Keierleber et al. “Design of Buchanan County, Iowa, Bridge, using Ultra High-Performance Concrete and pi beam cross section”. In: *2008 PCI National Bridge Conference*. 2008.

[25] Florida International University. *2008 – Jakway Park Bridge*. 2008. URL: https://utcdb.fiu.edu/project/2008-jakway-park-bridge/.

[26] Celik Ozyildirim. *Evaluation of Ultra-High-Performance Fiber-Reinforced Concrete*. Tech. rep. Virginia: Virginia Center for Transportation Innovation and Research, Federal Highway Administration, 2011, p. 23.

[27] Maher K. Tadros et al. “Ultra-High-Performance Concrete: A Game Changer in the Precast Concrete Industry”. In: *PCI Journal* 65.3 (2020). DOI: 10.15554/pcij65.3-06.

[28] Maher K. Tadros et al. “ABC Design of UHPC Decked I-Beam Vehicular Bridge in Ontario, Canada”. In: (2020).

[29] PCI Precast/Prestressed Concrete Institute. *PCI Document UHPC - Phase II (Draft version)*. Tech. rep. 2021.

[30] Yen Lei Voo. “An investigation into the behaviour of prestressed reactive powder concrete girders subject to non-flexural actions”. In: (2004). URL: https://doi.org/10.26190/unsworks/9955.

[31] AFNOR P18B. *NF P18-470 - National addition to Eurocode 2 - Concrete - Ultra-high performance fibre-reinforced concrete - Specifications, performance, production and conformity*. France, 2016.

[32] AFNOR P18B. *NF P18-710 - National addition to Eurocode 2 - Design of concrete structures: specific rules for Ultra-High Performance Fibre-Reinforced Concrete*. Vol. 33. April. France, 2016.

[33] Welf Zimmermann and Lutz Sparowitz. “Prefabricated UHPFRC parts and segmental flap method”. In: *fib Symposium Prague 2011*. Ed. by fib. Prague, 2011, pp. 803–806.

[34] Welf Zimmermann and Lutz Sparowitz. “Vorgespannte Fertigteile aus Ultrahochfestem Faserbeton”. In: *Beton- und Stahlbetonbau* 107.3 (2012), pp. 192–200. DOI: 10.1002/best.201100086.

[35] Bernhard Freytag et al. “Großversuch WILD-Brücke - Versuchsgestützte Bemessung einer UHPC-Bogenbrücke”. In: *Beton- und Stahlbetonbau* 104.3 (2009), pp. 134–144. ISSN: 00059900. DOI: 10.1002/best.200900663.

[36] Markus Hecht. “Practical use of fibre-reinforced UHPC in construction-production of precast elements for Wild-Brücke in Völkermarkt”. In: *Ultra High Performance Concrete and Nanotechnology in Construction, 3rd Intl. Symp. on Ultra High Performance Concrete and Nanotechnology for High Performance Construction Materials, Structural Materials and Engineering Series No. 19.* Kassel, 2012, pp. 889–896. ISBN: 9783862192656.

[37] Bernhard Freytag et al. “WILD-Bridge scientific Preparation for Smooth Realisation”. In: *Ultra High Performance Concrete and Nanotechnology in Construction, 3rd Intl. Symp. on Ultra High Performance Concrete and Nanotechnology for High Performance Construction Materials, Structural Materials and Engineering Series No. 19.* Kassel, Germany, 2012, pp. 881–888. ISBN: 9783862192656.

[38] Marco di Prisco et al. “The first P/R/SFRC bridge in Italy: Materials characterization, preliminary tests, design and construction features”. In: *fib 2022 Oslo, Concrete innovation for Sustainability.* Oslo, 2022.

[39] RDC. *UHPC for People blog - RDC.* URL: https://rdconcrete.com/uhpc-for-people/ (visited on 03/22/2021).

[40] Byung-Suk Kim et al. “Design and Construction of Innovative UHPC Pedestrian Cable Stayed Bridge in Korea”. In: *IABSE Symposium Report.* 2009, pp. 132–139. DOI: 10.2749/222137809796088657. URL: https://structurae.net/en/literature/id/10296655.

[41] KICT (Korea Institute of Civil Engineering & Building Technology). *Final report on development of fabrication technology and material model: Instructions for 80 MPa to 180 MPa-class SUPER concrete.* Seoul: KICT, 2019.

[42] K. Lynn Geren and Maher K. Tadros. “The NU Precast/Prestressed Concrete Bridge I-Girder Series”. In: *PCI Journal* 39.3 (May 1994), pp. 26–39. ISSN: 08879672. DOI: 10.15554/pcij.05011994.26.39.

[43] J. Kim Yail and Siriwardanage Thushara. “New LRFD-based prestressed concrete bulb-tee girders in Colorado”. In: *PCI Journal* 65.3 (2020), pp. 53–63. DOI: https://doi.org/10.15554/pcij65.3-03.

[44] Yen Lei Voo and Maher Tadros. “Taking Ultra-High-Performance Concrete to New Heights The Malaysian Wissahickon Memorial Bridge Philadelphia , Pennsylvania”. In: 5 (2016).

[45] CEN: European Committee for Standardization. *Eurocode 2: Design of concrete structures - Part 1-1: General rules and rules for buldings*. 2013.

[46] CEN: European Committee for Standardization. *Eurocode 1: Actions on structures*. 2013.

[47] Colegio de Ingenieros de Caminos Canales y Puertos, Asociacióni Técnica Española de Pretensado, and Instituto de Ciencias de la Construcción Eduardo Torroja. *E-6 Proyecto y Construcción de Puentes y Estructuras con Pretensado Exterior H.P. 10-96*. Ed. by Canales y Puertos Colegio de Ingenieros de Caminos. Madrid: Colegio de Ingenieros de Caminos, Canales y Puertos, 1996, p. 149. ISBN: 8438001203.

[48] CEN: European Committee for Standardization. *Eurocode 2: Design of concrete structures - Part 1-1: General rules and rules for buildings (Draft)*. 2020.

[49] Fedération internationale du béton (Fib). *Model Code for Concrete Structures 2010*. Lausanne, Switzerland, 2012.

[50] Fedération internationale du béton (Fib). *Model Code for Concrete Structures 2020 (Draft)*. Lausanne, Switzerland, 2020.

[51] P Y Blais and Marco Couture. "Precast, Prestressed Pedestrian Bridge-World's First Reactive powder concrete bridge". In: *PCI Journal* 44.5 (1999), pp. 60–71. ISSN: 0887-9672.

[52] Emmanuel Denarié Eugen Brühwiler. "Rehabilitation of concrete structures using Ultra-High Per- formance Fibre Reinforced Concrete". In: *The Second International Symposium on Ultra High Performance Concrete* 1 (2008), pp. 1–8. URL: https://infoscience.epfl.ch/record/121449/files/Paper%20Br%7B%5C%22%7Bu%7D%7Dhwiler%20Denari%7B%5C'%7Be%7D%7D%20UHPC%20Kassel.pdf.

[53] Yen Lei Voo, Stephen J. Foster, and Chen Cheong Voo. "Ultrahigh-Performance Concrete Segmental Bridge Technology: Toward Sustainable Bridge Construction". In: *Journal of Bridge Engineering* 20.8 (Aug. 2015). ISSN: 1084-0702. DOI: 10.1061/(asce)be.1943-5592.0000704.

[54] Andrew J. Giesler, Shannon Burl Applegate, and Brad D. Weldon. "Implementing Nonproprietary, Ultra-High-Performance Concrete in a Precasting Plant". In: *PCI Journal* 61.6 (2016). DOI: 10.15554/pcij61.6-03.

[55] N. Roux, C. Andrade, and M. A. Sanjuan. "Experimental study of durability of reactive powder concretes". In: *Journal of Materials in Civil Engineering* 8.February (1996), pp. 1–6.

[56] H. Almansour and Z. Lounis. "Innovative design approach of precast-prestressed girder bridges using ultra high performance concrete". In: *Canadian Journal of Civil Engineering* 37.4 (Apr. 2010), pp. 511–521. ISSN: 03151468. DOI: 10.1139/L09-169. URL: https://cdnsciencepub.com/doi/abs/10.1139/L09-169.

[57] Joost C. Walraven. "High performance fiber reinforced concrete: Progress in knowledge and design codes". In: *Materials and Structures/Materiaux et Constructions* 42.9 (2009), pp. 1247–1260. ISSN: 13595997. DOI: 10.1617/s11527-009-9538-3.

[58] Joost Walraven et al. "Self-compacting high-performance fiber concrete for foundations: Part 1 -experimental verification and design considerations". In: *Structural Concrete* July (2021), pp. 1–15. ISSN: 17517648. DOI: 10.1002/suco.202000440.

[59] Fausto Minelli and Giovanni A. Plizzari. "On the effectiveness of steel fibers as shear reinforcement". In: *ACI Structural Journal* 110.3 (May 2013), pp. 379–389. ISSN: 08893241. DOI: 10.14359/51685596.

[60] Florent Baby, Pierre Marchand, and François Toutlemonde. "Shear Behavior of Ultrahigh Performance Fiber-Reinforced Concrete Beams. I: Experimental Investigation". In: *Journal of Structural Engineering* 140.5 (2014), pp. 1–10. ISSN: 0733-9445. DOI: 10.1061/(asce)st.1943-541x.0000907.

[61] "The Ultra Girder: A Design Concept for a 300-foot Single Span Prestressed Ultra-High Performance Concrete Bridge Girder". In: *International Interactive Symposium on Ultra-High Performance Concrete* 2.1 (June 2019). ISSN: 0000-0000. URL: https://www.iastatedigitalpress.com/uhpc/article/id/9707/.

[62] European Concrete Platform. "C.6.2.2 Shear capacity of members without shear reinforcement". In: *Eurocode 2 Commentary*. (rev A 31-. Brussels, Belgium, 2008. Chap. C.6.2 Shear, p. 168.

[63] F. Vecchio and M. P. Collins. *The response of reinforced concrete to in-plane shear and normal stresses*. Toronto, 1982, p. 343. ISBN: 0-7727-7029-8.

[64] Evan C. Bentz, Frank J. Vecchio, and Michael P. Collins. "Simplified modified compression field theory for calculating shear strength of reinforced concrete elements". In: *ACI Structural Journal* 104.3 (2007), pp. 378–380. ISSN: 08893241.

[65] Fausto Minelli. "Plain and fiber reinforced concrete beams under shear loading: structural behaviour and design aspects". PhD thesis. University of Brescia, Italy, 2005, pp. 233–242.

[66] fib WP 1.4.1. *Bulletin 83. Precast tunnel segments in fibre-reinforced concrete*. 2017, p. 178. ISBN: 9782883941052.

[67] Paolo Martinelli et al. "Characterization tests for predicting the mechanical performance of SFRC floors: design considerations". In: *Materials and Structures/Materiaux et Constructions* 54.2 (Feb. 2021). DOI: 10.1617/S11527-020-01598-2.

[68] Mari Bøhnsdalen Eide and Jorun-Marie Hisdal. *Ultra High Performance Fibre Reinforced Concrete (UHPFRC) – State of the art. COIN Project report 44-2012*. 2012, p. 152. ISBN: 9788253612980. URL: www.coinweb.no.

[69] Antonio Marì Bernat et al. "Mechanical model for the shear strength of steel fiber reinforced concrete (SFRC) beams without stirrups". In: *Materials and structures* 53.2 (Apr. 2020), 28:1–28:20. ISSN: 1359-5997. DOI: 10.1617/S11527-020-01461-4. URL: https://upcommons.upc.edu/handle/2117/346436.

[70] Gobierno de España. *Código Estructural. Real Decreto 470/2021*. 2021.

[71] SIA 2052. *Béton fibré ultra-performanc (BFUP): Matériaux, dimensionnement et exécution*. Zurich, Switzerland, 2016.

[72] Comisión permanente del Hormigón. *EHE-08 Instrucción de Hormigón Estructural - Con comentarios de los miembros de la Comisión Permanente del Hormigón*. Tech. rep. 2010, p. 702.

[73] CEN: European Committee for Standardization. "Eurocode 2: Design of concrete structures: Part 2, Concrete bridges, Design and detailing rules". In: (2010).

[74] Sami Rizkalla et al. *Application of the LRFD Bridge Design Specifications to High-Strength Structural Concrete: Flexure and Compression Provisions*. 2007, p. 28. ISBN: 9780309424899. DOI: 10.17226/23269.

[75] Juan Ángel López et al. "First ultra-high-performance fibre-reinforced concrete footbridge in Spain: Design and construction". In: *Structural Engineering International: Journal of the International Association for Bridge and Structural Engineering (IABSE)* 24.1 (2014), pp. 101–104. ISSN: 10168664. DOI: 10.2749/101686614X13830788505793.

[76] Ben Graybeal. "Ultra-High Performance Concrete". In: *TechNote, FHWA-HRT-11-038* (2011), pp. 1–8. URL: https://www.fhwa.dot.gov/publications/research/infrastructure/structures/11038/.

[77] A. N. Dancygier and Z. Savir. "Effects of steel fibers on shear behavior of high-strength reinforced concrete beams". In: *Advances in Structural Engineering* 14.5 (Oct. 2011), pp. 745–761. ISSN: 13694332. DOI: 10.1260/1369-4332.14.5.745.

[78] Z. Savir, A. N. Dancygier, and A. Bentur. "On the toughness of high strength concrete with steel fibres of different lengths". In: *Role of Cement Science in Sustainable Development - Proceedings of the International Symposium - Celebrating Concrete: People and Practice*. 2003, pp. 127–136. ISBN: 0727732463. DOI: 10.1680/rocisd.32477.0012.

[79] Fuat Köksal et al. "Combined effect of silica fume and steel fiber on the mechanical properties of high strength concretes". In: *Construction and Building Materials* 22.8 (Aug. 2008), pp. 1874–1880. ISSN: 09500618. DOI: 10.1016/j.conbuildmat.2007.04.017.

[80] P. S. Song and S. Hwang. "Mechanical properties of high-strength steel fiber-reinforced concrete". In: *Construction and Building Materials* 18.9 (Nov. 2004), pp. 669–673. ISSN: 09500618. DOI: 10.1016/j.conbuildmat.2004.04.027.

[81] Özgür Eren and Tahir Çelik. "Effect of silica fume and steel fibers on some properties of high-strength concrete". In: *Construction and Building Materials* 11.7-8 (1997), pp. 373–382. URL: https://www.sciencedirect.com/science/article/pii/S0950061897000585.

[82] Vitor M C F Cunha. "Steel fibre reinforced self-compacting concrete (from micromechanics to composite behavior)". PhD thesis. University of Minho, 2010.

[83] Y. Mohammadi, S. P. Singh, and S. K. Kaushik. "Properties of steel fibrous concrete containing mixed fibres in fresh and hardened state". In: *Construction and Building Materials* 22.5 (May 2008), pp. 956–965. ISSN: 09500618. DOI: 10.1016/j.conbuildmat.2006.12.004.

[84] Norbert Randl and Tamás Mészöly. "Fibre effect on shear behaviour of UHPC beams". In: *fib Bulletin 95. Fibre Reinforced Concrete: From Design to Structural Applications*. Vol. 343. Oct. 2020, pp. 524–532. DOI: 10.35789/fib.BULL.0095.Ch53. URL: https://www.fib-international.org/publications/fib-bulletins/fibre-reinforced-concrete-from-design-to-structural-applications-pdf-detail.html#Ch53.

[85] Marco di Prisco et al. "On the identification of SFRC tensile constitutive behaviour". In: *Fracture mechanics of concrete structures. AA Balkema Publishers, Rotterdam* (2001), pp. 541–548.

[86] Thomás Lima de Resende, Daniel C T Cardoso, and Lidia C D Shehata. "Influence of steel fibers on the dowel action of RC beams without stirrups". In: *Engineering Structures* 221.July (2020). ISSN: 18737323. DOI: 10.1016/j.engstruct.2020.111044.

[87] Withit Pansuk et al. "Shear capacity of high performance fiber reinforced concrete I-beams". In: *Construction and Building Materials* 157 (Dec. 2017), pp. 182–193. DOI: 10.1016/j.conbuildmat.2017.09.057.

[88] Yen Lei Voo, Wai Keat Poon, and Stephen J. Foster. "Shear Strength of Steel Fiber-Reinforced Ultrahigh- Performance Concrete Beams without Stirrups". In: *Journal of Structural Engineering* 136.11 (Nov. 2010), pp. 1393–1400. ISSN: 0733-9445. DOI: 10.1061/(ASCE)ST.1943-541X.0000234.

[89] Estefanía Cuenca. *On Shear Behavior of Structural Elements Made of Steel Fiber Reinforced Concrete*. Springer Theses. Valencia (Spain): Springer International Publishing, 2015. ISBN: 978-3-319-13685-1. DOI: 10.1007/978-3-319-13686-8. URL: http://link.springer.com/10.1007/978-3-319-13686-8.

[90] R. Bornemann et al. "Ultra-hochleistungsbeton UHPC - herstellung, eigenschaften und anwendungsmöglichkeiten". In: *Beton- und Stahlbetonbau* 96.7 (2001), pp. 458–467. ISSN: 14371006. DOI: 10.1002/best.200100550.

[91] S Fröhlich and M Schmidt. "Influences on Repeatability and Reproducibility of Testing Methods for Fresh UHPC". In: *Ultra High Performance Concrete and Nanotechnology in Construction, 3rd Intl. Symp. on Ultra High Performance Concrete and Nanotechnology for High Performance Construction Materials, Structural Materials & Engineering Series No. 19*. Kassel: Kassel University Press GmbH, 2012, pp. 225–232.

[92] M Schmidt and Susanne Fröhlich. "Testing of UHPC". In: *2010 fib Congress and PCI Convention Bridge Conf. Proc.* Washington, D.C.: (pub.: Precast/Prestressed Concrete Institute, Chicago), 2010.

[93] F. Koksal, A. Ilki, and M. A. Tasdemir. "Optimum Mix Design of Steel-Fibre-Reinforced Concrete Plates". In: *Arabian Journal for Science and Engineering* 38.11 (2013), pp. 2971–2983. ISSN: 21914281. DOI: 10.1007/s13369-012-0468-y.

[94] Tim Soetens. "Design models for the shear strength of prestressed precast steel fibre reinforced concrete girders". PhD thesis. Gent University, 2015, pp. 158–167. URL: https://biblio.ugent.be/publication/5944364.

[95] PCI Precast/Prestressed concrete Institute. *Bridge design manual 3rd Edition, Second Release, August 2014*. 2014.

[96] Juan Navarro-Gregori et al. “Experimental study on the steel-fibre contribution to concrete shear behaviour”. In: *Construction and Building Materials* 112 (June 2016), pp. 100–111. ISSN: 09500618. DOI: 10.1016/j.conbuildmat.2016.02.157. URL: http://dx.doi.org/10.1016/j.conbuildmat.2016.02.157.

[97] J. Turmo et al. “Estudio del comportamiento a cortante de vigas de hormigón reforzado con fibras”. In: *Materiales de Construccion* 58.292 (Oct. 2008), pp. 5–13. ISSN: 04652746. DOI: 10.3989/mc.2008.40507.

[98] N. Randl et al. “Development of UHPC mixtures from an ecological point of view”. In: *Construction and Building Materials* 67.PART C (Sept. 2014), pp. 373–378.

[99] Rafael Ruiz, Leonardo Todisco, and Hugo Corres. “Conceptual design of HPFRC and UHPFRC road girder bridges”. In: *International fib Symposium - Conceptual Design of Structures 2021*. 2021. DOI: 10.35789/fib.PROC.0055.2021.CDSymp.P038.

[100] E. V. Sarmiento, M. R. Geiker, and T. Kanstad. “Influence of fibre distribution and orientation on the flexural behaviour of beams cast from flowable hybrid polymer-steel FRC”. In: *Construction and Building Materials* 109 (2016), pp. 166–176. ISSN: 09500618. DOI: 10.1016/j.conbuildmat.2016.02.005. URL: http://dx.doi.org/10.1016/j.conbuildmat.2016.02.005.

[101] Marco di Prisco, Francesco Iorio, and Giovanni Plizzari. “HPSFRC prestressed roof elements”. In: *RILEM TC 162-TDF Workshop* Test and Design Methods for Steel Fibre Reinforced Concrete (2003), pp. 161–188. DOI: 10.1617/2351580168.012.

[102] Liberato Ferrara and Alberto Meda. “Relationships between fibre distribution, workability and the mechanical properties of SFRC applied to precast roof elements”. In: *Materials and Structures/Materiaux et Constructions* 39.4 (2006), pp. 411–420. ISSN: 13595997. DOI: 10.1617/s11527-005-9017-4.

[103] Paolo Martinelli et al. “Characterization tests for predicting the mechanical performance of SFRC floors: identification of fibre distribution and orientation effects”. In: *Materials and structures* 54.3 (Feb. 2021), pp. 1–13. ISSN: 1359-5997. DOI: 10.1617/S11527-020-01593-7. URL: https://upcommons.upc.edu/handle/2117/335092.

[104] F. Ortiz Navas et al. “An experimental study on the shear behaviour of reinforced concrete beams with macro-synthetic fibres”. In: *Construction and Building Materials* 169 (2018), pp. 888–899. ISSN: 09500618. DOI: 10.1016/j.conbuildmat.2018.02.023. URL: https://doi.org/10.1016/j.conbuildmat.2018.02.023.

[105] Sergio H.Pialarissi Cavalaro et al. "Improved assessment of fibre content and orientation with inductive method in SFRC". In: *Materials and Structures/Materiaux et Constructions* 48.6 (2015), pp. 1859–1873. ISSN: 13595997. DOI: 10.1617/s11527-014-0279-6.

[106] Sergio H.P. Cavalaro et al. "Assessment of fibre content and 3D profile in cylindrical SFRC specimens". In: *Materials and Structures/Materiaux et Constructions* 49.1-2 (2016), pp. 577–595. ISSN: 13595997. DOI: 10.1617/s11527-014-0521-2.

[107] Steffen Grünewald et al. "Self-compacting high performance fiber concrete for foundations: Part 2—Fiber orientation and distribution". In: *Structural Concrete* 23.2 (2022), pp. 1018–1035. ISSN: 17517648. DOI: 10.1002/suco.202000441.

[108] "Comparison between methods to determine the fibre orientation factor of an HPFRC bridge box girder". In: *Construction and Building Materials* 269 (2021), p. 121291. ISSN: 09500618. URL: https://doi.org/10.1016/j.conbuildmat.2020.121291.

[109] ACI Committe 207. *ACI 207.1R-05 Guide to Mass Concrete*. Tech. rep. Reapproved. 2012, pp. 1–30.

[110] Asociación Española de Normalización. "EN 196-1: Methods of testing cement. Part 1: Determination of strength". In: (2018), p. 40.

[111] Asociación Española de Normalización. *EN 196-3: Methods of testing cement. Part 3: Determination of setting times and soundess*. 2017, p. 20.

[112] ASTM C939-87. *Standard test method for flow of grout (flow cone method)*. 2010.

[113] Asociación Española de Normalización. *EN 12350-5. Ensayos de hormigón fresco. Parte 5: Ensayo de la mesa de sacudidas*. 2020, p. 16.

[114] Asociación Española de Normalización. *EN 12390-3. Ensayos de hormigón endurecido. Parte 3: Determinación de la resistencia a compresión de probetas*. 2020, p. 24.

[115] ACHE. *Monografía M-2. Manual de tecnología del hormigón reforzado con fibras de acero*. 2000, p. 125.

[116] Antonio Mudadu et al. "The effect of fiber orientation on the post-cracking behavior of steel fiber reinforced concrete under bending and uniaxial tensile tests". In: *Cement and Concrete Composites* 93.July (2018), pp. 274–288. ISSN: 09589465. DOI: 10.1016/j.cemconcomp.2018.07.012. URL: https://doi.org/10.1016/j.cemconcomp.2018.07.012.

[117] J. Edgington and D. J. Hannant. "Steel fibre reinforced concrete. The effect on fibre orientation of compaction by vibration". In: *Matériaux et Constructions* 5.1 (1972), pp. 41–44. ISSN: 00255432. DOI: 10.1007/BF02479076.

[118] Giuseppe Tiberti et al. “An overview of the flexural post-cracking behavior of steel fiber reinforced concrete”. In: *Structural Concrete* 19.3 (June 2018), pp. 695–718. ISSN: 14644177. DOI: 10.1002/suco.201700068. URL: https://onlinelibrary.wiley.com/doi/10.1002/suco.201700068.

[119] Herbert Krenchel. *Fibre spacing and specific fibre surface*. Ed. by The Construction Press. 1975, pp. 69–79.

[120] K Schönlin. “Determination of the orientation, the content and the distribution of the fibres in fibre reinforced concrete”. In: 83.6 (1988), pp. 168–71.

[121] Estefanía Cuenca et al. “A material-performance-based database for FRC and RC elements under shear loading”. In: *Materials and Structures* 51.1 (Feb. 2018), p. 11. ISSN: 1359-5997. DOI: 10.1617/s11527-017-1130-7. URL: http://link.springer.com/10.1617/s11527-017-1130-7.

[122] Ling Zhi Jin et al. “Shear strength of fibre-reinforced reactive powder concrete I-shaped beam without stirrups”. In: *Magazine of Concrete Research* 72.21 (2020), pp. 1112–1124. ISSN: 1751763X. DOI: 10.1680/jmacr.18.00525.

[123] Karl Heinz Reineck and Leonardo Todisco. “Database of Shear Tests for Non-slender Reinforced Concrete Beams without Stirrups”. In: *Structural Journal* 111.6 (Nov. 2014), pp. 1363–1372. ISSN: 08893241. DOI: 10.14359/51686820.

[124] Leonardo Todisco, Karl Heinz Reineck, and Oguzhan Bayrak. “Database with shear tests on non-slender reinforced concrete beams with vertical stirrups”. In: *ACI Structural Journal* 112.6 (2015), pp. 761–770. ISSN: 08893241. DOI: 10.14359/51688055.

[125] Leonardo Todisco, Karl-Heinz Reineck, and Oguzhan Bayrak. “European design rules for point loads near supports evaluated with data from shear tests on non-slender beams with vertical stirrups”. In: *Structural Concrete* 17.2 (June 2016), pp. 135–144. ISSN: 14644177. DOI: 10.1002/suco.201500089. URL: https://onlinelibrary.wiley.com/doi/10.1002/suco.201500089.

[126] Leonardo Todisco, Oguzhan Bayrak, and Karl Heinz Reineck. “ACI-DAfStb database for tests on deep beams and comparisons with code provisions”. In: *Structural Concrete* 19.1 (Feb. 2018), pp. 296–304. ISSN: 1751-7648. DOI: 10.1002/SUCO.201700061. URL: https://onlinelibrary.wiley.com/doi/full/10.1002/suco.201700061%20https://onlinelibrary.wiley.com/doi/abs/10.1002/suco.201700061%20https://onlinelibrary.wiley.com/doi/10.1002/suco.201700061.

[127] Josef Hegger and Guido Bertram. "Shear carrying capacity of Ultra-High Performance Concrete beams". In: *Proceedings of the International FIB Symposium 2008 - Tailor Made Concrete Structures: New Solutions for our Society* (2008), p. 96. DOI: 10.1201/9781439828410.ch59.

[128] P. De Pauw et al. "Replacement of shear reinforcement by steel fibres in pretensioned concrete beams". In: *Proceedings of the International FIB Symposium 2008 - Tailor Made Concrete Structures: New Solutions for our Society* (2008), p. 104. DOI: 10.1201/9781439828410.ch67.

[129] In Hwan Yang, Changbin Joh, and Byung Suk Kim. "Shear behaviour of ultra-highperformance fibre-reinforced concrete beams without stirrups". In: *Magazine of Concrete Research* 64.11 (2012), pp. 979–993. ISSN: 00249831. DOI: 10.1680/macr.11.00153.

[130] Kevin Metje and Torsten Leutbecher. "Experimental investigations on the shear bearing behavior of prestressed ultra-high performance fiber-reinforced concrete beams with compact cross-section". In: *Structural Concrete* 22.6 (2021), pp. 3746–3762. ISSN: 17517648. DOI: 10.1002/suco.202100337.

[131] Rafic G. El-Helou and Benjamin A. Graybeal. "Shear Behavior of Ultrahigh-Performance Concrete Pretensioned Bridge Girders". In: *Journal of Structural Engineering* 148.4 (2022). ISSN: 0733-9445. DOI: 10.1061/(asce)st.1943-541x.0003279.

[132] Federal Highway Administration. "Structural Behavior of Ultra-High Performance Concrete Prestressed I-Girders". In: 8 (2006), p. 106. URL: http://www.tfhrc.gov/structur/pubs/06115/index.htm.

[133] Karl-Heinz Reineck and Daniel Dunkelberg. "ACI-DAfStb databases 2015 with shear tests for evaluating relationships for the shear design of structural concrete members without and with stirrups". In: (). URL: https://books.google.com/books/about/ACI_DAfStb_Databases_2015_with_Shear_Tes.html?hl=es&id=GNTYswEACAAJ.

[134] TC Membership. "RILEM TC 162-TDF: 'Test and design methods for steel fibre reinforced concrete' σ-ϵ-design method". In: *Materials and Structures/Materiaux et Constructions* 36.262 (2003), pp. 560–567. ISSN: 13595997. DOI: 10.1617/14007.

[135] Karl-Heinz Reineck and Daniel Dunkelberg. *ACI-DAfStb databases 2015 on shear tests for evaluating relationships for the shear design of structural concrete members without and with stirrups*. Ed. by Beuth Verlag GmbH. Berlin, 2017. URL: https://books.google.es/books/about/ACI_DAfStb_Databases_2015_with_Shear_Tes.html?id=GNTYswEACAAJ&redir_esc=y.

[136] Karl-Heinz Reineck and Birol Fitik. *ACI-DAfStb databases 2020 with shear tests on structural concrete members without stirrups*. DAfStb-Hef. Berling: Issued by Deutscher Ausschuss für Stahlbeton e.V. – DAfStb, 10787 Berlin, 2022.

[137] Eva O.L. Lantsoght. "Database of shear experiments on steel fiber reinforced concrete beams without stirrups". In: *Materials* 16.6 (2019), pp. 1–36. ISSN: 19961944. DOI: 10.3390/ma12060917.

[138] Enrico Faccin. "Experimental and analytical study on punching shear strength of steel fibre reinforced concrete flat slabs". PhD thesis. Università degli studi di Brescia, 2022.

[139] Jesús Miguel Bairán, Nikola Tošić, and Albert de la Fuente. "Reliability-based assessment of the partial factor for shear design of fibre reinforced concrete members without shear reinforcement". In: *Materials and Structures/Materiaux et Constructions* 54.5 (2021). ISSN: 13595997. DOI: 10.1617/s11527-021-01773-z.

[140] J Schlaich and K Schiifer. "Design and detailing of structural concrete using strut-and-tie models". In: 69.6 (1991), pp. 113–125. URL: https://scholar.google.com/scholar_lookup?title=Design%20and%20detailing%20of%20structural%20concrete%20using%20strut-and-tie%20models&author=J.%20Schlaich&publication_year=1991&pages=113-125.

[141] Jorg Schlaich, Kurt Schafer, and Mattias Jennewein. "Toward a Consistent Design of Structural Concrete". In: *PCI Journal* 32.3 (May 1987), pp. 74–150. ISSN: 08879672. DOI: 10.15554/pcij.05011987.74.150.

[142] E Mörsch. *Der Eisenbetonbau seine Theorie und Anwendung (Theory and Applications of Reinforced Concrete)*. Ed. by Verlag Konrad Wittwer. Stuttgart, 1902.

[143] Emil Mörsch. *Der Eisenbetonbau (Concrete-steel construction)*. Ed. by The Engineering News Publishing Company. Third. New York, 1909.

[144] W Ritter. "Die Bauweise Hennebique (The Hennebique system)". In: *Schweizerische Bauzeitung* (1899).

[145] A. Muttoni, J. Schwartz, and B. Thürlimann. *Design of Concrete Structures with Stress Fields*. Basel: Birkhäuser Basel, 1996. ISBN: 978-3-0348-9885-0. DOI: 10.1007/978-3-0348-9047-2.

[146] Aurelio Muttoni. *fib Bulletin 85. Towards a rational understanding of shear in beams and slabs*. Ed. by Ozzie Bayrak, Miguel Fernández Ruiz, and Walter Kaufmann. fib Bulletins. fib. The International Federation for Structural Concrete, May 2018. ISBN: 9782883941250. DOI: 10.35789/fib.BULL.0085. URL: https://www.fib-

international.org/publications/fib-bulletins/towards-a-rational-understanding-of-shear-in-beams-and-slabs-pdf-detail.html.

[147] ACI Committee 318/ACI 318R-19. *Building Code (ACI 318-19) and Commentary on Building Code Requirements for Structural Concrete (ACI 318R-19)*. 2019, p. 988. ISBN: 9781641950565.

[148] Stefano Campana et al. "Analysis of shear-transfer actions on one-way RC members based on measured cracking pattern and failure kinematics". In: *Magazine of Concrete Research* 65.6 (Mar. 2013), pp. 386–404. ISSN: 0024-9831. DOI: 10.1680/macr.12.00142. URL: https://www.icevirtuallibrary.com/doi/10.1680/macr.12.00142.

[149] Francesco Cavagnis, Miguel Fernández Ruiz, and Aurelio Muttoni. "Shear failures in reinforced concrete members without transverse reinforcement: An analysis of the critical shear crack development on the basis of test results". In: *Engineering Structures* 103 (Nov. 2015), pp. 157–173. ISSN: 01410296. DOI: 10.1016/j.engstruct.2015.09.015. URL: https://linkinghub.elsevier.com/retrieve/pii/S0141029615005787.

[150] Frank J Vecchio Collins and Michael P. "The Modified Compression-Field Theory for Reinforced Concrete Elements Subjected to Shear". In: *ACI Journal Proceedings* 83.2 (1986). ISSN: 0002-8061. DOI: 10.14359/10416. URL: http://www.concrete.org/Publications/ACIMaterialsJournal/ACIJournalSearch.aspx?m=details&ID=10416.

[151] Viktor Sigrist et al. "Background to the fib Model Code 2010 shear provisions - Part I: Beams and slabs". In: *Structural Concrete* 14.3 (2013), pp. 195–203. ISSN: 17517648. DOI: 10.1002/suco.201200066.

[152] R. C. Fenwick and Thomas Paulay. "Mechanisms of Shear Resistance of Concrete Beams". In: *Journal of the Structural Division* 94.10 (Oct. 1968), pp. 2325–2350. ISSN: 0044-8001. DOI: 10.1061/JSDEAG.0002092. URL: https://ascelibrary.org/doi/10.1061/JSDEAG.0002092.

[153] HPJ Taylor. "Investigation of the forces carried across cracks in reinforced concrete beams in shear by interlock of aggregate". In: *Cement and Concrete Association* 42.447 (1970), pp. 1–22.

[154] T Paulay and P J Loeber. "Shear transfer by aggregate interlock". In: *American Concrete Institute, ACI Special Publication* SP-042 (1974), pp. 1–15. ISSN: 01932527.

[155] Zdeněk P. Bažant and Pietro Gambarova. "Rough Cracks in Reinforced Concrete". In: *Journal of the Structural Division* 106.4 (Apr. 1980), pp. 819–842. ISSN: 0044-8001. DOI: 10.1061/JSDEAG.0005400. URL: https://ascelibrary.org/doi/10.1061/JSDEAG.0005400.

[156] Joost C. Walraven. "Fundamental Analysis of Aggregate Interlock". In: *Journal of the Structural Division* 107.11 (Nov. 1981), pp. 2245–2270. ISSN: 0044-8001. DOI: 10.1061/JSDEAG.0005820. URL: https://ascelibrary.org/doi/10.1061/JSDEAG.0005820.

[157] Tomaž Ulaga. *Betonbauteile mit stab-und lamellenbewehrung: verbund-und zuggliedmodellierung*. 280. vdf Hochschulverlag AG, 2003.

[158] Roberto Guidotti. *Poinçonnement des planchers-dalles avec colonnes superposées fortement sollicitées*. Tech. rep. École Polytechnique Fédérale de Laussane, 2010.

[159] J. Sagaseta and R. L. Vollum. "Influence of aggregate fracture on shear transfer through cracks in reinforced concrete". In: *Magazine of Concrete Research* 63.2 (Feb. 2011), pp. 119–137. ISSN: 0024-9831. DOI: 10.1680/macr.9.00191. URL: https://www.icevirtuallibrary.com/doi/10.1680/macr.9.00191.

[160] Miguel Fernández Ruiz. "The influence of the kinematics of rough surface engagement on the transfer of forces in cracked concrete". In: *Engineering Structures* 231 (Mar. 2021), p. 111650. ISSN: 18737323. DOI: 10.1016/j.engstruct.2020.111650.

[161] W J Krefeld and C W Thurston. "Contribution of longitudinal steel to shear resistance of reinforced concrete beams". In: *ACI Journal* 63.3 (1966), pp. 325–344. URL: https://www.scopus.com/inward/record.uri?eid=2-s2.0-0001660317&partnerID=40&md5=8230ec3a84d4a49c9e35c377cee2fd4a.

[162] H P Taylor. "Investigation of the dowel shear forces carried by the tensile steel in reinforced concrete beams". In: (1969).

[163] Theodor Baumann and H Rüsch. *Versuche zum studium der ver-dübelungswirkung der biegezugbewehrung eines stahlbetonbalkens*. Ernst, 1970.

[164] P. S. Chana. "Investigation of the mechanism of shear failure of reinforced concrete beams". In: *Magazine of Concrete Research* 39.141 (Dec. 1987), pp. 196–204. ISSN: 0024-9831. DOI: 10.1680/macr.1987.39.141.196. URL: https://www.icevirtuallibrary.com/doi/10.1680/macr.1987.39.141.196.

[165] Sandro Dei Poli, Marco Di Prisco, and Pietro G Gambarova. "Cover and stirrup effects on the shear response of dowel bar embedded in concrete". In: *Structural Journal* 90.4 (1993), pp. 441–450.

[166] Prodromes D Zararis. "Shear strength and minimum shear reinforcement of reinforced concrete slender beams". In: *ACI Structural Journal* 100.2 (2003), pp. 203–214. URL: https://www.scopus.com/inward/record.uri?eid=2-s2.0-0037497365&partnerID=40&md5=04dd57861d75a387ef8a188c497587ae.

[167] Thomas Pfyl. "Tragverhalten von Stahlfaserbeton". In: 15005 (2003), p. 145.

[168] Walter Kaufmann et al. “Shear transfer across cracks in steel fibre reinforced concrete”. In: *Engineering Structures* 186.December 2018 (2019), pp. 508–524. ISSN: 18737323. DOI: 10.1016/j.engstruct.2019.02.027. URL: https://doi.org/10.1016/j.engstruct.2019.02.027.

[169] Michael Rupf, Miguel Fernández Ruiz, and Aurelio Muttoni. “Post-tensioned girders with low amounts of shear reinforcement: Shear strength and influence of flanges”. In: *Engineering Structures* 56 (Nov. 2013), pp. 357–371. ISSN: 01410296. DOI: 10.1016/j.engstruct.2013.05.024.

[170] Andrea Monserrat López, Miguel Fernánez Ruiz, and Pedro Fco Miguel Sosa. “The influence of transverse reinforcement and yielding of flexural reinforcement on the shear-transfer actions of RC members”. In: *Engineering Structures* 234.February (May 2021), p. 111949. ISSN: 01410296. DOI: 10.1016/j.engstruct.2021.111949. URL: https://linkinghub.elsevier.com/retrieve/pii/S0141029621000997.

[171] Francesco Cavagnis, Miguel Fernández Ruiz, and Aurelio Muttoni. “An analysis of the shear-transfer actions in reinforced concrete members without transverse reinforcement based on refined experimental measurements”. In: *Structural Concrete* 19.1 (Feb. 2018), pp. 49–64. ISSN: 14644177. DOI: 10.1002/suco.201700145. URL: https://onlinelibrary.wiley.com/doi/10.1002/suco.201700145.

[172] Patrick Huber, Tobias Huber, and Johann Kollegger. “Investigation of the shear behavior of RC beams on the basis of measured crack kinematics”. In: *Engineering Structures* 113 (Apr. 2016), pp. 41–58. ISSN: 01410296. DOI: 10.1016/j.engstruct.2016.01.025. URL: https://linkinghub.elsevier.com/retrieve/pii/S0141029616000419.

[173] EN 12390-13. *Testing hardened concrete. Part 13: Determination of secant modulus of elasticity in compression*. Ed. by AENOR. Madrid, 2014, p. 18.

[174] J. Blaber, B. Adair, and A. Antoniou. “Ncorr: Open-Source 2D Digital Image Correlation Matlab Software”. In: *Experimental Mechanics* 55.6 (2015), pp. 1105–1122. ISSN: 17412765. DOI: 10.1007/s11340-015-0009-1.

[175] Nicola Gehri, Jaime Mata-Falcón, and Walter Kaufmann. “Automated crack detection and measurement based on digital image correlation”. In: *Construction and Building Materials* 256 (2020). ISSN: 09500618. DOI: 10.1016/j.conbuildmat.2020.119383.

[176] Nicola Gehri, Jaime Mata-Falcón, and Walter Kaufmann. “Refined extraction of crack characteristics in Large-scale concrete experiments based on digital image correlation”. In: *Engineering Structures* 251.November 2021 (2022). ISSN: 18737323. DOI: 10.1016/j.engstruct.2021.113486.

[177] B Li, Koichi Maekawa, and H Okamura. "Contact density model for stress transfer across cracks in concrete". In: *Journal of Faculty of Engineering, The University of Tokyo* 40 (Feb. 1989), pp. 9–52.

[178] Miguel Fernández Ruiz and Aurelio Muttoni. "On development of suitable stress fields for structural concrete". In: *ACI Structural journal* 104.4 (2007), p. 495.

[179] E Fehling and J Thiemicke. "Experimental Investigations on I-Shaped UHPC-Beams with Combined Reinforcement under Shear Load ". In: *Ultra High Performance Concrete and Nanotechnology in Construction, 3rd Intl. Symp. on Ultra High Performance Concrete and Nanotechnology for High Performance Construction Materials, Structural Materials & Engineering Series No. 19*. Kassel: Kassel University Press GmbH, 2012, pp. 477–484.

[180] Norbert Randl and Tamás Mészöly. "Load bearing behavior of UHPFRC beams reinforced with high grade steel". In: *Key Engineering Materials* 629-630 (2015), pp. 551–559. ISSN: 16629795. DOI: 10.4028/www.scientific.net/KEM.629-630.551.